Towards large-scale commercialization of fuel cells: Robust design optimization considering dimensional uncertainties in the flow distributors

THÈSE N^{O} 6899 (2016)

PRÉSENTÉE LE 27 AVRIL 2016

À LA FACULTÉ DES SCIENCES ET TECHNIQUES DE L'INGÉNIEUR
LABORATOIRE D'ÉNERGÉTIQUE INDUSTRIELLE
PROGRAMME DOCTORAL EN ENERGIE

ÉCOLE POLYTECHNIQUE FÉDÉRALE DE LAUSANNE

POUR L'OBTENTION DU GRADE DE DOCTEUR ÈS SCIENCES

PAR

Thierry Mikaël CORNU

acceptée sur proposition du jury:

Dr S.-R. Cherkaoui, président du jury
Dr J. Van Herle, directeur de thèse
Prof. P. H. Middleton, rapporteur
Prof. C. Pianese, rapporteur
Prof. D. Bonvin, rapporteur

ÉCOLE POLYTECHNIQUE
FÉDÉRALE DE LAUSANNE
Suisse
2016

Towards large-scale commercialisation of fuel cells: Robust design optimization considering dimensional uncertainties in the flow distributors

PAR

Thierry Mikaël CORNU

Remerciements

Je remercie avant tout **mon directeur de thèse**, *Dr Jan Van herle*, pour m'avoir accueilli dans son groupe et m'avoir encouragé à me lancer dans l'aventure doctorale. Je le remercie en particulier pour son dévouement à garantir le financement de ma thèse et pour instaurer un esprit de convivialité au sein de son groupe.

Mes remerciements vont aussi au *Prof. Daniel Favrat*, directeur du Laboratoire d'énergétique industrielle (LENI), qui m'a permis dès le premier jour de me sentir un collaborateur bienvenu dans son laboratoire.

Ma thèse a été financée essentiellement par SOLIDpower S.p.a. (SOFCpower-HTceramix), au travers du projet EFESO[1] puis par la Commission pour la technologie et l'innovation (CTI), dans le cadre d'un projet avec SWISSHydrogen SA (anciennement BELENOS Clean Power Holding de SWATCH group). Je remercie les personnes de ces sociétés qui ont permis d'intégrer le financement de ma thèse à ces projets, à savoir *Massimo Bertoldi*, *Olivier Bücheli*, *Alexandre Closset* et *Bahaa Roustom*.

I address my warmest acknowledgments to **all members of the jury** for having accepted to take this participative role in my thesis and for all their suggestions of improvements: *Dr Rachid Cherkaoui* (President), *Prof. Dominique Bonvin*, *Prof. Peter Hugh Middleton*, *Prof. Cesare Pianese*, and of course my advisor *Dr Jan Van herle*.

Pour leurs précieux **conseils scientifiques** et le temps qu'ils m'ont aimablement accordé, je remercie en particulier :
Dr Zacharie Wuillemin, *Dr Arata Nakajo* et *Dr Stefan Diethelm* pour avoir partagé leur grande expérience des piles à combustible ;
Dr Timm Faulwasser, *Prof. Fabio Nobile* et *Prof. Marco Picasso* pour m'avoir aidé à clarifier les aspects mathématiques du problème et à en réduire la complexité.

[1] Environmental-Friendly Electricity from Solid Oxide Fuel Cells.

Toute ma gratitude aux fées de l'**administration**, qui (r)accommodent tout ce qui peut l'être : *Chantal Donaghey*, *Sarah Duplan*, *Brigitte Fayet*, *Irène Laroche*, *Melody Meyer*, *Cécile Taverney*, *Alexandra Morrison* et *Suzanne Zahnd*.

Un grand merci aux **collaborateurs** de **SOLIDpower** et **SWISSHydrogen** et en particulier à *Zacharie Wuillemin*, *Diego Larrain*, *Yannik Antonetti*, *Massimo Bertoldi*, *Caroline Paccaud*, *Eva Saadé*, *Uwe Hannesen* et *Rexhep Gashi*.

Je remercie sincèrement **tous les étudiants** que j'ai eu la chance de superviser, qui ont apporté leur pierre à l'édifice. Remerciements particuliers à *Roberto Passini*, *Kevin Rosset*, *Pieter Dermont*, *Xavier Bednarek*, et *Arnault-Quentin Eggermont*.

Mille mercis à **tous mes amis et collègues** de feu le LENI, de FUELMAT, de l'IPESE et de l'EPFL en général. J'ai une pensée particulière pour *Matthias B. & D.*, *Samuel*, *Priscilla*, *Manuel*, *Laurence*, *Ema*, *Stefano*, *Jakob*, *Leandro*, *Tivi*, *Julien*, *Hossein*, *Nicolas B. & D.*, *Stéphane*, *Fabio*, *Nasibeh*, *Vaibhav*, *Alberto*, *Arata*, *Jean-Baptiste*, *Nils* et *Giorgio*. J'ai passé des moments incroyables grâce à vous, que ce soit autour d'un repas, d'un café (avec une « tranche de lard » svp !), d'une discussion passionnée se prolongeant entre deux portes, d'une bière, ou même en parlant de travail (si si !).

Remerciements spéciaux à *Stefano* — pour sa lecture d'une ébauche de mon manuscrit — ainsi qu'à *Manuel, Priscilla, Matthias D., Samuel, Jakob et Leonidas* — pour leur temps et conseils prodigués avant mon examen, et à *Matthias & Myriam B.* — pour tous les moments conviviaux entre amis qu'ils ont organisés.

Merci du fond du cœur à *Nicolas Flückiger*, *Audrey Kessler* et *Елена Жирная* qui m'ont permis de sortir un peu la tête de ma thèse (et désolé pour toutes les fois où le sujet de la discussion à dériver). Merci aussi à *Ioana Raluca Stancu* et *Gerrit Weber* pour leur écoute et leurs précieux conseils dans les moments difficiles.

Enfin et surtout, je remercie **ma famille**. Sans son soutien, affronter toutes les incertitudes qui ont surgit de partout dans ma thèse aurait été autrement plus désagréable. Merci infiniment à mes parents *Yvette & Sylvain* et à *ma sœur Cyndie*, ainsi qu'à ma tante *Lucienne*, ma marraine *Fabienne*, et mes grands-parents *Thérèse & Narcisse*.

MERCI aux 200+ personnes qui ont contribué par une action durable ou éphémère à rendre mes années de thèse plus agréables et enrichissantes, sans compter toutes celles qui travaillent dans l'ombre ou que j'aurais maladroitement oubliées (pardon !).

Hossein Afshari, Yannik Antonetti, Kevin Arrandel, Laura Augello, Germain Augsburger, Nordahl Autissier, Steven Beale, Rami Bechara, Helen Becker, Xavier Bednarek, Cédric Beetschen, Matthias & Myriam Bendig, Rafał Bernat, Massimo Bertoldi, Alexandre Bertrand, Manuel Bianco, Michel Bierlaire, Raffaele Bolliger, Dominique Bonvin, Nicolas Borboën, Navid Borhani, Noé Bory, Isabelle & Jacques Bouverat, Romain Brunner, Olivier Bücheli, Stéphane Bungener, Priscilla Caliandro, Jean-Baptiste Carré, Dilan Celebi Ayse, Alexandre Chainho, Rachid Cherkaoui, Carinne Christinaz, Alexandre Closset, Víctor Codina, Paul Constantine, Yvette & Sylvain Cornu, Cyndie Cornu, Ariane Cornu, Manuel Crivelli, Jonathan Demierre, Christopher Dennison, Pieter Dermont, Nicolas Descoins, Stefan Diethelm, Chantal Donaghey, Matthias Dubuis, Jaka Dujc, Mikaël Dumortier, Sarah Duplan, Alexis Duret, Carole Dusonchet, Richard Dwight, Arnault-Quentin Eggermont, Soumaya El Kadiri, Yuriy Elesin, Adriano Ensinas, Emanuele Facchinetti, Antonin Faes, Timm Faulwasser, Daniel Favrat, Brigitte Fayet, Samira Fazlollahi, Nicolas Flückiger, Gregory François, Jean-Marie Fürbringer, Irwin Gafner, François Gallaire, Rexhep Gashi, Martin Gassner, Léda Gerber, Michela Geri, Christine Gil, Sami Goekce, Thérèse & Narcisse Gogniat, Mara Gagnebin, Kyriaki Goulouti, Fabio Greco, Uwe Hannesen, Samuel Henchoz, Gianluca Iaccarino, Angel Iglesias, Julien Jakubowski, Keith Jamison, Quentin Jeangros, Maziar Kermani, Samir Kerrache, Audrey Kessler, Stefanie Keuler, Young Min Kim, Eddy Koch, Jérémie Koch, Jakub Kupecki, Christian Landry, Irène Laroche, Diego Larrain, Jonas Lätt, Dirk Lauinger, Andreas Lesch, Lindsay Lessard, Pénélope Leyland, Henning Lübbe, Christopher Lythcke-Jørgensen, Gunda Mader, Hossein Madi, Mirco Magnini, Virginie Maillard, François Maréchal, Mardit Matian, Elfie Méchaussie, Gianluca Menghini, Ramanunni Menon, Fabien Meyer, Melody Meyer, Alberto Mian, Hugh Middleton, Olivier Millioud, Jonathan Mitchell, Vinit Mittal, Laurent Monnard, Stefano Moret, Alexandra Morrison, Gaudenz Moser, Arata Nakajo, Tuoung-Van Nguyen (Tivi), Fabio Nobile, Luis Eric Olmedo, Martin Ouwehand, Caroline Paccaud, Andrea Panizza, Alessandra Parisio, Roberto Passini, Emanuela Peduzzi, Bruant Perrinjaquet, Philip Peschke, Quoc Nhat Nam Pham, Cesare Pianese, Gaia Piazzesi, Marco Picasso, Michele Pisaroni, Sabine Pochon, Stéphane Poitel, Nasibeh Pouransari, Pierre Queloz, Jakob Rager, Alberto Ravagni, Paul Ressler, Giorgio Rinaldi, Jean-Loup Robineau, Kevin Rosset, Georges Roessler, Bahaa Roustom, Eva Saadé, Leandro Salgueiro, Mark Sawley, Pieter Schmal, Nils Schüler, Andreas Schüler, Vaibhav Singh, Paul Stadler, Ioana Raluca Stancu, Régis Straubhaar, Élisabeth & Joseph Paratte/Surdez, Fabienne & Michel Surdez, Annie, Dorian, Maëlle, Odile & Romain Surdez, Laura Swiler, Sylwia Szczukiewicz, Philippe Thalmann, Pietro Tanasini, Cécile Taverney, Quentin Theurillat, John Thome, Laurence Tock, Oliver Todd, Stefan Trabut, Trach-Minh Tran, Leonidas Tsikonis, Jan Van herle, Luc Veya, Nicolas Videau, Catherine Vinckenbosch, Frank Vöhringer, Anna Sophia Wallerand, Gerrit Weber, Pierre Wilhelm, Lucienne & Nicolas Willemin, Amandine, Dhiraj & Vimala Willemin, Truusje Winkel, Zacharie Wuillemin, Suzanne Zahnd, Achim Zanker, Morgane Zwahlen, Елена Жирная

Les Breuleux, le 13 avril 2016.

Thierry Cornu

Abstract

The present and future challenges that humanity is facing regarding *consumption and supply of energy* constitute the context of this research. The technology in which we are interested is the *fuel cell*, mainly because of its high efficiency for the conversion of fuels into electricity and heat. More specifically, the types of fuel cell considered are solid-oxide (SOFC) and polymer electrolyte (PEFC) fuel cells.

To take part in the reduction of the consumption of fossil fuels and of the emissions of greenhouse gases and of pollutants, fuel cells should first become a more attractive alternative technology. The finality of this study is hence to tackle remaining obstacles hindering their large-scale commercialization; namely, to reach a balanced and competitive combination of *production cost*, *lifetime*, and *density of performance*.

The originality of this research lies in the simultaneous tackling of these challenges via the *management of uncertainties* during the *design* of fuel cell stacks. The approach is hence to take actions "upstream" rather than "downstream". Particularly, a novelty is to account for the effect of the *manufacturing variability* on the homogeneity of the performance and on the related risk of degradation, or even failure. We focus on dimensional tolerances of the parts whose function is to distribute the flows as homogeneously as possible into the fuel cell. The technical objective is to find a robust optimal solution, i.e., a solution which is optimal also in terms of a lowered sensitivity to imperfections, such as geometrical distortions.

Besides, this research also deals with the challenges associated with the management of uncertainties in the context of combining *optimization of geometries (design)* and modelling based on *computational fluid dynamics (CFD)*. Taken alone, these techniques were proven to be powerful tools of analysis and of synthesis. They are however computer intensive. When used together, the insight they can offer is even greater, but we face, even with today's high-performance computing (HPC) infrastructures, the *dilemma of accuracy versus tractability*, which is even more problematic in the context of *uncertainty management* as will be shown.

Therefore, efforts were dedicated to find ways to unravel this dilemma, in the prospect of achieving the optimization, under uncertainty, of the design of fuel cells. In particular, approximate models were investigated, notably *reduced-order modelling* and *metamodelling* techniques.

The results of this research relate to both methodology and technology. Among the methodological results, surrogate models are evaluated in the prospect of their use (tractability vs. accuracy). Guidelines are given for the management of uncertainties in this context, and for future researches.

From a technological point of view, it was shown, first, that accounting for dimensional tolerances in the design of fuel cells is crucial. Then, the effect of these uncertainties were quantified, giving clearer insight on the best ways to deal with them. Last but not least, optimization of the design was carried out accounting for the uncertainties. Deterministic optima were compared with stochastic optima, revealing weaknesses of the deterministic approach and potential for improvements of the designs when considering, quantitatively, the uncertainties.

Last, and maybe more important, while conducting these investigations, we were able to raise numerous original (or re-formulated) questions, giving birth to novel tracks for improvements and to a fertile ground for further researches.

Keywords

Fuel cells; Computational fluid-dynamics (CFD); Uncertainty quantification (UQ); Robust design optimization (RDO); Stochastic optimization; Optimization under uncertainty (OUU); Surrogate modelling. Lifetime; Durability of performance; Reliability; Cost.

Résumé

Les défis présents et futurs auxquels l'humanité fait face en matière de *consommation et d'approvisionnement en énergie* constituent le contexte ce cette recherche. La technologie qui nous intéresse est la *pile à combustible*, principalement en raison de sa haute efficacité pour la conversion de combustibles en électricité et en chaleur. Plus spécifiquement, nous avons considéré les piles à combustible à oxyde solide (SOFC) et à électrolyte en polymère (PEFC).

Afin de participer à la réduction de la consommation de combustibles fossiles et des émissions de gaz à effet de serre et de polluants, il est nécessaire que les piles à combustible deviennent une technologie alternative plus attractive. La finalité de cette étude est ainsi de s'attaquer aux obstacles freinant leur commercialisation à large échelle. Il s'agit de parvenir à une combinaison compétitive et équilibrée en terme de *coût de production*, de *durée de vie*, et de *densité de performance*.

L'originalité de cette recherche réside dans le fait que ces défis sont relevés simultanément via la *gestion des incertitudes* durant la *conception* de la pile à combustible. L'approche est ainsi de prendre des mesures en amont plutôt qu'en aval. En particulier, une innovation consiste à prendre en compte les effets de la variabilité de fabrication sur l'homogénéité des performances et sur le risque connexe de dégradation, voire de défaillance. L'accent est mis sur les tolérances dimensionnelles des pièces responsables de la distribution, aussi homogène que possible, des écoulements à l'intérieur de la pile à combustible. L'objectif technique est de trouver un optimum robuste, c'est-à-dire une solution qui soit optimale aussi en terme d'une sensibilité minimum aux imperfections, telles que des distorsions géométriques.

Par ailleurs, cette recherche traite aussi des défis associé à la gestion des incertitudes dans le contexte de la combinaison d'une *optimisation géométrique* et d'une modélisation basée sur la *simulation numérique des fluides (CFD)*. Prises séparément, ces techniques ont fait leurs preuves comme outils d'analyse et de synthèse performants. Elles sont néanmoins gourmandes en ressources de calcul. Utilisées conjointement, elles permettent encore plus de clairvoyance, mais nous faisons alors face, même avec les infrastructures de calcul à haute performance contemporaines, au dilemme de l'*exactitude contre la faisabilité (solubilité)*, qui est encore plus problématique dans le contexte de la *gestion des incertitudes*, comme nous le montrerons.

En conséquence, des efforts ont été entrepris pour résoudre ce dilemme, dans la perspective de l'accomplissement de l'optimisation, sous incertitudes, de la conception de piles à combustible. En particulier, l'utilisation de modèles approximatifs de substitution a été examinée, notamment les techniques de modélisation d'ordre réduit et de méta-modélisation.

Les résultats de cette recherche ont donc trait à la fois à la méthodologie et à la technologie. Parmi les résultats méthodologiques, des modèles de substitution ont été évalués dans la perspective de leur utilisabilité (solubilité contre exactitude). Des recommandations sont données pour la gestion des incertitudes dans ce contexte, et pour des recherches ultérieures.

D'un point de vue technologique, nous montrons, en premier lieu, que tenir compte des tolérances dimensionnelles lors la conception des piles à combustible est crucial. Deuxièmement, les effets des incertitudes ont été quantifiés, permettant de donner un aperçu plus clair des meilleures moyens pour les atténuer. Enfin et surtout, l'optimisation de la conception a été réalisée en tenant compte des incertitudes. Des optima déterministes sont comparés aux optima stochastiques, révélant les faiblesses des premiers et le potentiel d'amélioration de la conception lorsque l'on prend en considération, quantitativement, les incertitudes.

Enfin, et peut-être plus important encore, en conduisant ces investigations, nous avons pu soulever de nombreuses questions inédites, donnant naissance à de nouvelles pistes d'amélioration et à un terreau fertile pour de futures recherches.

Mots-clés

Pile à combustible ; Simulation numérique des fluides ; Quantification d'incertitudes ; Optimisation robuste du design ; Optimisation stochastique ; Optimisation sous incertitudes ; Modélisation de substitution. Durée de vie ; Durabilité des performances ; Fiabilité ; Coût.

"The whole problem with the world is that fools and
fanatics are always so certain of themselves,
and wiser people so full of doubts."
Bertrand A. W. Russel

À tous ceux qui ont cru en moi.

À tous les incertains.

Foreword

The following text is an excerpt from "This Thing For Which We Have No Name — A Conversation With Rory Sutherland", in *Edge.org* [1]. Since I read it during the elaboration of this thesis, I cannot tell it inspired me for the subject. I was already interested in uncertainties. But, in my opinion, these few words strikingly point out why uncertainty is a matter of interest; not only for fuel cells, and even from a philosophical perspective.

> *"[W]e think there is such a thing called perfect reason. That we should be able to deploy reason and logic in every decision we make, when most of the time we simply don't have enough information to do so or the cost of acquiring that information will be absurd, or the information is not available in a comparable form. You know, it's very difficult — weighting. If you're looking at three or four variables in parallel when buying a car, what relative weighting do you attach to things? Are they linear? Are they even sort of monotonic in terms of how we perceive them?*
>
> *[...]*
>
> *First and foremost, let me give you a business example. The single best thing the London Underground did in terms of improving passenger satisfaction per pound spent wasn't faster, more frequent, later running trains, it was putting dot matrix display boards on the platform to tell you how long you were going to have to wait for your next train. There's something about the human brain, for whatever reason, which hates uncertainty. That's an interesting case because if you research how can you improve the Underground, most people would have said, "I want faster trains. I want more frequent trains." They would not have said, "I want less uncertainty." […] And you're both happier, you make better use of the time but you're also vastly less stressed in that period. Now, simply knowing that is really, really important. We don't like uncertainty."*

On these words, I wish you a good and hopefully interesting read.

Structure of the document

This thesis involves several fields, which are interlaced. Most of the readers will be specialized in one of them and have less knowledge of others. Therefore, we have tried to achieve a good balance of providing the right information. Furthermore, the ideas cannot be developed in all the necessary details sequentially, since some depend on others, and since it would impinge the understanding of the broader chains of reasoning. So, as much as possible, the document is decomposed by first giving overviews of the ideas, then dwelling progressively into details, and by relying on cross-references to relevant parts of the document.

The first part of the document will mostly discuss the methodology and its elaboration. Intermediate results will be presented to support the decisions that were taken. Since the methodology is a compound of several techniques, I chose to organize and divide the discourse according to these blocks. Interactions between them will be emphasized were appropriate.

The main techniques used are: numerical (flow) modelling, sensitivity analyses, design and analysis of computer experiments, sampling, statistics, uncertainty quantification, surrogate modelling, optimization, and the particular case of optimization under uncertainty. Several methods and sub-methods exist for each of these general techniques. They will be presented in more or less detail, depending on their usage in the frame of this thesis.

Remark:

For the sake of brevity and legibility, the trademarked and registered names of products or companies are shortened to their simpler form and put in small capitals. As an example, ANSYS® Fluent™ becomes ANSYS FLUENT, or simply FLUENT.

Almost all references to places in the document can be accessed with an hyperlink. When you hover the mouse over one cross-reference, the cursor will change shape..

Words or phrases in ***bold italics*** are defined in the *Glossary & index*, p. 309.

Chapter 1 — Introduction

Overview, context, motivations, objectives, originality, scope, and technological background of the thesis.

Chapter 2 — State of the art

Literature review regarding fuel cells, especially numerical modelling, design optimization, manufacturing uncertainty, general overview of methods and techniques for or related to the optimization under uncertainty. Highlight where and how this thesis contributes to fill a gap in the "state-of-the-art".

Chapter 3 — Description of the problem

Emphasis on the challenges that we meet when tackling the problem

Chapter 4 — Modelling approaches

Presentation of the main modelling blocks and assumptions regarding the physical phenomena and the stochastic processes.

Chapter 5 — Sensitivity to simulator's attributes

Study of the effect of simulator's attributes on the tractability and on the accuracy. The main goal of this chapter is to answer the question: how to build a simulator suitable for optimization under uncertainty of the design of fuel cells?

Chapter 6 — Sensitivity to decision variables

Study of the effect of controllable variables on performance indicators of fuel cells. The main goal of this chapter is to answer the question: which are the most significant variables for the evaluation of fuel cells "quality", that should therefore be chosen as decision variables in the subsequent optimization?

Chapter 7 — Characterization of the uncertainties

This chapter presents the characterization that was carried out for the input uncertainties, from experimental measurements to their interpretation in the form of statistical data, and resulting modelling as probability distribution functions.

Chapter 8 — Propagation of the uncertainties

Study of the effect of the input uncertainties on the outputs. Focus on geometrical distortions.

Chapter 9 — Optimization under uncertainty

Case studies of optimization of the design of fuel cells. From deterministic to stochastic optimization. Quantification of the uncertainty of the deterministic solution. Comparison and analysis of various scenarios.

Outline of contents

List of symbols & acronyms

This list of symbols is not exhaustive. Some symbols that only appear locally are described where they are used or are self-explanatory. You will find first acronyms and abbreviations, next special symbols by themes, an finally symbols sorted alphabetically (Latin and Greek letters).

Convention of notations

A space is used when multiplying variables to better distinguish groups of symbols which represent a single variable, e.g., $Q = M_{\mathrm{H_2}}\,\Delta_{\mathrm{r}}h$. A middle dot is used when confusion is still possible (e.g., with units, kg/(m · s))
Square brackets [ ] are used instead of parenthesis ( ) to indicate a functional relationship (e.g., $f[x]$, $\Delta_{\mathrm{r}}h[\mathrm{H_2}]$), so that such expressions cannot be confused with multiplication of variables.
Vectors, matrices, and tensors are in bold characters.

Otherwise, the composition of this thesis follows as much as possible the recommendation of NIST, about the writing of quantities, values, and units. (http://physics.nist.gov/cuu/Units/checklist.html).

Units different than in the next tables are sometimes used, especially when they lead to values closer to unity (e.g., mbar instead of Pa).

Glossary & index

Words or phrases in ***bold italics*** are defined in the *Glossary & index*, p. 309.

ACRONYMS & ABBREVIATIONS

AC/DC	Alternate current / direct (continuous) current
ANOVA	Analysis of variance
ASC	Anode-supported cell
ASR	Area specific resistance
BOP	Balance of plant

BPP	Bi-polar plate
CDF	Cumulative distribution function
CFD	Computational fluid dynamics
CHP	Combined heat- and power- generation (cogeneration)
CPU	Central processing unit (one core)
DACE	Design and analysis of computer experiments
DOE	Design of experiments
EORMS	Encyclopaedia of operations research and management science
FC	Fuel cell
GDL	Gas diffusion layer
FDP	Fluid distribution pattern
GPU	Graphical processing unit
HPC	High-performance computing
IID	Independent and identically distributed (random variables)
I-V	Current-voltage (polarisation) curve
IVM	International vocabulary of metrology
KKT	Karush-Kuhn-Tucker conditions
LENI	Laboratoire d'énergétique industrielle
LHV	Lower heating value
LHS	Latin hypercube sampling
LSM	Lanthanum strontium manganite ($La_{1-x}Sr_xMnO_3$)
LZO	Lanthanum zirconate ($La_2Zr_2O_7$)
MAD	Mean absolute deviation: $\frac{1}{n}\sum_i^n \lvert x_i - \bar{x_i} \rvert$
MCFC	Molten carbonate fuel cell
MCMC	Markov chain Monte Carlo
MCS	Monte Carlo simulations
MEA	Membrane electrode assembly
MIC	Metallic interconnect
MOO	Multi-objective optimization
MSE	Mean squared error: $\frac{1}{n}\sum_i^n \left(\hat{\theta} - \theta_i\right)^2$
OCV	Open circuit voltage
OUU	Optimization under uncertainty
PDF	Probability distribution function
PE(M)FC	Polymer electrolyte (membrane) fuel cell, also known as proton exchange (membrane) fuel cell
PEN	Positive electrode – electrolyte – negative electrode (cell, membrane)
PROSOFC	Production and reliability oriented SOFC cell and stack design

QOI	Quantity of interest
RMS	Root mean squares (a.k.a. quadratic mean): $\sqrt{\frac{1}{n}\sum_i^n x_i^2}$
RMSD	RMS deviation (or E for error): $\sqrt{\frac{1}{n}\sum_i^n \left(\hat{\theta} - \theta_i\right)^2}$
ROM	Reduced-order model(ling)
RSD	Relative standard deviation (a.k.a. coefficient of variation)
RSM	Response surface methodology
RV	Random variable
SMLPM	Standard millilitre per minute (STP as defined by UIPAC are $T = 273.15$ K and $p = 10^5$ Pa)
SSA	Six sigma analysis
STD	Standard deviation: $\sigma[X] = \sqrt{\mathrm{E}[(X-\mu)^2]}$, with $\mathrm{E}[X] = \mu$
SOFC	Solid oxide fuel cell
SRU	Single repeating unit (= individual repeat element)
SZO	Strontium zirconate
TPB	Triple phase boundary
UQ	Uncertainty Quantification
YSZ	Yttria-stabilized zirconia; yttria = oxide of yttrium: Y_2O_3, zirconia = dioxide of zirconium: ZrO_2
ZHAW	Zürcher Hochschule für Angewandte Wissenschaften (Zurich University of Applied Sciences)

SYMBOLS BY THEMES

Constants

e	Elementary charge:	$1.602\,176\,6208 \times 10^{-19}$	C
$\mathcal{F} = e\mathcal{N}_\mathrm{A}$	Faraday constant:	96 485 332.89	C/kmol
$k_\mathrm{B} = \frac{\mathcal{R}}{\mathcal{N}_\mathrm{A}}$	Boltzmann constant:	$1.380\,648\,52 \times 10^{-23}$	J/K
$\mathcal{N}_\mathrm{A}$	Avogadro constant:	$6.022\,140\,857 \times 10^{26}$	1/kmol
$\mathcal{R}$	Universal ideal-gas constant:	8 314.4598	J/(kmol·K)
σ_SB	Stefan-Boltzmann's constant:	$5.670\,367 \times 10^{-8}$	W/(m²·K⁴)

Non-dimensional numbers

Gr_{L}	Grashof number (characteristic length L)	—
Kn	Knudsen number	—
Ma	Mach number	—
Nu_{L}	Nusselt number (characteristic length L)	—
Pr	Prandtl number	—
Ra_{L}	Rayleigh number (characteristic length L)	—
Re_{L}	Reynolds number (characteristic length L)	—
Sc	Schmidt number	—
Sh	Sherwood number	—

Operators and other shortcut notations

Δx	Difference between two values of x ; $\Delta x = x_2 - x_1 \equiv {}_1^2\Delta x$
$\Delta x_{/ref}$	Relative difference, with reference *ref*
$x_{/ref}$	Ratio relative to reference *ref*
$\prod[\ ]$	Product
$\sum[\ ]$	Sum
$\frac{dy}{dx}$	Total derivative
$\frac{\partial y}{\partial x}$	Partial derivative
$\boldsymbol{\nabla}$	Nabla (spatial partial derivatives)
$\boldsymbol{\nabla^2}$	Laplacian[1], $\boldsymbol{\nabla^2 u} = \boldsymbol{\nabla} \cdot (\boldsymbol{\nabla u})$
$\propto$	Proportional to (linearly)
$\forall$	For all
$\exists$	There exists
$\dot{x}$	Per unit of time (1/s)
x'	Per unit of length (1/m)
x''	Per unit of surface (1/m²)
x'''	Per unit of volume (1/m³)
$\tilde{x}$	Per unit of mole
$[\ ]$	Interval, or function of
$\{\ \}$	Ensemble
$\hat{\theta}$	Estimation of a parameter θ (statistic)
$\bar{x}$	Sample mean of x (arithmetic mean, or simply mean)

[1] We write the Laplacian $\boldsymbol{\nabla}^2$ instead of $\boldsymbol{\Delta}$ to avoid confusion with the operator of difference, Δ.

$\mathrm{E}[X]$	Expected value of X (expectancy)
$\mathrm{Var}[X]$	Variance of X
$\mathrm{Cov}[X,Y]$	Covariance of X and Y
$\mu[X]$	Average of X
$\langle x \rangle$	Average of x, when $\bar{x}$ is inconvenient
$\sigma[X]$	Standard deviation of X

Sub- and superscripts

$_{\mathrm{a}}$	Air
$_{\mathrm{b}}$	Bulk
$_{ch}$	Channel (also, c)
$_{e}$	Element
$_{\mathrm{f}}$	Formation (e.g., enthalpy-change of formation)
$_{\mathrm{f}}$	Fuel
$_{\mathrm{g}}$	Gaseous
$_{\mathrm{h}}$	Hydraulic (diameter)
$_{i}$	Species i, or item i (regarding)
$_{\mathrm{l}}$	Liquid
$_{p}$	Isobaric, at constant pressure
$_{\mathrm{r}}$	Reaction (e.g., enthalpy-change of reaction)
$_{\mathrm{s}}$	Solid
$_{\mathrm{A}}$	Anode, anodic
$_{\mathrm{C}}$	Cathode, cathodic
$_{\mathbb{D}}$	Design (regarding)
$_{\mathrm{E}}$	Electrolyte, electrolytic
$_{\mathbb{N}}$	Nominal value
$_{\mathbb{U}}$	Uncertain
$_{V}$	Isochoric, at constant volume
$_{\mathrm{cell}}$	Cell
$_{\mathrm{IE}}$	Condition of independent elements (not stacked)
$_{\mathrm{ST}}$	Condition of stacked elements
$_{\mathrm{el}}$	Electricity (regarding)
$_{\mathrm{th}}$	Thermodynamic (regarding, heat)
$^{\ominus}$	At standard state (thermodynamic)

$_{\text{ref}}$	Reference
$_{\text{in}}$	Inlet
$_{\text{out}}$	Outlet
$_{\text{min}}$	Minimum
$_{\text{max}}$	Maximum
$_{\text{eff}}$	Effective
$_{\text{lam}}$	Laminar
$_{\text{turb}}$	Turbulent
$_{\text{st}}$	Stack
$_{\text{tot}}$	Total
$_{\text{sys}}$	System
$_{\text{sim}}$	Simulated
$_{\text{mix}}$	Mixture
$_{\text{yr}}$	Yearly

SYMBOLS BY ALPHABETS

Latin letters

A	Area of surface	m^2
a	Speed of sound	m/s
C_i	Concentration (volumetric) of species i	$kmol/m^3$
c_i	Mass fraction of species i	kg/kg
$\tilde{c}_i$	Molar fraction of species i	kmol/kmol
c_p	Specific heat capacity at constant pressure	J/(kg·K)
c_V	Specific heat capacity at constant volume	J/(kg·K)
D	Diameter	m
d	Margin of error	
E_a	Activation energy	kJ/kmol
$\mathcal{E}$	Electrochemical potential	V
E	Expectancy	
f	Friction factor	—
$f[\ ]$	Objective function(s)	
G	Gibbs free energy	J
g	Mass-specific Gibbs free energy	J/kg

$\boldsymbol{g}[\ \ ]$	Inequality constraints (functions)	
H	Height	mm
h	Mass-specific enthalpy	J/kg
h	Heat transfer coefficient	W/(m²·K)
h	Height (smaller)	mm
$\boldsymbol{h}[\ \ ]$	Equality constraints (functions)	
I	Electrical current (magnitude)	A
I_n	Identity matrix of dimension n	—
j	Current density (electrical)	A/m²
L	Length	M
m	Mass	kg
$\dot{m}$	Mass flow rate	kg/s
$\widetilde{m}_i$	Molar mass (or $\mathcal{M}$)	kg/kmol
$\mathcal{N}_{\dots}$	Number of …	—
N	Mole (quantity of)	kmol
$\dot{N}$	Molar flow rate	kmol/s
n	Number in enumeration (e.g., iterations, samples)	—
$\wp$	Probability	—
P	Perimeter	m
p	Pressure	Pa
Q	Heat	J
R	Resistance (electrical, ionic, hydraulic)	
S	Entropy	J/K
T	Temperature	K
t	Time	s
t	t-Student parameter	—
U	Bulk velocity (magnitude)	m/s
U	Difference of electrical potential / voltage	V
$[u, v, w]$	Velocity components along Cartesian coordinates	m/s
V	Volume	m³
$\dot{V}$	Volumetric flow rate	m³/s
W	Width	
w	Width (smaller)	
$\boldsymbol{x}$	General input vector (e.g., decision variable)	
$[x, y, z]$	Cartesian coordinates A standard referential is defined in figure 10.1, p. 310.	m
$[X, Y, Z]$	General random variables	

Greek letters

α	1 − Level of confidence	—
α	Thermal diffusivity	m²/s
β	Level of confidence: $\beta = 1 - \alpha$	—
β	Volumetric thermal expansion coefficient	1/K
Γ	RMSD flow uniformity	—
γ	"Worst" flow uniformity (min/mean)	—
$\Delta\ldots$	Difference (operator)	
$\delta\ldots$	Relative deviation of a quantity with respect to the reference	—
ε	Emissivity	—
ϵ	Residue	
η	Efficiency	—
η	Overpotential (loss)	V
$\boldsymbol{\theta}$ ϑ	Parameters (set)	
κ	Thermal conductivity	W/(m·K)
κ	Permeability	m²
λ	***Air-excess ratio***	—
μ	Dynamic (molecular) viscosity	kg/(m·s)
ν	Kinematic viscosity	m²/s
$\prod[\quad]$	Product of	
ρ	Density (volumetric mass)	kg/m³
ϱ_l	Coefficient of linear correlation	—
$\sum[\quad]$	Sum of	
σ	Electrical conductivity	S/cm
σ	Ionic conductivity	S/cm
τ	Tortuosity	—
Υ	Fuel utilization (or u_f)	—
Φ	Potential (voltage)	V
ψ	Porosity	—
ω	Set of uncertain variable	
Ω	Domain	

"Computers are capable of delivering wrong answers
to high degrees of precision if care is not exercised."
Rob Best, CAPE Subject Group
The Use of Computers by Chemical Engineers

CHAPTER 1

Introduction

Several levels of goals, of challenges, of trade-offs, and of choices.

The context, motivation, and objectives of this research are introduced going from the general situation to the particular problem. More details and references to the literature are progressively given to justify why the research topic is relevant and why the approach chosen to address it is original. A more extensive literature review is done in Chapter 2.

Words or phrases in ***bold italics*** are defined in the *Glossary & index*, p. 309.

1.2 Overview of the thesis

This section gives a brief overview of the context, motivations, objectives, and means of this thesis. More extensive developments are given afterwards.

1. Context

Fuel cells allow an efficient conversion of hydrogen and hydrocarbon fuels into electricity and heat. This quality should help preserve our environment.

2. Motivations

Fuel cells have lots of advantages, making them a promising technology for the conversion of energy. Despite this, they are not yet a fully viable alternative to legacy technologies. Apart from reducing the ***production cost*** of fuel cell stacks, enhancing both their long-term ***reliability*** and their ***durability of performance*** count among the major challenges to achieve their large-scale commercialization.

The thesis is that these issues can be tackled together (at least partially) by accounting for ***uncertainties*** during the design of the product. A methodology and tools are needed to manage this task in a reasonable time.

3. Objectives

The proposed research will focus on finding scientific solutions addressing the main challenges together, i.e., *durability of performance*, *reliability*, and *cost*[1] of the fuel cell stacks. More specifically, the purpose is to design robust fuel cell stacks by managing the uncertainties that otherwise create obstacles to their large-scale commercialization. To be able to achieve this, a first goal is to develop a careful methodology and associated numerical tools.

4. Means

Investigations are conducted towards the above objectives by developing and applying computer simulations and algorithms, such as computational fluid dynamics (CFD) and surrogate modelling, uncertainty quantification (UQ) via Monte Carlo simulations (MCS) improved with advanced sampling techniques and variance reduction techniques, and optimization under uncertainty (OUU).

1.3 Context and motivations

1.3.1 Living with our environment – ultimate motive

We, human beings, put a lot of pressure on "our" environment through our activities and quest of ever increasing "comfort" — i.e., consumption of goods and services. This consumption impacts the availability of limited raw resources, whether for the production of goods or of (energy) services. Besides, the processes of transformation of raw resources are almost always accompanied by the generation of some emissions in the form of pollutants and/or of so-called green-house-gases. The later, such as carbon dioxide (CO_2) and methane (CH_4), are in part responsible for the climate changes, through the increase of the average temperature of the Globe. Besides, consequences for health are also alarming in large urban areas where pollution is concentrated. These

[1] Although indirectly: we did not perform ourselves a cost analysis or implement a cost model. We rely on empirical evidence of the relationship between cost and, e.g., tolerances or amount of material provided by our industrial partner and many studies.

topics take more importance year after year in the political, economic, and social circles, as reflected by the media. The *United nations conference on climate change* (COP21/CMP11) is precisely taking place when writing these lines.

It is therefore desirable to reduce: 1) consumption of raw resources, and 2) emissions of green-house-gases and of pollutants in the production of goods and services.

Fortunately, pursuing the first goal is usually favourable to the second one. We shall note that the first and most effective measure is to reduce the production (consumption) of goods and services. However, this is not a topic for which scientific research and technical innovations are of great help; this matter is rather cultural, social, political, and economic.

Need for more efficient and cleaner technologies

Another mean to pursue both of these goals is to create and use more efficient technologies. Here, efficient should be understood as a measure including the resources consumed by the technological product during its entire lifetime: design, production, operation, and recycling or disposal.

The emissions of green-house-gases and/or of pollutants can be further reduced by employing *cleaner* technologies, i.e., which produce less of such emissions irrespective of their efficiency. Again, the measure should encompass the entire lifetime of the technology.

1.3.2 Fuel cells as a technological solution

The technology to which this thesis applies — fuel cells — addresses the problem from the perspective of the *efficient conversion of resources into energy services*. Our modern societies use two forms of energy in large quantities: electricity and heat. Many researches show that fuel cells are good candidates as a technology for the efficient conversion of hydrogen and hydrocarbon fuels into electricity and heat [2–7]. Indeed, fuel cells are promising devices able to *convert the chemical energy contained in a fuel directly into electrical (and thermal) energy*, without the intermediate of a thermodynamic cycle. This leads to a higher energy-conversion efficiency than with intermediate processes: the energy service extracted from a given amount of fuel as input is higher. As a consequence, the emissions of CO_2 are also proportionally reduced. Besides, *at the condition that hydrogen is produced cleanly*, the emissions are only water vapour when using hydrogen as a fuel.

More generally, advantages of fuel cells are:

- No combustion:
  - More efficient;
  - No emissions of pollutants such as NO_x;
  - Quiet, low noise;
- No movement of solid parts:
  - Less noise, less complex, less wear, and more reliable (from this viewpoint);
- High efficiency even at partial load;
- Modularity, from watts to megawatts;
- Fuel flexibility (for high-temperature fuel cells).

Moreover, the application-range of fuel cells is large. Depending on the type of fuel cells, they are suitable for distributed generation, residential and industrial cogeneration, and mobile applications (e.g., transport).

A technological background to SOFC and PEFC is given in § 1.6, p. 19.

1.3.3 Obstacles to the widespread use of fuel cells

Considering all their advantages, one may ask "why a large-scale commercialization of fuel cells has not yet happened?"

They have been studied and developed intensely the last three decades. Despite this theoretical and experimental background, and although remarkable progress is being achieved, the technology is only starting to become fully *marketable and economically viable* (i.e., competitive without subsidy [8]).

Several reasons exist to explain it. Of course non-techno-economic reasons exist, which may be overlooked, such as political, social, and cultural matters, as well as the all-too-common inertia to adopt a new[2] technology. But the main reason is probably that — despite recent improvements — their ***total cost of ownership*** (without consideration of externalities) is still too high to be attractive as a competitive alternative to "legacy" technologies, such as power plants relying on combustion of fossil fuels or on nuclear fission.

[2] Fuel cells are not a novel invention, though: the first descriptions of the principle were given in 1839 by William Groove and Christian F. Schönbein; they were used as auxiliary power units in the Gemini and Apollo space missions [9]. However, it is only for around three decades that they have been developed in view of becoming a common alternative to other legacy technologies.

Whereas excellent and reproducible performance was proven (e.g., DC efficiency of 70 % with DIR at the LENI), the remaining obstacles for succeeding in a broad deployment are hence ***durability of performance*** (e.g., target less than 0.2 % degradation of performance per thousands of hours), ***reliability*** (e.g., no cell cracking), and power-specific **cost of production** (e.g., 500 $/kW).

Fuel cells are still expensive to manufacture, and whereas they are efficient, they are not yet for long enough (at a useful operating power) to compensate for the investment.

Along with performance, this thesis proposes to address the issues of lifetime and of cost. However, the originality of this research lies in that these challenges are addressed indirectly, but all together, through the prism of the *management of uncertainties* during the design of fuel cell stacks. More details about the relationships between lifetime, cost, and uncertainties, are given in the next sections.

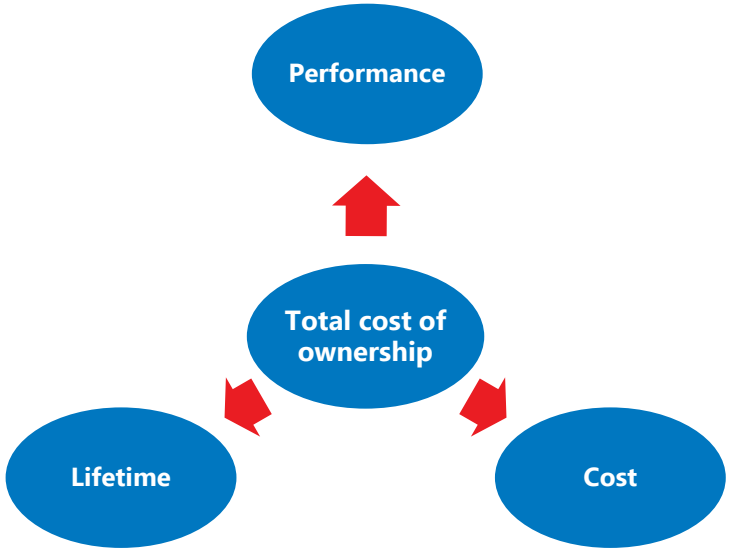

Figure 1.1 Total cost of ownership of a product is a function of its performance (efficiency), its lifetime, and its cost.

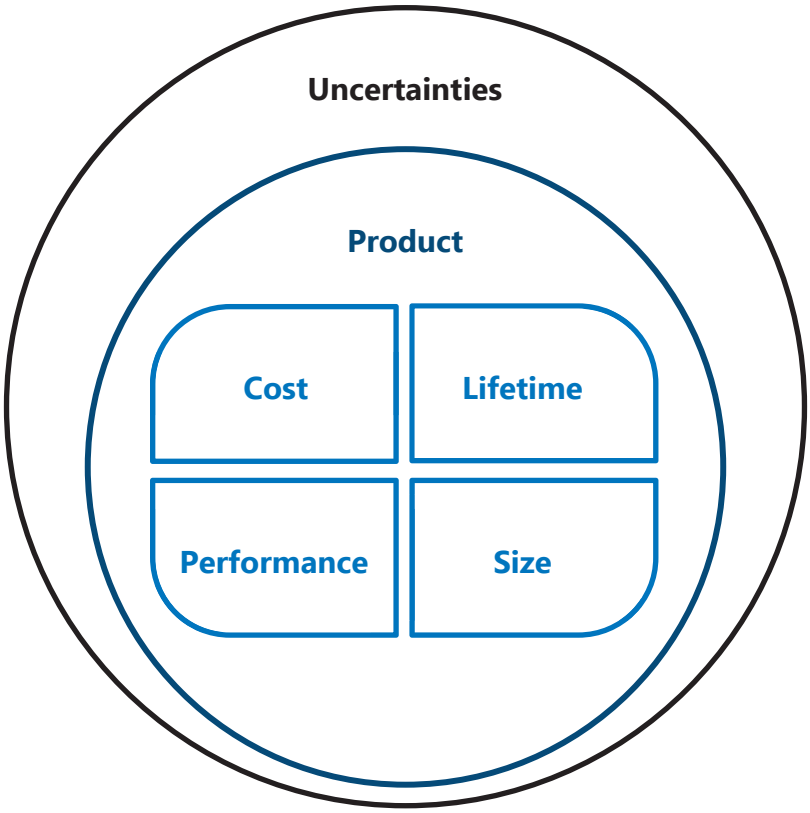

Figure 1.2 Illustrations of key aspects of a product, with uncertainties interfering in all of them.

1.3.4 General factors affecting total cost of ownership

Why is the lifetime of fuel cells too short, and why are they too expensive?
First, it should be noted that these gaps are only true compared with the current alternative technologies (with their infrastructure, and the price of their corresponding raw resources). Then, it is also crucial to keep in mind that lifetime and cost are linked, at the minimum from a purchaser's point of view: for a same service (performance density), potential customers would accept to buy at a high cost if lifetime is correspondingly worth the investment (and vice-versa). As a consequence, the two main objectives are to minimize the production cost and to maximize the lifetime of fuel cells, while keeping or improving their already good performance. These objectives are usually conflicting.

1. Performance

Ways to increase the output power of a fuel cell stack are:

(a) Increase the number of cells.

(b) Increase the amount of fuel injected in each cell.

(c) Increase the electric current drawn per amount of fuel injected.

(d) Increase the (average) output voltage of the single cells.

It should be noted that these actions are actually not independent, and have limits. In particular, c) and d) are linked through the current-voltage (IV) characteristic of the fuel cell.

Electrical efficiency is increased when (c) or (d) is achieved with a magnitude bigger than the reduction of the other. The system efficiency also depends on the energy lost in the balance-of-plant components. This loss mainly arises from the drop of pressure across the system, which must be compensated by a compressor with an imperfect efficiency.

2. Size

The size of the system is often wished *as small as possible* for a given performance (high power density). This is especially true for (small-size) mobile applications, such as cars, buses, small boats, and all smaller mobile devices. Although in a lesser extent, it is also true for stationary applications, such as residential cogeneration.

Reducing the size can have a positive effect on cost (e.g., because less material is used), but not necessarily: it needs tighter integration, miniaturisation, and management of issues arising from them. Furthermore, miniaturisation can have a detrimental effect on performance and on lifetime (see e.g. Chapter 9); and thereby, on total cost of ownership.

3. Lifetime

The ***lifetime*** of the product depends on its ***reliability***, on its ***durability of performance***, and on the *minimum performance guaranteed* by the manufacturer.

For a given designed fuel cell, using it at a higher performance most often means stressing (wearing) it more, so that a failure becomes more probable (reliability-issues), and the rate of (permanent) ***degradation of performance*** increases (durability-issues). As mentioned, miniaturisation (i.e., increasing performance density) can also put limit on lifetime.

Last but not least, lifetime also depends on the quality of the product, in terms of the quality of manufacturing parts, of assembly of them, of the chosen materials, etc. Besides, there usually is a significant relationship between these qualitative aspects and the cost of production.

4. Cost of production

Trying to *reduce costs* puts pressure on the choice of material and of manufacturing processes, on the quality of assembly, on the control of quality / accepted quality (yield), and thereby on the intrinsic quality of the design. However, it does not mean that it is impossible to reduce these costs, while keeping or even increasing lifetime. This is where optimization, or continuous improvement, can help, especially if an integrative approach is used.

Of course, fuel cells being a relatively new technology, ***production costs*** can hopefully be reduced by mass-production (economy of scale). Until recently though, it seems that this aspect was deemed insufficient or judged too risky by lots of investors, so that fuel cell companies had to rely largely on subsidies. Other levers are to reduce the need of *raw materials* (or replace expensive ones by cheaper ones) and of expensive *manufacturing- and assembly-processes*. These depend on the *design* of the product, among which geometrical and material aspects play an important role. As mentioned, design is also crucial for performance and lifetime. However, the ***quality*** *of the production*, i.e. the ***accuracy*** with which the product is manufactured, also affects the production cost, the performance, and the lifetime. The goal is hence to find a trade-off, which allows to reduce the total cost of ownership.

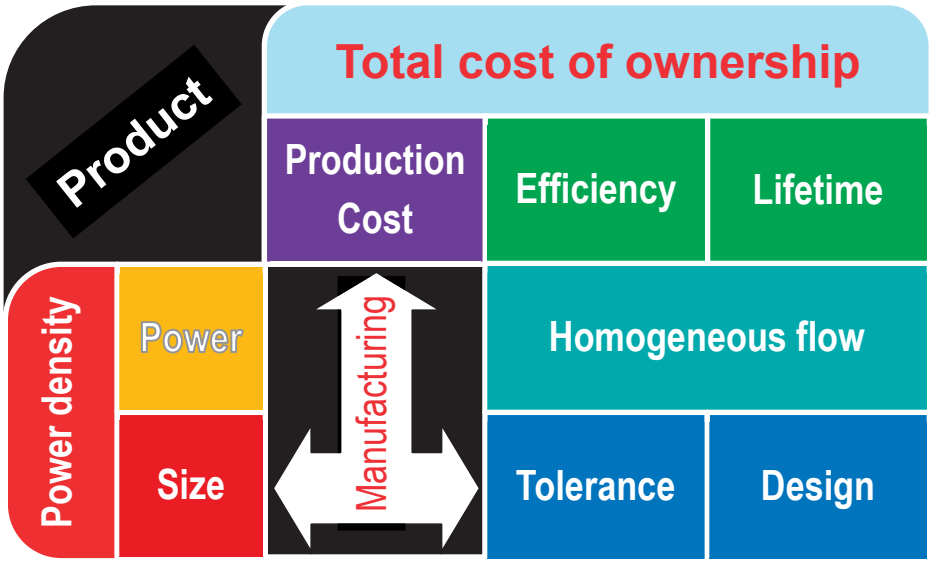

Figure 1.3 Total cost of ownership of a fuel cell, with factors related to design and manufacturing.

As an example, a strong relationship exists between performance and cost for PEFC, because the catalyst responsible in large part for performance is particularly expensive (the catalyst is usually platinum).

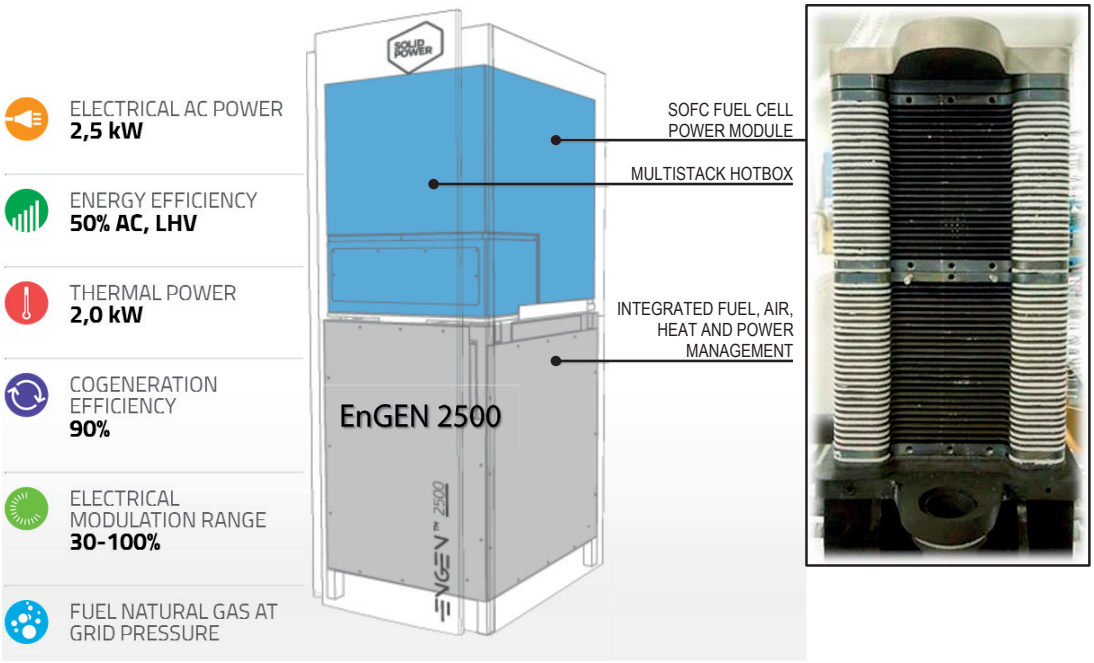

Figure 1.4 SOFC system "EnGEN 2500" commercialized by SOLIDpower.

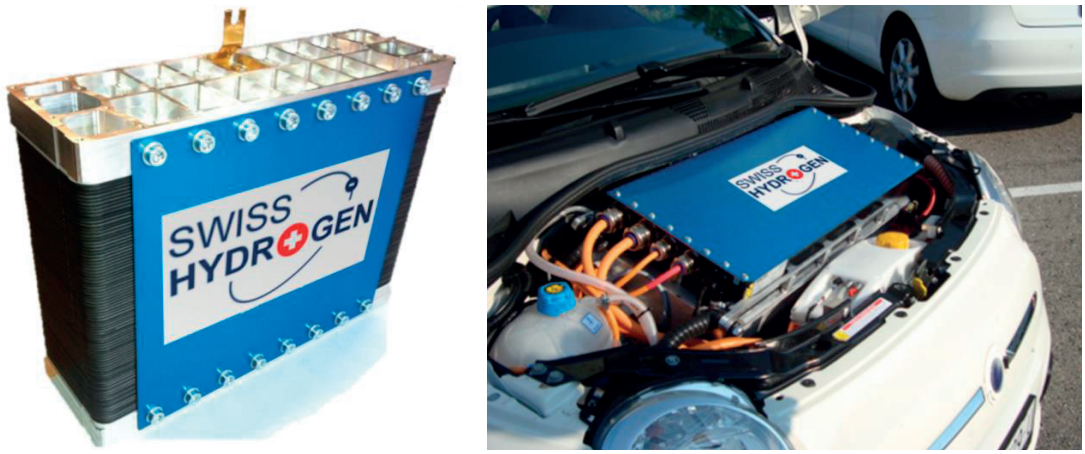

Figure 1.5 Fuel cell stack (left) and fuel cell system installed in the electric Fiat 500 (right) developed by SwissHydrogen [10].

Figure 1.6 illustrates the typical trade-off that exists between cost of production and cost of failure. Cost of failure is the cost of replacing or repairing a product under warranty; it may also include indirect cost of losing customers. In this example, the cost of a failure increases faster than linearly. Conversely, the cost of production tends to increase exponentially (asymptotically) when targeting zero failure. It however does not tend to zero when failure is certain. It should be noted that these curves correspond to optima (Pareto points). In other words, there exist cases where cost of production and cost of failure are higher for the same probability of failure. Remark: the cost due to an imperfect yield (products which do not pass the qualification) can be regarded either as a cost of production or as a cost of failure.

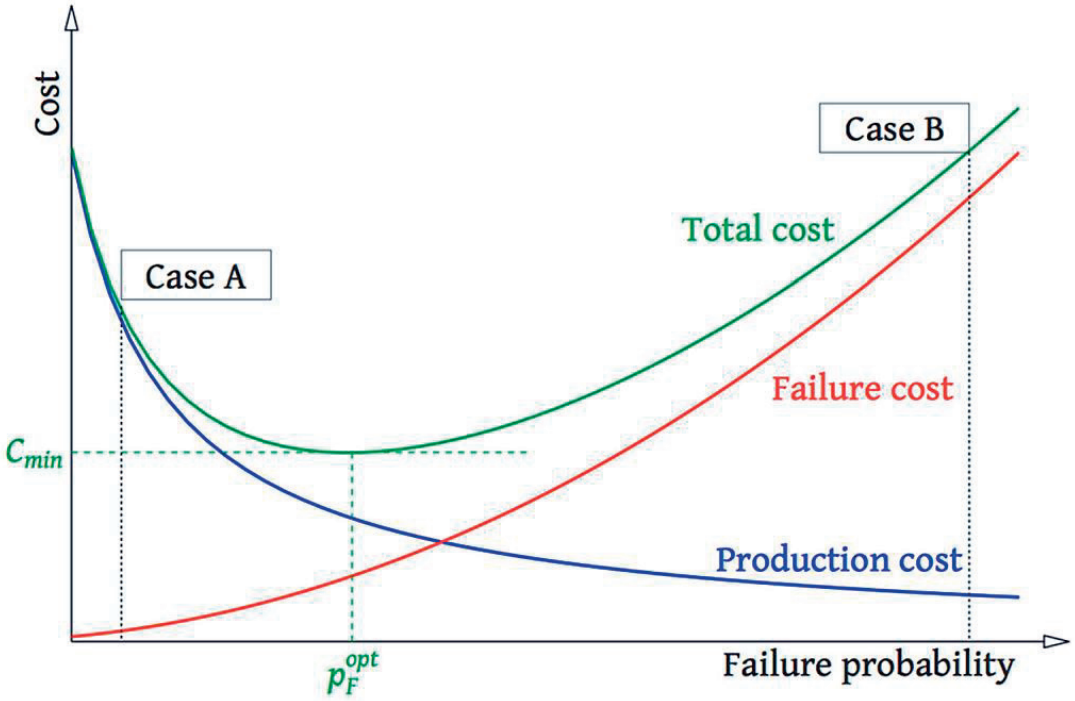

Figure 1.6 Cost factors governing the design and cost-optimal reliability level (failure probability). Reproduced from the "description of work" of the project PROSOFC[3] [11].

1.3.5 Technical factors limiting the performance, its durability, and/or reliability

Several factors were reported to be responsible for limiting the performance and reliability of SOFCS, such as electrode degradations by poisoning, formation of an insulating layer (cathode), re-oxidation (anode), ageing processes (grain growth, inter-diffusion of species, change in microstructure), thermo-mechanical stresses, thermal losses which activate/accelerate degradation (e.g., Joule losses), issues with the gas distribution, or with the sealing of the elements, etc. [12–17]. One other source of limitations are uncertainties / variabilities, which by the way can be the cause of some of the aforementioned issues.

[3] Production and reliability oriented SOFC cell and stack design.

1. Manufacturing costs and tolerances

Economic competitiveness must be taken into account. The constant need to reduce costs puts restrictions on the choices of a suitable FDP geometry, appropriate manufacturing processes, and their corresponding tolerances — leading to compromises. This adds a new level to modelling and to design, because, while performance and reliability issues are closely related to the distribution of the gaseous flows within the FDP, the flow distribution itself may be strongly influenced by geometrical inaccuracies, and hence by dimensional tolerances. Indeed, in practice, the manufacturing tolerances and the accuracy of assembly are known to have a large impact on the quality of the flow distribution, as illustrated by Huang et al. [18]. In their study, they showed experimentally and with numerical simulations that "an improvement of the flow uniformity in interconnects can effectively remove local hot spots on the positive electrode-electrolyte-negative electrode (PEN) and increase the peak power density of the single-cell stack at least up to 11 %".

Moreover, not only the performance and reliability of a single cell are affected by the flow distribution, but also the quality of the whole stack depends on a homogeneous distribution within *and among* repeat elements [19]. Consequently, the dispersion of repeat elements' quality among the stack is also of major importance.

However, so far and to the best of our knowledge, previous studies in literature do not account for inaccuracies of production and their influences on performance and reliability from the viewpoint of flow distribution. In particular, numerical simulations are commonly carried out with the designed geometries, free from any flaws or defects. Similarly, analytical models generally deal with simplified geometries. Liu et al. [20] already used MCS with a finite element analysis model to study the effect of dimensional error, but their work on PEFC was focused on the mechanical pressure-distribution that influences contact-resistance.

2. Role of design by virtual prototyping

Computer-aided-design tools are acknowledged to be an effective means to reduce the cost of R&D: it avoids the production of many intermediate prototypes and of the experimental benches to test them. Basically, virtual (computerized) prototypes and experiments is a complement to physical ones.

Reducing cost of R&D is useful to reduce the total cost of ownership, especially for a technology which is not yet mainstream (mass-produced). However, when it comes to uncertainties, some drawbacks of physical experiments are transposed to numerical models, since they are usually built and calibrated based on them. When care is not

taken, the advantages of computer design can then become drawbacks (e.g., a common numerical computation, being essentially deterministic, avoids or "hides" uncertainties, but the fact that these do exist in the real-world should not be forgotten).

Observations (general in engineering):

- Numerical modelling is increasingly used for the accelerated development of products.
- Numerical optimization is increasingly used to push the limits of performance, cost, quality, … of a product. And find better trade-offs, e.g. about those in figure 1.6.

This leads to an issue, because ***deterministic optimization*** usually ***activates*** some ***constraints*** of the optimization problem. As soon as stochastic processes (i.e., reality) enter into play, these constraints are violated and the product will either fail or wear quicker. Besides, people tend to have excessive confidence in computer models. The problem is not that they are less valuable than experiments, but that their results can "look so much like" those of an experiment[4]. Besides, models have their root in some experiments (observations of the real-world) — from values of coefficients to the form of relationships between physical quantities. This "translation" is however not free from uncertainties.
Moreover, to satisfy a budget, in terms of available computer resources and time constraints, the complexity of a model often has to be reduced; especially when the model is used in a process involving many evaluations (such as sensitivity analyses, uncertainty quantifications, or optimizations). These simplifications further reduce the ***accuracy*** of the models.

1.3.6 Accuracy versus tractability

One of the challenges of our research was to deal with two conflicting needs:

- Computations need to be accurate enough, such that the effect of the uncertainty that we are interested in are not drawn into uncertainties (errors) due to the computing accuracy (models of physical phenomena, but also techniques to estimate the statistics of interest, for instance; number of samples, etc.)
- Computations must remain tractable (computer resources and time).

[4] For instance, a model may give an answer which looks reasonable, but for which conditions an experiment would have failed with clear signs (e.g., overheat), whereas the simulator omits such signs.

Hence, compromises are also needed here, as well as a methodology which allows to maximize the valuable information one can get in a given time-span. Also, it is necessary to be able to quantify (estimate) what is the degree of accuracy of the resulting statistics.

Remark

We want to consider uncertainties / variability errors / lack of information / complexity in the data (information) that are used to take decisions about design.
Computer models help in the design process (analysis and synthesis). Even when these models are thoroughly verified, validated, and calibrated with experimental measurements, they remain imperfect to predict a "large spectrum of reality" when used deterministically.
To account for uncertainties, it is desirable to consider the related variables with stochastic rather than deterministic inputs to the model. We should make clear that the goal of this thesis is not to make the *model* more robust, nor is it really to quantify the sensitivity of the *model*'s responses to uncertainties; ultimately, it is rather the *real product* which we want to make robust.
So, the stochastic model should be — *ideally*[5] — an accurate representation of the real (stochastic) product. Actually, it is necessary and sufficient that the model allows to take decisions for the design of the real product such that it satisfies some criteria.
Accounting for uncertainty allows: 1) to model reality more closely (more accurately), since ***aleatory uncertainties*** are present in reality; and 2) to account for the remaining lack of agreement of the model with reality, whether this disagreement is due to a lack of knowledge or a decision taken to reach a compromise (i.e., ***epistemic uncertainties***).

[5] Ideally, because it is probably impossible.

1.4 Objectives of this thesis

The objectives of this thesis articulate around technological and methodological goals.

1.4.1 Towards large-scale commercialization of fuel cells

Enhancing both long-term reliability and durability of performance of fuel cell stacks counts among the major challenges to achieve their commercialization. In fine and regarding the big picture, the aim of the thesis is hence to *investigate solutions* to:

- *Maximize the quality* of the system, measured in terms of:
  - *performance* (at least maintain), composed mainly of:

    (i) efficiency

    (ii) and power density;
  - *lifetime,* which can be decomposed in:

    (i) *durability* of performance,

    (ii) and *reliability*.
- *Minimize costs*[6], without severely compromising the quality of components and thereby of the device itself (see also figure 1.6).

A possible approach to formulate this problem would be to minimize the total cost of ownership. However, it would need, ideally, to solve an integral over time, with decision variables pertaining to design and to operation, with known cost functions for the materials, the manufacturing processes, the fuel, the rate of interests, and with many other variables related to industrial mass-production and distribution. Besides, large conjectural fluctuations and uncertainties of various nature should be implemented on top of that. While interesting and topical with the subject of uncertainties, it would clearly go beyond the scope of this thesis, where much has yet to be done to deal with uncertainty on the design of flow distribution and patterns, and the dilemma of getting tractable *and* accurate simulations.

Before going further, we must highlight that only indirect indicators of lifetime and cost will be used, for similar reasons as just stated.

[6] Manufacturing costs are especially targeted, although other production costs may also be reduced: e.g., costs related to assembly, quality control, yield, or balance-of-plant.

1.4.2 Technological goals

To pursue the main aim stated above, we chose to focus on the design of the fluid distribution pattern responsible for a homogeneous distribution of the fields of the physical variables, notably the flow fields. The goals are then:

- To characterize the design uncertainties[7] (inputs of the model), especially those regarding the geometry of the fluid distribution patterns.
- To quantify the uncertainties of the outputs by propagating the former.
- To use design optimization under uncertainty as a tool to better understand the trade-offs and the relationship between dimensions, tolerances, and topologies.
- To suggest measures of improvements and of quality control.

1.4.3 Methodological goals

The objective of this research is to develop and implement a methodology for the design and optimization of fuel cell stacks under uncertainty.

Optimization under uncertainty (OUU) is particularly challenging in terms of computational efforts, especially with numerical models involving CFD or similar simulation means. Hence, efficient implementations of OUU for such engineering problems are needed and paramount. In addition to a well-defined methodology for performing OUU of fuel cells, some outcomes of the study are guidelines for future designs, as well as quantification and characterization of input and output uncertainties.

The methodological approach is generic to many other multi-disciplinary design engineering problems where complex nonlinear coupled phenomena are involved and interact with stochastic processes. Thanks to this generality, both the know-how and the implemented tools can be transposed to different fuel cell technologies, or different fluid flow technologies having similar topology (heat exchangers, lab-on-a-chip, etc.).

[7] We do not mean the uncertainty prior to the decision about which design choices are better; but uncertainty which still exists after that decision, about the physical variables associated to design, such as dimensions, shapes, composition of materials, ….

1.4.4 Scope of the thesis' goals

Reasons for the limitation of scope are given in the body of the thesis.

This thesis deals with the *design* of *planar fuel cells*. The category of fuel cells considered are *solid oxide fuel cells* and *polymer-electrolyte fuel cells*. The focus is put on *accounting for uncertainty* during the design procedure: using *uncertainty quantification* and *optimization under uncertainty*. The main uncertainties considered are *geometrical tolerances*, which are ***aleatory uncertainties***. The main variables of decision for the design concern the geometry of the *fluid distribution pattern*. Regarding physical phenomena the emphasis is correspondingly put on *fluid mechanics*.

Some simplifications could not be avoided to achieve tractable computations:

Operating conditions are obviously considered, but this thesis does not deal with the control of these variables, nor on their optimization, whether deterministic or stochastic. The focus is put on *meso- and macroscopic phenomena* (not on nano- or micro-structural aspects of the materials, or of diffusion into porous media, or of the details of electrochemical reactions). The focus is on the "averaged" behaviour of the fuel cells, so that we study the *steady state*. If no steady state can be achieved during the real operation, we assume that, *in average*, the behaviour of the fuel cell is well represented by a steady state mathematical model[8].

Without being able to cover every aspect in fuel cell technology in a single research (in particular, issues about the microstructure of materials are not dealt with in detail here), this study will focus on a scientifically challenging subject — namely *managing uncertainty* —that is relevant towards achieving the stated finality.

1.5 Original contributions

The novelty of the planned research is the consideration of uncertainties, particularly geometrical uncertainties, to find robust optimal solutions, i.e., solutions which are optimal considering uncertainties. Basically, this means that one additional objective is considered: robustness.

To the best of our knowledge, we are the first to carry out such a research about application of optimization under uncertainty of the design of fuel cell stacks with geometry

[8] Our reasoning is similar to the use of Reynolds-averaged Navier-Stokes (RANS) equations for modelling turbulent flows, which are time-averaged and can be used in steady state. The model should capture and resolve the average (steady state) behaviour.

at the centre of the OUU: geometry appears as decision variables, uncertain variables, constraints and/or objectives.

The contribution of this work can be divided in terms of methodology and applications (in the form of guidelines and solutions to industrial design).

Fuel cells are intrinsically a technology which requires several disciplines to function. Here, we brought along yet other topics to study and develop these devices. The innovation mostly lies at the intersection of the corresponding scientific fields. Most of the efforts were deployed to find ways to tie links between the fields' techniques, to take advantage of the powerful tools offered by some to build on others: e.g., to include UQ in design optimization, apply OUU to CFD, build or calibrate surrogate models thanks to DACE[9] or optimization, etc. Of course, to achieve that, it was also necessary to gather enough knowledge of each field, but it was not possible to *master* any of them without risking to hinder and slow down the construction of these bridges.

Figure 1.7 shows the various fields of knowledge and their relationships as used in the frame of this thesis.

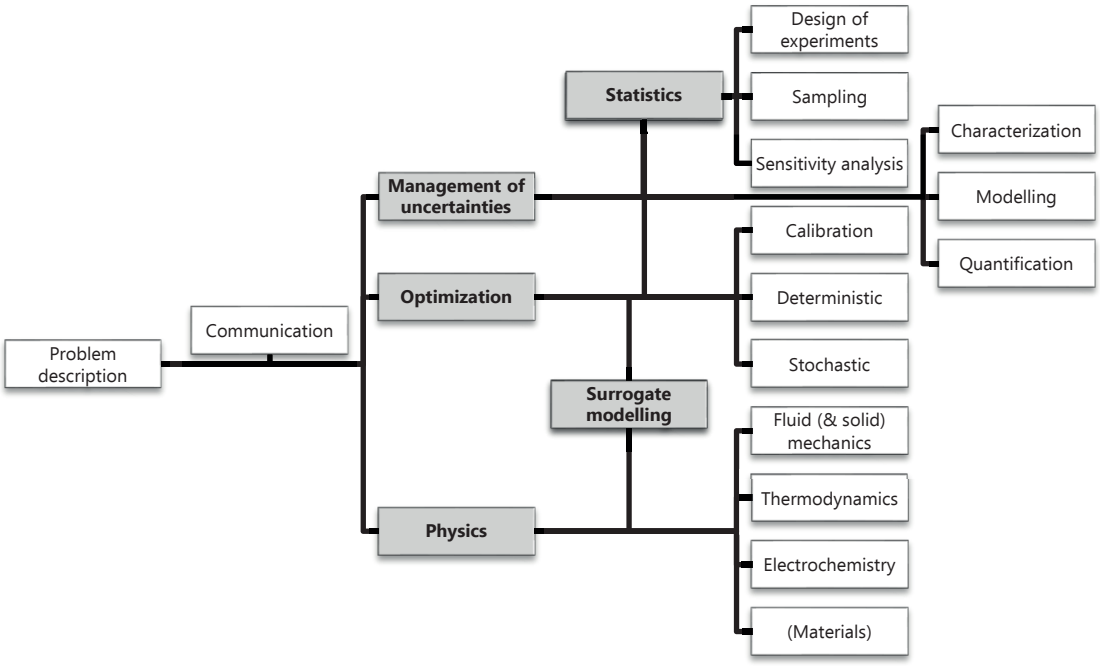

Figure 1.7 Scheme showing the various fields of knowledge and their relationships as used in the frame of this thesis.

[9] Design and analysis of computer experiments.

1.6 Technological background

This section gives a brief technical description of the functioning of fuel cells, more specifically SOFC and PEFC. The modelling aspects and physical phenomena are further described in 87Chapter 4, with § 4.3.2 dedicated to *Electrochemistry*, p. 94.

1.6.1 Working principle of fuel cells

From an electrochemical point of view, fuel cells are similar to traditional batteries: chemical energy contained in reactants is directly converted into electricity through electrochemical reactions (oxidation-reduction). Fuel cells differ mainly by a continuous supply of fuel and oxidizer (usually air).

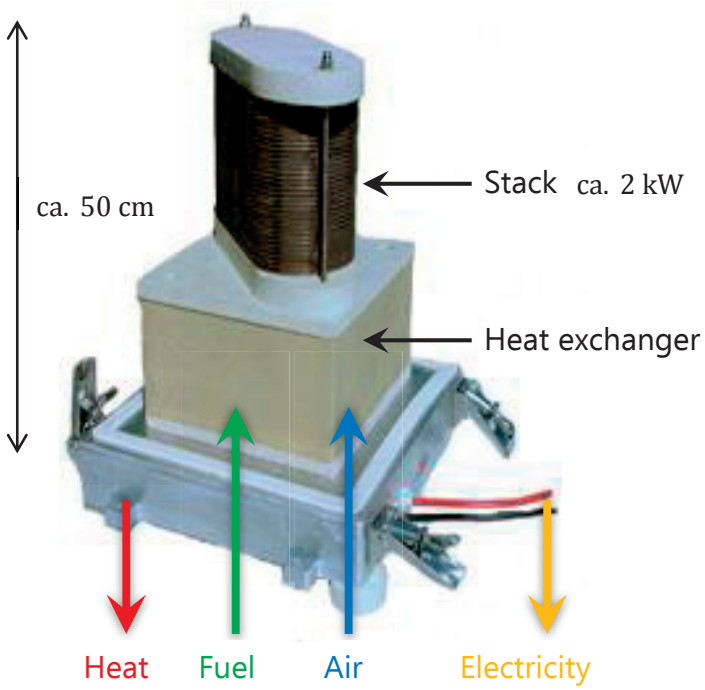

Figure 1.8 Inside view of a so-called "hotbox" showing the fuel cell stack on top of the heat exchanger.

A fuel cell is basically composed of an electrolyte separating a cathodic and an anodic compartment. The *anode* and *cathode* (electrodes) surround the *electrolyte* (membrane). Together, these three layers form the membrane-electrodes assembly (MEA). The MEA is surrounded by an interconnector on each side. The anode is continuously supplied with fuel, and the cathode with oxidizer. The fuel and oxidizer are isolated to avoid combustion.

The principle is to allow the electrochemical reaction of the fuel with the oxidizer, but in such a way that the electrons exchanged in the reaction must flow through a different path than the ion. The flow of electrons through this external electrical circuit generates an electrical current. This flow is made possible by the redox potential difference that is created between the electrodes.

To simplify the presentation, we present here the case where the fuel is hydrogen.

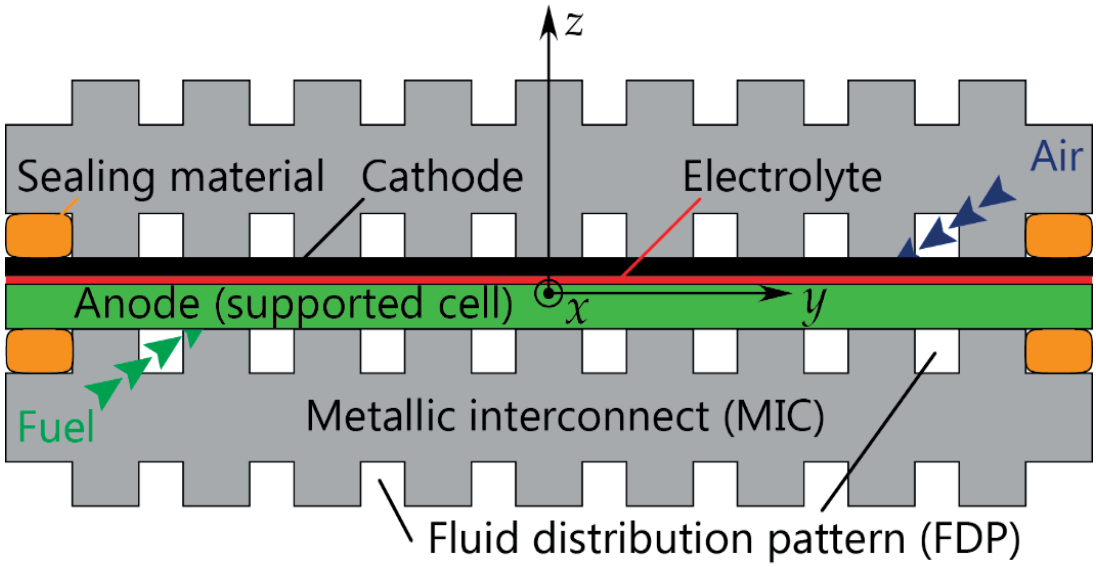

Figure 1.9 Schematization of a repeat element for a planar SOFC.

1. Anode

- Dissociation of hydrogen:

$$H_2 \rightarrow 2\,H^+ + 2\,e^- \tag{1.1}$$

2. Electrolyte

The electrolyte must be a good ionic conductor (for either anion or cation), but must be gas-tight and an electronic insulator.

3. Cathode

- Dissociation of oxygen:

$$\tfrac{1}{2}\,O_2 + 2\,e^- \rightarrow O^{2-} \tag{1.2}$$

4. MEA: anode-electrolyte-cathode

Fuel and oxidizer are separated by the gas-tight MEA.

- Oxidation of hydrogen; global reaction:

$$H_2 + \tfrac{1}{2}\,O_2 \rightarrow H_2O \tag{1.3}$$

5. Interconnectors

The interconnectors have several functions:

- Collect and conduct the electrons towards the external electrical circuit;
- Provide a suitable path to supply the electrodes with their respective reactants, and to evacuate the products;
- Provide the mechanical strength;

6. Sealing

Sealing material is needed to prevent the combustion of fuel with the oxidizer, and to prevent leakages to/from the ambient air (or any other fluid) surrounding the fuel cell.

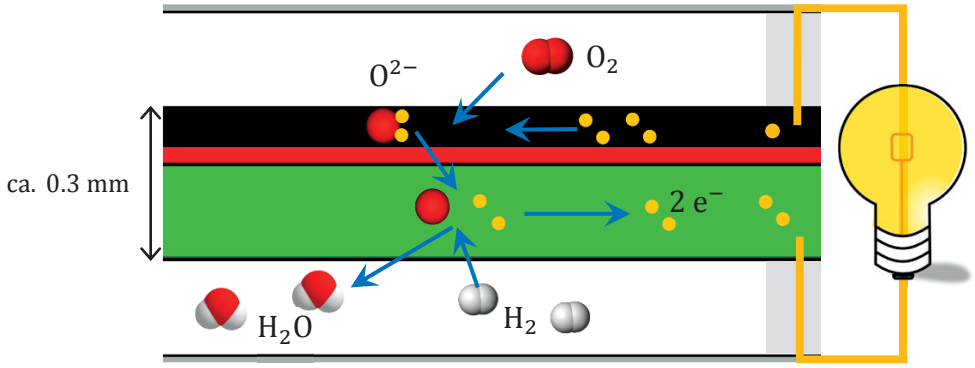

Figure 1.10 Detail of the scheme in figure 1.10. Steps of the electrochemical reaction of hydrogen with oxygen in the cell leading to the flow of electrons.

The scale up of the power is achieved by stacking several elements, which are electrically connected in series; therefore, current drawn from the stack equals that drawn

from each element, whereas the voltage of the stack equals the sum of the voltage of the elements.

There exist planar and tubular configuration of fuel cells. This thesis deals with the planar configuration, which is attractive for compactness (volumetric power density) and cost (relatively easy and cheap production). It however imposes challenging constraints (mechanical, thermal, sealing, pressure drop).

There exist many variants of MEA. For instance, the part of the cell giving most of the mechanical strength may be either the anode, the electrolyte, or the cathode. SOLIDpower, our industrial partner producing SOFC, uses anode-supported cells (ASC).

There exist many configurations for the supply of fuel and oxidant. The main "architectures" are characterized by co-flow, counter-flow, or cross-flow.

1.6.2 PEFC specifics

The electrolyte is a polymeric membrane, which conducts protons (H^+, hydrogen-ion). As a consequence, water[10] is formed at the cathode, which usually must be constantly humid to be conductive.

1. Specific advantages

- Low temperature
- High specific power
- Suitable for mobile applications (even small)

2. Specific drawbacks

- Need pure hydrogen, because it does not tolerate even small amounts of carbon monoxide in the fuel; inflexibility of the fuel.
- Cost of the catalyst (platinum)
- Usually need a coolant (extra circuit/layer)
- Water management is critical (keep electrodes and electrolyte humid, but avoid flooding at the cathode)
- Management of biphasic flows

[10] Depending on the operating conditions, the gas mixture at the cathode can be saturated with water-vapour, with minimal amount of water in liquid form.

1.6.3 SOFC specifics

The electrolyte is a solid oxide, which conducts ions of oxygen. The products are hence formed at the anode (steam, and carbon dioxide when the fuel contains carbon). This has a consequence on the molar and mass balance, and thereby on the properties of the mixture (viscosity, density) flowing in the anodic and cathodic compartments, as will be discussed later.

SOFCs mainly distinguish themselves with elevated operating temperature $(650\ ℃ \text{ to } 850\ ℃)$. SOFCs are especially appropriate for the cogeneration of electricity and heat.

The porous anodic and cathodic catalyst-layers are separated by a thin $(10\ \mu m)$ dense oxygen-ion conducting ceramic electrolyte-layer (yttria-stabilized zirconia, YSZ). Oxygen-ions at the cathode are transferred through the electrolyte to the Ni-catalyst at the anode where electrochemical reaction takes place with the fuel (e.g., H_2, CO, CH_4, higher hydrocarbons, or even alcohols). Between inlet and outlet, the gaseous fuel flows along the anode and is hence gradually converted by oxygen into the reaction-products (i.e., H_2O and CO_2).

The anode-supported-cell (ASC) configuration is employed by several research groups (us included) for the benefit of reducing the operating temperature[11] (from $1\,000\ ℃$ to $\leq 800\ ℃$), allowing better durability and lower cost. In this configuration, the mechanical strength of the cell is given by a thick anode, which is coated with a thin electrolyte.

A repeat element of a planar anode-supported SOFC is sketched in figure 1.9. Typical dimensions for such an element are $[3 \ldots 5]$ mm in z-direction and $[50 \ldots 100]$ cm^2 in xy-plane (active area of the cell).

1.6.4 Specific advantages and drawbacks of SOFCs

1. Specific advantages

- High efficiency (high temperature)
- Fuel flexibility (tolerate hydrocarbons, e.g., natural gas: internal steam reforming of methane is therefore possible.)

[11] The ionic conductivity of the electrolyte strongly depends on temperature. A thinner electrolyte allows to operate at lower temperature, while achieving similar ionic-resistive losses.

2. Specific drawbacks

- High temperature
- Cost of materials to resist high temperature and corrosive environment at those temperatures
- Heavier materials
- Chromium in stainless steel is a source of pollutants (for cathode)

1.7 Collaborations

1.7.1 Industrial partners

This work was carried out in collaboration with industrial partners. Namely, SOLIDpower S.p.a.[12] and BELENOS Clean Power Holding Ltd[13]. This work contributed to the research and development of some of their fuel cell products. They are acknowledged for the opportunity given to learn from their technology, to build from it, and to apply to it some of the ideas developed along this thesis.

Confidentiality

Due to intellectual property, we are unfortunately not allowed to describe some confidential matters, such as geometries of the real products and other proprietary information.

1.7.2 Colleagues and students

Priscilla Caliandro is warmly acknowledged for her contribution to Chapter 6, p. 167.

Special acknowledgements are due to Arata Nakajo for his review of an early version of Chapter 6 and for having provided his data and routines to compute degradation criteria (p. 244). He also contributed to this work by informing me about the existence of a MATLAB code to solve a resistive network and sharing is knowledge about it

[12] Formerly a joint company under the name HTceramix SA (Yverdon, Switzerland) and SOFCpower S.p.a (Mezzolombardo, Italy).

[13] The fuel cell activities are now developed under the name of SWISSHydrogen SA.

(p. 125). This code was graciously provided by Prof. W. K. S. Chiu from the University of Connecticut [21–23].

Kevin Rosset is acknowledged for his contribution to this work in the frame of a semester project (10 ECTS). He implemented a first version of the resistive network (p. 125) and tried it on a test case.

Pieter Dermont and Xavier Bednarek are acknowledged for their contribution to this work in the frame of their semester project (10 ECTS). They participated in the investigations to improve the agreement between a 2D and 3D flow model (p. 102).

Roberto Passini is acknowledged for his contribution to this work in the frame of his semester projects (3 × 10 ECTS). He participated in the sensitivity analysis to the attribute of the simulator, Chapter 5, p. 139. Then, he did a preliminary sensitivity analysis on the effect of constrictions in channels (in relation to § 9.3, p. 255).

First part

Search of a methodology: What are the right tools?

« Toute certitude est par essence contradictoire avec
la philosophie de la recherche. »
Pierre Joliot
La Recherche passionnément

CHAPTER 2

State of the art

This chapter presents the state of the technology and of the research. The issues approached in this thesis are given priority.

2.1 Fuel cells (PEFC, SOFC)

Considerable literature is dedicated to the study of fuel cells. Detailed **numerical models** were elaborated for theoretical *analysis:* e.g., Jeon et al. [24] implemented a 2D CFD model of anode-supported SOFCs, which accounts for transport phenomena and diffusivity using a continuum micro-scaled model based on statistical properties. Their model is able to calculate the contribution of the different overpotentials.

Numerical tools are also used extensively for the *synthesis and optimization* of designs: e.g., Bi et al. [25] employed 3D, isothermal, electrochemically inert CFD simulations with the objective of maximizing the flow uniformity among the cells in planar SOFC stacks.

Experimental works are applied for both *exploration and validation:* e.g., Lee et al. [26] showed enhanced performance and reliability with functionally graded (i.e., multi-layered) electrodes and glass-based compression-seal gaskets for a planar SOFC stack.

Still, literature is scarce on one of the major (and multifaceted) sources of problem: *uncertainties*. They are associated to the notion of potential risks (hence costs), notably up to the failure of the device.

2.1.1 Distribution of the flows: a critical factor

Each component of an SOFC stack plays an important role and has to be thought together with its interactions with other components. Several studies show that **distributing the gas as uniformly** as possible over the active area is a necessary condition to

achieve a sound product [13,18,27–29]. This is essential on one hand to get a homogeneous consumption of the fuel at the anode, and on the other, at the cathode, to supply air such as to provide adequate cooling [13,18,27–29]. If that condition is not met, increased losses and degradations are likely to occur at the anode because of concentration polarization and of the inherent risk of re-oxidation, which might lead to the breakage of the cell [13,18,27,28]. Besides, the repeat element may be subjected to thermal stresses. Hence, a good design of the component responsible for distributing the gas, namely the fluid distribution pattern (FDP), is critical. Nevertheless, to design the geometry of the FDP is challenging because not only the flow uniformity is an objective, but also adequate electrical and thermal conductivity, moderate thermo-mechanical stresses, etc., are targeted. Among the constraints, the design has to achieve the integration of sealing areas, gas manifolds, etc., as well as to deal with manufacturing aspects [13,28]. Reinert et al. [30] stressed that the actual, local fuel utilization in many cases does not equal the set, global fuel utilization defined by the electrical current and the global fuel flow rate because of possible leakages or of an inhomogeneous fuel distribution to the fuel cell stack layers. This is illustrated in figure 2.1.

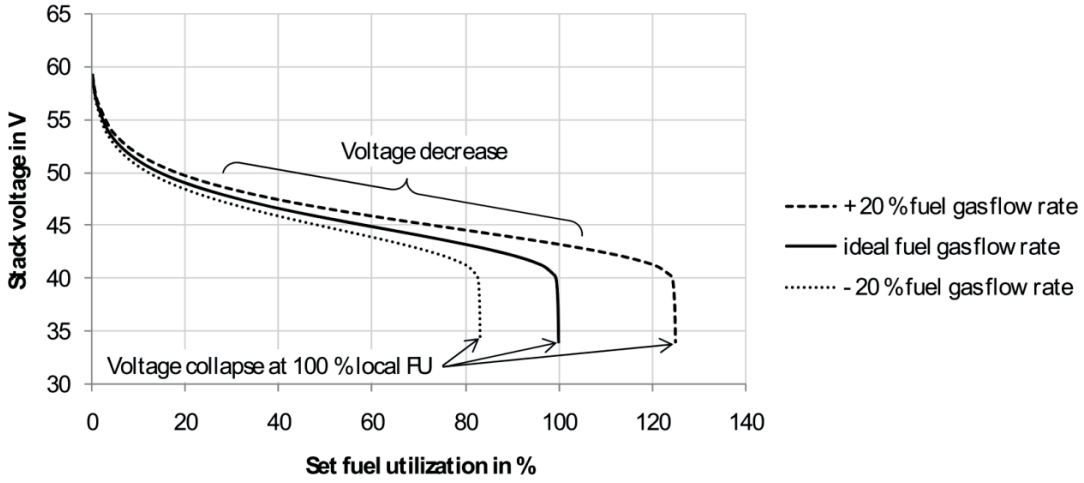

Figure 2.1 Actual, local vs. set, globally averaged fuel utilization (FU) [30]

2.1.2 Manufacturing variability (aleatory uncertainty)

So far and to the best of our knowledge, literature is scant about studies accounting for inaccuracies in production and their impacts on performance and lifetime. In particular, numerical simulations are commonly carried out with the designed geometries, without any flaws or defects. Similarly, rather extreme simplifications of the geometries are commonly used in analytical models, assuming, rightfully or not, that their

effect is negligible. Yet, ample evidence exists that variability can have a major incidence on the product behaviour. Indeed, manufacturing imperfections lead to greater heterogeneity of the flow field; yet, flow uniformity within fuel cells was shown to be paramount.

Rammouse et al. [31] studied the processing parameters and their influence during the manufacture of anode-supported SOFCs. A method based on standardization and systematization was described, but the distributions of processing parameters were not related to corresponding distributions of performance or reliability (only aggregate betterment). Hence, their study does not inform on the relative importance of parameters, or on their possible interactions. However, it provides quantitative evidence about some manufacturing variabilities, as shown in figure 2.2 and figure 2.3.

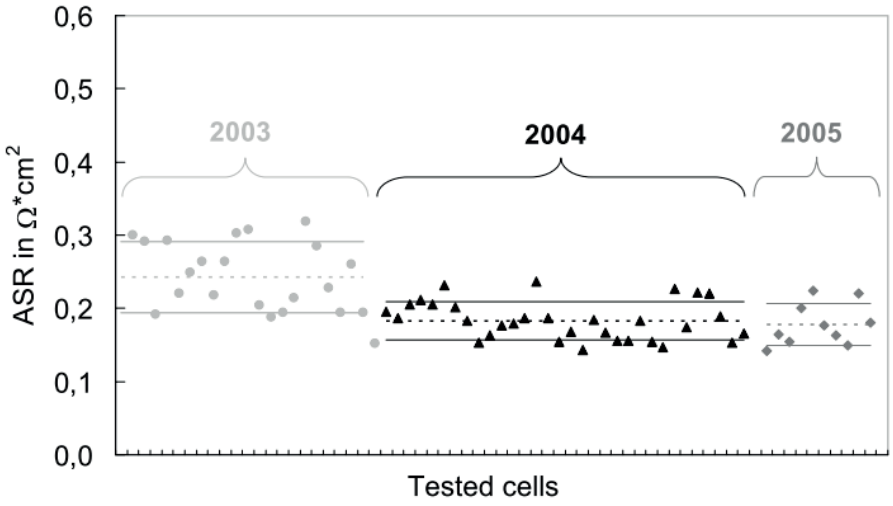

Figure 2.2 Cell electrical performances [31].

At the LENI, Wuillemin et al. [13] modelled and studied the influence of imperfect sealing in an SOFC, which may lead to detrimental consequences. Comparison with post-experiment analyses showed that the developed CFD model predicts accurately the location of parasitic combustion and the existence of redox cycles during polarization. The results show that a detailed modelling approach including the imperfections of the system is a powerful tool for a better understanding of degradation and for the design of more reliable products.

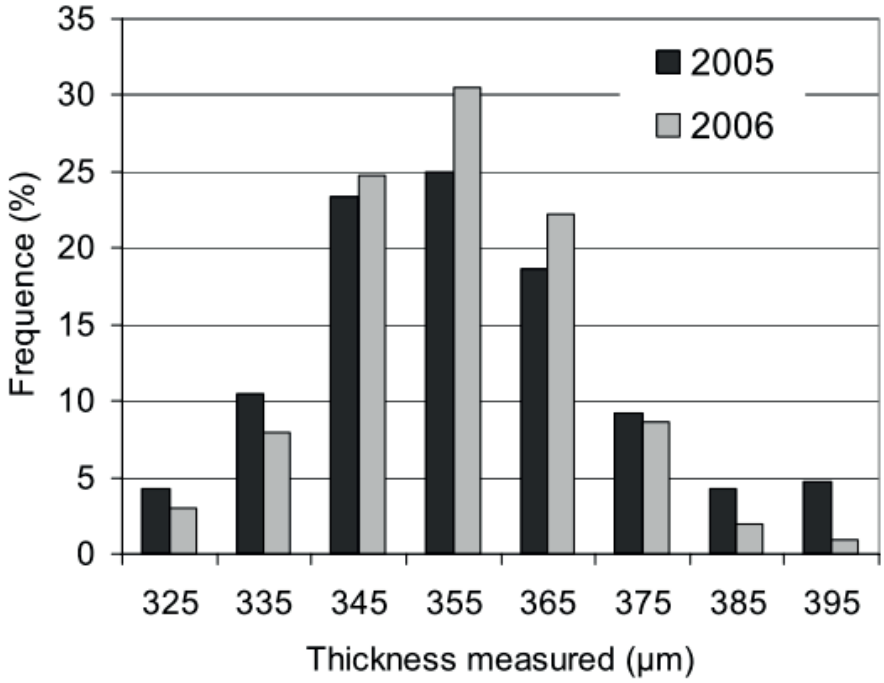

Figure 2.3 Statistical analysis of tape thickness distribution [31].

Bertoldi et al. [2], from SOLIDpower S.p.a., pointed out the variability of characteristic dimensions, requiring strict quality-control measures for the production of SOFC stacks.

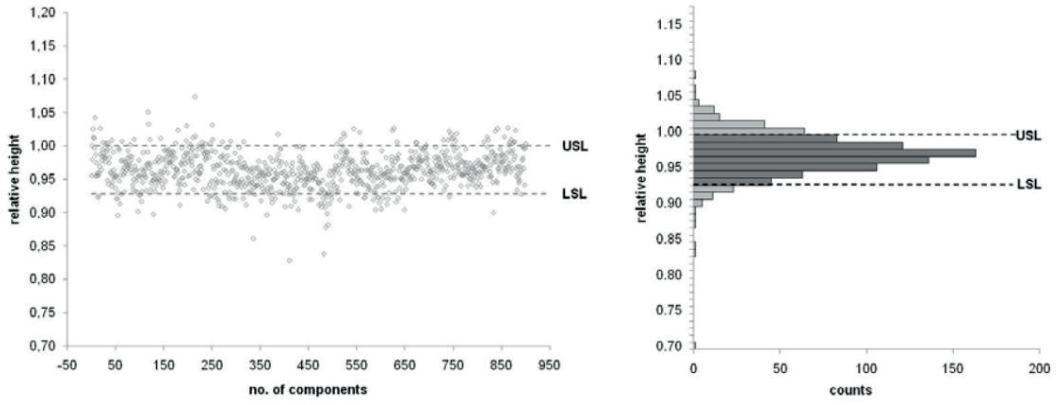

Figure 2.4 Variability of a characteristic height for a series of 900 components sequentially produced. Data are normalised on USL (upper specification limit) [2].

Sun et al. [32] proposed a methodology to design SOFC stacks based on probabilities, though an algorithmic optimization was not done.

> *"The method takes into account the randomness in SOFC material properties as well as the stresses arising from different manufacturing and operating conditions. […] Finite element analyses were used to predict the electrochemical and thermal mechanical responses of SOFC stacks with different geometric variations and under different operating conditions."*

2.1.3 Optimization of the design

As shown, it is obviously needed to consider the variability of manufacturing processes during the design of fuel cell stacks. Some researchers conducted design optimization, while explicitly taking into account these processes.

Wu et al. [33] analysed the parametrized performance of PEFC by using the Taguchi method and a neural network. In addition to showing that the method is functional, they pointed out that, according to the analysis of variance, the performance of PEFCs is significantly affected by the operating temperature and pressure.

Chen et al. [34] optimized the design of bi-layer interconnectors for SOFC with design of experiment (DOE) based on the Taguchi method and a 2D CFD model. For the studied grid-staggered pattern, the height of the channel was shown to be the most significant factor among those analysed.

Peng et al. [35] optimised the shape of flow channels for hydro-formed metallic bipolar plates in PEFC to maximize both reaction-efficiency and formability. The same authors [36] then investigated a flexible forming process via numerical simulations and experiments.

Although considering the manufacturing processes, these studies lack the notion of a heterogeneous distribution of the quality, which is inherent to the variability of these processes. Consequently, the optimum that is found is likely not robust.

2.1.4 Monte Carlo simulations for uncertainty quantification

Monte Carlo simulations have been used for a few years now in the field of SOFC. Until recently, however, MCS were used primarily in their "kinetic" form, focusing on the micro-structure of materials [e.g., 37].

Seidenberger et al. [38] estimated the distribution of water and mechanisms of degradation in PEFC using 3D MCS. Uncertainties related to manufacturing or to operating conditions were, however, not considered.

Liu et al. [20] used MCS with a finite element analysis to study the effect of dimensional tolerances. The scope of their work on PEFC was limited to the calculation of the contact-resistance as a function of the mechanical pressure-distribution; they did not consider the distribution of the flow.

2.1.5 Towards robust design — Optimization under uncertainty

Subramanyan et al. [39,40] performed a multi-objective optimization of hybrid SOFC power-plants under uncertainties, which were characterized and quantified. The optimization is conducted at the level of the entire system (macro-model).

Zhao et al. [41] presented a parametric design-method with neural network relationships and fuzzy relationships considering uncertainties and applied it to SOFC. Their objective function is composed of three performance indicators and one cost indicator. The partial pressure of hydrogen and the operating temperature were selected as the "design" [sic] variables to optimize. Hence, an optimal *operating condition* was found, which actually tells nothing about the quality of the design itself. Moreover, the uncertainties in question were generated by non-deterministic relationships, not from the stochastic distribution of parameters. As a consequence, no insight can be obtained about the sensitivity to design parameters — and more importantly — although the computed optimum is robust with respect to uncertainties on the relationships used for the evaluation of the objective function, this optimum is not robust in the sense of being less sensitive to variations of the design parameters.

2.1.6 Uncertainties in measurements and for diagnostics

Hernandez et al. [42] presented a stochastic approach for the diagnosis of PEFC faults. PDF of cell voltage was used as a clustering parameter. Operation modes leading to failure were clearly identified, allowing a classification of flooding and electrode contamination failure.

Gazzarri et al. [43] modelled the degradation in an SOFC stack. A sensitivity analysis (with interactions) was carried out, and a non-invasive diagnostic technique was proposed to identify degradation modes in situ, based on impedance spectroscopy.

Momma et al. [44] carried out an uncertainty analysis in SOFC performance testing. Uncertainties of measurements and their propagations when combined for the final result were analysed.

Oliviera et al. [45] studied the uncertainties of measurements with MCS and analysed the reliability of measured values in the evaluation of electric variables of PEFCs and SOFCs.

2.2 Uncertainty and optimization in other fields

2.2.1 Monte Carlo simulations and alternatives

Robust design methods and Monte Carlo simulations (MCS) have been applied in other engineering fields.

Putko et al. [46] implemented an approach for input uncertainty propagation and robust design in a quasi 1D Euler CFD code using sensitivity derivatives, and validated the method with statistical moments generated through MCS. The method was applied on a subsonic flow through a variable area nozzle — first with propagation of geometric uncertainties, and then with propagation of flow parameter uncertainties. The drawback of such a method is the need to have access to and modify a CFD code. It is a so-called intrusive approach.

Crossland et al. [47] developed a flexible object-oriented modelling framework for representing uncertainty in early variant design. MCS were associated to a risk model to design automobile interior trim.

Huang et al. [48] completed a tool for predicting machining tolerances via MCS, with accumulation of several operations and their associated errors. The purpose is a rapid evaluation of alternative process plan decisions.

Kumar et al. [49] implemented a robust design method using Bayesian MCS and applied it to a CFD analysis of a compressor blade. Their model deals with manufacturing uncertainties and allows for multi-objective optimization.

Witteveen et al. [50] proposed a monomial chaos approach for efficient uncertainty quantification in nonlinear problems. The method was applied to uncertainty quanti-

fication of the Burgers equation and to a 2D boundary layer flow problem, then compared the results with those of the MCS, of the perturbation method, of the Galerkin polynomial chaos method, and of a nonintrusive polynomial chaos method.

Bowman [51] presented an efficient gradient-based tolerance optimization using MCS. The goal of the method is to select the optimal tolerances for achieving the desired yield ("acceptance rate") of functional assembly at the minimum cost. The method was shown to be powerful for dimensional tolerances (i.e., accuracy of distances), but is problem-specific and cannot deal with geometrical tolerances (i.e., such as parallelism, circularity, or flatness) and other kinds of uncertainties.

It is clear that a "pure" Monte-Carlo implementation[1] over a detailed physical model is not appropriate for carrying out the intended optimization under uncertainty. Indeed, finding optima is much more efficient with methods that not only rely on randomness, but have a kind of "smart" deciding rules or behaviour (e.g., heuristics), to reduce the number of evaluations until an optimum is found with a suitable convergence (confidence).

There exist several enhancements to the basic MCMC algorithm and some alternatives, which may be especially profitable when applied to intensive computations such as OUU with CFD models. Among nonlinear "global" optimization methods, gradient-based are distinguishable from non-gradient-based methods. About the former, well known techniques are Newton's method, steepest descent, conjugate gradient, and sequential quadratic programming (SQP). Gradient-based methods find local optima with high reliability and converge with few iterations, but are usually unable to escape a local optimum. However, they are often not well suited to stochastic processes and systems, for which either the response to the input is not clearly defined mathematically (do not satisfy continuity, derivability …) or whose response is given by a "black-box" at some stage (proprietary software). Gradient-based methods are only directly applicable and fully efficient when the objective- and constraint- functions can be *explicitly* described with mathematical (in)equations, which is a major hindrance. Otherwise, the gradient must be evaluated numerically, by several realizations of the "black-box" simulator, which is time-consuming and may not be accurate enough to orient the algorithm in the right direction. Stochastic methods will find a good solution with high probability, but it is not guaranteed to even be a local optimum.

[1] By "pure" Monte-Carlo, we mean random draws in a uniform distribution, without any enhancement.

Remark: The adjoint-solver[2] as implemented in FLUENT still has several limitations. For instance, models such as porous-jump and compressible gases are not supported, neither are boundary conditions of type mass flow inlet. So, it cannot be used effectively in the frame of this thesis.

Among non-gradient-based methods of optimization, many are stochastic. Most of them rely on (MC)MC-based algorithms, such as simulated annealing (SA), reactive tabu search (RTS), variable neighbourhood search (VNS), and reliability-based optimization (RBO), among which belong first-order reliability and second-order reliability methods (FORM and SORM). Another category uses response surface methodology (RSM), such as indirect optimization based on self-organization (IOSO). Other methods are based on (meta-) heuristics: reactive search optimization (RSO), memetic, swarm-based, and evolutionary (genetic) algorithms belong to this category.

[2] The adjoint-solver computes the sensitivity derivatives. Being able to use it would allow efficient computation of the derivatives.

"What happens is fact, not truth.
Truth is what we think about what happens."
Robert McKee

CHAPTER 3

Description of the problem

The purpose of this chapter is to give a more accurate description of the problem that we addressed. We give some examples. We also point out the challenges.

3.1 Idea

The idea is that the quality of any manufactured product is notably affected by the variability of diverse characteristics with respect to the ideally designed product. These imperfections are frequently the sources (causes) of durability or reliability issues (consequences). Since phenomena are highly coupled, it is stressed that, in their turn, some causes may be the consequences of other causes, and vice-versa.

Those variations can be described as a probability — for one manufactured product — to achieve a certain value among a statistical distribution for a given variable (known as a random variable). Such a distribution can be characterized with several statistics, among which the *mean* and the *standard deviation* are common. An important point is that the mean is not necessarily equal to the value targeted by the design stage.

3.2 Typical geometry at play

Figure 3.1 shows the geometry of a fluid distribution pattern. The illustration corresponds to the design of bipolar plates of a PEFC. However, apart from the presence of a coolant, the elements are common to SOFCs.

3.2.1 Importance of flow distributors on the performance

As said in the literature review, flow distributors play a large role on the performance. But also on the lifetime, because a cell which is less stressed will be less affected by degradations. Figure 3.2 illustrates this issue.

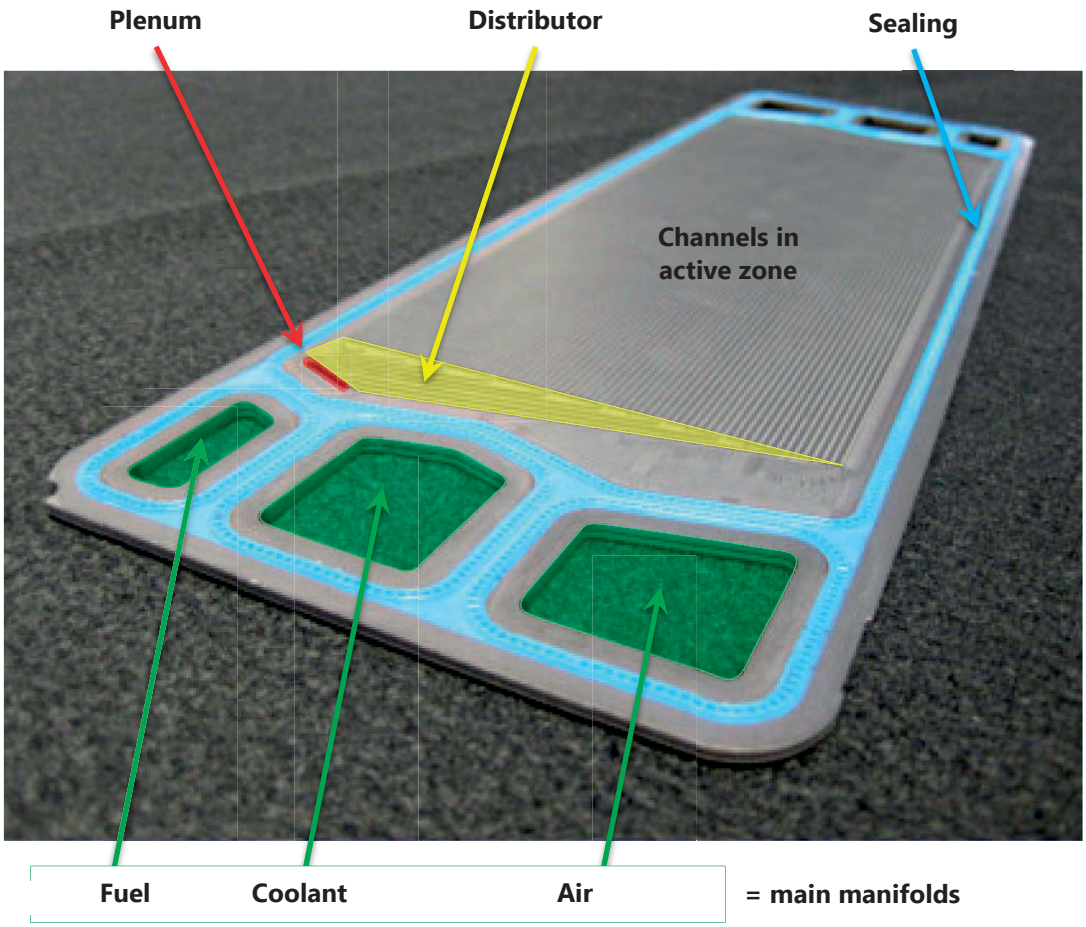

Figure 3.1 Example of the geometry of a fluid distribution pattern. Design of bipolar plates of a PEFC [10].

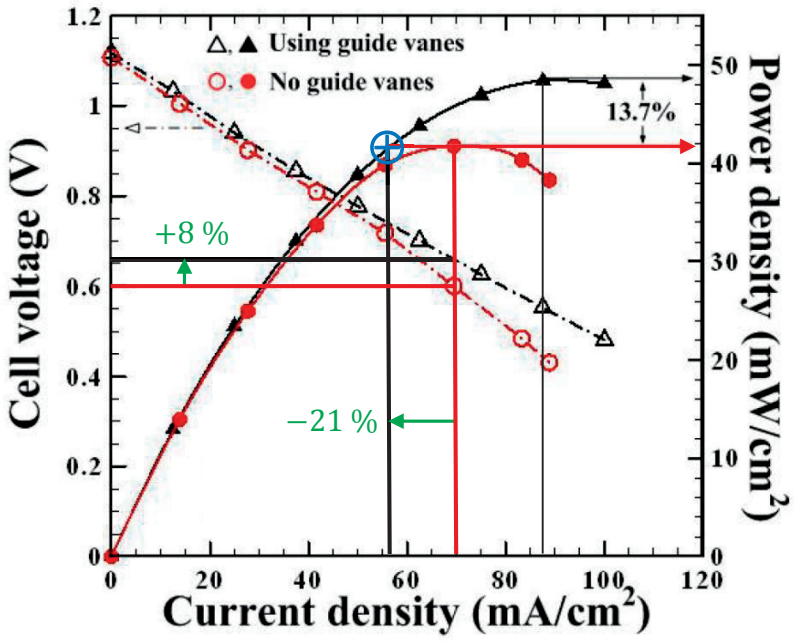

Figure 3.2 Power-generating characteristics of two sets of identical single-cell stacks except using different flow distributors [52].

Operating conditions: 720 ml/min of air as an oxidant and 640 ml/min of 62.5 % H_2 + 37.5 % N_2 (molar) as a fuel; T = 850 °C.

3.2.2 Importance of dimensions of channels

The dimensions of the distributors, and particularly of the channels or other flow paths in the active area, are crucial to a uniform flow distribution. It is sensitive to their variability, and more so if they are small.

Height of channels, H (deterministic) is wished as small as possible — yet not too small. It influences, among others:

- Pressure drop;
- Flow uniformity;
- Electrical efficiency;
- System efficiency (blower);
- Material cost;
- Specific power;
- Diffusion.

Accounting for variability of the height of the channel is important for flow uniformity, and it is linked to:

- Reliability and durability issues;
- Efficiency limitation (fuel utilization);
- Manufacturing costs (specialized processes);
- Quality control costs;
- Production yield.

Dimensional variability impacts uniformity of most fields (v, j, T).

Figure 3.3 highlights the small dimensions of the channels, compared to the large size of the other parts, including the manifolds (hollow part not physically visible). Figure 3.4 shows that uncertainty can also arise from basic computer assisted drawing.

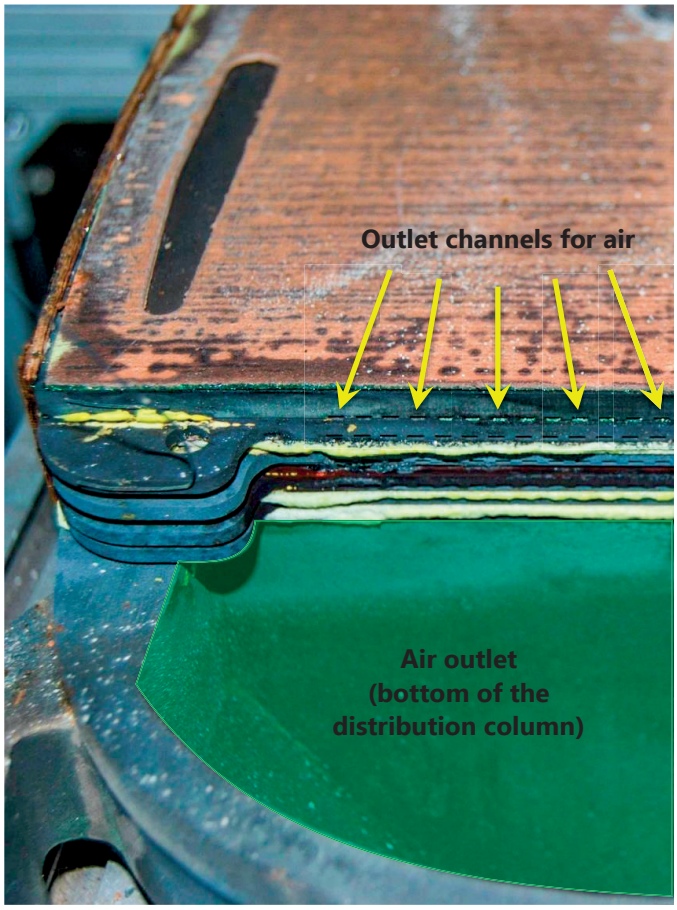

Figure 3.3 Quarter view of an SOFC short stack (after operation), which emphasizes the contrasting length-scales at play: the distribution column is much bigger than the channels. The width of internal channels is even shorter by ca. 75 %.

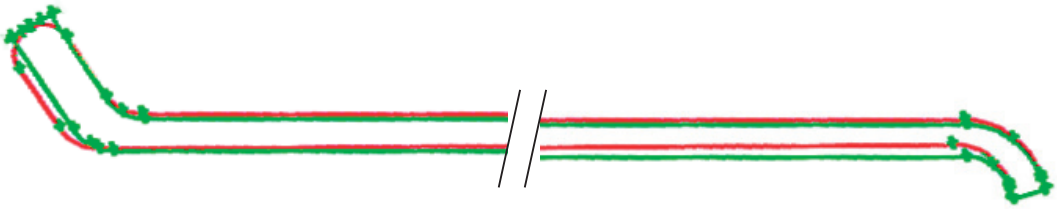

Figure 3.4 Example of deviation of models in the *design phase*.
Green curves: drawing of a rib in GAMBIT meshing software, corresponding to an improved flow distribution.
Red curves : geometry as (re)drawn on DASSAULT CATIA by our industrial partner based on a STEP file generated with GAMBIT.

3.2.3 Why is deterministic optimization dangerous?

Deterministic and stochastic optimization, subject to inequality constraints, are differentiated schematically in figure 3.5. For simplicity of representation, the objective function is supposed to be uncertain only with respect to two random variables, resulting in a probability distribution function (PDF) for the objective whose support is bidimensional. Several aspects should be highlighted: (1) the PDFs of the random variables are not necessarily identical for different targeted design values; (2) the PDF of the objective function is often not linear with the PDFs of the random variables (hence the need for specialized methods); and (3) the deterministic optimum is generally not robust since it almost always leans on a constraint boundary. As an example, the deterministic optimum in figure 3.5 would not be robust even if the dispersion was nearly zero. The PDF associated with the deterministic optimum when accounting for variability is sketched here with a bigger dispersion than the PDF for the robust optimum. Yet this is not generalizable.

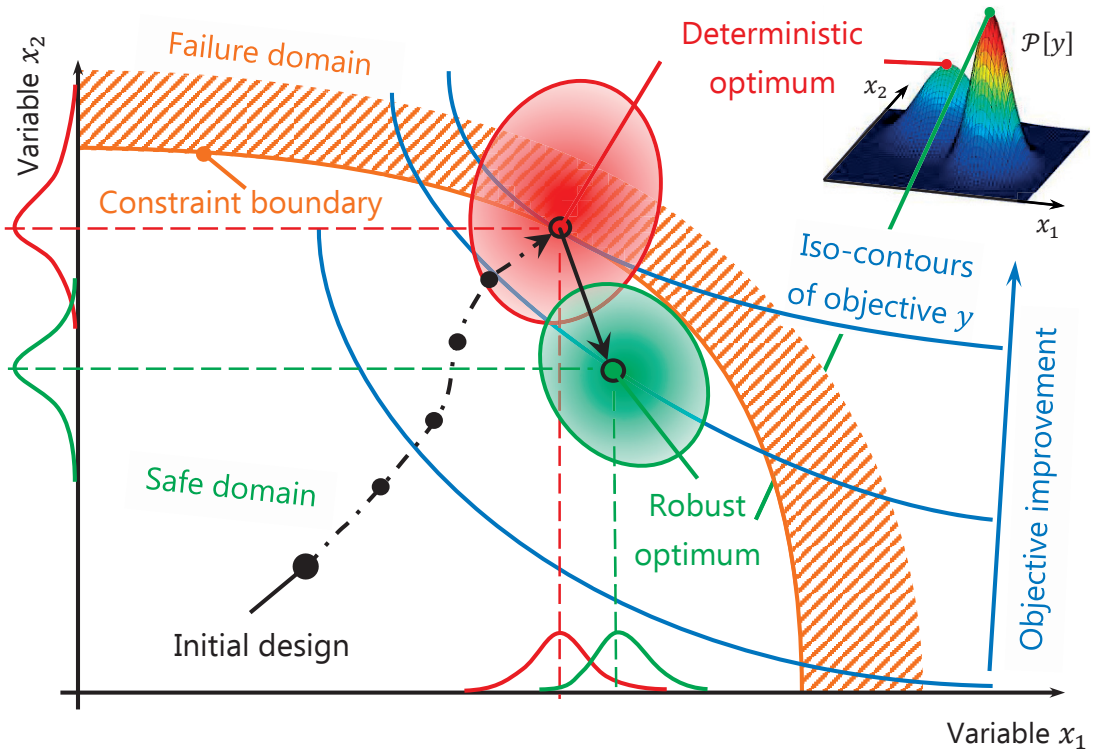

Figure 3.5 Schematization of deterministic vs. robust design optimization.

3.3 Steps

The main stages of this investigation are:

1. Assess available methods for OUU and implement the most appropriate

A common way to study the effect of uncertain inputs on the outputs of a complex system is to apply so-called Monte Carlo simulations (MCS), e.g., based on Markov-chain Monte Carlo class of algorithms (MCMC). The principle of this group of methods is to evaluate the outputs of a system for a lot of input combinations drawn from statistical distributions. MCS are useful for two distinct purposes of interest:

Analysis of existing systems, e.g., definition of quality controls or comparison with post-operation diagnosis;

Synthesis of new systems, e.g., through numerical (robust design) optimization.

Regarding the procedure, the second is basically like the first, with the addition of an optimization stage. The steps of the procedure and further explanations are exposed in § 5. *Perform an OUU of an SOFC stack with interacting imperfections*, below.

2. Implement heterogeneous distributions in the modelling tools

Adaptation of the developed CFD model was necessary to allow the implementation of uncertainties. About geometrical imperfections, routines generating such deformations on the CFD mesh were implemented.

3. Analyse the influence of manufacturing tolerances

It consists of analysing the influence of dimensional and geometrical tolerances. Characterization by measurements on real components is needed.

4. Validation of the models

Statistical model

The procedure to validate the outcomes of the statistical analysis is: to validate the deterministic simulations, to validate the modelling of uncertainty, and to verify the code linking the deterministic simulator with the stochastic computations.

Nevertheless, since resources for physical experiments are limited, we may not have enough available statistical data to truly validate the model. Therefore, methods such as statistical hypothesis testing will be used to assess the confidence interval, which indicates the degree of reliability of the estimate.

Since the validation takes place before the OUU, it is carried out on a non-optimal design. The design obtained with the OUU may fall outside the domain of validity.

Another aspect which is worth highlighting is that some heterogeneities (variability) may be the consequences of the (stochastic) degradation of the fuel cell, i.e., not necessarily observable at the first usage of the product, nor directly inherent to its design or its manufacture.

5. Perform an OUU of an SOFC stack with interacting imperfections

An optimization under uncertainty (OUU) is composed of the processes outlined in figure 3.6.

First, it is worth mentioning that the procedure involves two main intermixed stages:

Simulation of the system with samples drawn from the distributions of the uncertain variables;

Optimization of the system by adjusting a set of decision variables for minimizing the objective function, while satisfying constraints.

Inputs with heterogeneous distributions (non-uniform probability distribution) are stochastic (random) variables given to the models, which hence return as many sets of outputs as sets of inputs that were sampled. These outputs are themselves stochastic variables, from which statistics of interest are aggregated (such as mean and standard deviation of quantities of interest). These statistics are then used to compute an objective function, which is minimized through optimization of a selected set of design variables. Deterministic iterates or stochastic iterates are used depending on the optimization algorithm to update these variables. Although operating conditions are not subject to the optimization under uncertainty, they may be (deterministic) variables, too. Constrained, multi-objective, and discrete integer optimization can also be performed in the OUU paradigm.

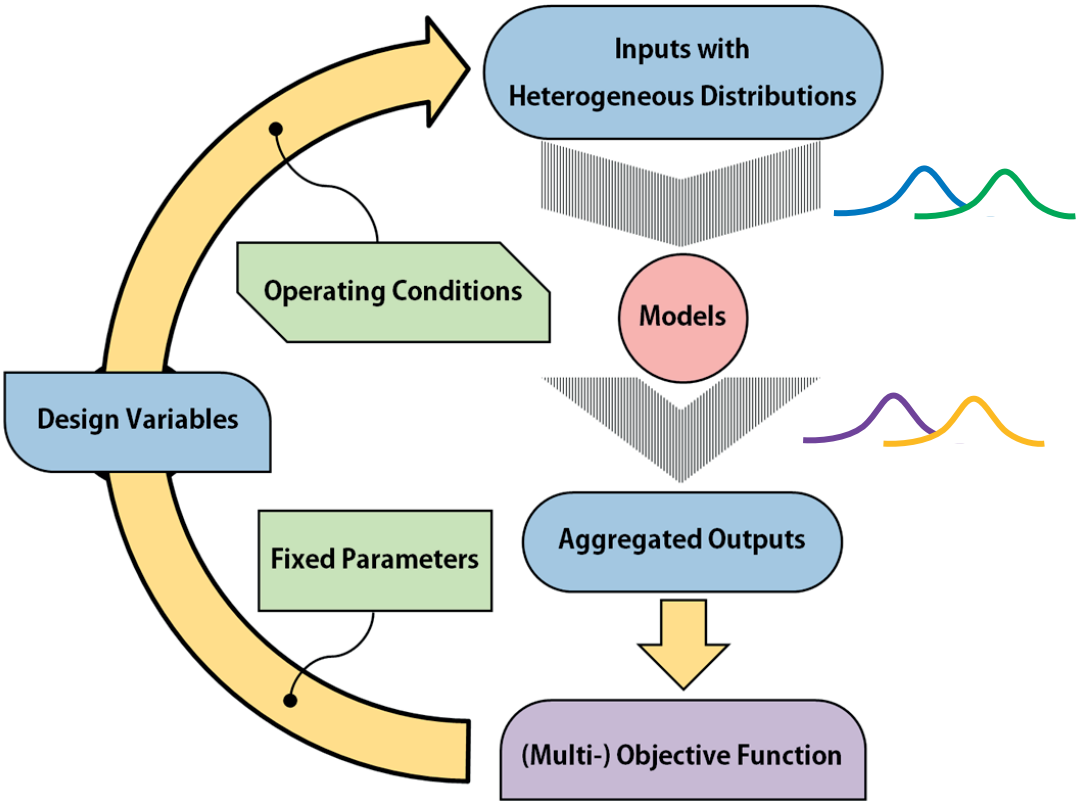

Figure 3.6 Diagram of the optimization, under uncertainty, of the design.

To obtain a reliable estimate of the objective function under uncertainty, hundreds to thousands of parameter-sets should be simulated to evaluate the stochastic responses of the system. The optimization loop is carried out for the objective function aggregated from such a batch of simulations. Consequently, a batch of many simulations must be processed for each set of design variables subject to the optimization, and each set of operating conditions. Besides, the phenomena are highly nonlinear, hence implying a vast amount of iterations in the optimization loop and in the simulations. Furthermore, CFD models are typically intensive in both resource and time. As a consequence, methods for both sampling and optimization have to be chosen carefully for efficient computations.

Optimization under uncertainty is particularly challenging with resource- and time-intensive numerical models, such as CFD. Indeed, when accounting for uncertainty, each tested set of parameters subject to the optimization requires many evaluations of the stochastic responses of the system to obtain a reliable estimate of the objective function. Hence, a paramount need exists for efficient implementation of OUU for such engineering problems. The methodological approach is generic to any challenging multi-disciplinary optimization of an engineering problem where complex nonlinear

coupled phenomena are involved and interact with stochastic processes — requiring thorough fundamental understanding. Thanks to this generality, both the know-how and the implemented tools can be transposed to other domains than SOFCs.

3.4 Quantities of interest

The quantities that we are interested in getting a quantification (under uncertainty) are in particular:

- Efficiency (system, electrical, …);
- Electrical power output, and its density (+ potential and current);
- Indicator of flow uniformity (fuel utilisation → efficiency and lifetime);
- Corresponding decision (design) variables, such as geometrical dimensions;
- Indicator of degradation.

Since we consider a stochastic framework, the value of the quantities in which we are interested may be the mean, the standard deviation, a probability, or any other ***statistic*** or combination of statistics of those quantities.

3.4.1 Choice of indicator of flow uniformity

At least one criterion must be defined to assess the uniformity of the flow — which is a relative quantity — and therefore the "optimality" of the geometry. There exist several ways of measuring the degree of uniformity (of the flow). The most common (in fluid dynamics) is the root-mean-square of differences over the domain of interest. However, in our case, we focus in variations occurring at a scale above *ca.* 1 mm. Indeed, the microstructure of the cell (and of the GDL where present) is such that (or should be such that) these variations are heavily damped (cancelled) ; dominance of diffusion rather than that of convection (advection). Besides, all the constraints on the geometry in the active zone are such that the characteristic widths (of the cross-section) of the flow path are of that order (ca. 1 mm). It is therefore straightforward to use an indicator of uniformity which is based on the variations of flow averaged in these subdomains.

An observation of the field of velocity and of the streamlines coloured by velocity allows a qualitative appreciation (as does the pressure field, but less intuitively). To measure quantitatively the irregularity of the flow, one method is to plot the velocity

against the y coordinate (transverse). More precisely, it concerns the component of velocity parallel to the mean flow (u_x). Another way to quantify the homogeneity of the flow field is to use an index of flow uniformity used for instance by Huang et al. [53].

$$\Gamma_u = 1 - \left(\frac{1}{N_c} \sum_{c=1}^{N_c} \left[\frac{\overline{u_x[c,x]} - \overline{u_x[x]}}{\overline{u_x[x]}} \right]^2 \right)^{0.5} \tag{3.1}$$

where N_c is the number of intervals or "channels", $\overline{u_x[c,x]}$ is the mean x-component of velocity at channel c and at position x, and $\overline{u_x[x]}$ is the mean velocity along the x-line. A perfect flow uniformity is indicated by $\Gamma = 1$ and the worst situation by $\Gamma = 0$.

In our case, we generalise this definition to the flow rate. Indeed, what is important is the supply of the species. This definition accounts for possible variations of density (depends on mixing composition and temperature), a more accurate indicator is given by the mass flux:

$$\Gamma[x] = 1 - \left(\frac{1}{N_c} \sum_{c=1}^{N_c} \left[\frac{\dot{m}[c,x] - \dot{m}[x]}{\dot{m}[x]} \right]^2 \right)^{0.5} \tag{3.2}$$

As a matter of fact, the density varies only slightly along the transversal direction (y). Finally, it should be noted that the uniformity of the flow is not a sufficient criterion. Actually, the homogeneity of the species distribution is the key factor (see remark below).

The case of solid oxide fuel cells

For solid oxide fuel cells, it is the minimum local flow rate which is critical. In the case of channels, the most underfed channel is hence the most limiting.

The index of flow uniformity is therefore defined here as:

$$\gamma = \frac{\min[\dot{\boldsymbol{V}}_c]}{\text{mean}[\dot{\boldsymbol{V}}_c]} \tag{3.3}$$

with $\dot{\boldsymbol{V}}_c$ the vector regrouping the volumetric flow rate in each channel c of a cell element. Alternatively, if the fluid distribution pattern is not composed of channels, c represent the mesh-cell (smallest local division in a simulation). Also, for the distribution in a stack of cell elements, c would represent the cell element.

A perfectly homogeneous flow distribution is indicated by $\gamma = 1$, which is the maximum value γ can take. The minimum and worst value is $\gamma = 0$ in principle. However, one of the advantages of this indicator is that $\gamma < 0$ indicates a reversed flow. This indicator is used in most of this document. We compare it to Γ in more detail in § 4.6.1, p. 126.

In Chapter 8 (p. 213), we used a slightly different indicator of flow uniformity, which is the *deviation* of *mass* flow rate between the minimum and the average. So, it is basically equivalent to $\delta = \gamma - 1$ (with γ defined for mass flow rate instead of volumetric flow rate). This opposition gives the advantage that δ shows directly by how much in percent a channel (or element) is underfed. The best value is $\delta = 0$ and the worst value is $\delta = -1$ without reversed flow ($\delta < 1$ otherwise).

For a single repeat element, this deviation is expressed as:

$$\delta_{\min}^{\mathrm{IE}}[el] = \frac{\min\left[\dot{M}_{ch}^{\mathrm{IE}}\right] - \dot{M}_{\mathrm{ch}}^{\mathrm{mean}}}{\dot{M}_{\mathrm{ch}}^{\mathrm{mean}}},\ \forall\ el \tag{3.4}$$

For stacked repeat elements, the flow rate deviation in (3.4) for individual repeat elements becomes:

$$\delta_{\min}^{\mathrm{ST}}[el] = \frac{\min\left[\dot{M}_{ch}^{\mathrm{ST}}\right] - \dot{M}_{\mathrm{ch}}^{\mathrm{mean}}}{\dot{M}_{\mathrm{ch}}^{\mathrm{mean}}},\ \forall\ el \tag{3.5}$$

For both indicators, the ideal channel flow rate $\dot{M}_{\mathrm{ch}}^{\mathrm{mean}}$ is the same, as it refers to the *nominal* — average — flow per element:

$$\dot{M}_{\mathrm{ch}}^{\mathrm{mean,\ ST}} = \frac{\dot{M}_{\mathrm{stack}}}{\mathcal{N}_{\mathrm{el}}\,\mathcal{N}_{\mathrm{ch}}} = \frac{\dot{M}_{\mathrm{el}}^{\mathrm{mean,\ ST}}}{\mathcal{N}_{\mathrm{ch}}} = \frac{\dot{M}_{\mathrm{el}}^{\mathrm{simu}}}{\mathcal{N}_{\mathrm{ch}}} = \dot{M}_{\mathrm{ch}}^{\mathrm{mean,\ IE}} \tag{3.6}$$

Why flow uniformity instead of another indicator?

Actually, what is important is that each chemical species participating in the reactions is homogeneously distributed at the triple-phase boundary (TPB), which is the interface where the reactions occur. However, a model representing such a micro (nano) scale, while at the same time needing to represent the macroscale, would make the problem computationally intractable. Moreover, flow uniformity is a determinant factor for the species uniformity. It is even the sole factor if 1) the species are well mixed in the flow at inlet or mixing occurs before the active zone and 2) the reaction rate is homogenous. The latter depends mostly on the *uniformity of:* 1) the flow itself, 2) the

temperature, 3) the properties of the cell's microstructure, and 4) the properties of constituting materials. The field of temperature depends on the boundary conditions, the geometry, the flow itself, and the reaction-rate itself (coupling). In consequence, uniformity of these factors is key, and that of flow is crucial. As said, the scope of this thesis is not to consider in detail the material and microstructure aspects of the fuel cells. It is therefore assumed that another research (thesis) is dedicated to the optimal design of those aspects such that their negative and potentially interacting effects are minimized (i.e., guaranty their homogeneity where required and/or a low sensitivity to heterogeneity, e.g. through optimization under uncertainty).

3.5 Introduction to uncertainties

The purpose of this section is to explain:

- What are uncertainties (definitions)? Where and when do they occur?
- Why accounting for them is important?
- How uncertainties can be qualified (described, characterized, classified)?
- How uncertainties can be quantified, reduced, and "optimized for"?

Basic definition: an uncertainty is a loose/fuzzy concept describing a lack of certainty about a proposition. It raises the "philosophical" question: "How certain are we about a given certainty?"

Uncertainty is also a measure (qualitative or quantitative) of the degree to which something is uncertain (believed to be). Note that we usually assimilate a source of uncertainty to an uncertainty.

Uncertainties [epistemic uncertainties] result from different sources covering many aspects, including design decisions not yet taken, lack of specification details, missing information, characteristics estimated with rules-of-thumb, or alternative, non-ideal behaviour models, — whereas *variabilities* [***Aleatory uncertainties***] include aspects such as manufacturing inaccuracies[1], variable environmental and operating conditions, or evolution due to ageing.

Figure 3.7 shows the main kinds of input and output variables which may be uncertain in the frame of our study. Note that although we considered the issues of uncertainties with a general approach, the robust optimization that we performed in the closing chapter of this thesis involves only uncertainty on the height of the channels as input

[1] Manufacturing inaccuracies are especially relevant for ceramic components, which are used in SOFCs.

to the model. It is important to realize that the model or system itself is uncertain due to its constituents being uncertain. Typically, the physics can be described more or less accurately: e.g., phenomena considered or not, formulations of the boundary conditions, sub-models used to compute a property, factors not well adjusted, or even an entire field of knowledge not considered ("neglected").

3.5.1 Why should we quantify uncertainties?

One could ask, why bother with UQ when safety factors can be applied? First, safety factors should not be confused with ignorance factors[2]. Second, in addition to refine safety factors, UQ can provide valuable information. Among others:

- Uncertainty quantification is an essential part of validation.
- It can provide a rigorous measure of confidence, and hence, confidence.
- It supports decision making, and highlights priorities.
- UQ is an integral part of robust (design) optimization.
- It may shed light on "hidden" or unintuitive features.

3.5.2 How to describe uncertainties qualitatively?

Uncertainties can arise from many sources and can take different "forms" (sub-concepts). Besides, some disagreements exist in the literature about what is an uncertainty and what is not (among these sub-concepts).

[2] A *safety factor* is computed based on documented theoretical or experimental grounds, whereas an *ignorance factor* is only chosen based on impressions or by just guessing (e.g., to allocate twice as much time for a task than the duration which initially came to mind).

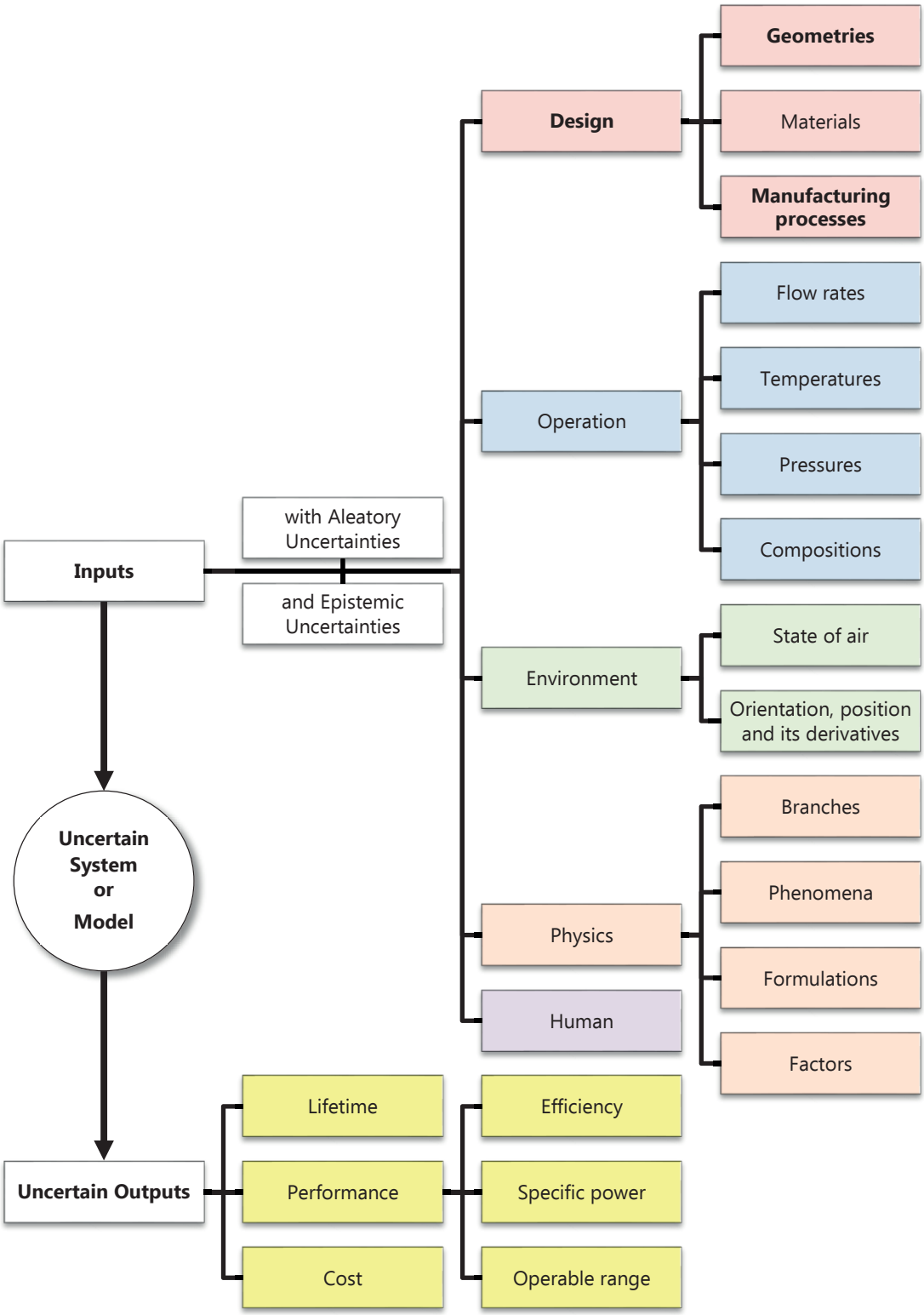

Figure 3.7 Main kinds of input and output variables which may be uncertain.

1. A common way of classifying uncertainties:

The formulation of this section is inspired from a presentation by Todd Oliver during the lectures series on UQ in CFD at the Von Kármán Institute, Belgium [54].

> *"Consider a proposition A. Is A true? At least three reasons why we may be uncertain:"*

Aleatory uncertainty refers to the case where the variable is, in essence, a random variable.

Truth of *A* varies "randomly".

Examples of aleatory uncertainties

- The number of six after two draws of a dice.
- The height of a channel.

Epistemic uncertainty: *A* is objectively either true or false but given current information, we cannot conclusively establish which.

It refers to the case where the variable can in essence be known exactly to a given precision, but the data is not available (e.g., cannot be measured with such precision or at all).

Oberkampf et al. [55] define epistemic uncertainty as *"any lack of knowledge or information in any phase or activity of the modelling process."*

O'Hagan and Oakley [56] distinguish aleatory and epistemic uncertainty as follows:

> *"Aleatory uncertainties are described as arising from inherent variabilities or randomness in systems, whereas epistemic uncertainties are due to imperfect knowledge."*

Examples:

- The diameter *D* is larger than 2 mm.
- The number of six after two draws of a dice.
- Answering the question "which model is most accurate" ?

Vagueness describes the case where the proposition is not clear (specific) enough to be definitely true or false.

Example: the diameter D is large (yes/no). "Large" is too ambiguous (relative), especially without context.

It is important to realize that the same **uncertain variable** can be either epistemic or aleatory depending on the context (i.e., the aim of the study and the statement of the problem). Example: the number of six after two draws of a dice can be known exactly if an experiment is planed carefully enough, in a reproducible (or at least predictable) manner.

Usually, **human error (mistakes)** are not considered as uncertainties. Indeed, they should be avoided (eliminated). For instance, if one makes a mistake while doing an experiment, it should be repeated without the mistake. But what happens if the mistake is not seen, or not acknowledged? In other words, what is the degree of certainty that a set of data does not contain any human error? Following this argument, we include (hidden) human errors in the sources of uncertainties.

Similarly, ***vagueness*** and ***ambiguity*** should be eliminated, especially when they can be assimilated to human errors. Again, they nevertheless exist, and create uncertainties, which may not be easily reduced, nor easily detected.

3.5.3 How to characterize uncertainties quantitatively?

Let $x = x_{\mathbb{U}}$ be an uncertain variable (input) and F a quantity of interest which depends on it (output). The knowledge of the relationship is often not known a priori. Figure 3.8 schematizes more or less sophisticated means to get information about how our quantity of interest behaves with variation of the uncertain variable. Typical approaches are:

(a) *Deterministic analyses* (ignore uncertainties) is the most basic (non-) approach; not represented in the figure.

(b) *Local sensitivity analyses:* the local derivative of F with respect to x is estimated/computed at some given value(s) x_0 of the input variable. The local slope represents the local sensitivity.

(c) *Extreme cases:* for an interval of possible values of x, $[x_{\min} \dots x_{\max}]$, what is the resulting interval of F, $[F_{\min} \dots F_{\max}]$? As illustrated, unless the function is proven to be monotonous, it is dangerous to assume that extreme values of x lead to extreme values of F.

(d) *Probabilities:* for a given probability distribution function of x, $\mathcal{P}_x$, what is the resulting distribution $\mathcal{P}_F$ of our quantity of interest F?

(e) *"Hybrid":* combination of the above means.

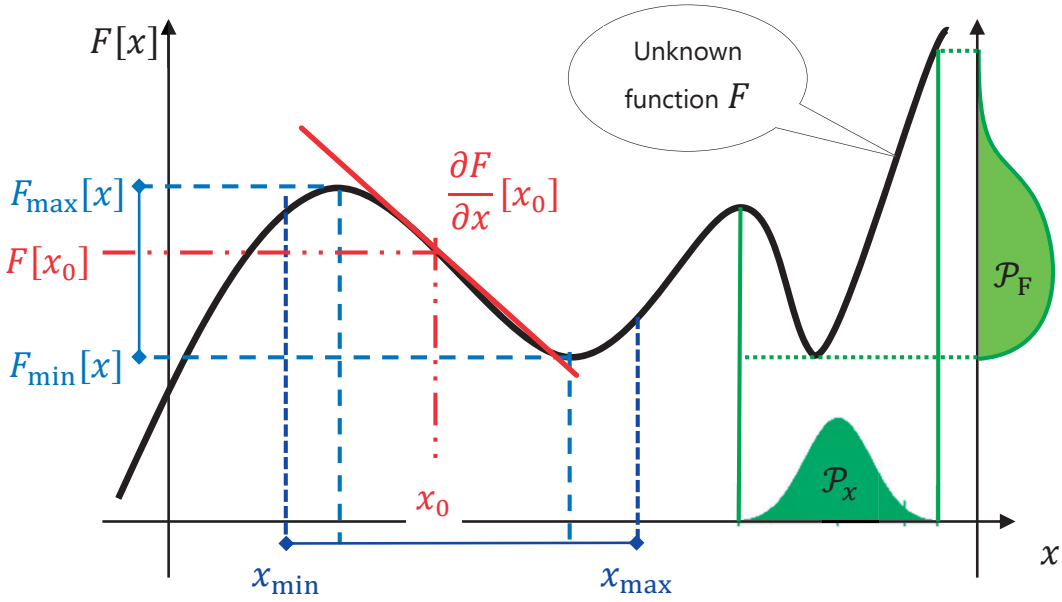

Figure 3.8 Schematic illustration of various means to quantify the effect of an uncertain variable x on a quantity of interest F.

In both academic and industrial contexts, (a) and (b) are still the most common practices.

The definition of the input uncertainties is critical. As in "garbage-in / garbage-out".

For instance, the value of a quantity is often described as $V = [X - Y \ldots X + Z]$, often with $Y = Z$. But what does it mean? X is usually assumed to be the mean, but it could be the median. Z and Y can be based on the extreme observed values [min ... max], or on the standard deviation, or on a quantile $[10^{\text{th}} \ldots 90^{\text{th}}]$, or on 3 σ, etc. Even when this is defined, it does not tell much about the statistical distribution of values.

3.6 Examples of issues

3.6.1 Effect of variable spreading of the sealing material

This example corresponds to a real-case issue that occurred with the design of our industrial partner. They diagnosed performance and reliability issues after a change of sealing material for a new sealing paste. Investigations hinted that the cause was a bad airflow distribution at the cathode induced by an inappropriate position of the sealing. Actually, several uncertainties and variabilities concerned the sealing: the dispenser may not distribute the paste as uniformly as wished, or not with enough accuracy; the paste, although solidifying when drying, may spread more or less during assembly and during operation at high temperature.

Simulations were therefore carried out to study the flow behaviour when accounting for a few scenarios about the uncertainty around the spreading of the paste. It consisted on the implementation of various widths of bypasses.

Data:

- A new pattern is used at the cathode in order to lower pressure drops.
- This new pattern relies, in the critical entry region, on the sealing paste to define the flow field; this aspect will be addressed in particular.
- Principal direction is now parallel to the mean flow.
- The height of the FDP has been increased to 0.95 mm.
- The sealing paste spreads towards the pattern.

Objectives:

- Analyse the flow field at the cathode with the current FDP.
- Estimate the pressure drop.
- Predict the behaviour of the flow according to risks of manufacturing inaccuracies.

Remark:

It was demonstrated [57] that pressure drops are essentially dependent of the height of the pattern. The orientation of the pattern does not affect much pressure drops.

Modelling conditions

Five geometrical situations were considered in order to account for the uncertainty about the location of the sealing paste, at inlet and at outlet.

- Large, medium, thin, and obstructed bypasses between the pattern and the sealing paste; dimensions and scheme are available below;
- Asymmetric spreading of the paste.

The flow field was computed without electrochemical reactions and with the assumption of perfect seals[3]. Properties of the flow are the following:

- Air at $T = 750$ °C, $p = 1$ atm, with $\lambda = 4$
- Mass flow rate $\dot{M} = 5.611 \cdot 10^{-5}$ kg/s for a flow rate of hydrogen equal to 6 ml/(min · cm^2) with a cell of active area equal to 50 cm^2.

Geometries

The medium bypass is wider than the thin bypass by ca. 1.5 mm, while the large bypass is once again ca. 1.5 mm wider. Figure 3.9 shows a scheme of these bypasses, along with a superposition of the SOLIDWORKS drawing from which the thin bypass results and a photography of the paste deposition, which a priori involves a medium or maybe large bypass.

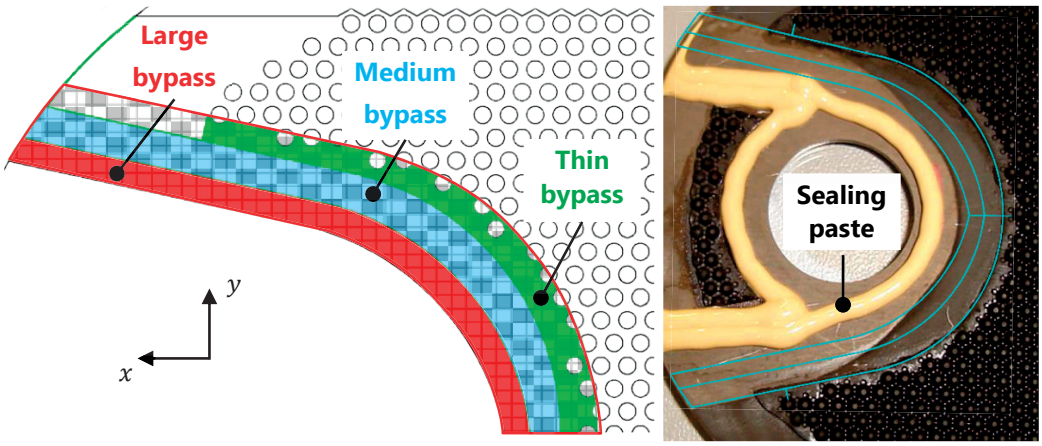

Figure 3.9 Width of the bypass of the air flow between the sealing paste around the fuel manifold and the pattern of cones at cathode.

[3] We studied this question[e.g., 13,57]. The material used previously was slightly porous; the new material ensure a much better gas-tightness.

Results and discussion

Pressure drop

Results reveal that pressure drops are sensitive to the width of the bypass. However, once a minimum width is reached (medium bypass), it has little further effect.

Table 3.1 Global pressure drop between inlet and outlet for various widths of the bypass between the sealing paste and the pattern of cones ($h = 1$ mm).

Width of bypass	Pressure drop [mbar]
Large	15
Medium	16
Thin	24
Obstructed (zero)	36

Distribution of the flow

As visible on the figures below, the distribution of air strongly depends on the width of the bypass. When it is obstructed, the flow field is absolutely not homogeneous (nearing zero on the central axis, close to outlet and inlet) . As a consequence, the middle of the cathode is under-supplied with air. The situation is opposite at the border of the cell; this is less critical. In comparison, at the anode, the worst deviation of the bulk velocity is 1.6 and it is about 1.2 with the optimized pattern.

Figure 3.11 shows the evolution of the flow uniformity along the length of the cell. It highlights a critical situation if the bypass is obstructed. The situation improves significantly when the bypass widens. However, the maximum uniformity does not correspond to the largest bypass, but rather to the medium (overall) or thin one (towards outlet).

One of the major problems resulting from these observations is that the behaviour of the flow is strongly linked with the distribution of the inaccuracies due to the spread of the sealing paste. In other words, the more a solution is reproducible, the more confidence one has with the constancy of the flow field (and accordance with the prediction from simulations).

A homogeneous distribution of the air between stack elements will be sensitive to the FDP thickness and to the bypass width. The latter has furthermore a significant impact on the air distribution within the repeat element itself. The impact of the sealing paste

deposition on the bypass width and on the resulting flow distribution is further illustrated in the following section.

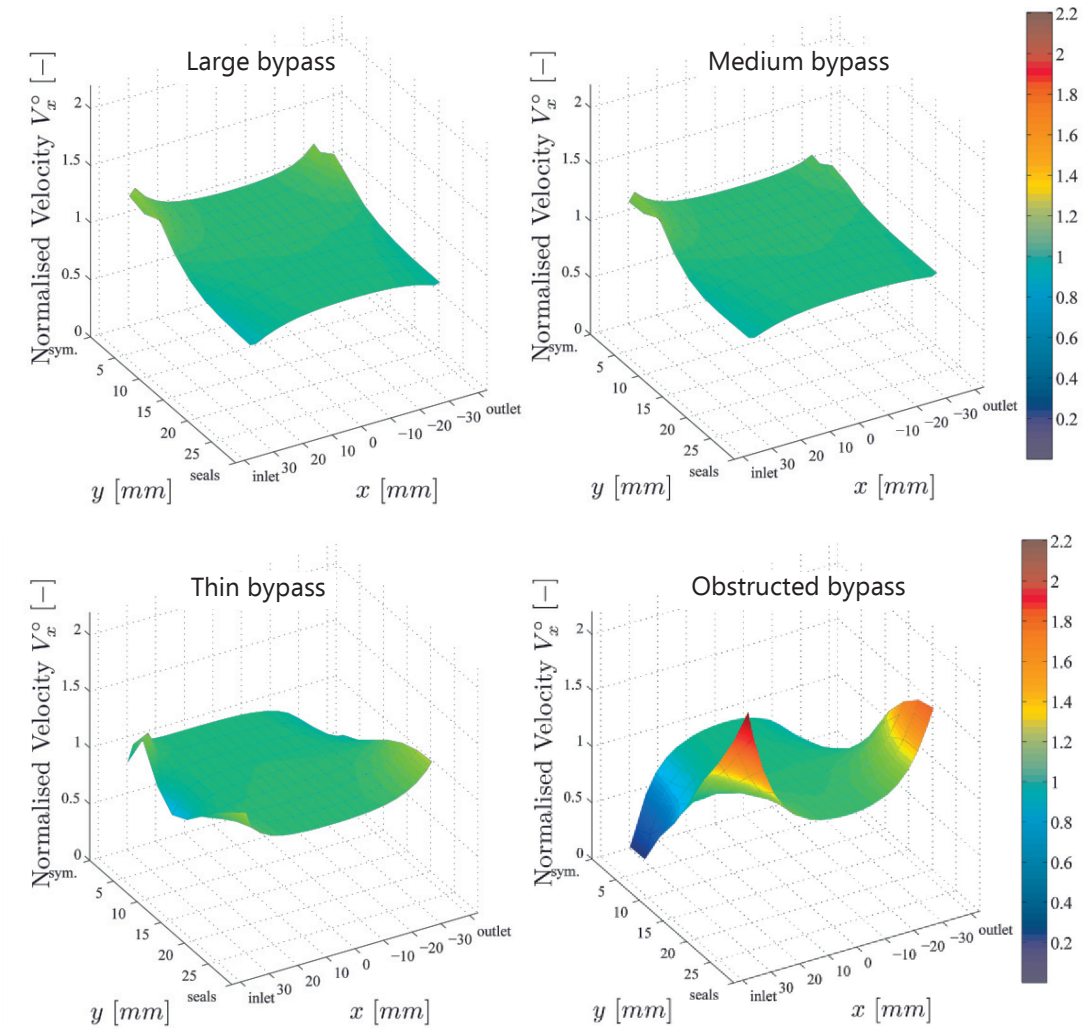

Figure 3.10 Flow deviation [—] in function of the width of the bypass (ideal = 1). Conditions: flow only, OCV, $h = 1.0$ mm.

Risk of asymmetry

Cases where the bypasses are asymmetric are probable. We studied the worst scenarios for flow distribution, i.e., when they differ in the transversal direction (y). However, we simulated only mild asymmetries (one increment), judging that the probability of meeting extreme ones is low (e.g., obstructed and large bypasses). Besides, we believe

that the results below are convincing enough that the flow is poorly distributed even with mild asymmetries.

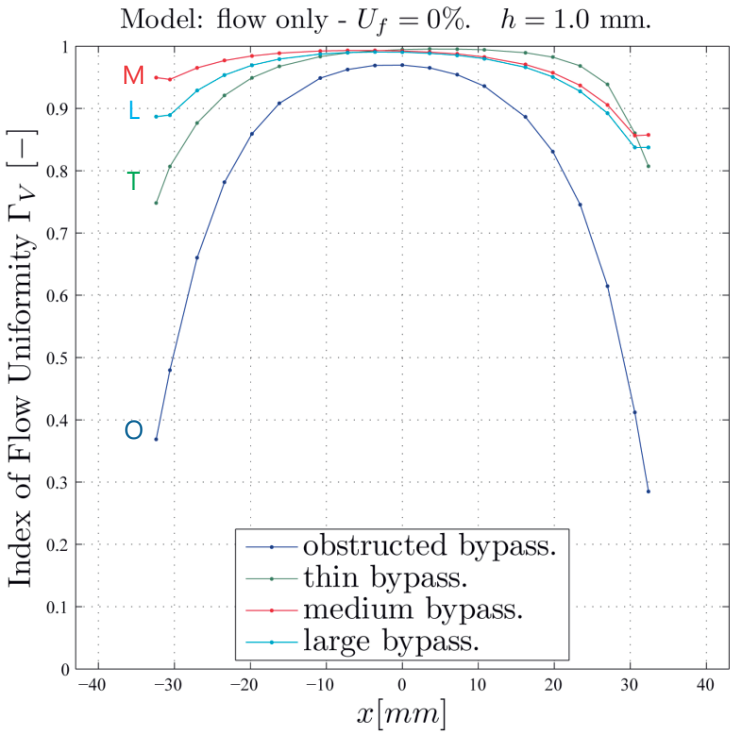

Figure 3.11 Index of flow uniformity [—] along the length of the cell with the width of the bypass as parameter (ideal index = 1).

Figure 3.12 shows the field of velocity when the bypass is obstructed on the top and is thin on the bottom. Air flows preferentially along the less resistive path (thin bypass), so the distribution is asymmetric. It is emphasized in figure 3.13, which shows the streamlines coloured by particle of fluid. The red line indicates where the fluid splits between "top and bottom", showing the strong asymmetry.

Figure 3.14 shows the flow deviation on the cell when the bypasses are thin on the right and obstructed on the left. With maximal deviations of 1.8 and 0.1 with respect to the mean flow (unity). With respectively 50 % and 30 % of deviation, thin & medium and medium & large bypasses are better, but still subject to asymmetric flow (figure 3.15). This asymmetry lowers even more the amount of oxygen on one side of the cathode. Figure 3.16 shows the evolution of the flow uniformity along the length of the cell.

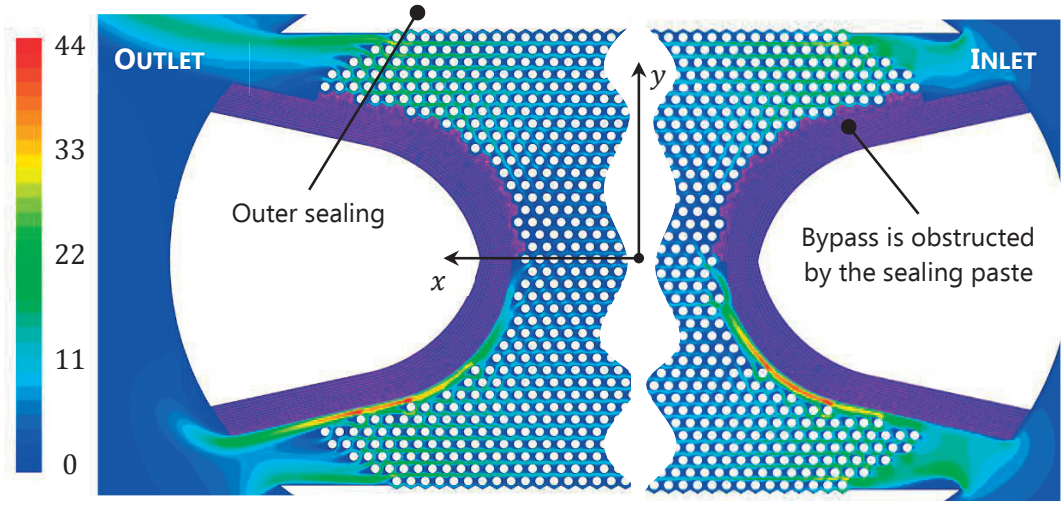

Figure 3.12 Velocity magnitude [m/s]. Top: obstructed bypass; bottom: thin bypass. The flow is strongly deflected towards the thin bypass.

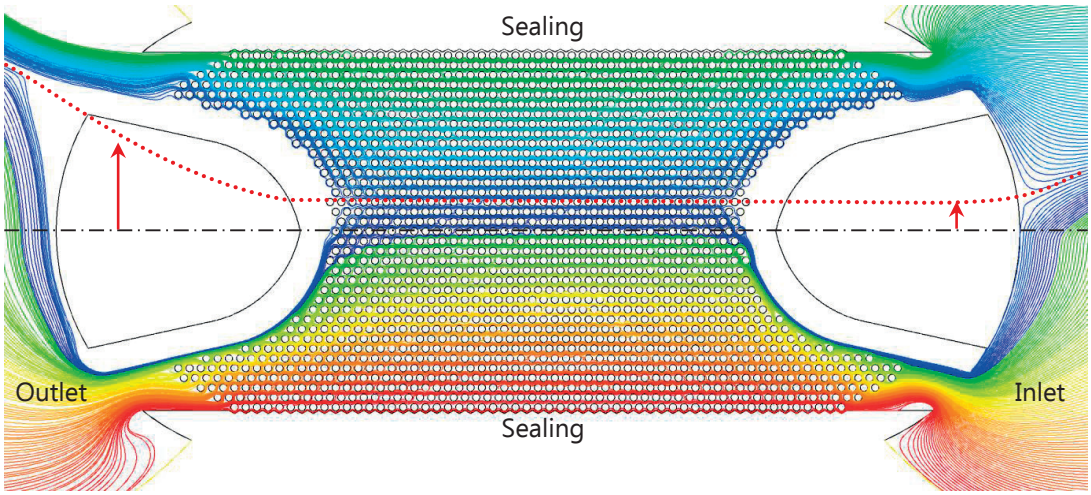

Figure 3.13 Streamlines coloured by particle of fluid. Top: obstructed bypass; bottom: thin bypass. A large portion of the flow follows the thin bypass.

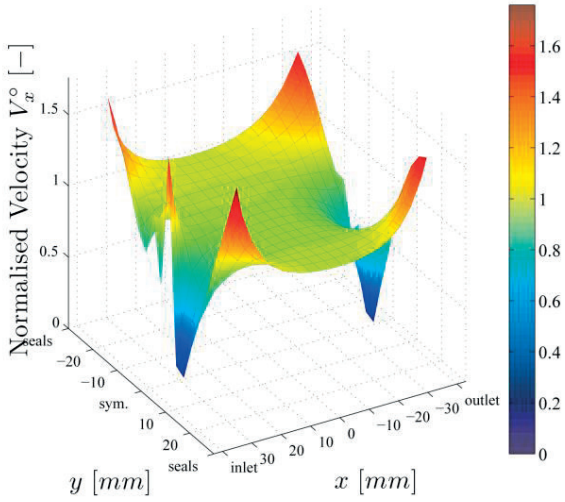

Figure 3.14 Critical situation of asymmetric width of bypasses: thin and obstructed. Conditions: flow only, OCV, $h = 1.0$ mm.

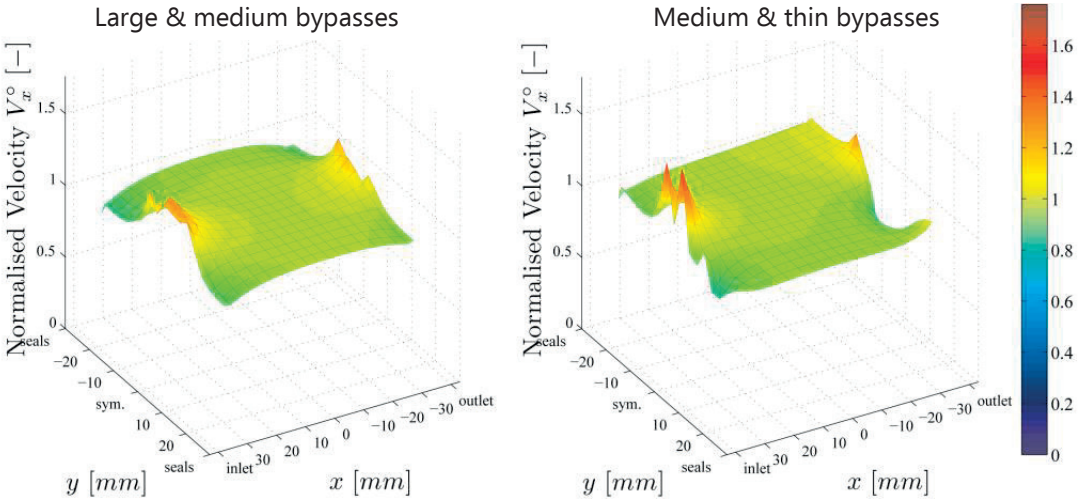

Figure 3.15 Flow deviation [—] in function of the width of the bypass (ideal = 1). Conditions: flow only, OCV, $h = 1.0$ mm.

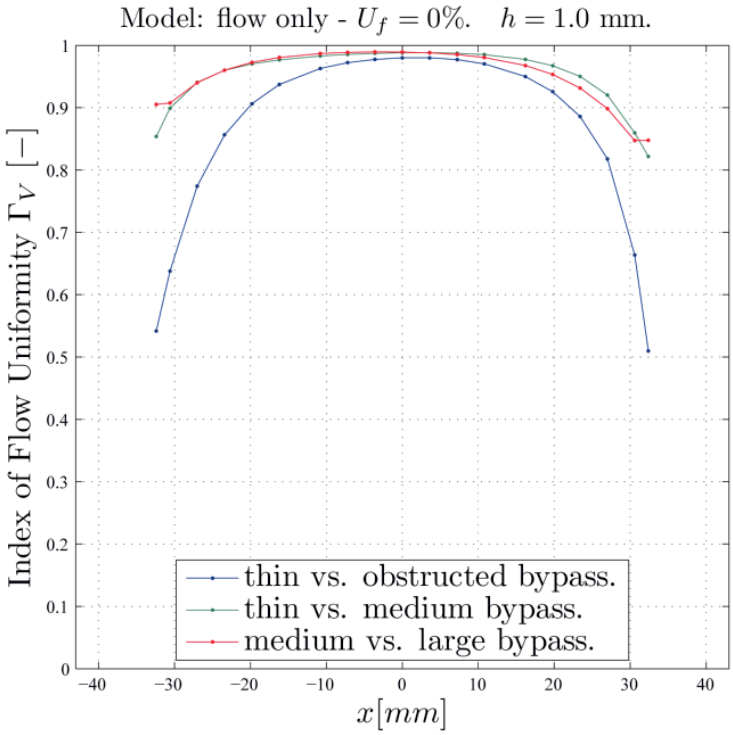

Figure 3.16 Index of flow uniformity [—] along the length of the cell with the width of the asymmetric bypasses as parameter (ideal index = 1).

Variability of the height of the pattern

Another issue happened with the previous design. At ca. 70 mbar, the pressure drops measured with a new pattern were out of specifications. Measurements of the height of the pattern pointed out that it was twice lower than targeted (ca. 0.5 mm instead of ca. 1 mm). Since these measurements were post-operation, it is however uncertain whether they correspond to operating conditions. A CFD simulation for $h = 0.5$ mm indeed predicts a pressure drop of 70.1 mbar, which is in agreement with the experimentally recorded value. We could therefore confirm with confidence that the low height measured corresponds to operating conditions, and that it was the cause of the large pressure drop. The design was correspondingly adjusted to make sure that the height of the pattern is close to 1.0 mm.

Table 3.2 Global pressure drop between inlet and outlet for the nominal height of the pattern (1.0 mm), and for the measured height (0.5 mm).

Height of pattern [mm]	Pressure drop [mbar]
0.5	70
1.0	15

Conclusions

The way the sealing paste is spread has a strong impact on the air distribution and pressure drops. The worst situation occurs when the sealing paste obstructs the bypass between the FDP and the sealing paste. In that case, the midline of the cell near both the inlet and the outlet is very poorly supplied with oxygen. Besides, the distribution of the flow is particularly inhomogeneous in such a situation. Another important point to stress regarding the spread of the paste is the risk of asymmetry, to which the distribution is very sensitive.

If a symmetric medium bypass is ensured, then distribution is better and total pressure drop is acceptable.

It should be stressed that even if simulations show better results with a larger bypass, they are not optimal at all. An important matter to keep in mind is that the real seal deposition is likely to have a less regular form than the geometry assumed here.

Hence, the control over the application and the spread of the paste is a critical point. If the process is not mastered, then the distribution of the flow and the reliability of the stack cannot be mastered.

Recommendations to our industrial manufacturing partner

We could give three main guidelines:

- It must be ensured that bypasses are large enough and as symmetric as possible.
- Pressure drops are more sensitive to the width of bypasses than to the orientation of the pattern.
- The air distribution within the element and within the stack is sensitive to the spread of sealing paste. The control and quality of the process is thus essential for a satisfactory stack operation.

3.7 Challenges to solve for this thesis

3.7.1 Generalities

Solving such a problem meets several challenges, of various nature. We discuss:

(1) the obstacles that make an exclusively experimental approach inadequate.

   (a) Measurements of the flow distribution (response);

(b) Measurements of the actual geometrical dimensions (input);

⇨ Both in a stochastic framework, i.e., accounting for variability.

(2) the main difficulties with an approach using numerical simulations.

General issues:

(a) Nonlinearity of the phenomena, i.e., nonlinear effects of factors on responses.

(b) Interplay of phenomena at different length-scales (and time-scales), e.g. about fluid flow, electrochemistry, heat transfer, etc.

(c) High dimensionality in many ways:

- parameters (e.g., operating conditions, different scenarios);
- decision variables;
- uncertain variables, including sampling of their distribution;
- spatial dimensions;
- discretization;
- many channels (or elements of a pattern) in an elementary cell;
- many elementary cells in a stack;

⇨ ***Combinatorial explosion*** of some variables (so-called ***curse of dimensionality***).

(d) Discrete variables potentially needed in the optimization.

(e) Inaccessible or insufficient information by experimental measurements.

3.7.2 Challenges in the experimental framework

It was clear from the beginning that, although we planned to focus on a numerical study, any experimental result that could support our work would be beneficial. Therefore, we searched whether there exist experimental ways to:

(i) either completely replace the need for computerized experiments for the uncertainty quantification of a specific design;

(ii) or *validate the statistical model* (characterization of the input uncertainties and convergence of their propagation to an accurate PDF);

(iii) or at least, *validate*[4] *the modelling of physics* (flow distribution), especially among cells in the stack.

The outcomes of our investigations are that — for the respective purposes (i to iii) — even for a specific (and realistic) design, it is not tractable, or at least particularly challenging, to either take:

(A) measurements of sufficient *accuracy*:

(1) either because the technique is *too intrusive*;

(2) or because it relies on *indirect measurements*, with an associated model intrinsically containing significant uncertainties;

(3) or because the technique does not allow to *cover enough space* of the cell with a desirable resolution (precision);

and/or:

(B) measurements in sufficient *quantity*:

(1) either because of (A.3);

(2) or because the technique cannot be applied on several samples with enough *repeatability* (i.e., sufficient accuracy) for a sound *statistical analysis*;

(3) or because the time and cost for (B.2) make the approach unpractical.

Below, we discuss in more detail the issues related first to the measurement of the flow distribution (output) and then to the measurements of the geometrical dimensions (inputs) .

1. Measurement of the flow distribution (output)

It is particularly difficult, or close to impossible (unpractical), to do a proper validation and especially to get accurate measures of the flow distribution within many (all) channels of an element — not even mentioning a stack, especially in operation; nor repeating measurements on other samples for statistical purposes.

[4] With *validate*, we mean that results *not only looks like reasonable*, but that numerical and experimental results are quantitatively in agreement (i.e., that their interval of confidence largely overlap), while accounting for their respective uncertainties, and that the corresponding level of confidence is acceptable in view of the uncertainty quantification.

Aside from a personal research of potential solutions, extensive discussions with Dr Navid Borhani [58] and Dr Philip Peschke [59] lead to the conclusion that no practical solutions exist in the current state of the art. Addressing this particular problem would have implied an entire thesis according to N. Borhani.

Table 3.3 Advantages and drawbacks of available techniques for direct or indirect measurements of flow uniformity.

Techniques	Advantages	Drawbacks
Particle image velocimetry (e.g., micro-PIV)	☑ Minimal intrusion ☑ High resolution of the flow field (detailed velocity profile which can be integrated to get local flow rates) ☑ Potentially high accuracy	☒ Need transparency: not the actual manufactured pieces, and no functioning fuel cell. ☒ Small "window" at a time, maximum ca. 10 × 10 mm^2. ☒ Need for a dedicated test bench able to shift the measurements elsewhere in a reproducible way. ☒ Channels cannot be tracked simultaneously
Dye-ink or smoke imaging	☒ Intrusion can be controlled, cancelled ☒ Large area covered ☒ Conceptually simple ☒ Easy implementation (for a rough estimate) ☒ No special equipment required ☒ Cheap	☒ Need a transparent top-view ☒ Not trivial to introduce the coloured agent homogeneously in the stream, such as to get accurate measurements. ☒ May not be accurate enough for our purpose
Hot-wire anemometers	☒ Relatively accurate measurement of the flow rate in small geometries	☒ Intrusion increases with reduction of channel's dimensions.

Techniques	Advantages	Drawbacks
		☒ Difficult to implement one in each channel. ☒ Expensive (several hot-wire anemometers) ☒ Need calibration of each.
Change of static pressure	☑ Conceptually simple ☑ Relatively easy implementation in several channels ☑ No special equipment required ☑ Cheap	☒ Intrusive (holes and resulting non-smoothness) ☒ Not accurate enough[5]
Temperature-sensitive liquid crystals with step-change of inflow temperature	☑ Negligible intrusion ☑ Large area covered with ease (200 cm^2 not a problem)	☒ Not accurate enough for our physical problem and our purpose
Infrared imagery with step-change of inflow temperature	☒ Negligible intrusion ☒ Large area covered with ease (200 cm^2 not a problem)	☒ Not accurate enough for our physical problem and our purpose
Coriolis flow-rate metre	☑ Non-intrusive ☑ Accurate	☑ Impossible to implement for the measurement of flow rates in several adjacent paths (channels). ☑ Expensive

[5] This was tried by BELENOS without success, notably due to leakages and too much intrusion.

2. Measurements of the geometrical dimensions (inputs)

To characterize the distribution of the input uncertainties, it is desirable to take measurements of the relevant geometrical dimensions of the FDP. It is relatively easy to collect such data before assembling and using a fuel cell stack. But what is really interesting is to characterize these dimensions *after assembly*, and if possible, *as they are during operation*. This is not a trivial distinction. Unfortunately, neither option is ideal.

The former can be carried out relatively easily and with good accuracy (e.g., with a laser). It is even imaginable to automate the process to collect a large amount of samples in a reasonable time frame. However, plenty of uncertainties remain about how much these data are actually representative of the situation after assembly and in operation. Indeed, assembly can be partly responsible for the variability and/or systematic deviation with respect to the nominal dimensions; the mechanical response of the materials (e.g., bending, crushing, withdrawal of sintering) due to constraints and high temperature[6], is difficult to predict accurately, and can be inhomogeneous; on top of that, the heterogeneities of the contacting or diffusion layers, of the cell, and of the sealing material, can also take part in the variability of the internal dimensions.

The only method that we know, which would allow to characterize the internal dimensions of the stack *during operation*, is x-ray tomography. This technique is however extremely expensive and we lack the experience to state whether it would actually be feasible in that case. The second approach is hence to characterize the dimensions *after assembly and after operation*. The main drawback in this case is that the procedure is intrusive and destructive, with all the associated uncertainties. This approach was nevertheless tried, by cutting the stack transversally. This is the subject of Chapter 7.

Remark: Most of the uncertainties discussed above are epistemic.

3.7.3 Challenges in the computational framework

Size and complexity of the problem

The problem is:

- multi-dimensional in the physical space;
- multi-scale (length-scale);

[6] This applies especially to SOFCs.

- multi-dimensional in terms of number of variables, since it involves uncertain and decision variables.

Here is a simple, rather optimistic estimation of the computation time for an optimization under uncertainty of one specific design, with model and mesh of average "size", assuming, based on previous experience:

(a) 5 hours per simulated operating point (OP) and per core (high-end 2012);

(b) Speed-up ratio ca. 5 from 1 to 8 cores per job (8 cores per OP);

(c) 1 000 stochastic evaluations of OP per set of design variables (SDV);

(d) 10 OPs per SDV (performance map evaluation);

(e) 10 jobs of 8 cores ran simultaneously in the inner loops;

(f) 100 iterations per OUU of SDV (outer loop of OUU algorithm).

Sun-clock duration $= (5\ [\mathrm{h}]/5) \cdot (1000) \cdot (10/10) \cdot 100 = 10^5\ [\mathrm{h}] > 11$ years, non-stop.

These numbers show that with current computing facilities available at hand, the computing time must be reduced at least by a factor 100 for this study to be feasible in the context of a thesis.[7]

In addition to duration, temporary data storage may be a bottle-neck if care is not taken to optimize the amount of data… Indeed, total number of simulations in the case above would be 1 million. Even if results are aggregated in a 100 kB file for each simulation, total data would amount to 100 GB per study.

Last but not least, a major limitation is the number of licenses of proprietary software that can be accessed simultaneously. In fact, this limitation determines the methods and models that can be used.

[7] Not to mention the fact that exploitation of HPC clusters' rarely exceed 5 years.

1. Example of sizes of computer-models and respective computation time

Table 3.4 gives an insight of the computing effort necessary to solve various kinds of simulated cases. Note that the cases cannot be compared one-to-one, because they were not all run under the same conditions or to achieve the same precision (different modelling, geometries, discretization, computer, etc.). All the computation times correspond to a simulation ran on 4 cores, but not always on the same machine. Even so, we believe it can serve to clarify some order of magnitude.

Table 8.3 gives further insight of the particularly large computing effort, which was necessary for the study described later in Chapter 8.

Figure 3.17 shows that the scalability is not linear, i.e. not perfect, for a typical CFD simulation corresponding to our problem ran on several cores (HPC cluster *Pleiades 2a* in this case). Indeed, on a single core, the simulation takes ca. 50 min, while it takes ca. 8 min on 16 cores, instead of ca. 3 if it would scale linearly.

Table 3.4 Computing effort for various kinds of simulated cases.
The computation times indicated correspond to one single evaluation of the model (i.e., one set of parameters).

Cases	ID	Dim.	Repeated divisions[1]	x	y	z	Mesh cells[2]	Mesh density	Time
		—	—	mm	mm	cells	kilo	cells/mm^2	min
half fuel cell with pins	C1	2D	1 000	150	35	1	550	105	40
full element (Chapter 5, SA)	C2	3D	1	81	2	40	120	19	1.5
section of element w/ coolant, PEFC	C3	3D	7	230	9	30	685	11	150
fuel flow (Chapter 8, UQ)	C4	3D	12	65	41	11	500	17	20
fuel flow (constriction)	C5	3D	20	24	41	10	280	28	2
air flow 80-cells stack	C6	2D	80	85	205	1	1 800	103	75
air flow 3D	C7	3D	64	80	90	10	1 500	21	15
air flow 2D	C8	2D	64	80	90	1	230	32	3
air flow full channels	C9	2D	64	70	90	1	830	10	20

[1] Number of divisions in the geometry which are repeated, such as pins, channels, or elements. The total number of mesh cells which are necessary to get accurate enough results typically increases with the number of divisions along a constant dimension.

[2] Rounded to the nearest 5 000.

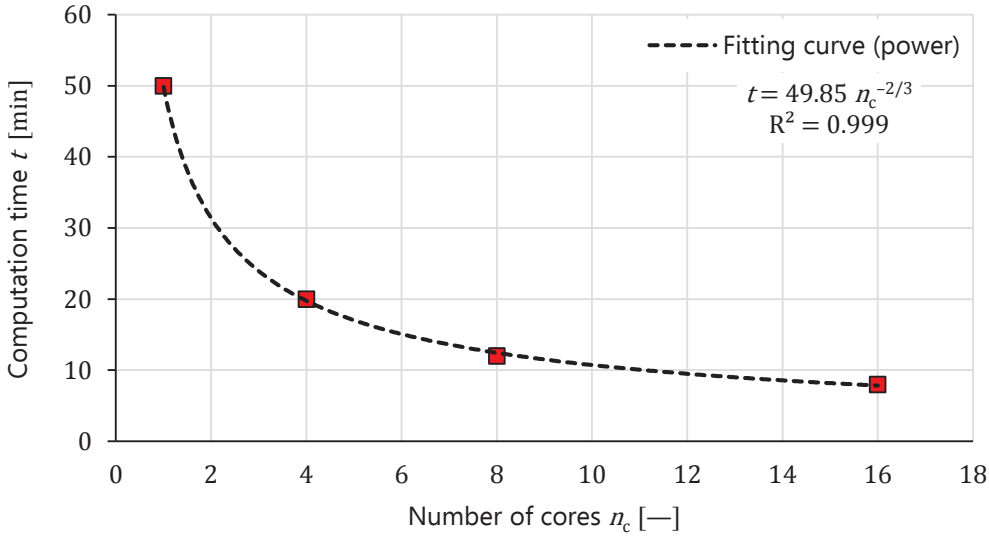

Figure 3.17 Scalability of a typical simulation: computation time versus number of cores. Case of 3D fuel flow used for UQ study, 500 000 mesh cells. Uncertainty on time is 1 min (size of the square marks).

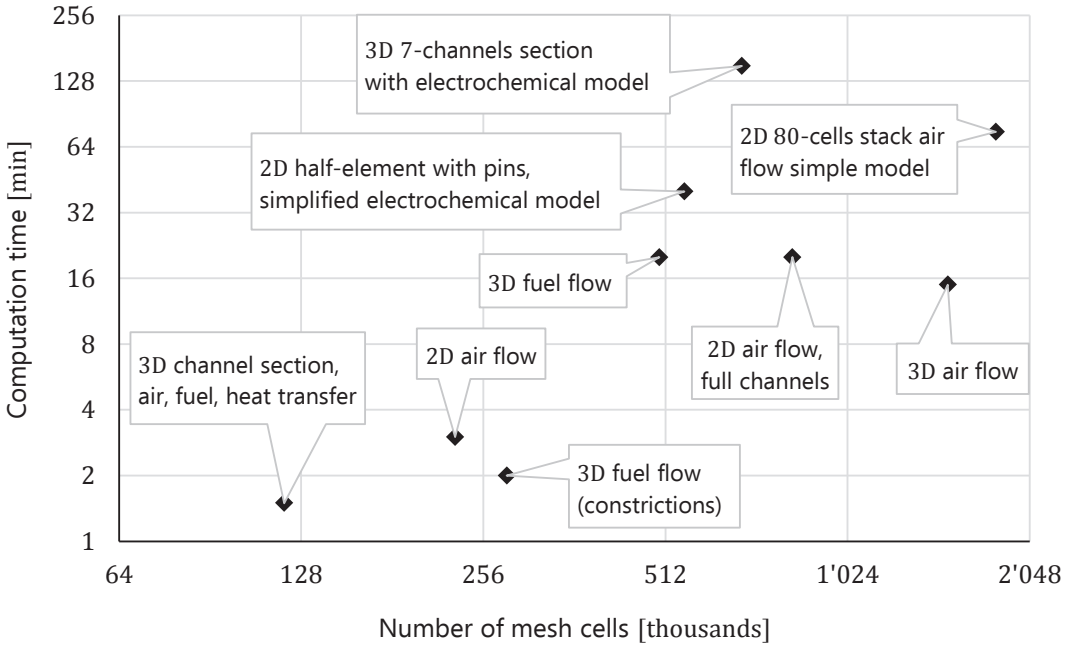

Figure 3.18 Computation time versus the number of mesh cells for various cases.

2. Available computer resources

Table 3.5 Characteristics of the computer resources available during our research.

Characteristic	Laptop	Desktop	Pleiades 2a	Pleiades 2b	Bellatrix
Date of service	2010-2016	8.2013-2019	2005-2012	2006-2012	2013-2017
Kind	Laptop	Desktop		HPC clusters	
Computer model	Dell Precision M4400	Own assembly	Dell PE1425	Dell PE1950 & Fujitsu-Siemens RX200	Dell/ Serviware
Nodes	1	1	120	210	424
Sockets/node	1	1	1	2	2
Cores/socket	2	6	1	2	8
Total cores	2	6	120	840	6 784
Model of processor	Intel Mobile T9600	Intel i7 3930K	Intel Xeon EM64T LV	Intel Xeon 5150	Intel Xeon E5-2660
Clock [GHz]	2.8	3.2 (3.8)[1]	2.8	2.67	2.2
L2 cache, kB/core	3 072	256	1 024	2 048	256
L3 cache MB/socket	—	12	—	—	20
RAM/core [GB]	2	10.7	4	2	2
RAM/node [GB]	4	64	4	8	32
RAM peak bandwidth per node [GB/s]	6.4 DDR2-800	68.3 DDR3-2133	6.4 DDR2-400	21.3 DDR2-667	102.4 DDR3-1600
Inter-connectivity	—	—	Gigabit Ethernet switch 432 Gbit/s		InfiniBand QDR 2:1
Peak Gflop/s per core	11.2	25.6	5.6	5.34	17.6
Global peak Tflop/s	0.0112	0.1536	0.672	4.4856	119

[1] Overclocked CPU.

3. Available software licences

There were 50 *shared* ANSYS FLUENT software licences made available to the EPFL's collaborators. This puts a boundary on the maximum number of simulations that can be ran simultaneously: in practical terms[2] around 6 during working hours and usually 10 to 20 otherwise.

4. Other potential challenges with computing resources

The following aspects are not as such the subject of this thesis. However, anyone involved in a similar adventure should not underestimate their importance, because they are, by the very nature of such work, also at the core of it.

Software licenses: Their number puts a limit on the number of simultaneous runs that are possible. Expensive proprietary software is therefore not the best option if a sound alternative exists.

Software compatibility:

– related to interfacing of software (with some proprietary software, some data may not be accessible, or not in an adequate form)

– related to operating system: multi-platform software are advantageous. Indeed, while HPC clusters run almost exclusively on LINUX nowadays[3], a workstation is however necessary to prepare and test the cases, where MICROSOFT WINDOWS is still the "only" adequate choice for using some CAD software such as CATIA or SOLIDWORKS (DASSAULT SYSTEMS).

Architecture/organization: All HPC clusters can compute, but not all are appropriate depending on the "structure" of the problem. What are its limits, e.g., on the file system / file exchange / disk read/write speed; queues.

Reliability: HPC clusters happen to fail and need maintenance. The frequency of these failures and of these lacks of availability must be taken into account. A direct consequence is that the code should save the data regularly, and organized in a way such that a computation can be resumed from a "checkpoint" if necessary. Besides, it should be noted that the operating lifetime of the HPC

[2] We wrote a script whose goal is to run as many simulations in parallel as possible, *while ensuring that at least five new users can request a license* at the time of deciding whether to launch a new one or wait. Otherwise, our automatic program would take all remaining licences, e.g. for Monte Carlo simulations, progressively blocking access to everyone else.

[3] Linux was used on 92 % of the top 500 super-computers as of June 2010 (almost 98 % in June 2015). Source: http://www.top500.org/statistics/details/osfam/1

cluster is usually no more than 4 years.
Management of disk space.

Technical issues: the "ubiquitous" need for debugging, scripting, interfacing, … of computer codes.

3.7.4 Reduction of the computing effort

Reduction of computing efforts must be of at least a factor 100, as stated above. To achieve this target, it is necessary to act on every lever available. Namely, to implement efficiently: (1) model, (2) uncertainty quantification, (3) model evaluation of objective function, and (4) design optimization algorithm. Item (1) includes the level of modelling for the physics of the fuel cell, but also the models used for the uncertainties.

The third stage was underestimated: computing the objective function from the results of one simulation is usually a quick straightforward algebraic calculation. Yet, the idea here is to evaluate the quality (in a general sense) of a product. The question raised is: should the whole operating map be evaluated to quantify the quality? For each candidate design and each perturbation? In case the answer is yes, the number of simulations increases substantially. Therefore, a practical method must be found for the evaluation of the objective function.

Taking the most out of HPC resources available is of course not negligible either.

Item:

(1) is parallelizable but not well scalable (single simulations based on discretized models);

(2) is parallelizable as long as stochastic variables are assumed independent and a suitable method is used to construct the estimator (no classic online update);

(3) is fully scalable, relying on independent operating points for the creation of a performance map;

(4) is parallelizable in a certain extent, e.g., if classical gradient-based optimization methods are not used (the gradients of recent implementation of *fmincon* for instance can be evaluated in parallel, but the algorithm still iterates sequentially).

It is important here to distinguish the two main stages of an OUU, namely item 2), nested into item 4). Both are computationally intensive and hence the best method should be chosen to minimize run-time. Efforts to minimize computing time of 2) are especially beneficial since it is nested into 3), itself nested into 4). Same reasoning is

also true for 1). Care should nevertheless be taken when reducing model complexity since it is at the core of accuracy (validity).

Domain spaces of 2) to 4) must be covered to ensure the confidence in the solution (global picture). The resulting total, multi-dimensional search space, is huge. The search space for continuous variables is infinite in essence…; the required precision (discretization) and the sensitivity of the responses to input changes ultimately determine the number of evaluations necessary. The domain space of 2) is usually quite large in essence because it is usually necessary to sample from probability distribution functions to get the pdf of the outputs. Domain space of 3) is constrained and can be restricted to the region known to be of interest, leading to high reduction potential. Search space for the design variables (4) may be rather large, even if it is constrained, because of nonlinearities. It would be even more complicated if some design variables are discrete (either on a continuous support, or not, i.e., either Boolean or nominal (representing a category)).

3.7.5 Uncertainties associated to models

We could have called this section “the paradox of UQ”, or the “dilemma of this thesis”.

Uncertainties associated to models have as consequence that performing an optimization under uncertainty is only reasonable if their impact on the (optimal) solution is less than for other kinds of uncertainty — from one order of magnitude at least. The best would be, of course, to carry out an optimization considering each potential design-, operating-, uncertain- … variable. Nevertheless, some decisions must be taken since computation time is already considerable in OUU, as seen before.

Following this observation, the idea is to consider modelling uncertainty as a constraint for reducing the model complexity such that computation is feasible, while providing accuracy with one order of magnitude better than influences of other uncertainties. In a sense, it means solving a multi-objective optimization problem where model “complexity” is minimized and accuracy maximized (optimal model “complexity”).

The problem might also be taken the other way round, and wait for HPC evolution, which is fast: i.e., carry out OUU taking into account model uncertainties and neglecting all others. The advantage of this approach is that simplistic models could be considered, drastically reducing the computational effort. Nonetheless, it raises the question of how sound the solutions may be. Indeed, with such an approach, model uncertainties may well restrict the robust design to domains less worthwhile than current practical solutions (already proven functional by experience or common sense).

To sum up, availability of more powerful computing facilities might be waited for; or, evolution of HPC could be anticipated and hence, methodology could be developed and implemented such that software and protocols are ready when adequate hardware is available. The second choice sounds reasonable, since a PhD thesis is supposed to cover a subject that is original and in advance with respect to industry standard and at the edge of state-of-the-art.

In any case, the goal of this thesis is first to develop and implement a methodology for OUU applied to fuel cells.

3.7.6 Tracks to come to a tractable solution

As was discussed, it is necessary to act on all the available levers to be able to solve such a problem.

The elements (letters) below correspond to the one in § 3.7.3, p. 74.

(a) The model should be as quick to compute as possible. However, its accuracy is also important, such as to provide usable results. So it should be "efficient", in terms of runtime over accuracy.

(b) Take advantage of the computing power as efficiently as possible: code well scalable and parallelizable.

(c) The uncertainty quantification method should be as efficient as possible.

(d) The quality of the design can be assessed thoughtfully with as few evaluations of the model as possible (operating conditions).

(e) Similar as (b), but in addition to parallelizable, manage to get access to enough computing resources (hardware/license of software).

(f) The optimization algorithm should be as efficient as possible.

It should be noted that the whole problem can also be made quicker to solve by reducing its scope. That is, for instance, not only the model can use a coarser discretization or a rougher approximation to compute the local current density in each channel of each cell of a stack, but also, one could judge unnecessary (or not worthwhile) to compute the current density at this level of detail, or to even compute it at all. Similarly, the number of uncertain and decision- variables, as well as the complexity of the objective function, can be reduced. When using a simpler, less accurate, model (function), a point exists when not using it makes more sense and can actually lead to better decision (if otherwise they would be misguided).

Let's make a new estimation, assuming that the time-contribution of points (a), (c), (d), and (f) can all be divided by 5 on average:

Sun-clock duration $= (1\ [\mathrm{h}]/5) \cdot (200) \cdot (2/10) \cdot 20 = 160\ \mathrm{h}$, which is close to a full week of non-stop computation. This is much more reasonable than 11 years.

One of the difficulties arises from the fact that some variables associated to the geometry are both decision variables (optimization) and uncertain variables (uncertainty quantification). This complicates the problem essentially for the following reasons:

(1) Geometry is the first building block of the problem, so that every step should be updated in a way or another (more work for the engineer and for the computer).

(2) Parametrization of geometry can be challenging, especially if one wishes to keep a low number of variables and to avoid absurd situations (with constraints). Besides, it may lead to discontinuities (singularities) in the mathematical problem.

(3) Meshes of good quality are determinant for the quality of the results; the solver may not converge with a poor mesh. So, meshes must be carefully parameterized, too.

(4) Changes in topology are especially difficult to deal with automatically.

(5) The domain of the computation changes.

"Essentially, all models are wrong,
but some models are useful."
George E. P. Box

CHAPTER 4

Modelling approaches

The objective of this chapter is to describe the main modelling approaches considered in this thesis. We first enumerate the most basic elements.

4.1 Existing software (packages)

The list of software below is not exhaustive, but it covers a selection of computer programs, which provide at least some of the necessary qualities to address our problem.

Modelling, CFD especially

- ANSYS FLUENT (CFX)
- COMSOL
- STARCD, STARCCM
- NUMECA
- OPENFOAM

Geometry and meshing

- ANSYS Mesher
- ANSYS ICEMCFD
- TRELIS (as replacement for GAMBIT) /

Analyses *(DACE, RSM, SSA, Optimization, etc.)*

- ANSYS DESIGNXPLORER
- MATLAB

- DAKOTA
- DYNARDO OPTISLANG
- MODEFRONTIER
- GPROMS (PSE) → equation solver, focus on both modelling and analyses

Rationale for the choice of software or code

The criteria were: functionality, price, documentation, parallelizable/ HPC, operating system, open-source (i.e., possible to see how it works, and potentially modify/add code), and of course, previous experience.

GPROMS can be interfaced with ANSYS CFD and with MATLAB. A fuel cell module exists, but after discussion with Dr Pieter Schmal [60] (Head Academic office at PSE), it cannot be licenced to academic institutions because it includes proprietary information.

Given our experience with FLUENT, it was natural to keep this choice for CFD modelling, despite the changes not always being absent of bugs since ANSYS bought it. COMSOL could have been an interesting choice, given a rather flexible licence policy (to run cases in parallel), new users in our research group, tight coupling with MATLAB, and a relatively nice equation editor. However, when it comes to complex 3D geometries of industrial designs, COMSOL is usually recognised as weaker than ANSYS (at least at that time). For instance, it would probably have been convenient for the geometries considered in Chapter 9, but less so for those deformed in Chapter 8 and even less for some studies performed for our industrial partners.

OPENFOAM certainly has two advantages : open-source and free of charge. We believed however that the experience built on FLUENT — also from previous researchers in the group — and the relatively large amount of licences at EPFL were in favour of FLUENT.

ANSYS decided to stop licencing GAMBIT; but we met a lot of trouble with the new ANSYS software for pre-processing. So, we switched to ICEMCFD and TRELIS for meshing. Regarding analyses, ANSYS DESIGNXPLORER helped a bit, but it is currently slow and "buggy", so we preferred to rely on MATLAB and DAKOTA for the management of the analyses. OPTISLANG (coupled with ANSYS) would probably have been a good alternative. However, at that moment, our group was not yet involved in the project "PROSOFC" with the company selling it (DYNARDO), so the licences and proprietary nature of the software were the factors to discard it (temporarily).

4.2 Pre-processing aspects of CFD

4.2.1 Geometry

When we study a geometry of our industrial partners:

The geometry used in the CFD code is exported in STEP format from 3D drawings of the product (either from CATIA or SOLIDWORKS, CAD software). After importation in the meshing tool, they are then simplified and re-parameterized as necessary depending on the study. Both of these procedures often involve lots of reconstruction.

Otherwise:

The geometry is created and parameterized from scratch in the meshing tool, as needed.

4.2.2 Meshing

To get as accurate a solution as possible, the quality of the mesh of the calculation-domain represented by the geometry should be as high as possible. Some common indicators are:

- Local resolution of the mesh (discretization)
- Gradient of sizes of the mesh cells
- Aspect ratio
- Skewness (ESS, EAS)

It is not trivial to parameterize the mesh, such that when updating the parameters of the geometry, the quality of the updated mesh is kept sufficient. This is however critical in the frame of building a metamodel, performing an uncertainty quantification, or an optimization. Indeed, the time spent on meshing manually each new instance would make such approach intractable.

Typically, (fully) automated meshing techniques (e.g., Delaunay triangulation) use triangular elements, because they work with any geometry and the resulting quality is relatively robust to geometrical changes. However, triangular-based meshes have two major drawbacks:

- For the same discretization error, the number of mesh cells is larger.
- The quality of the mesh is intrinsically lower, especially in boundary layers and where the fluid flows mostly in a rectilinear way (like in channels)

We therefore focused on parameterizing the meshes such as to get quadrangular elements where it is advantageous. Triangular elements were used where they offer better quality (e.g., acute angles, or for transition in complex geometries), and where we did not succeed to parameterize quadrangular-based zones robust to changes of geometrical parameters (triangular elements adapt more easily).

Remark:

When some parameters control the *topology* of a geometry, it is often preferable to construct one parameterized mesh for each topology. In that case, the choice of the corresponding mesh-file is controlled with the topological parameters.

4.3 Modelling of physics – Choice of models

We need a simulator which is as efficient as possible (tractability × accuracy). Therefore, the number of equations and the system that they form should be as simple to solve as possible, whereas still providing the adequate accuracy for the intended purpose. Sometimes, it is possible and beneficial to use algebraic formulations, either analytical expressions or (semi)-empirical correlations. Sometimes, a detailed CFD model (at least as a reference/source) is unavoidable. However, most often it is possible to include some simplifications in the CFD model. Literature data, algebraic formulations (correlations), or our own tests were used to assess where such simplifications can be applied.

For instance, when a flow is fully developed, it is possible, with good accuracy, to reduce the computation of the pressure drop to an algebraic model (0D). The evaluation of the length of the entrance region is therefore necessary to know where the flow is fully developed.

4.3.1 Nature of the fluid flows

We are dealing with internal flows.

1. Laminar versus turbulent flows

This point (1.) is inspired from Incropera et al. [61].

The definition of the Reynolds number for internal flows in a channel is:

$$Re_{D_\mathrm{h}} = \frac{\rho\, u_\mathrm{m}\, D_\mathrm{h}}{\mu} = \frac{u_\mathrm{m}\, D_\mathrm{h}}{\nu} \tag{4.1}$$

with u_m the mean (bulk) velocity of the fluid over the cross-section of the channel and D_h its hydraulic diameter:

$$D_\mathrm{h} = \frac{4\,A}{P} \tag{4.2}$$

with A the area and P the (wetted) perimeter of the cross-section.

In a fully developed flow, the critical Reynolds number corresponding to the *onset* of turbulence is $Re_{D_\mathrm{h},\,\mathrm{c}} \approx 2\,300$. Much larger Reynolds numbers ($Re_{D_\mathrm{h}} \approx 10\,000$) are needed to achieve fully turbulent conditions. The transition to turbulence is likely to begin in the developing boundary layer of the entrance region. For laminar flow ($Re_{D_\mathrm{h}} \lesssim 2\,300$), the hydrodynamic entry length may be obtained from an expression of the form [1]

$$x_{\mathrm{fd,\,h,\,lam}} \approx 0.05\, Re_D\, D_\mathrm{h}$$

This expression is based on the presumption that fluid enters the tube from a rounded converging nozzle and is hence characterized by a nearly uniform velocity profile at the entrance. Although no satisfactory general expression exists for the entry length in turbulent flow, we know that it is approximately independent of the Reynolds number and that, as a first approximation [2],

$$10 \lesssim x_{\mathrm{fd,\,h,\,turb}} \lesssim 60\, D_\mathrm{h}$$

For the purposes of this text, we shall assume fully developed turbulent flow for $(x/D_\mathrm{h}) > 10$.

The mean velocity of an internal flow is defined as the velocity linked to the mass flow rate:

$$\dot{m} = \rho\, \dot{V} = \rho\, u_\mathrm{m}\, A_\perp \tag{4.3}$$

2. Entrance of fully developed regions (thermally, hydrodynamically)

The extent of the entry region depends on whether the flow is laminar or turbulent. We used usual correlations to estimate it.

3. Incompressible vs. compressible flows

When the speed of the flow tends to zero, any fluid behaves like an incompressible fluid. We therefore use the Mach number to judge whether the flow can be assumed incompressible with minimal loss of accuracy.

$$Ma = \frac{u_\mathrm{m}}{a} = \frac{u_\mathrm{m}}{\sqrt{\gamma\, P/\rho}} = \frac{u_\mathrm{m}}{\sqrt{\gamma\, \mathcal{R}\, T/\widetilde{m}}} \tag{4.4}$$

with the ratio of the specific heats $\gamma = c_P/c_V$.

The rule of thumb is that the error is smaller than 10 % when $Ma < 0.3$.

$$Ma = \frac{u_\mathrm{m}}{a} = \frac{\dot{M}}{\rho\, S}\frac{1}{\sqrt{\gamma\dfrac{P}{\rho}}} = \frac{\dot{M}}{S}\frac{1}{\sqrt{\gamma\, \rho\, P}} \qquad \text{or also:}$$

$$Ma = \frac{\dot{M}}{S}\,\frac{1}{P}\sqrt{\frac{\mathcal{R}\, T}{\gamma\, \widetilde{m}}} \tag{4.5}$$

(pluriatomic ; monoatomic ideal gas)

$\widetilde{m} \in ca.\,[2\,;\,44]$ $\qquad$ (H_2 ; CO_2)

So, the "worst case" (high Mach number) is for low pressure, small molar mass, high temperature, and large mass-flux (variation of $\gamma \in [1.33\,;\,1.67]$ is negligible in comparison). In all cases that we studied, either the Mach number was much lower than 0.3 (usually $Ma < 0.1$), or the design was clearly weak (e.g., bad flow uniformity, bad robustness, large pressure drop).

Remark:

A guideline can be drawn: from the point of view of the uniformity of the flow conditions (their "robustness"), high-speed flows are not desirable. One of the reasons is flow compressibility. So, when designing the fuel cell stack, an eye should be kept on the value of the Mach number. It is relatively easy to achieve this. We will see that other factors should "ring an alarm" before this one (Reynolds number, turbulence, dominance of inertial effects).

Navier-Stokes equations for incompressible[1] flows are:

[1] Which means that effects of compressibility on the flow are neglected (negligible), not that the fluid (e.g., air), is incompressible.

$$\rho \left(\frac{\partial \boldsymbol{u}}{\partial t} + (\boldsymbol{\nabla u}) \cdot \boldsymbol{u} \right) = -\boldsymbol{\nabla} p + \rho \, \boldsymbol{g} + \mu \, \boldsymbol{\nabla^2 u} \tag{4.6}$$

Gravity is neglected since the regime of the flow is forced convection. Furthermore, we are interested in the flow when steady-state is reached, or time-averaged quantities if the flow is intrinsically unsteady.

$$\rho \, (\boldsymbol{\nabla u}) \cdot \boldsymbol{u} = -\boldsymbol{\nabla} p + \mu \, \boldsymbol{\nabla^2 u} \tag{4.7}$$

4. Biphasic vs. monophasic flows

The fluids in SOFCs are gases ($T > 600$ °C). In PEFCs, gases are usually wished saturated in humidity, but liquid water is undesirable (risk of flooding of the cathode). Biphasic flow simulations are notoriously complex and computationally intensive even for "academic problems". Given the context and objectives of this thesis, they would be intractable. We assume that the operating conditions are adjusted adequately, such that gases are saturated in humidity all along the fluid distribution pattern, without significant (effect of) condensation. We are however convinced that this aspect calls for further investigations by the community and is of high interest.

5. Pressure drop

The pressure drop along a channel of length L and hydraulic diameter D_h:

$$\Delta p = f \frac{1}{2} \rho \, u_\mathrm{m}^2 \frac{L}{D_\mathrm{h}} \tag{4.8}$$

The Darcy-Weisbach (or Moody) friction factor f depends on the regime of the flow and on the geometry of the cross-section. For a fully developed laminar flow, it is:

$$f = \frac{c_\mathrm{s}}{Re} \tag{4.9}$$

With c_s a coefficient that depends only on the shape of the cross-section. It is sometimes called the Fanning friction factor.

We rewrite 4.8 with conserved quantities ($\dot{M}$ or $\dot{V}$, depending on the situation). For a fully hydrodynamically-developed laminar flow, the pressure drop along a channel is then:

$$\Delta p = \frac{\mu}{2}\frac{c_s\,L}{D_h^2}\,u_m = \frac{\nu}{2}\frac{c_s\,L}{A\,D_h^2}\,\dot{M} = \frac{\mu}{32}\frac{c_s\,P^2}{A^3}\,L\,\dot{V} \tag{4.10}$$

To fix ideas, $c_s \cong 64$ for circular channels. For rectangular channels, it depends on the ratio *a/b* of the sides. It is 57 for a square and 96 for an infinite or null ratio (asymptotically thin channel, $a \ll b$ or $a \gg b$).

Note that in these conditions, the hydraulic diameter simplifies as follows: square: $D_h = a$; asymptotically thin channel: $D_h = 2a$, with a the smallest side (which is limiting). Obviously, $D_h = d$ for a circular channel.

For fully turbulent flow in a channel of relative roughness e/D:

Colebrook (transcendental expression, implicit in f):

$$\frac{1}{\sqrt{f}} = -2.0\log\left[\frac{e/D}{3.7} + \frac{2.51}{Re_D\sqrt{f}}\right] \tag{4.11}$$

Smooth surface condition ($e/D \rightsquigarrow 0$), Pethukov:

$$f = (0.790\ln[Re_D] - 1.64)^{-2} \quad \text{with} \quad 3\,000 \lesssim Re_D \lesssim 5\times 10^6 \tag{4.12}$$

Churchill, explicit approximation covering laminar and turbulent flow regime:

$$\begin{aligned} f &= 8\left(\left(\frac{8}{Re}\right)^{12} + (A+B)^{-1.5}\right)^{\frac{1}{12}} \\ A &= (2.457\ln[((7/Re)^{0.9} + 0.27\,e/D)^{-1}]\,)^{16} \\ B &= \left(\frac{37530}{Re}\right)^{16} \end{aligned} \tag{4.13}$$

In developed form:

$$f = 8\left(\left(\frac{8}{Re}\right)^{12} + \left\{\left(2.457\ln\left[\left(\left(\frac{7}{Re}\right)^{0.9} + 0.27\frac{e}{D}\right)^{-1}\right]\right)^{16} + \left(\frac{37530}{Re}\right)^{16}\right\}^{-1.5}\right)^{\frac{1}{12}} \tag{4.14}$$

4.3.2 Electrochemistry

The model for the electrochemistry and for the system (balance-of-plant components) is largely inspired from [62] and [63], which are themselves based on [13,15,27,64–66] . Some modifications were made to implement our set of assumptions (e.g., stationary

behaviour) and additional information about the flow. Typically, we replaced the averaged values by approximation of local values. We also implemented the local fuel and air utilization, depending on the flow uniformity that we compute, instead of the global (set) value. Basically, the model relies on an equivalent-circuit approach to compute the cell potential (its components) and the other related quantities [15].

The Butler-Volmer equation is [67]:

$$j = j_0 \left(\exp\left[\frac{\alpha_\mathrm{A}\, \nu_e\, \mathcal{F}}{\mathcal{R}\, T} \left(E - E_\mathrm{eq} \right) \right] - \exp\left[- \frac{\alpha_\mathrm{C}\, \nu_e\, \mathcal{F}}{\mathcal{R}\, T} \left(E - E_\mathrm{eq} \right) \right] \right) \tag{4.15}$$

Where j is the electrode current density [A/m^2], j_0 the exchange current density, E the electrode potential, E_eq the equilibrium potential, α_A and α_C respectively the anodic and cathodic charge transfer coefficient. The activation overpotential can be introduced in (4.15(4.15) according to $\eta_\mathrm{act} = E - E_\mathrm{eq}$.

$$\rho[\mathrm{mix}] = \frac{\widetilde{m}[\mathrm{mix}]\, p_0}{\mathcal{R}\, T} \tag{4.16}$$

$$p^\mathrm{in}[\mathrm{O_2}] = p_0\, n^\mathrm{in}[\mathrm{O_2}] \tag{4.17}$$

$$\dot{N}^\mathrm{in}[\mathrm{H_2}] = \frac{\dot{V}^\mathrm{in}[\mathrm{H_2}]\, \rho[\mathrm{H_2}]}{\widetilde{m}[\mathrm{H_2}]} \tag{4.18}$$

$$\dot{N}^\mathrm{react}[\mathrm{H_2}] = \Upsilon\, \dot{N}^\mathrm{in}[\mathrm{H_2}] \tag{4.19}$$

$$I = \frac{\nu_e\, \mathcal{F}\, \dot{N}^\mathrm{react}[\mathrm{H_2}]}{\mathcal{N}_\mathrm{cells}} \tag{4.20}$$

$$\eta^\mathrm{Nernst} = \frac{\Delta_r \tilde{g}[\mathrm{H_2}]}{\nu_e\, \mathcal{F}} \tag{4.21}$$

$$j = \frac{I}{A_{\text{active}}} \tag{4.22}$$

The overpotential for activation at the cathode is modelled from the Butler-Volmer equation, with the charge transfer coefficients $\alpha_{\text{A \& C}} = 0.5$, which simplifies to [65]:

$$\eta_{\text{C}}^{\text{act}} = \frac{2\mathcal{R}\,T}{\nu_e\,\mathcal{F}}\ \text{asinh}\left[\frac{j}{2\,j_{0,\,\text{C}}}\right] \tag{4.23}$$

with the cathodic exchange current density:

$$j_{0,\,\text{C}} = 2\ \frac{\mathcal{R}\,T}{\mathcal{F}}\ k_{0,\,\text{C}}\ \exp\left[\frac{-E_{\text{C}}^{\text{act}}}{\mathcal{R}\,T}\right] \tag{4.24}$$

The anodic overpotential due to activation is neglected since it is relatively small in comparison to that at the cathode (this may differ depending on the cell technology). The anodic overpotential due to concentration is formulated as [66]:

$$\eta_{A}^{\text{diff}} = -0.5\ \frac{\mathcal{R}\,T}{\mathcal{F}}\ \ln[1 - \Upsilon_{\text{loc}}] \tag{4.25}$$

The overpotential due to concentration at the cathode-side is formulated as:

$$\eta_{\text{C}}^{\text{diff}} = -0.5\ \frac{\mathcal{R}\,T}{\mathcal{F}}\ \ln\left[1 - \frac{\Upsilon_{\text{loc}}}{\lambda_{\text{loc}}}\right] \tag{4.26}$$

The overpotential due to the dissociation of oxygen at the cathode is calculated with:

$$\eta_{\text{C}}^{\text{diss}} = \ R_{0,\,\text{C}}\left(\frac{p^{\text{in}}[\text{O}_2]}{p_0}\right)^{-0.5} j\,\exp\left[\frac{E_{\text{C}}^{\text{diss}}}{\mathcal{R}\,T}\right] \tag{4.27}$$

The ohmic drop related to the electrolyte is modelled as:

$$\eta_{E}^{\text{ionic}} = \frac{j_{\text{tot}}\,h_{\text{E}}}{\sigma_{\text{E}}^{\text{ionic}}} \tag{4.28}$$

with the ionic conductivity of the electrolyte modelled as:

$$\sigma_{\text{E, ionic}} = \sigma_{0,\,\text{E}}\ \exp\left[\frac{-E_{\text{E}}^{\text{act}}}{\mathcal{R}\,T}\right] \tag{4.29}$$

The ohmic drop related to the MIC is modelled with resistors:

$$\eta_{\mathrm{MIC}} = (R_{\mathrm{mic1}} + R_{\mathrm{mic2}})\, I \tag{4.30}$$

The resulting cell potential is given by:

$$\eta^{\mathrm{cell}} = \eta^{\mathrm{Nernst}} - \eta_{\mathrm{C}}^{\mathrm{diss}} - \eta_{\mathrm{C}}^{\mathrm{diff}} - \eta_{\mathrm{C}}^{\mathrm{act}} - \eta_{\mathrm{E}}^{\mathrm{ionic}} - \eta_{\mathrm{A}}^{\mathrm{diff}} \tag{4.31}$$

The electrical power delivered by the stack is hence:

$$P_{\mathrm{el}} = \mathcal{N}_{\mathrm{cells}}\, \eta^{\mathrm{cell}}\, I \tag{4.32}$$

The other quantities of interest follow:

$$sP_{\mathrm{el}} = \frac{P_{\mathrm{el}}}{A_{\mathrm{active}}} \tag{4.33}$$

$$\varepsilon_{\mathrm{V}} = \frac{\eta^{\mathrm{cell}}}{\eta^{\mathrm{Nernst}}} \tag{4.34}$$

$$\varepsilon_{\mathrm{thermo}} = \frac{\Delta_{\mathrm{r}} g[\mathrm{H_2}]}{LHV[\mathrm{H_2}]} \tag{4.35}$$

$$\varepsilon_{\mathrm{I}} = \Upsilon \tag{4.36}$$

$$\varepsilon_{\mathrm{el}} = \varepsilon_{\mathrm{thermo}}\, \varepsilon_{\mathrm{V}}\, \varepsilon_{\mathrm{I}} \tag{4.37}$$

$$\varepsilon_{\mathrm{el}} = \frac{P_{\mathrm{el}}}{\dot{N}^{\mathrm{in}}[\mathrm{H_2}]\, LHV[\mathrm{H_2}]} \tag{4.38}$$

$$P_{\mathrm{blowers}} = \frac{\Delta p[\mathrm{air}]\, \dot{V}^{\mathrm{in}}[\mathrm{air}]}{\varepsilon_{\mathrm{blower}}} \tag{4.39}$$

$$\varepsilon_{\text{sys}} = \frac{\varepsilon_{\text{ACDC}} \left(P_{\text{el}} - P_{\text{blowers}}\right)}{\dot{N}^{\text{in}}[\text{H}_2]\, LHV[\text{H}_2]} \tag{4.40}$$

4.4 Modelling of uncertainties – Choice of models

Several sources of uncertainties can affect the fuel cells. Ideally, all identified uncertainties should be taken into account. To keep the computation tractable, we focused on uncertainties related to the design, rather than the operation, of the fuel cell.

At first, we modelled actual geometrical deformations with function of forms, that we applied to the original geometry (more details in Chapter 8). However, we realized that averaged deformations applied to an entire flow path (channel) are sufficient to characterize the effect on the flow distribution (in our context). Therefore, we strived to rather characterize the uncertainty on the channels by taking measurements on a real stack (more details in Chapter 7). This is important in order to link such average deformations with actual manufacturing tolerances and other production inaccuracies. The idea is to extract a statistical model from the measurements, in order to get a probability distribution function or at least parameters of a theoretical PDF (e.g., Gaussian) fitting well with the empirical one. Note that by taking measurements on a stack after operation, we also directly take into consideration the possible variations due to assembly and operation.

4.5 Surrogate modelling – Choice of technique

4.5.1 Reduced order modelling

Several techniques exist to reduce the size of a problem. It is common in most fields of sciences to analyse a system by neglecting variations in some dimensions, especially in time and space.

We investigated ways to reduce the dimensions of the problem in the context of the flow distribution into fuel cells. The following section deals in particular with fluid dynamics.

1. "Porous media" for modelling hydraulic resistors

It is common to approximate the flow in a rather uniform pattern by implementing an "equivalent porous medium". It has been widely used in fuel cells, with success, including in a study by the author [12,57,68]. We will show hereafter some instances where this technique reaches limitations.

First, we describe several situations and ways where porous media can be beneficial to reduce the requirement in computing resources. Mathematical models are discussed further. It is not an exhaustive list, but shows the main idea with a dummy model condensing typical usages (see figure 4.1). The geometry of a fluid distribution pattern may contain channels, staggered pins of various shapes, interrupted channels, steps or other sudden changes in direction. Some other elements will be discussed later and are not shown here.

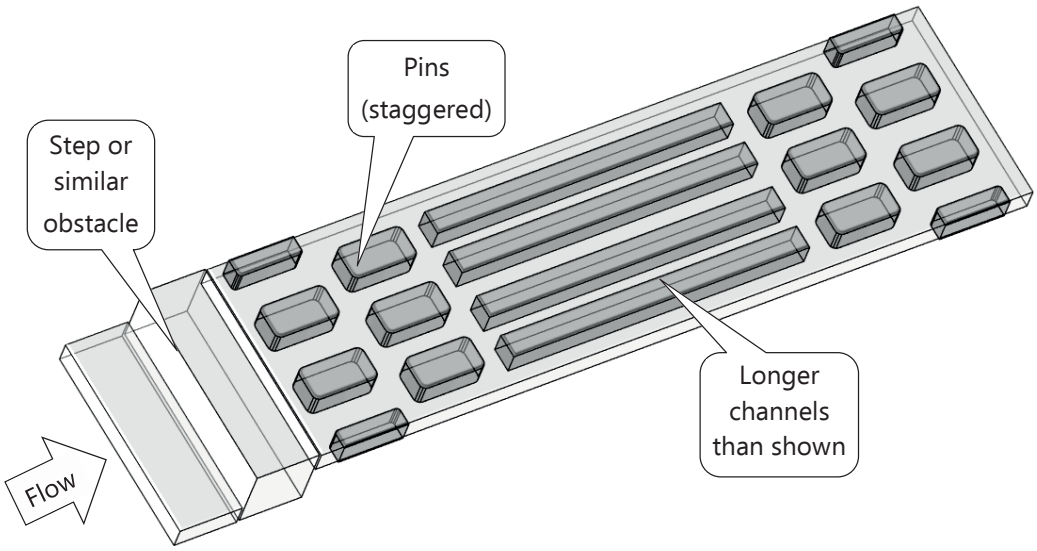

Figure 4.1 Scheme of some typical elements which can form part of a 3D model of a fluid distribution pattern (dimensions and position for illustration only).

When meshing a geometry for CFD applications, it is common and good practice to "clean" the CAD geometry from small features which would otherwise prevent the creation of a mesh of good quality, especially when these features do not impact the flow significantly (i.e., less than the loss of accuracy due to a poor mesh/solution). The modifications discussed here go further.

The large difference of the characteristic dimensions in the geometry often leads to unnecessary large number of mesh cells to keep a mesh of good quality (e.g., small

such as space between pins, cross sections of channels, versus big such as length of channels, manifolds, and plenums). Figure 4.2 schematizes some simplifications that can be implemented for the model in figure 4.1. Long uninterrupted channels, where the flow is fully developed, can be replaced by a 1D porous interface having the same hydraulic resistance. A large, homogeneous pattern of pins (staggered or not) can be replaced by a homogeneous porous medium (3D), with anisotropic resistances if necessary. A simple step or obstacle to the flow can be replaced by a porous medium tuned to provide an equivalent resistance (in an adequate range of flow rate). Note that in this example, the step does not imply any difficulty to get a mesh of quality since the geometry is basic. It was however useful as a last resort in a couple of situations.

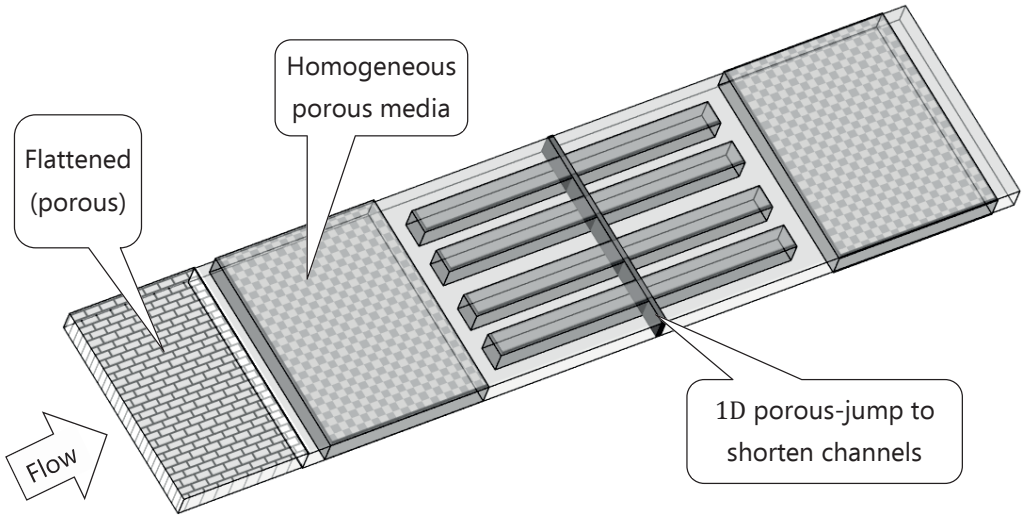

Figure 4.2 Example of use of artificial porous media to simplify a 3D model. Basically, they are helpful to reduce the number of mesh elements and sometimes to improve the quality of the mesh. Both allow a lower computation time and a better convergence (more precision)[2].

The aforementioned simplifications can save many mesh cells, many poor quality mesh cells, and therefore many hours of computation and of engineering (drawing and meshing). Still, planar fuel cells are made of essentially "flat" geometries (apart from the manifold of a stack). So, it is reasonable to consider sparing that extra third dimension (vertical, *z*), usually involving at least ca. 10 layers of mesh cells per flow domain, and some computation overhead due to the coupling.

[2] Precision may be increased this way, but in principle such artifice leads to lower accuracy.

Figure 4.3 shows some further simplifications that can be implemented to convert a 3D model in a 2D model, *but correcting it for the lacking dimension*. The 1D porous-jump is unchanged. The main difference is the introduction of finite permeabilities in the domain wherever the height (3rd dimension) is small, which is basically everywhere in fuel cells. Indeed, resistance to flow due to that dimension is only negligible when it is much smaller than the other dimension of the cross section (asymptotic case of a flow between infinite parallel planes).

Note that in 2D, it may be beneficial to keep geometric features such as pins, since computing resources are already significantly spared by removing one dimension.

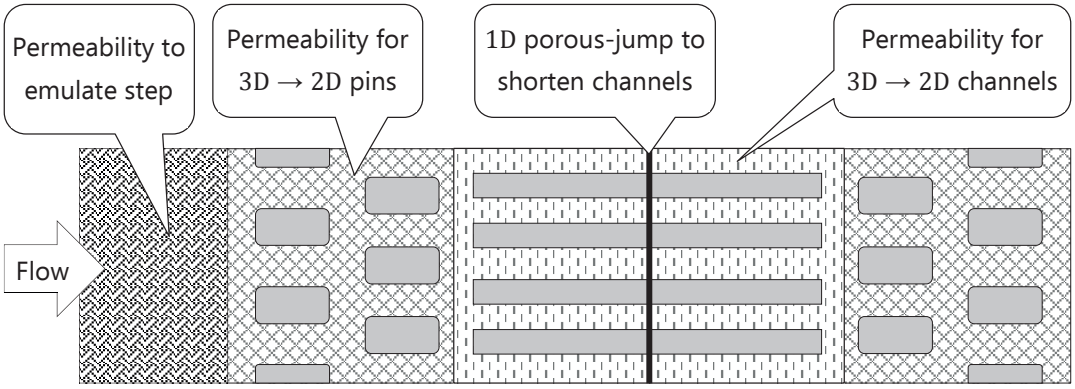

Figure 4.3 Example of use of artificial porous media to further simplify a 3D model into a 2D model. The idea is similar than for figure 4.2. However, the necessary values of (im)permeability are different (except for 1D porous-jump).

Basis to all corrections

The basic idea for each of these corrections is to use the law of Darcy for porous media:

$$\dot{V} = \frac{\kappa}{\mu} S \frac{|\Delta p|}{L} \tag{4.41}$$

With κ $[m^2]$ the permeability of the porous medium. This law can be written locally in terms of the velocity and of the gradient of pressure.

$$\boldsymbol{\nabla} p = -\frac{\mu}{\kappa} \boldsymbol{u} \tag{4.42}$$

To model an artificial loss of pressure proportional to velocity, the right-hand term is added to the Navier-Stokes equation. Note that in CFD software, it is usually implemented in a porous domain, but the permeability (or terms of resistance) can be set independently from the porosity, which can stay 1.

2. 3D with porous media and 1D porous-jump

To avoid modelling the flow in long channels (rectilinear) for which a good estimation can be computed with algebraic expressions, so-called *porous-jumps* (to create jumps of pressure) can be used. The idea is to place a surface in the middle of a shorter version of the channel, and attribute it a virtual length and permeability.

A number of considerations should however be cared for:

- This approximation is strictly valid only for fully-developed laminar flows.
- As with other instances of virtual permeability, the profile of velocity is flattened when crossing this surface. The flow must therefore re-develop after it.

The consequences are that the computation of the parameters for these porous-jumps are not straightforward. Usually, we advise to keep a long enough section of channel before the porous-jump, such that the flow can fully develop before reaching it (so that it is not necessary to compensate for the side upstream of the face). The same advice holds for the downstream section, in order to guaranty a fully-developed flow at the end of the channel. Indeed, the distribution and the pressure drop where the flow exits the channel depends significantly on the profile of velocity. Lastly, since the flow must re-develop after the porous-jump, the resulting overall pressure drop is overestimated. In practice, for most of the cases considered, the difference was negligible (< 0.5 %). Otherwise, the difference can be accounted for by casting it into the parameters of the porous-jumps; either by estimating it a priori, or a posteriori.

3. 2D corrected

As said, some authors already used Darcy corrections to adjust a 2D model for the 3D reality. However, to the best of our knowledge, either the situations always satisfy the underlying hypothesis (e.g., thin single serpentine channels), such that no significant disagreement with reality is noticed, or the Darcy corrections are adjusted each time a different situation arises for which no analytical or accurate correlation exists. For our purpose (OUU), it is however not tractable to rely on non-automatic adjustment.

We therefore looked for a generalized expression valid in the situations encountered for our designs, or an automated and quick procedure to identify the values of permeabilities that minimize the disagreement between the 3D model and the 2D model.

Approach based on correlations for the friction factor

J. Dujc et al. at ZHAW proposed the following corrections [69,70] to the 2D steady-state incompressible Navier-Stokes equations:

$$\frac{5}{6}\rho\left((\boldsymbol{\nabla u})\cdot\boldsymbol{u}\right) = -\boldsymbol{\nabla}p + \mu\,\boldsymbol{\nabla^2 u} - \underline{\frac{12\,\mu}{H^2}\,\boldsymbol{u}} \tag{4.43}$$

The density is corrected by a factor $5/6$ and a term following Darcy's law is introduced (underlined). The corresponding permeability is therefore $\kappa = H^2/12$, with H the height of the cross section (the reduced dimension). It therefore assumes that the velocity profile along that dimension is described by a Hagen-Poiseuille flow, i.e. an essentially 2D flow between two infinite parallel planes (figure 4.4).

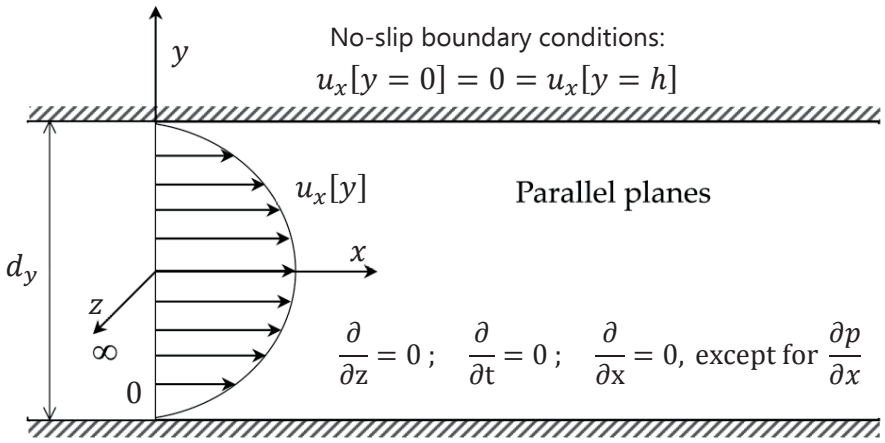

Figure 4.4 Hagen-Poiseuille flow between two parallel planes.

The solution to the Hagen-Poiseuille flow is given by the following equations:

$$u_x[y] = \frac{1}{2\mu}\frac{\mathrm{d}p}{\mathrm{d}x}\left(y\,d_y - y^2\right) \quad ; \quad u_y = 0 \quad ; \quad u_z = 0 \tag{4.44}$$

$$u_\mathrm{b} = \frac{\int_0^{d_y} u[y]\mathrm{d}y}{\int_0^{d_y}\mathrm{d}y} = \cdots = \frac{1}{12\,\mu}\frac{\mathrm{d}p}{\mathrm{d}x}{d_y}^2 \tag{4.45}$$

$$\frac{\mathrm{d}p}{\mathrm{d}x} = \frac{12\mu}{{d_y}^2}\,u_\mathrm{b} \tag{4.46}$$

The correction seems valid and relatively accurate for the cases addressed by Dujc [69]. When $w \gg h$, the resistance induced by the side walls is negligible with respect to the top and bottom walls. Furthermore, in a single serpentine channel, inaccuracies about the resistance to flow have no major consequences: the pressure drop will deviate in same proportion than the resistance; the fluid properties which depend on the pressure of the mixture will only be slightly inaccurate. But the fluid can only flow in that single channel, rather than choose the path of least resistance.

Our applications involve multiple paths for the flow and the condition $w \gg h$ is not satisfied — especially because these dimensions are subject of the optimization, so can potentially vary out of the domain of validity.

We look for a more general correction, which accounts for the parameters of the cross-section, and not only for its height.

Using the expression of the pressure gradient for a laminar, fully developed flow in a channel (3D):

$$\frac{\mathrm{d}p}{\mathrm{d}x} = \frac{c_\mathrm{s}}{Re}\frac{1}{2}\rho\, {u_\mathrm{b}}^2 \frac{1}{D_\mathrm{h}} = \frac{c_\mathrm{s}\,\mu}{2{D_\mathrm{h}}^2}\, u_\mathrm{b} \tag{4.47}$$

For a given channel, our goal is to conserve the gradient of pressure and the bulk velocity:

$$\left.\frac{\mathrm{d}p}{\mathrm{d}x}\right|_{2\mathrm{D}} = \left.\frac{\mathrm{d}p}{\mathrm{d}x}\right|_{3\mathrm{D}} \qquad ; \qquad u_\mathrm{b}|_{2\mathrm{D}} = u_\mathrm{b}|_{3\mathrm{D}} \tag{4.48}$$

Adding a term of dissipation according to Darcy's law to the 2D model:

$$\frac{12\mu}{{d_y}^2} + \frac{\mu}{\kappa} = \frac{c_\mathrm{s}\,\mu}{2{D_\mathrm{h}}^2} \tag{4.49}$$

Which leads the impermeability for the correction:

$$\left.\frac{1}{\kappa}\right|_{2\mathrm{D}\to 3\mathrm{D}} = \frac{c_\mathrm{s}}{2\,{D_\mathrm{h}}^2} - \frac{12}{{d_y}^2} = \cdots = \frac{c_\mathrm{s}\,{d_y}^2 - 24\,{D_\mathrm{h}}^2}{2\left(D_\mathrm{h}\,d_y\right)^2} \tag{4.50}$$

Using the hydraulic diameter for a rectangular channel (or as first approximation for a trapezoidal one):

$$D_\mathrm{h} = \frac{4\,A}{P} = \frac{2\,w\,h}{w+h} \tag{4.51}$$

And noting that to compute the flow in the plane Oxy with a 2D model, then $w \equiv d_y$ and $h \to \infty$, the expression of the impermeability becomes:

$$\frac{1}{\kappa}\Big|_{\mathrm{2D}\to\mathrm{3D}} = \frac{c_\mathrm{s}\, w^2 - 24\, {D_\mathrm{h}}^2}{2\left(D_\mathrm{h}\, w\right)^2} = \cdots = \frac{(w+h)^2\, c_\mathrm{s} - 96\, h^2}{8\, w^2\, h^2} \tag{4.52}$$

Table 4.1 Particular cases of the correcting impermeability.

case	c_s $[-]$	$1/\kappa$ $\left[\mathrm{m}^{-2}\right]$
$w \ll h$	96	0
$w \gg h$	96	$\frac{12}{h^2}$
$w = h$	57	$\frac{16.5}{w^2}$
$d \coloneqq w = h$	64	$\frac{20}{d^2}$

Remark:

It is emphasized that in fuel cells, for good reasons, the height of the channels is usually not bigger than their width. On the contrary, the width is often bigger than the height, to minimize the height of the stacks (and material), the resistance to electric current, and to avoid diffusion-limitation along the vertical gradients of concentration that form with the consumption and production of species at the electrodes. So, we are not in presence of the only case for which an uncorrected 2D approximation is valid.

Test on straight channels of varying dimensions of cross-section

These 2D corrected models were confronted to the 3D case, on straight channels of varying width and height of the cross-section. The length[3] of the channels is 1 metre. The width is varied in the interval $\left[0.2\,;3\right]$ mm and the height in the interval $\left[0.1\,;2\right]$ mm. So, the aspect ratios fall in the interval $[0.1\,;30]$. Latin hypercube sampling was used to cover the space with 100 samples. The simulations were done with ANSYS FLUENT V15. The update of the two extreme points failed (issue with automatic meshing) so they were discarded. The flow rate was chosen low enough to ensure laminar conditions in each case $\left(\max\left[Re_{D_\mathrm{h}}\right] = 130\right)$.

[3] The actual length of the channels are usually about 5 to 10 times shorter. But here we are interested only in the *relative difference* between the models ; we use longer channels in this comparison to easily avoid managing the effects of boundary conditions, which are not the interest here.

Figure 4.5 compares the pressure drop obtained with the 2D corrected models, relative to the 3D case (zero line). The 2D uncorrected model is not represented in this figure, since it underestimates the real pressure drop by as high as 100 %. Figure 4.6 compares all models in absolute terms. Our model (TCO) intersects the model "ZHAW" at an aspect ratio of ca. 4.5. The green curve tends asymptotically to the real case for large aspect ratio, as expected, but is inaccurate otherwise, especially for $W/H < 2$ (up to 14 % underestimation). Our model makes a "wave" shape around the zero line, with a maximum overestimation of ca. 4 % and minimum of ca. 7 %. Overall, the RMSD of our model, 2.4 %, is 3.4 times better than that of ZHAW. However, the interval of interest for our applications is typically bigger than 2 and may go up to 10 or more in areas of distribution (e.g., plenum).

So, we decided to take over the advantages of both model, by merging them, as shown in figure 4.5 (TCO_ZHAW). A conditional statement switches the relation used when $W/H = 4.5$. The RMSD is reduced down to 1.87 %. Besides, the relative difference is kept below 2 % (absolute) for all aspect ratios bigger than ca. 2.

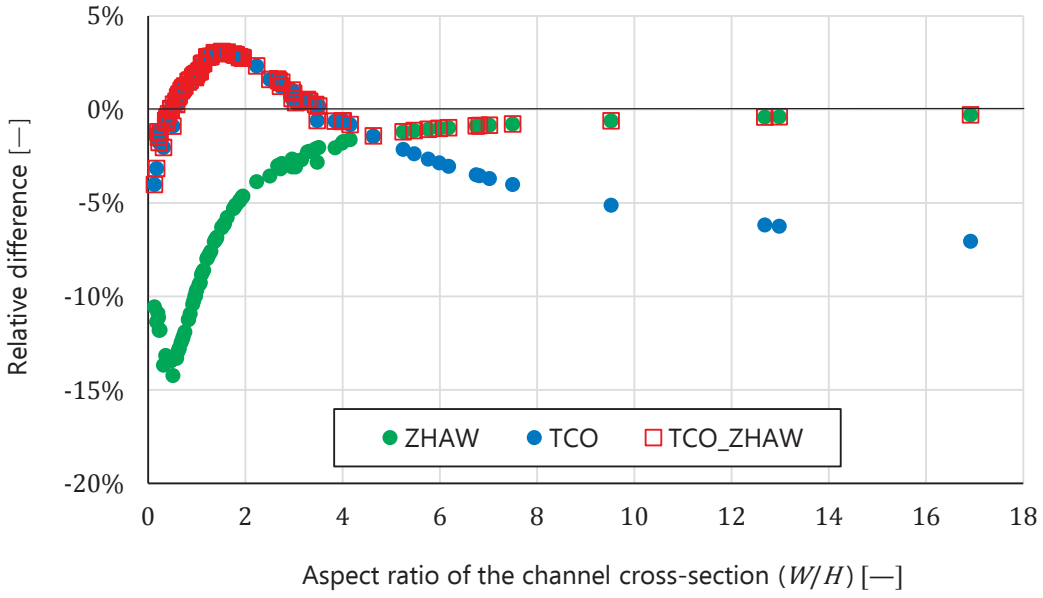

Figure 4.5 Relative difference of the pressure drop obtained with 2D corrected models and 3D values in function of the aspect ratio of the channel cross-section defined as width over height.

Remaining issues

First, the 2D correction, without further fine-tuning, may not be accurate enough for our purpose. Indeed, whereas 2 % difference on the evaluation of the pressure drop (hydraulic resistance) is good, especially for a 2D model, it may cause problem in the uncertainty quantification since it is at the root of the flow distribution.

Second, these results are valid only for straight channels, with a rectangular cross-section and for fully developed flow.

The next section investigates a more accurate and sophisticated approach for the correction of a 2D model. In that section, we will discuss results obtained with both approaches when applied to more complicated geometries.

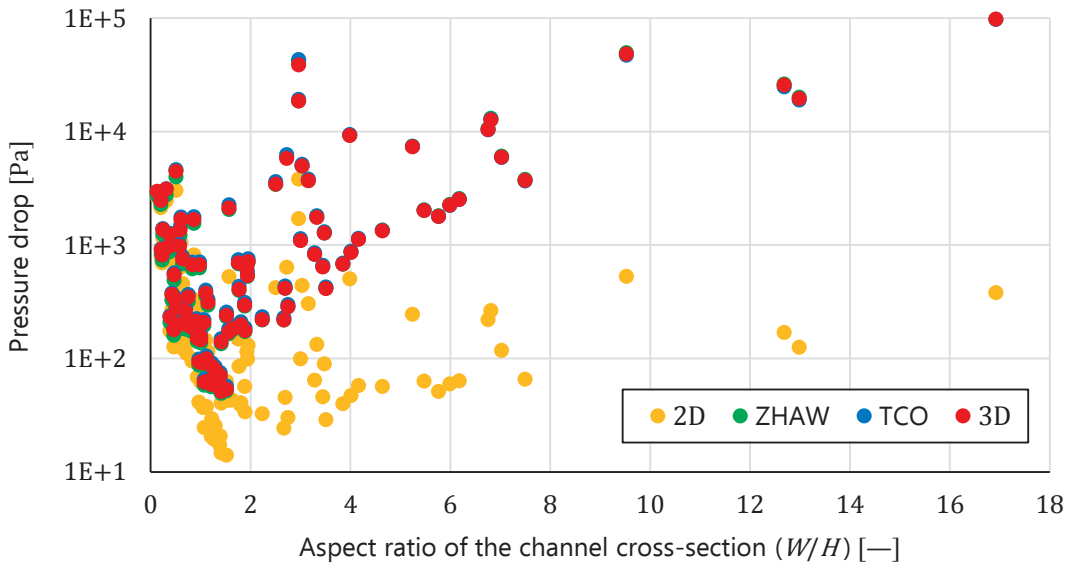

Figure 4.6 Pressure drop in function of the aspect ratio of the channel cross-section. The length of the channel is 1 metre. The data points "2D" correspond to the model without correction.

4.5.2 Analytical approach

1. Flow in a rectangular hollow duct

In general, channels in a fuel cell or other devices with flow distributors have a cross-section which is rectangular or approximately rectangular. Under strong assumptions

(laminar, fully developed flow, with constant properties), an analytical solution to the equations of Navier-Stokes exists for such ducts (e.g., [71,72]). The profile of the longitudinal velocity is given by:

$$u_x[y,z] = \frac{4\,h^2}{\pi^3\,\mu}\,\frac{dp}{dx}\sum_{n,\,\text{odd}}^{\infty}\frac{1}{n^3}\left(1-\frac{\cosh\left[n\,\pi\,\frac{y}{h}\right]}{\cosh\left[n\,\pi\,\frac{w}{2\,h}\right]}\right)\sin\left[n\,\pi\,\frac{z}{h}\right] \tag{4.53}$$

And the gradient of pressure is given by:

$$\left.\frac{dp}{dx}\right|_{3D} = \frac{-12\,\mu\,u_b}{h^2}\left(1-\sum_{n,\,\text{odd}}^{\infty}\frac{1}{n^5}\,\frac{192}{\pi^5}\,\frac{h}{w}\tanh\left[n\,\pi\,\frac{w}{2\,h}\right]\right)^{-1} \tag{4.54}$$

Velocities are naturally zero along coordinates y and z.

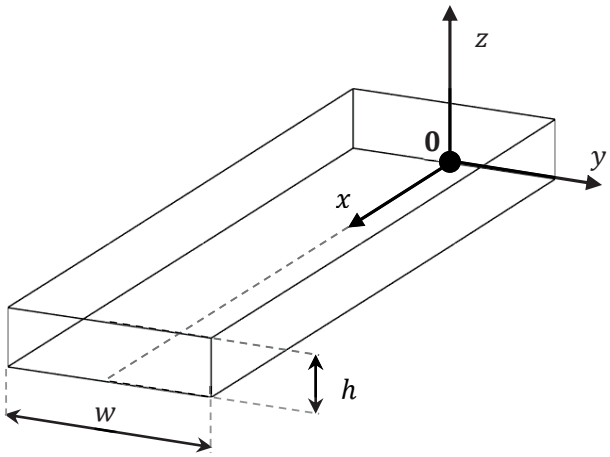

Figure 4.7 Scheme of a straight channel with a rectangular cross-section.
Walls with no-slip velocity condition at: $y = [-w/2\,;\,w/2]$ and $z = [0\,;\,h]$.

To model this flow problem in 2D with a correction from a virtual porous medium (Darcy), the Navier-Stokes equations are solved in 2D with laminar and steady-state conditions. The dimension which is considered infinite in this 2D model is the height[4]. So, the pressure drops due to the top and bottom walls (in reality) are modelled with a virtual permeability. The modified Navier-Stokes equations are again:

[4] We are interested in the distribution of the flow among several channels in the plane Oxy. To get a 2D model in that plane, we therefore need to assume h infinite (top and bottom walls inexistent) even though usually $h < w$ in our cases. The consequences will be discussed further.

$$\rho\,(\boldsymbol{\nabla u})\cdot\boldsymbol{u}-\frac{\mu}{\kappa}\,\boldsymbol{u}=-\boldsymbol{\nabla}p+\mu\,\boldsymbol{\nabla^2 u} \tag{4.55}$$

Shaking a bit the maths of the previous equations and boundary conditions leads to the solution:

$$u_x[y]=\frac{\kappa}{\mu}\,\frac{dp}{dx}\left(\frac{\cosh\left[\frac{y}{\sqrt{\kappa}}\right]}{\cosh\left[\frac{w}{2\sqrt{\kappa}}\right]}-1\right) \tag{4.56}$$

$$\left.\frac{dp}{dx}\right|_{2\mathrm{D}}=\frac{-\mu\,u_\mathrm{b}}{\kappa}\,\frac{1}{\left(1-\frac{2\sqrt{\kappa}}{w}\,\tanh\left[\frac{w}{2\sqrt{\kappa}}\right]\right)} \tag{4.57}$$

The relation between the pressure drop and the bulk velocity is not anymore linear (with slope $-\mu/\kappa$).

We wish to conserve the pressure drop and the bulk velocity between the 3D and 2D models. So, the permeability κ is computed to satisfy both conditions. The resulting transcendental equation is solved numerically. Note that κ depends only on the geometric dimensions of the duct's cross-section. So, we could imagine to use it as an alias to model variabilities of the height (third dimension).

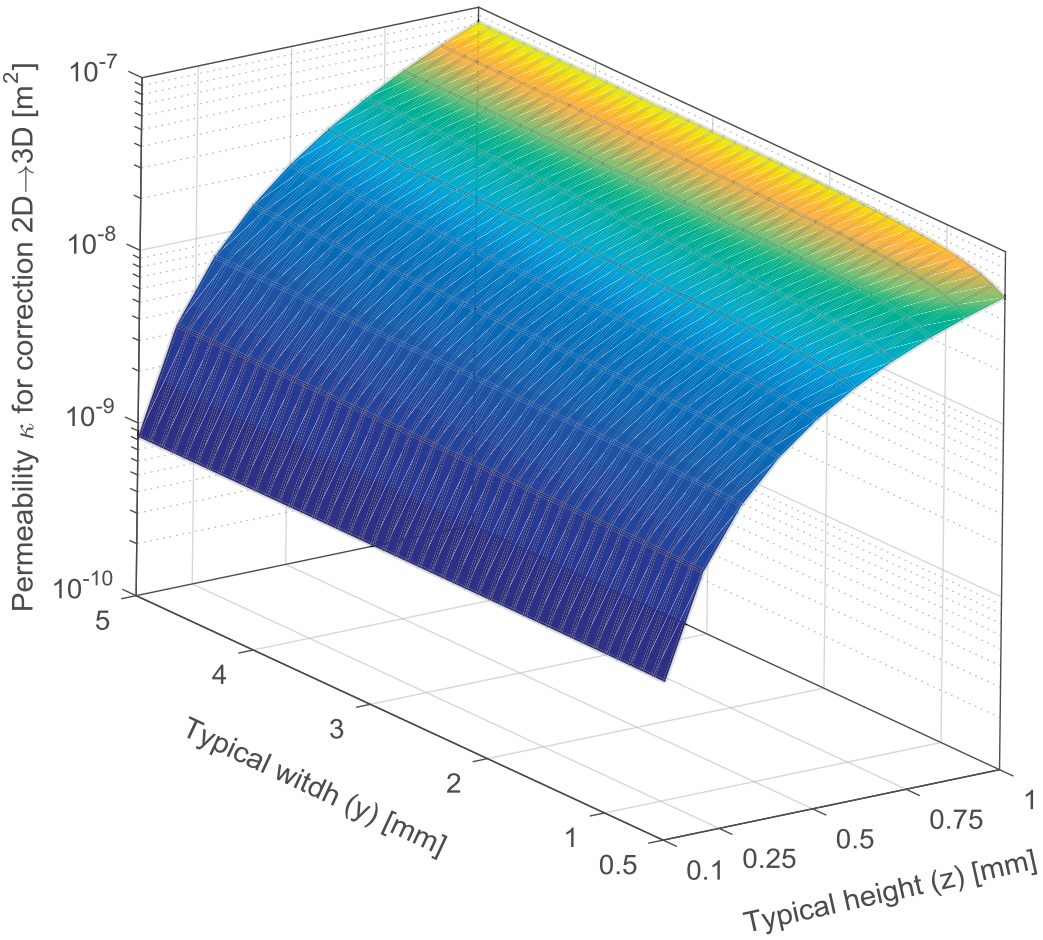

Figure 4.8 Values of the virtual permeability κ in function of typical height and width of cross-section to flow in fuel cells.

With this "Darcy correction", it is possible to obtain the correct values of the hydraulic resistances. Therefore, for a given flow rate (bulk velocity), the pressure drop is consistent with that of the 3D model.

The introduction in 2D of a resistive term with a finite permeability is accompanied by a side effect: as visible in figure 4.10, the Poiseuille profile between two infinite parallel planes (blue curve) is flattened when adding the permeability (green curve). An undesirable consequence of this side effect will be discussed further.

2. Flow in irregular ducts and geometries

According to figure 4.10, a 3D-like representation of the flow can be reproduced accurately by adding a virtual permeability in the 2D geometry. However, this is rigorously

true only for *fully-developed*, *laminar*, *steady-state* flows in *rectangular*[5] channels. Yet, the geometry of the FDP may include curved channels, sudden change of cross-sections, of direction, as well as steps, plenum, convergent and divergent, etc. Therefore, the previous analysis can only be used as a starting point. A more sophisticated procedure is necessary to compute adequate permeabilities for those zones. It is discussed in the next sections.

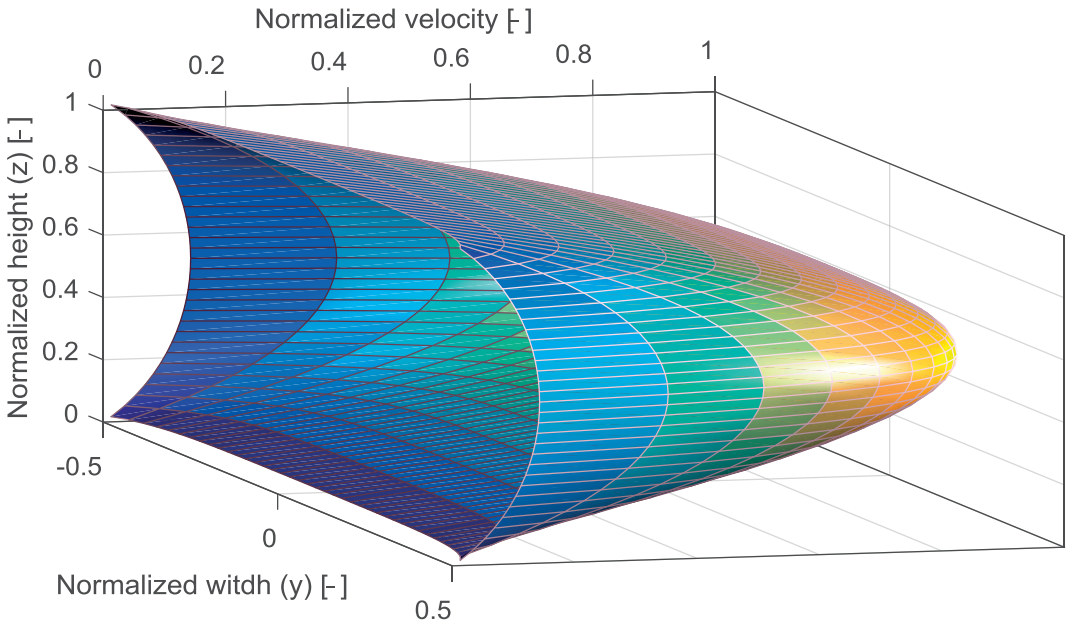

Figure 4.9 3D profile of the fully-developed velocity in a rectangular channel of aspect ratio $y/z = 4.25$.

[5] Or any other regular geometry for which an analytical solution exist, such as a triangle or an ellipse (circle).

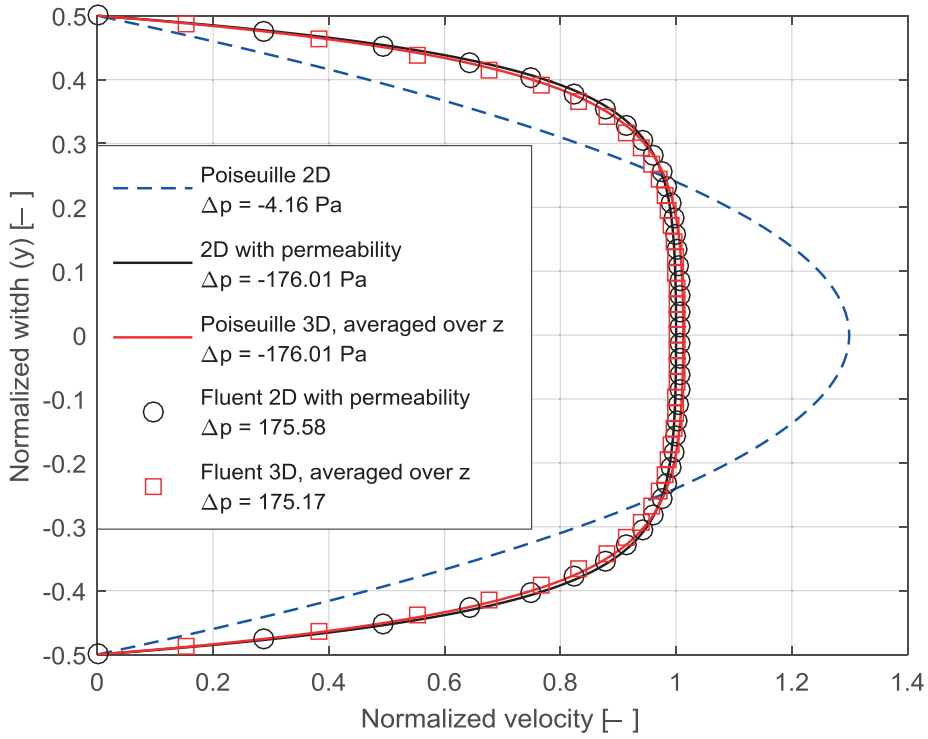

Figure 4.10 Fully developed profiles of velocity in a rectangular channel with an aspect ratio of 4.25. Profiles in 3D are "projected" on y coordinates by taking the area-weighted averaged over z for each y.

Lines refer to analytical solutions and markers to numerical solutions. The bulk velocity is conserved (area under the profile).

3. Procedure to automatize the calibration of the 2D model

Geometry

The geometry was decomposed in sub-domains. Figure 4.11 presents a general scheme[6] of a fluid distribution pattern, with zones and interfaces where respectively permeabilities were set and numerical measurements were taken.

[6] We cannot disclose the detail of the geometry for confidential reasons.

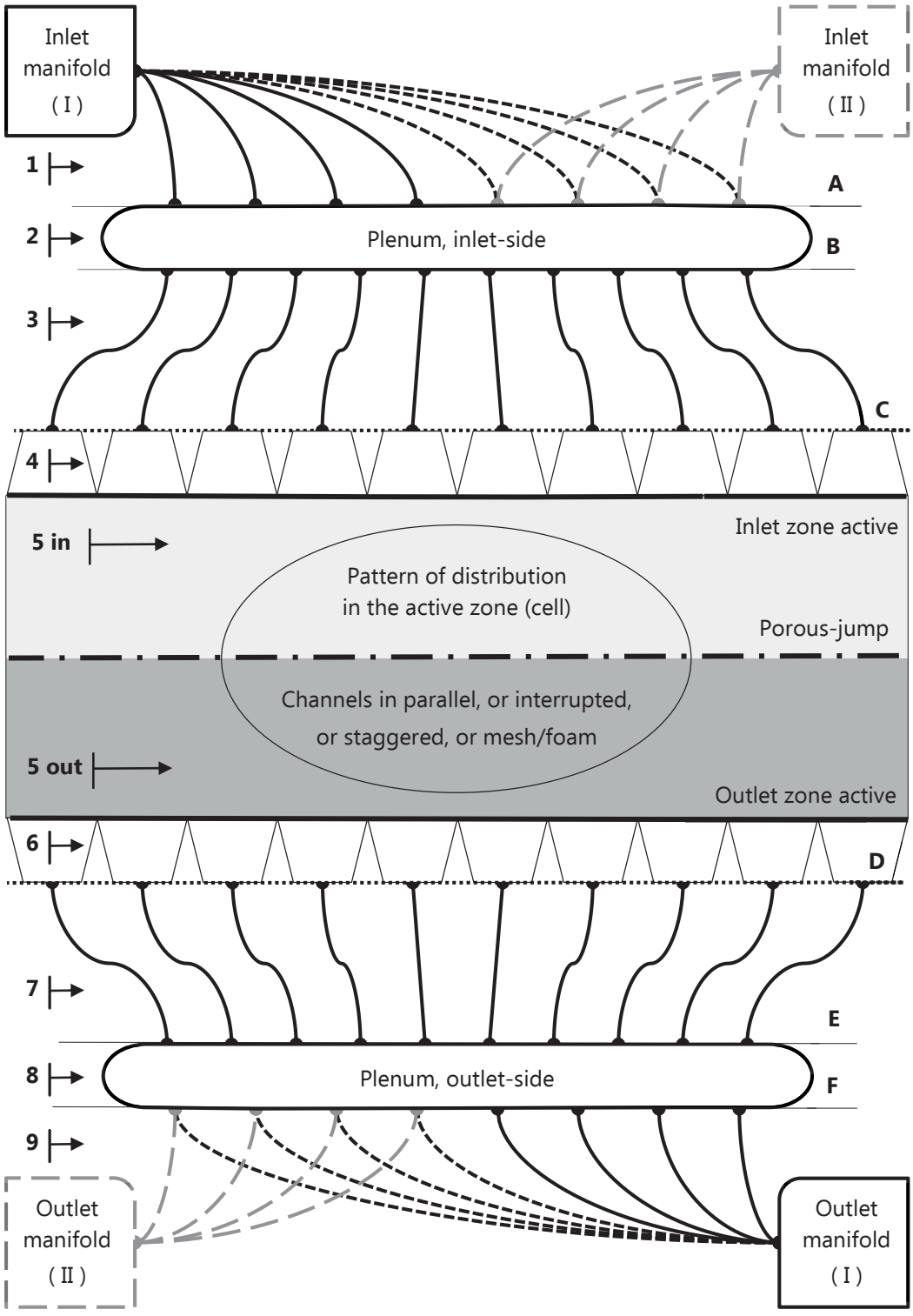

Figure 4.11 Generalized scheme of a fluid distribution pattern at the level of the elementary fuel cell. Positions and dimensions are for illustration only. Some elements are optional. Zones of various nature are numbered, while letters identify their interfaces. See also text.

Mesh and boundary conditions

The 2D geometry is a vertical projection of the 3D geometry. This transition allows to reduce the number of mesh cells by a factor 5 at least, usually ca. 10. The addition of porous-jumps to shorten the long channels further allows to reduce the number of mesh cells (typically by a factor 4). The greater the number of channels, and the longer they are, the more beneficial this technique is (also, more accuracy is kept with longer channels). In the example considered here, the final mesh consisted of ca. 200 000 mesh cells instead of ca. 6 000 000.

Division of the geometry in zones

The geometry is divided in distinct zones. Each duct with a single inlet and a single outlet constitutes a different zone. In addition, the channels in the active area are divided in two pieces by the porous-jump. Parts with multiple inlets or outlets, or both, are attributed distinct zones. They are usually not divided, since the exact separation of streamlines is not known a priori, and depends on the operating conditions. More detail about the advantages and drawbacks of this choice will be discussed later.

Permeability of porous "volumes"

In FLUENT, the surface (fluid domain) of each zone n is attributed a permeability κ_n in the `Porous Zone` tab of the `Fluid` panel. The procedure to compute these permeabilities is explained below.

Inlet flow rates and profiles

For each inlet, the corresponding *mass flux*[7] [kg/(m^2 s)] is extracted from the 3D results[8] and imposed to the 2D inlet, such that bulk velocities are conserved if the density is unchanged: $\rho\, u_\mathrm{b}|_{2D} \coloneqq \rho\, u_\mathrm{b}|_{3D}$. Moreover, to avoid inaccuracies due to re-development of the flow in inlet zones, we also extract the 3D velocity profiles. The 2D profiles are created by averaging (weighted) over the third dimension and with a correction to account for the virtual permeability of the corresponding zone.

[7] In 2D, the mass flow rate [kg/s] depends on the reference depth (3rd dimension), which is only used for post-processing in FLUENT.

[8] Either experimental results, if they were available, or results from a 3D simulation, as in our case.

Outlet pressures

The pressure relative to the gauge is usually set to zero (average) at outlets for a first simulation (3D). However, with several outlets, the gauge pressures after computation are typically not exactly zero for every outlet (e.g., relative standard deviation of 80 %). So, the outlet pressures are extracted from the 3D results and imposed in 2D: $p_{\text{out}}|_{\text{2D}} \coloneqq p_{\text{out}}|_{\text{3D}}$.

Source (sink) of mass

Like in 3D, the production (respectively consumption) of species is modelled via a volumetric source (sink) of mass, $\dot{\rho}$. The only difference is that the "volume" corresponding to the 2D surface where the source is imposed is defined according to a reference "depth" in FLUENT (h_{ref}, which appears in the expression of the volume and of the mass flow rate).

$$\dot{\rho} = \frac{\dot{M}_{\text{in}} - \dot{M}_{\text{out}}}{V} \quad \left[\frac{\text{kg}}{\text{m}^3\ \text{s}}\right]$$

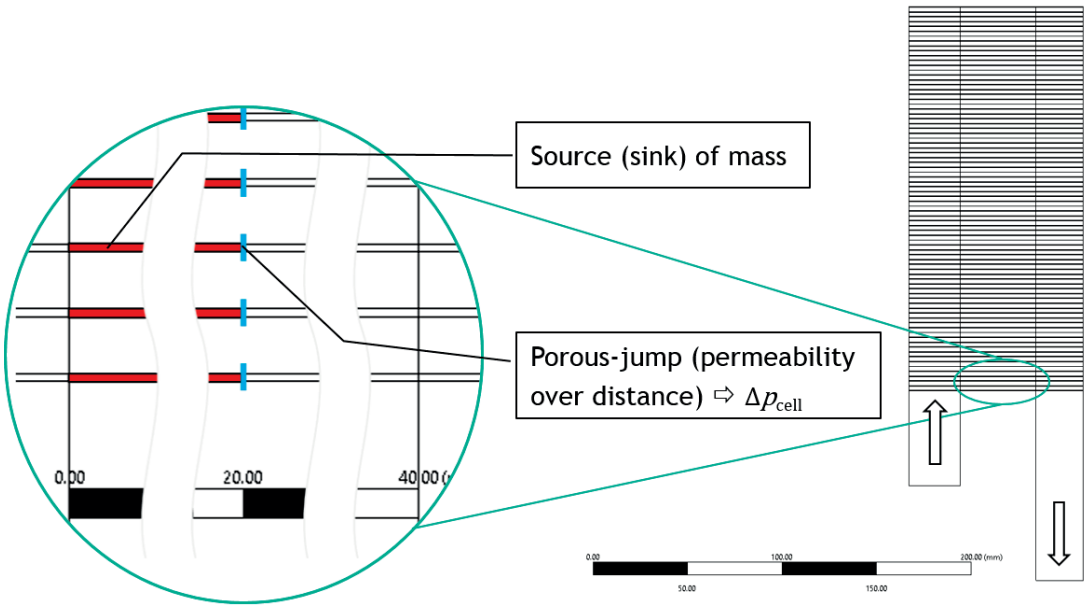

Figure 4.12 View of the implementation of porous-jump and of source of mass in a 2D model.

This illustration corresponds to a model at the level of a stack of 80 cells, but the principle is identical for a repeat element. The source of mass can also be placed after the porous-jump or distributed in both chunks of channels. Numerical instabilities seem to be reduced with the two last cases.

Porous-jumps

The change of pressure across a porous-jump is $\Delta p = -\frac{\mu}{\kappa}\, u_\mathrm{b}\, \Delta x$, with μ and u_b the dynamic viscosity and bulk velocity of the *flow crossing* a membrane of permeability κ and width Δx. To compute the correct value of κ, it is important to use values of μ and u_b corresponding to the state when crossing the membrane, i.e., accounting for the source of mass. The width Δx is set in software; the surface representing the membrane in the mesh has no width.

Description of the calibration procedure

The goal is to minimize the differences of information gathered between the 2D and the 3D model.

Initialization of the permeabilities

To choose reasonable initial values for the permeabilities is essential to allow — or at least improve — the convergence of the following optimizations. The aforementioned semi-analytical method to estimate the permeabilities is useful here.

Three procedures were tried to calibrate correctly and as quickly as possible the 2D model with the 3D results, by adjusting the permeabilities. In each case, the focus was to minimize the disagreement of the flow rates in channels of the active zones between 2D and 3D. This disagreement was quantified in terms of the root-mean-square of relative differences (RMSD).

1. Using *fgoalattain* and *fmincon* in MATLAB

This procedure was not conclusive. The optimisation algorithm behind *fgoalattain* and *fmincon* computes gradients to search the minimum. Unfortunately, the current version of the *adjoint-solver* of FLUENT does not support porous zones. So, the gradients can only be evaluated numerically, by running simulations. Moreover, the algorithm must compute the gradients for each permeability κ_n, which are the variables of decision ($n = 42$ in our test). Last but not least, the strong nonlinearity of the simulations with respect to the values of κ_n always induced a divergence of the flow solver or of the algorithm. It is indeed time-consuming to evaluate numerically several gradients of a

highly nonlinear functional by running a "black-box" simulator. The nonlinearity and the "blindness" of the algorithm regarding the black-box, results in high risk of inaccurate evaluation of gradients, leading the algorithm to take a wrong direction.

2. Calibration by comparison of the static pressures

A more robust approach was necessary. The idea is to find optimal κ_n such that pressures in 2D matches those in 3D at several interfaces of "measurement". These interfaces correspond to the divisions in zones of distinct permeabilities. Since the 2D pressures at outlet are imposed equal to those in 3D, permeabilities are iteratively changed from downstream to upstream, such as to satisfy:

$$^{3D}_{2D}\Delta[p_{u:d}] = p_{u:d}|_{3D} - p_{u:d}|_{2D} < \epsilon$$

where $u{:}\,d$ indicates the interface between adjacent zones u upstream and d downstream with permeabilities κ_i and κ_j and ϵ is a tolerance threshold. When several upstream interfaces belong to a single porous zone (i.e., one permeability), the maximum deviation of pressure is minimized.

Permeabilities are changed as follows:

$$\kappa_d^{new} = \kappa_d \left(1 - \beta \frac{^{3D}_{2D}\Delta[p_{u:d}]}{p_{u:d}|_{2D}}\right) \tag{4.58}$$

with $\beta \in]0, 1]$ an adjustable factor of relaxation to control convergence. With equation (4.58), when the static pressure is overestimated in 2D, the permeability is increased to correct it, and vice-versa. To reach a stable calibration, the permeabilities must be updated based on a well converged simulation. So, to use low values of β is wise.

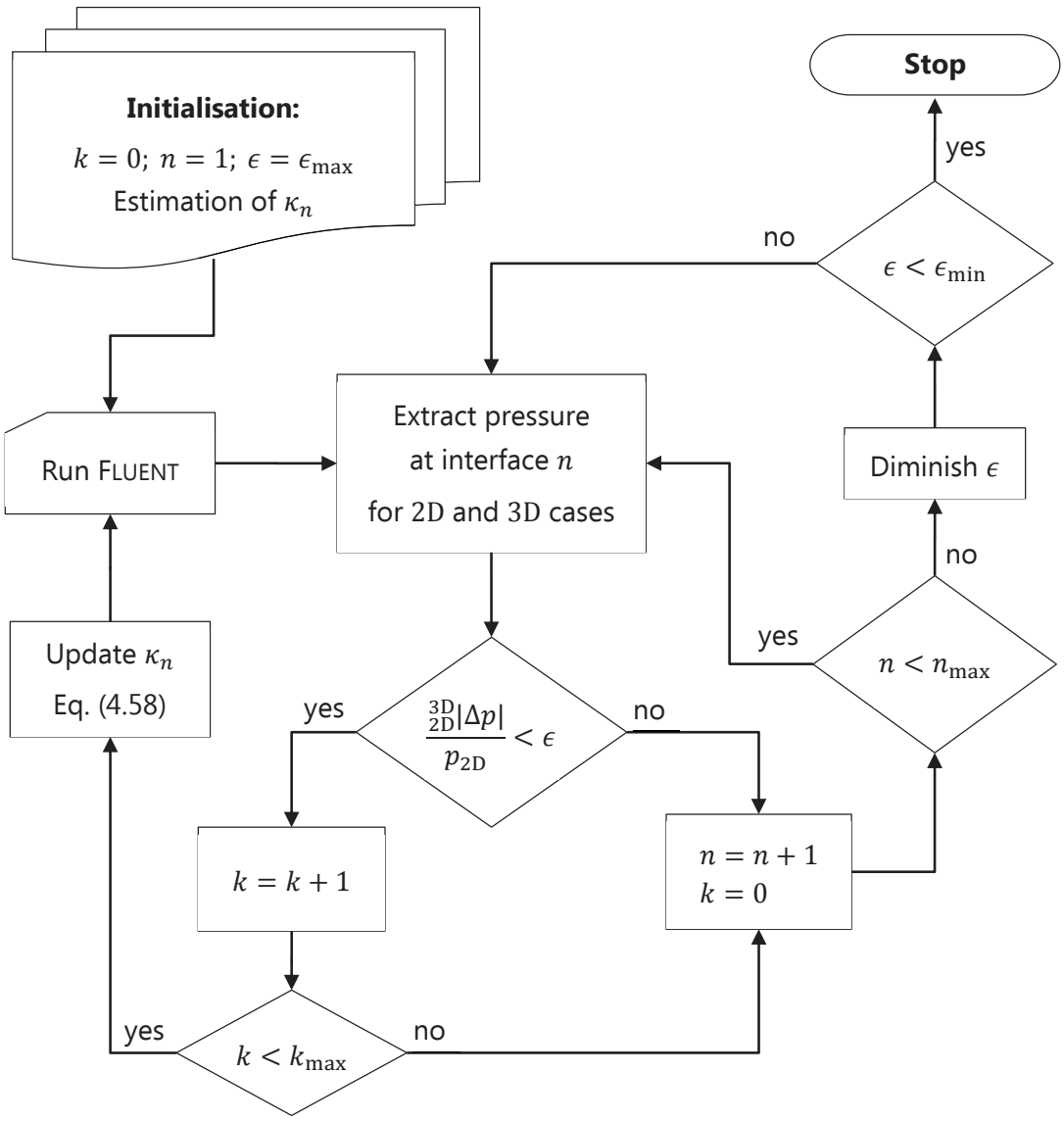

Figure 4.13 Simplified diagram of the iterative procedure to calibrate the 2D model by comparing static pressures with those obtained with the 3D model.

A counter k is used to avoid spending too much iterations for adjusting one permeability κ. Indeed, the flow in every channel is coupled and interacts with each permeability. The procedure is similar when comparing flow rates.

3. Refinement of calibration by comparison of the flow rates

From the point of view of the performance and lifetime of the fuel cells, accurate knowledge of the flow rates (distribution) is more interesting to us than the local pressure of the fluid. The following procedure is used as a refinement to the previous one.

Since flow rate is conserved in the distribution network (except in the active zone), the degree of freedom to adjust them is less than for the pressures. So, it is only useful to compare 2D and 3D flow rates at one interface along each full branch (i.e., without separation of flow). Nonetheless, to reach a correct flow rate, there is freedom to update the permeability of any of the zones belonging to such a branch. It is convenient to update only one zone with the equivalent resistance necessary. It is preferable when possible to keep a low permeability in zones subject to inertial effects (channels upstream of an enlargement, and the enlargement itself). Indeed, those are damped when the permeability is decreased.

Otherwise, the procedure is basically similar as above, except that here flow rates instead of pressures are compared between 3D and 2D. Besides, the permeability is increased to compensate an *under*estimated flow rate in the corresponding zone.

4. Using *globalsearch* and *patternsearch* in MATLAB

Since the response to the simulation is nonlinear and it seemed that *fmincon* and *fgoalattain* get stuck on local optima (when they terminated), we tried alternative algorithms to search for a global optimum, or at least other local optima. *Globalsearch* seemed a good candidate, since it generates many start points stochastically, but still uses *fmincon* (gradient-based) for a fast convergence to the solution. With it, we could decrease the disagreement between 2D and 3D, compared to *fgoalattain* and *fmincon* (alone). However, the results seem not to be reproducible consistently and it is slow to test all the start points not discarded by the heuristic procedure of *globalsearch*.

We considered that it is a good sign that the response of the simulation is not smooth, probably in part due to the behaviour of the flow solver when provided with input variables for which it cannot (easily) find a physical solution (e.g., problem of convergence, reversed flow, etc.). Therefore, we tested algorithms not relying on gradients. According to MATLAB documentation [73], *patternsearch* is usually the most successful and efficient of "derivative-free-optimization" solvers implemented in the software. Contrary to others (*particle swarm* and *genetic algorithm*), it is proven to converge to at least a local optimum. *Simulated annealing* also has a proof of convergence, but only under very slow cooling schedule. In addition, "*The pattern search algorithm is robust in relation to objective function failures. This means patternsearch tolerates function evaluations resulting in* `NaN`*,* `Inf`*, or complex values.*" [73].

Patternsearch proved successful, by providing a solution similar to our own "fluid-mechanics" based algorithm. Note that only the value of the objective function is almost equal: RMSD of central flow rates of 37.6 % (our approach) and 36.8 % (*patternsearch*).

The values of the "optimal" permeabilities however differ by several order of magnitudes, leading to much larger pressure drops. Since we focus on the uniformity of flow distribution irrespective of the pressure level, constraints have not been set for pressures to avoid this situation. If we did, a solution similar to our approach would probably have been reached, but we let freedom to the algorithm in the hope to further minimize the difference between 2D and 3D.

Remark about computation time

The computation time for all the aforementioned attempts of calibration was considerable. To reach a better solution than our initialisation, it always took more than ca. 16 hours of computation on 3 cores (at 3.2+ GHz with *Desktop* in Table 3.5).

Analysis of the results

The following results correspond to the best of the optima found, for which the pressure level is as in our 3D model (i.e., minimization with our algorithm). It can be noted already that a RMSD of ca. 38 % highlight the inability of that approach to provide accurate enough information for the intended purpose.

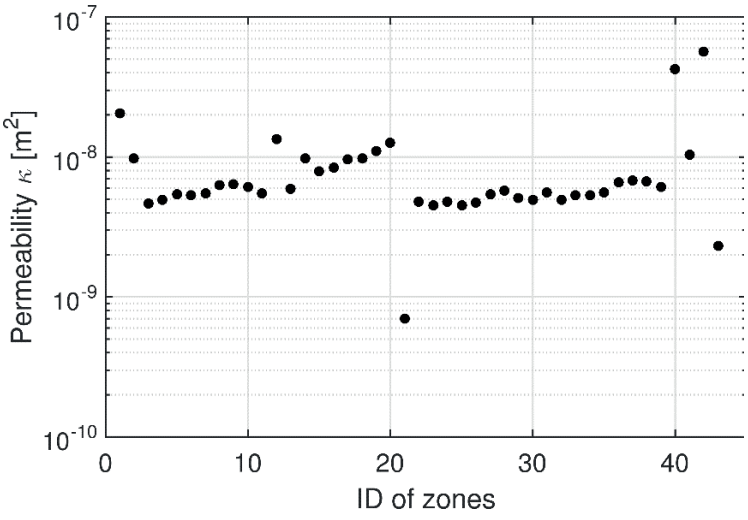

Figure 4.14 Values of the permeabilities set for each zone, to minimize the difference between the 2D and 3D models (more particularly the RMSD of the flow rates in the central channels.

On the synthetic view of figure 4.15, pressures and flow rates on the right seem to match rather well. A look at the leftmost graph nevertheless sheds light on the rather

large remaining relative differences between 2D and 3D, especially for flow rates and at certain locations. Figure 4.16 shows the flow rates in more detail and figure 4.17 shows the pressures. It can be seen on the latter that the pressures are well matched, easily falling into the ±10 % bands (ca. 2.5 % maximum difference). The case is completely different for the flow rates. They almost fall within these bands, but with much more variations. Actually, the large discrepancy for interfaces D, E, and F, for instance, would not be too dramatic for our future use of the model. The discrepancy in the central channels are much more problematic. Indeed, the index of flow uniformity in the active zone would be unreliable with differences of up to 20 %. Besides, the shape of the flow distribution itself is not reproduced. In the next section, we discuss with an illustrative example the factors responsible for such disagreement between 2D (corrected) and 3D.

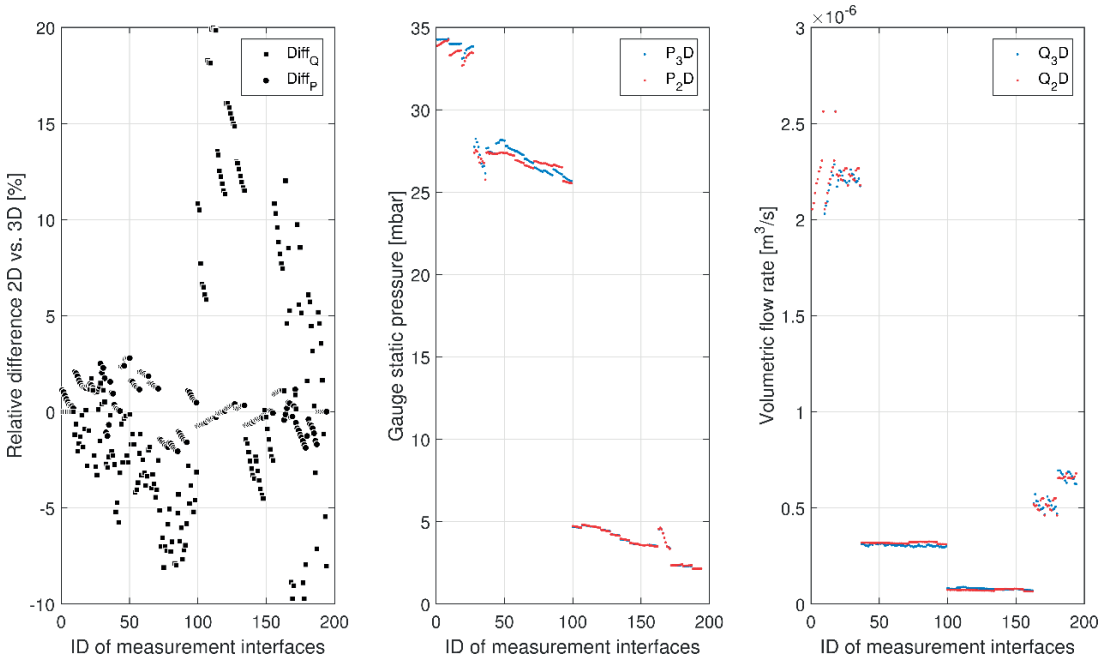

Figure 4.15 Synthetic view of the 2D vs. 3D results. See next figures for details. Inlet at ID = 0, outlet at ID = 200.

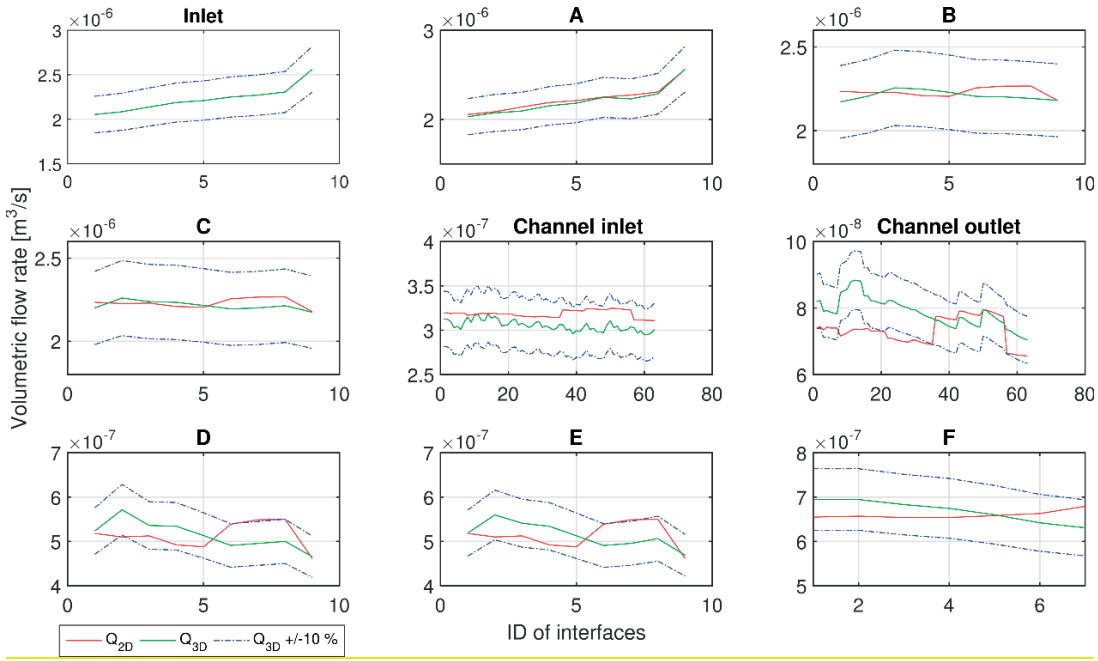

Figure 4.16 View of detail for the comparison of the 2D and 3D flow rates. Q is the volumetric flow rate.

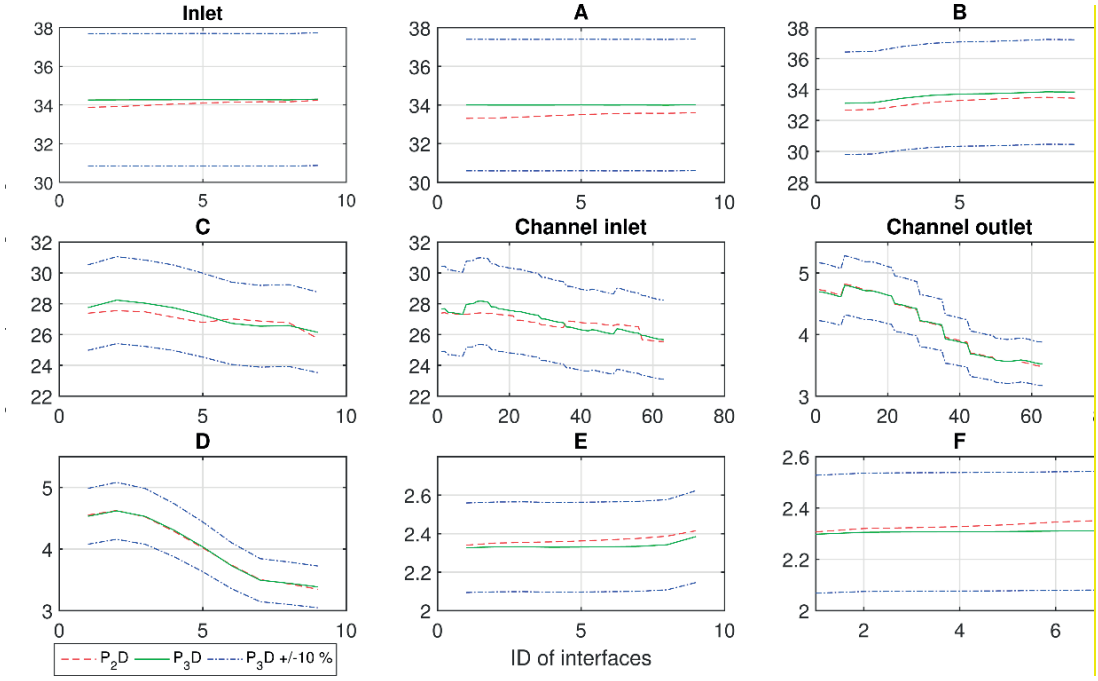

Figure 4.17 View of detail for the comparison of the 2D and 3D pressures.

Inertial effect not reproduced by the corrections

The main identified reason for the aforementioned discrepancy is that the inertial effects cannot be reproduced by, or should we say due to, the correction (set with virtual permeabilities). A major issue when adding a virtual permeability is indeed the diminution of the inertial effects. Indeed, the Darcy term $\left(-\frac{\mu}{\kappa}\,\boldsymbol{u}\right)$ added to the Navier-Stokes equation is directly proportional to velocity and not to the spatial variation of velocity like the convective and diffusive terms: $(\boldsymbol{\nabla u})\cdot\boldsymbol{u}-\nu\,\boldsymbol{\nabla^2 u}$. Hence, any characteristic of flow distribution which depends substantially on inertial effects, such as jets and sudden change of direction, cannot be correctly reproduced. They are "damped".

Figure 4.18 shows a typical geometry where such a problem occurs. Our point is better highlighted with this geometry, because the flow behaves completely differently when the gas is supplied from one side or from the other. Both models capture a difference of behaviour, but the 2D model fails to match with the 3D.

The convergence of each case was checked with residuals, by monitoring the convergence of the flow rate in the channels, and with the mass balance. All relative measures are lower than 10^{-3}. The overall pressure drop is slightly higher (ca. 7 %) for case A. For case A and B, the pressure drop computed with the 2D corrected model underestimates that of the 3D model by ca. 4 %. In large part, this is due to the intermediate distributor zone, which is subject to a uniform permeability, whereas in reality (3D), dissipation due to flow friction against the lower and upper walls (inexistent in 2D) is higher in regions with high velocities.

Figure 4.18 clearly emphasizes that for case B, 2D corrected and 3D models do not match. The maximum relative error is 10 %, and the MAD is 7 %. Conversely, both models match relatively well for case A, exhibiting a maximum relative error of 2.3 % and a MAD of 1 %. For both cases, the error is not systematic, since there are over and under-estimations of the flow rate in approximately same proportion (mean of errors is close to zero). Interestingly, flow uniformity of case A is also significantly better than for case B: for A the deviation of the maximum is 1.3 % (1.1 % in 2D) and 2.1 % (1.4 % in 2D) for the minimum, whereas for B they are respectively 8.6 % (8.0 % in 2D) and 8.7 % (3.0 % in 2D). From these numbers, it is also clear that for case B, the 2D corrected model underestimates the deviation of the minimum flow by almost a factor 3. So, we believe that it would be dangerous to take decisions with the 2D corrected model when such cases can occur. The risk is besides exacerbated if an (optimization) algorithm bases its decision with such results (hiding the reasoning and bigger picture to the engineer).

Nevertheless, an important conclusion can be drawn from this example. Indeed, it seems that the main reason explaining that the flow uniformity is better for A than for B is the same reason explaining that agreement between 2D and 3D is better for A than for B. The supplying channel at inlet of A is around twice as large as that of B (and so is the bulk velocity). The inertial effects are hence more pronounced for B than for A ($Re = 1\,374$ vs. 787) even if the height, being smaller, is limiting the change of hydraulic diameter. Interestingly, this inertial effect (creation of a jet) is, in this situation, preponderant over the inclination of the inlet channel, which is disadvantageous for A.

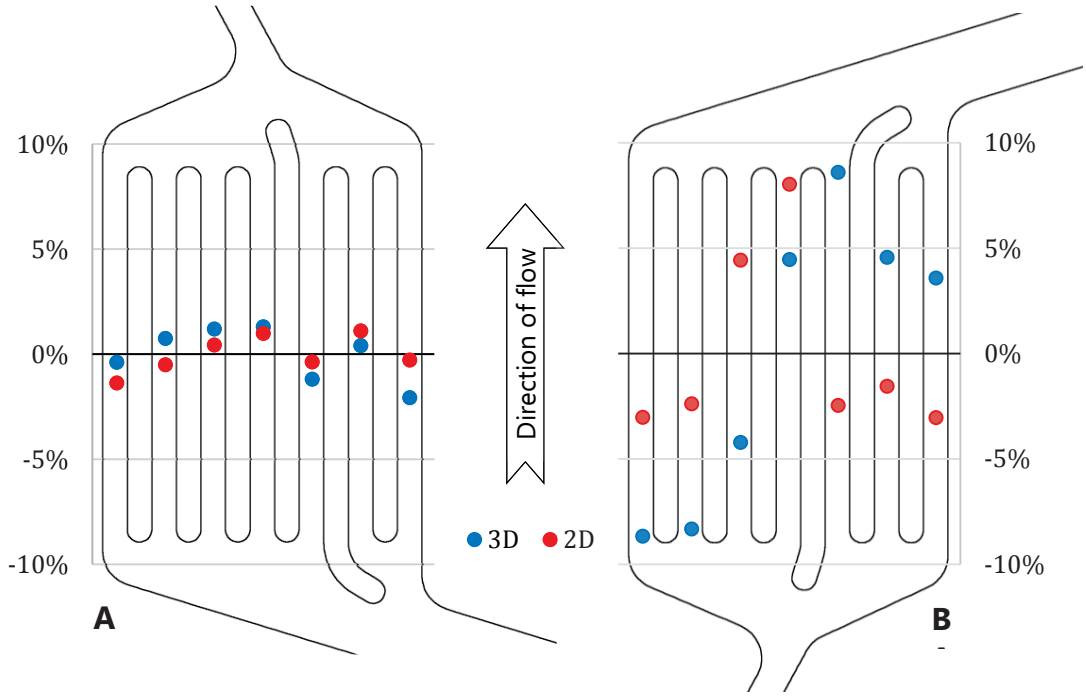

Figure 4.18 Deviation of the flow rate into the channels relative to the mean flow. Comparison of CFD-results with 3D and 2D with Darcy corrections.
Note: channels were shortened for illustration (ca. 20 × longer).

Conclusion for the 2D corrected model

As discussed, even with lengthy calibration of the corrections for particular geometries, the 2D model is unable to match the 3D model with sufficient accuracy at the level of the flow rates. It should be noted that the model could be refined, for instance by:

- Using a nonlinear correction, i.e., with two or more coefficients instead of only one (permeability)

- Subdivide even more the domain of computation, to assign a correction at a smaller scale. Typically, zones connected to several channels could be divided in as many zones.

Yet, even if more accurate predictions could be obtained with such solutions, it would not be adequate for our goal. Indeed, calibration would still be required when the geometry is changed (either during the uncertainty quantification, or the optimization). So, increasing the complexity and the number of variables to optimize for would be, in our opinion, counterproductive. The 3D model could actually be quicker to run, while keeping its intrinsic higher accuracy.

Actually, since we are mainly interested in the flow distribution — rather than the detailed flow profile (velocity vectors and pressures) — an alternative approach may be to further reduce the dimensions and the coupling of the problem. The related investigation is the subject of the next section.

4. 0D or quasi 1D — hydraulic network (lumped model)

In addition to the aforementioned reason, another motivation for the development of this model was the need for a quick model to develop the tools related to the uncertainty quantification and the optimization of the design (testing and debugging).

We use the analogy with electric circuits, keeping consistent units for power:

$$\Delta\Phi = R_{\mathrm{el}} I \;\Rightarrow\; \Delta P = R_{\mathrm{h}} \dot{V} \tag{4.59}$$

We test the flow distribution of a standard configuration taken from [52]. The resistive network flow model was calibrated with a 3D CFD model, but only at the level of the manifold (virtual resistances).

The main hypotheses are:

- Laminar or linearized turbulent flow regime;
- Fully developed flow;
- Constant (or averaged) parameters along the duct's segment ($v, P_{\perp}, A_{\perp}$).

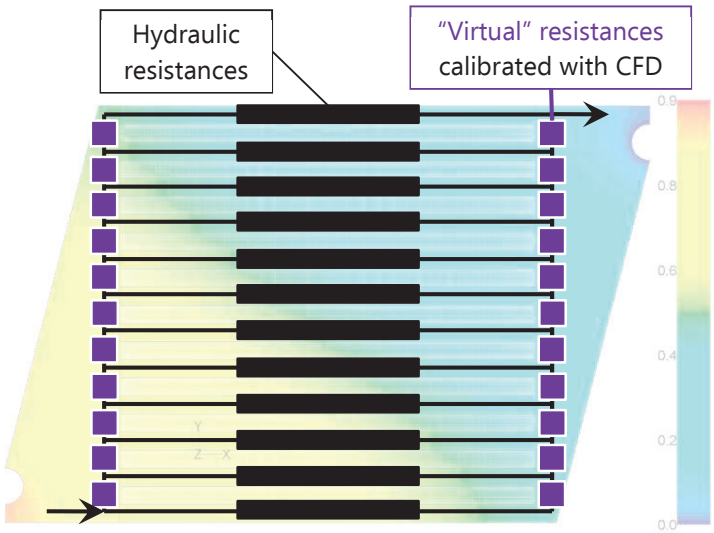

Figure 4.19 Scheme of the resistive network used to model the FDP shown underneath in transparency.

To solve the resistive network, we used a MATLAB code graciously provided by Prof. W. K. S. Chiu from the University of Connecticut [21–23].

The original application of the code is not flow network, but it was relatively easy to adapt it for our needs. Besides, the code was made ca. 15 times faster, partly by tailoring it to our purpose, and partly by reorganizing it (pre-allocation, vectorization, avoiding slow usage of MATLAB, etc.).

4.6 Uncertainty quantification – Choice of technique

4.6.1 How to treat the combinatorial problem?

Statement of the problem

Consider $\mathcal{N}_c$ channels. Their dimensions are random variables. We assume that they are manufactured with the same tolerances (identically distributed random variables). Let's also first assume that the random variables are also independent.
Consider that their PDF is described by $\mathcal{N}_s$ samples.
We are interested in the global pressure drop and in the distribution of flow in the channels.

To fully describe the stochastic responses to the variability of the dimensions, the number of evaluations of the system is hence:

$$\mathcal{N}_{\text{eval}} = \mathcal{N}_{\text{s}}^{\mathcal{N}_{\text{c}}} \tag{4.60}$$

Even if the PDF of a characteristic dimension of the channels could be represented accurately enough with $\mathcal{N}_{\text{s}} = 3$ samples, the number of evaluations for 16 and 64 channels would be respectively of the order of 10^{7} and 10^{30}. With $\mathcal{N}_{\text{s}} = 30$ samples, it would be respectively 10^{23} and 10^{94}.

The following question was raised: Let's consider that only one channel (or a few) is represented by a random variable, and all other channels are attributed the nominal value (average). The channel is either chosen randomly, or with a priori knowledge of which channel's variability has the most effect on the responses. Is the resulting simulation representative of the reality (which is, that all channels can vary)?

A basic example

To investigate and illustrate our point, we considered the simple network illustrated in figure 4.20.

Figure 4.21 clearly shows two important points:

- If all channels are subject to variability, it is fundamental to attribute a distinct random variable to each of them, and therefore to sample for all of them. If the variables vary synchronously (full dependence), it is unnecessary, but it is the only, unlikely, case.

For instance, by sampling one channel out of 64, the prediction would be: there is 20 % chance that a channel is underfed by 5 %. But when accounting for all channels, the risk is basically 100 %. In that case, there is 20 % chance that a channel is underfed by 15 %. So, 20 elements in a stack of 100.

- The indicator γ is more relevant than Γ to emphasize strong local flow deviation, and therefore to judge the risk of degradation. Furthermore, the cumulative distribution function (CDF) of γ displays a wider range of values. As a consequence, the slope is less sharp, giving the ability to take decision in a more nuanced manner, rather than "on/off".

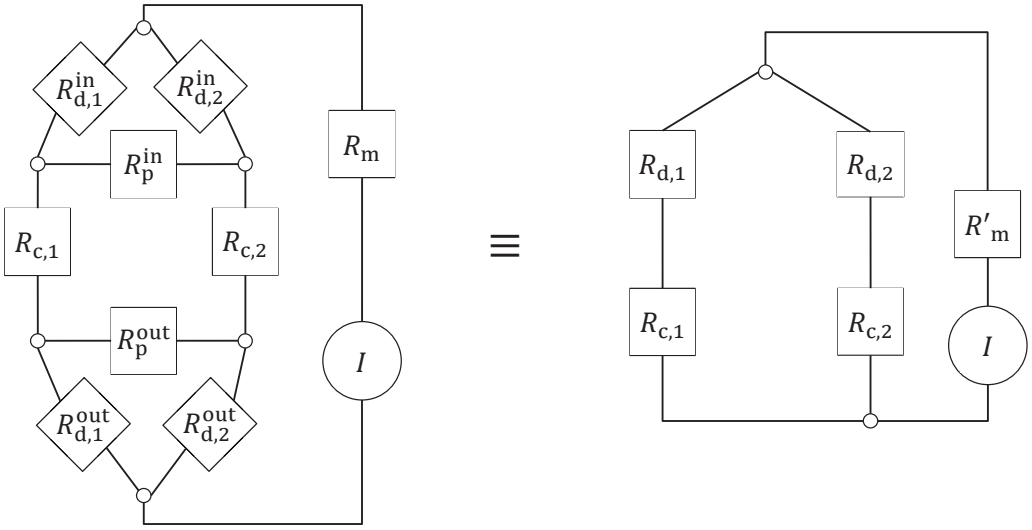

Figure 4.20 Simple hydraulic resistive network with analogy to electricity. Kennely's theorem allows the transformation $\mathrm{Y} \to \Delta$: left and right circuits are equivalent.

R_m, R_d, R_p, and R_c are the resistance of respectively: the manifolds, the distributors, the plenums or transversal channels, and the channels. The exponent "in" and "out" stand for inlet and outlet sides, respectively. Following relation (4.59), the electrical current can be assimilated to the flow rate (volumetric); similarly, the difference of potential between two nodes (voltage) is replaced by a difference of pressure.

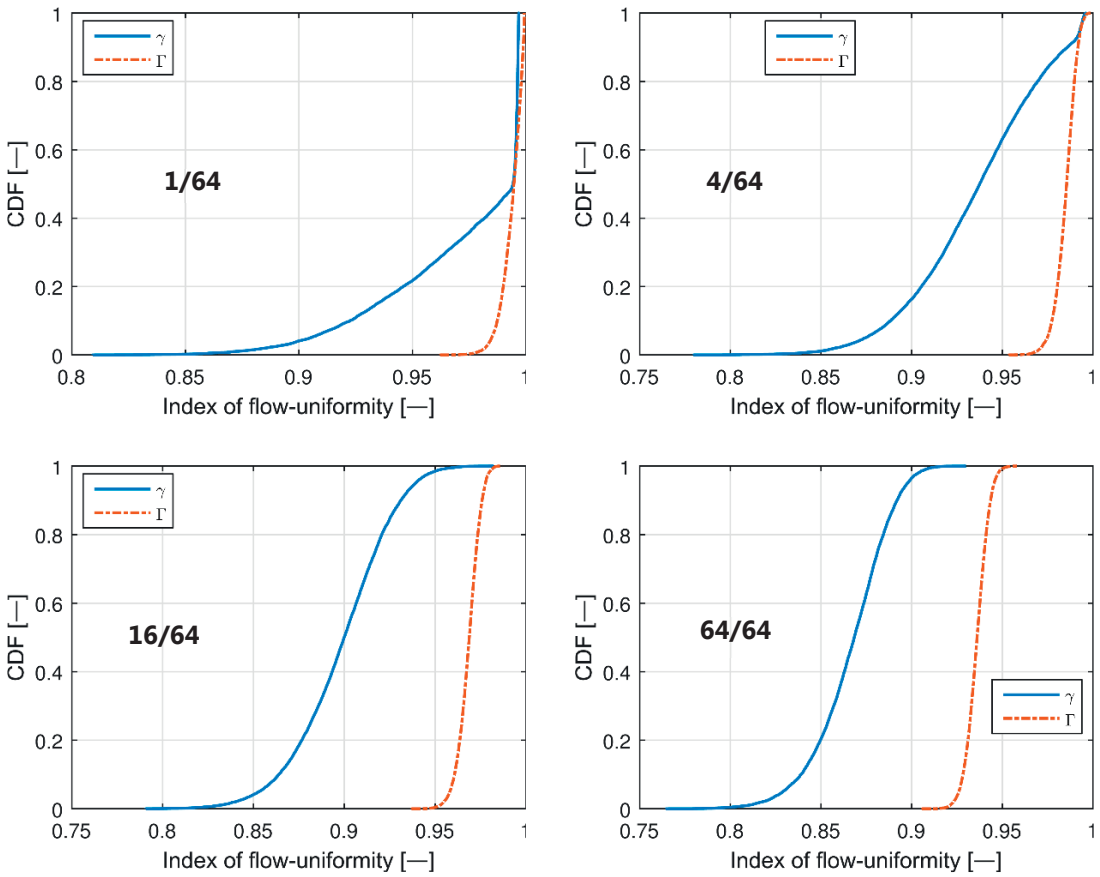

Figure 4.21 Cumulative distribution function for two different indexes of flow uniformity (γ and Γ). The design is made of 64 parallel channels. The four subfigures correspond to the number of channels whose dimensions are attributed random variables. They follow a normal distribution, centred on the nominal value, with 3 % of the smallest dimension as standard deviation. 10 000 samples were drawn for each case.

2. Dependence and correlation of the random variables

The effect of random variables on the responses is not the same if they are independent random variables or not[9]. Dependence of the variability of the dimensions can arise and depend on the manufacturing process, assembly, and operation. The variables may be positively or negatively correlated. Figure 4.22 is an example of potential negative correlation. It shows a misalignment and distortion of a rib separating two channels. As a consequence, while the width of one channel will reduce, the width of the

[9] Normally distributed and uncorrelated does not imply independent.

other will increase. Note that this is only true under the assumption that other ribs vary independently. A positive correlation can arise for instance when a part is machined: the width of a groove decreases as the tool (e.g., drill) wears.

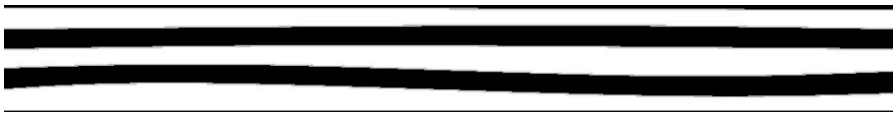

Figure 4.22 Illustration of misalignment and distortion of the ribs (black) between channels. The contours were extracted from a photograph of a real product, without stretching.

4.6.2 Some strategies to tractability vs. accuracy

We are interested in strategies to get accurate information on the output uncertainties in as few simulations as possible (and as quick simulations as possible). The outputs are random variables and $\mathcal{N}$ simulations provide $\mathcal{N}$ realizations of them, from which we can derive estimations of their statistics. We also want information about the quality of the ***statistics***, preferably "online". This is useful to avoid running an arbitrarily large number of simulations when only a few are necessary to achieve a desired level of accuracy. For instance, when the variability of the input is lower, or when the sensitivity of the response is lower.

1. Online recursive update of mean and variance

A *numerically stable* online algorithm to compute the mean and the variance is [74]:

Initialisation: $\bar{x}_0 = 0, \quad SSD_0 = 0$

Updated sample mean: $\bar{x}_k = x_{k-1} + \frac{x_k - \bar{x}_{k-1}}{k}$

Updated sum of squares of differences: $SSD_k = SSD_{k-1} + (x_k - \bar{x}_{k-1})\,(x_k - \bar{x}_k)$

Updated sample variance: ${s_k}^2 = \frac{SSD_k}{k-1}, \quad k > 1$

Update population variance: ${\sigma_k}^2 = \frac{SSD_k}{k}$

2. Variance reduction with control variates

Many techniques exist to reduce the variance of an estimation: e.g., conditioning, stratified sampling, importance sampling, draw recycling, antithetic draws, control variates, … We implemented ***control variates***.

Here is an outlook of the method.

Consider X an output of the simulation, for which we desire to estimate its expectancy:

$$\theta = \mathrm{E}[X]$$

Note that X is a random variable, which can already be a statistic. For instance, we are interested in the expectancy of the minimum flow rate which occurs in a fuel cell, or the expectancy of the average flow rate in one element.

We can reduce the variance of the estimation of θ by using the information we know from another output of the simulation, Y, for which we know its true expectancy: $\mathrm{E}[Y] = \mu_Y$

$$Z = X + c\,(Y - \mu_Y)$$

$$\mathrm{E}[Z] = \mathrm{E}[X] = \theta$$

$$\mathrm{Var}[Z] = \mathrm{Var}[X + c\,Y] = \mathrm{Var}[X] + c\,\mathrm{Var}[Y] + 2\,c\,\mathrm{Cov}[X, Y]$$

The goal is to minimize $\mathrm{Var}[Z]$. By deriving twice the expression, it can be shown that $\mathrm{Var}[Z]$ is minimum for:

$$c^* = -\frac{\mathrm{Cov}[X, Y]}{\mathrm{Var}[Y]}$$

Since $\mathrm{Cov}[X, Y]$ and $\mathrm{Var}[Y]$ are usually not known, we use their sample estimates:

$$\widehat{\mathrm{Cov}}[X, Y] = \frac{1}{n-1}\sum_{r=1}^{R}(X_r - \bar{X})\,(Y_r - \bar{Y})$$

$$\widehat{\mathrm{Var}}[Y] = \frac{1}{n-1}\sum_{r=1}^{R}(Y_r - \bar{Y})^2$$

An estimator of θ with a reduced variance (controlled with Y), is then:

$$\hat{\theta} = \bar{X} + c^*\,(\bar{Y} - \mu_Y)$$

And the improvement (reduction) of the variance is:

$$\frac{\mathrm{Var}[Z]}{\mathrm{Var}[X]}$$

Example

Figure 4.23 shows an example of the use of control variates for estimating the system efficiency. The chosen control variate is the height of the channels at cathode. Not only the variance at a given number of simulations is reduced (MSE bands are narrower), but also the controlled mean converges more quickly than the sample mean towards the "true" (population) mean.

So, we can achieve the same precision with less simulations. It is useful also in the context of optimization, where noisy responses are not desirable, especially if gradient-based algorithms are used.

Furthermore, it is especially useful when used as a criterion to stop the sampling loop, rather than arbitrarily choose a high number of samples. It allows to reduce the number of simulations in regions of the problem where the response is less sensitive to input variability, or when the input variability is lower.

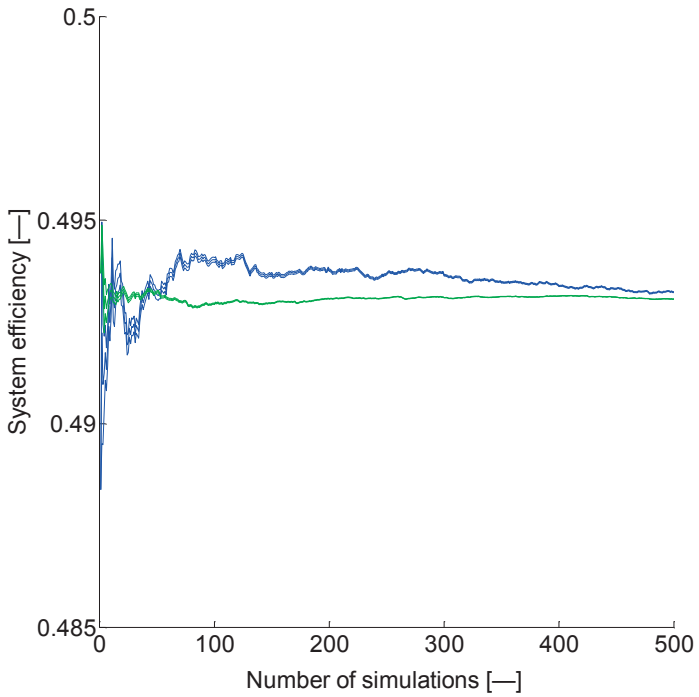

Figure 4.23 Sample mean and MSE bands (blue) versus controlled mean and MSE bands (green) as function of the number of simulations. Example for the system efficiency. The chosen control variate is the height of the channels at cathode.

3. Latin hypercube sampling

Compared to (pseudo)random sampling (pure Monte Carlo), Latin hypercube sampling (LHS) is an efficient way to get more precise statistical estimates with a given number of samples [75]. The idea is to better cover the space of the random inputs.

It should be noted, however, that all samples generated with LHS (or other DOE techniques) should be used to fully take advantage of its properties. Therefore, control variates are less useful with LHS than with "pure" random samples; but it is also less needed, since statistics based on LHS converge faster.

4. Statistical analysis with bootstrapping

Bootstrap is a technique which allows to estimate more precisely the statistics of random variables, when a given number of realizations are available. It is especially useful to have a better estimation of the MSE of such statistics[10]. The basic idea is to resample from these realizations to improve the estimation of the statistic. It is an inexpensive computation, since the values corresponding to the realizations are already available when bootstrap is applied. However, it is usually overkill to draw more than $R = 100$ "bootstrap" re-samples or to apply bootstrap in steps smaller than R (except for the sake of displaying a smoother curve of convergence). The convergence of the bootstrapped MSE of the standard deviation of various quantities of interest is shown on Figure 4.24. For this example, the rate of convergence is basically identical for each quantity. It shows that ca. 500 simulations are necessary to achieve $\mathrm{MSE}[\sigma] = 10^{-3}$ and ca. 2 500 additional simulations (so 6 times the resources) if a threshold of 10^{-4} is desired.

[10] The mean is the only statistic for which an analytical expression exists for its MSE as a function of the number of realizations.

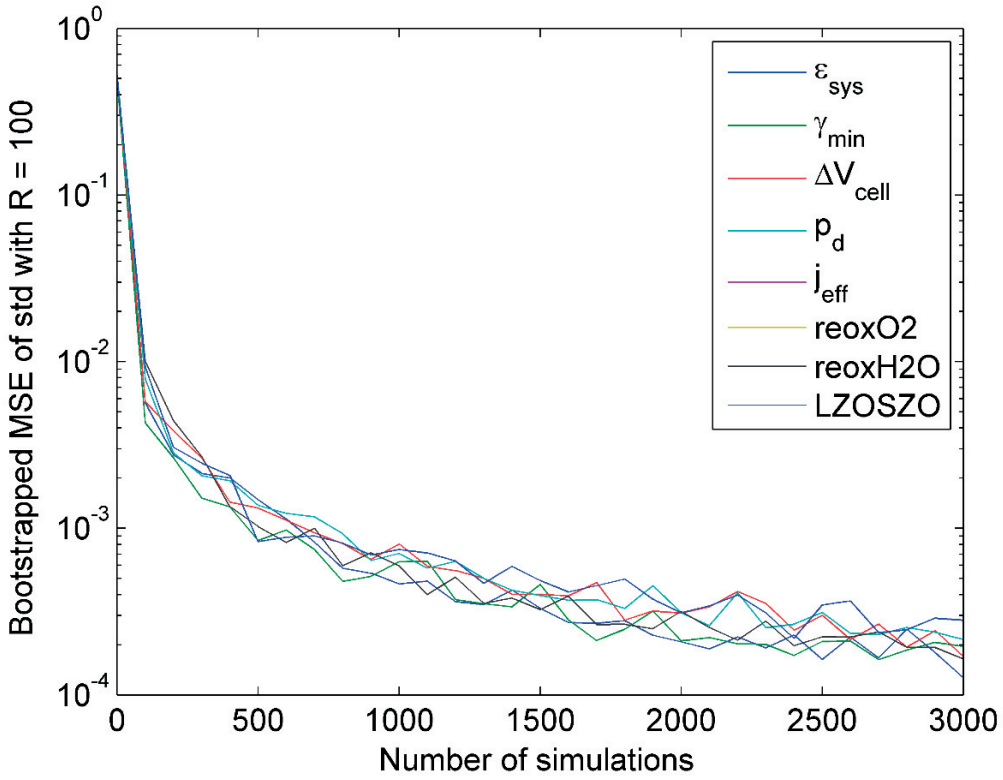

Figure 4.24 Mean square error of the standard deviation of the outputs as function of the number of simulations. 100 bootstrapped samples were drawn to compute the MSE with a step of 100 simulations.

Second part

Surrogate modelling: tractability vs. accuracy

This part describes the research conducted to build an efficient simulator, i.e., a programmed mathematical model whose ratio "accuracy over computational resources" is adequate for the intended purpose.

« La science consiste à passer d'un
étonnement à un autre. »
Aristote

CHAPTER 5

Sensitivity to simulator's attributes

5.1 Introduction

The purpose of this chapter is to analyse the sensitivity of the ***simulator accuracy*** and of its related ***computational resources*** to its ***attributes***. By attributes of the simulator, we mean all choices in the software (simulator), which together form the function of transfer between the "true" inputs of interest and the outputs. An attribute consists of a "name" (or key) and a "value". It may be a quantity, but is often a more complex object, such as the choice of a physical model or of a numerical method.

The *factors* of the following sensitivity analysis are the attributes of the simulators. The *responses* are 1) estimators of the computational accuracy and 2) indicators of the computational resources (***tractability***). The objective is to analyse the effect of the factors on the responses — in other words, the sensitivity of the responses to the factors.

It is possible to estimate, without actually running simulations, the effect of some attributes on the computational resources (especially memory, storage, and to some extent, time). However, estimating their effect on the computational accuracy usually requires running the simulator.

5.1.1 Indicators of tractability and accuracy

1. Typical indicators of tractability

- CPU time;
- RAM: minimum 2 GB per million of mesh cells;
- Space for data storage (on disk);
- Number of iterations of the solver (usually less important than time).

2. Typical indicators of accuracy

Basically, the indicators of accuracy are the quantities of interest, such as for instance:

- Velocity;
- Pressure (drop);
- Mole fractions of species;
- Temperature and/or heat flux;
- Cell voltage, or current density if voltage is imposed;
- Electrical efficiency.

Often, only global quantities are ultimately necessary (e.g., efficiency, average of temperature or voltage, etc.). Nevertheless, it may be desirable to consider some local values (profiles or fields) during the sensitivity analysis, because they tend to be more sensitive to changes, and their variance is therefore easier to capture precisely.

3. Combination of indicators

Most of the time, several quantities are important. For example, if the temperature is computed accurately but the voltage is largely overestimated, then the simulator does not provide valid information about voltage. Besides, as stated above, information about local values is sometimes desirable. We therefore need a technique to aggregate the results. Among the various existing aggregation technique, we use the root mean square difference (RMSD) to compute a single indicator out of n indicators:

$$\widehat{\Phi} = \sqrt{\frac{1}{n}\sum_{k=1}^{n} \Delta\Phi_{\mathrm{rel},\,k}} \tag{5.1}$$

with $\Delta\Phi_{\mathrm{rel}}$ the relative difference to the *reference* value:

$$\Delta\Phi_{\mathrm{rel}} = \frac{\Phi}{\Phi_{\mathrm{ref}}} - 1 \tag{5.2}$$

The case and values of reference are discussed below. For several local and global values, we simply repeat the process: the relative difference of the local values are aggregated into global RMSDs, before computing a final single indicator by taking the RMSD of those RMSDs.

5.1.2 Generalized procedure

Main assumption and its justification

The absolute ***accuracy*** of a simulator cannot usually be determined (***exactness*** of the model and ***precision*** arising from its implementation in a program). Therefore, we must use a *simulator of reference* as a replacement for a hypothetic perfectly accurate simulator. Ideally, the reference is the most detailed, valid, simulator available. It is *assumed* to be the closest to the "true" real-world situation, which would be represented by a perfectly accurate simulator (i.e., exact model implemented with infinite precision). The motivations for this choice are that:

- the most detailed simulator is also the most computationally intensive;
- we have no proof that the quantities of interest of the real-world situation that are computed can be measured with greater accuracy;
- even if a simulator is more accurate than the reference to which it is compared, the magnitude of the difference is still indicative of the effect of the factors on the responses.

Based on this last point, we can also choose as a reference a simulator which provides an intermediate level of precision. In that case, it is however not considered as the most precise, and hence not the most accurate.

Decisions to improve attributes to get a better simulator

Therefore, the following decisions can be taken based on the results of the sensitivity analysis:

- If the effect of a factor is negligible on accuracy *and* tractability, then for this factor, its level (value, property) can be chosen freely.
- If the effect of a factor is negligible on accuracy only, whereas tractability is significantly affected, then the level of the factor which corresponds to the most tractable simulator is chosen.
- If the effect of a factor is negligible on tractability only, whereas accuracy is significantly affected, then the level of the factor which corresponds to the most accurate simulator is chosen.
  Alternatively, a level allowing accurate enough simulations can be chosen if the increase in tractability is judged worthwhile the loss of accuracy (surplus of accuracy).

- If the effect of a factor is significant on computing- accuracy *and* tractability, then:
- Is there a level of this factor for which the simulator is accurate *and* tractable enough?
- If yes, it is chosen (the best compromise).
- If no, the problem cannot be solved under the wished requirements of accuracy *and* tractability. It must be investigated whether the requirements can be loosened or what prejudices arise from their non-fulfilment.

Figure 5.1 illustrates the conceptual flowchart used to build an adequate simulator for optimization under uncertainty. The processes (rectangles) are described in the next sections. Programming depends on modelling and both can affect accuracy and tractability, but it is useful to distinguish them. Indeed, modelling affects accuracy mostly regarding exactness, rather than regarding precision for what concerns programming.

Improve the tractability of the simulator

The tractability of the simulator is improved by first acting on the factors that have the most effect on tractability and the least effect on accuracy. To achieve this, we can sort the factors according to the ratio:

$$R_f = \frac{a_f\left[\widehat{\Phi_{\mathrm{T}}}\right]}{a_f\left[\widehat{\Phi_{\mathrm{A}}}\right]} \tag{5.3}$$

with a_f the effect of the factor f on the estimator $\widehat{\Phi}$ of accuracy (A) or tractability (T).

With modern computers, "over-precision" is a common tendency, so that the lack of accuracy often comes more from a lack of exactness than a lack of precision. Besides, around such a level of precision as used nowadays, the need for computer resources increases faster with increase in precision than accuracy does. Therefore, when improving tractability is desirable, a good practice is usually to first act on factors affecting accuracy, then those affecting precision, and lastly those affecting exactness.

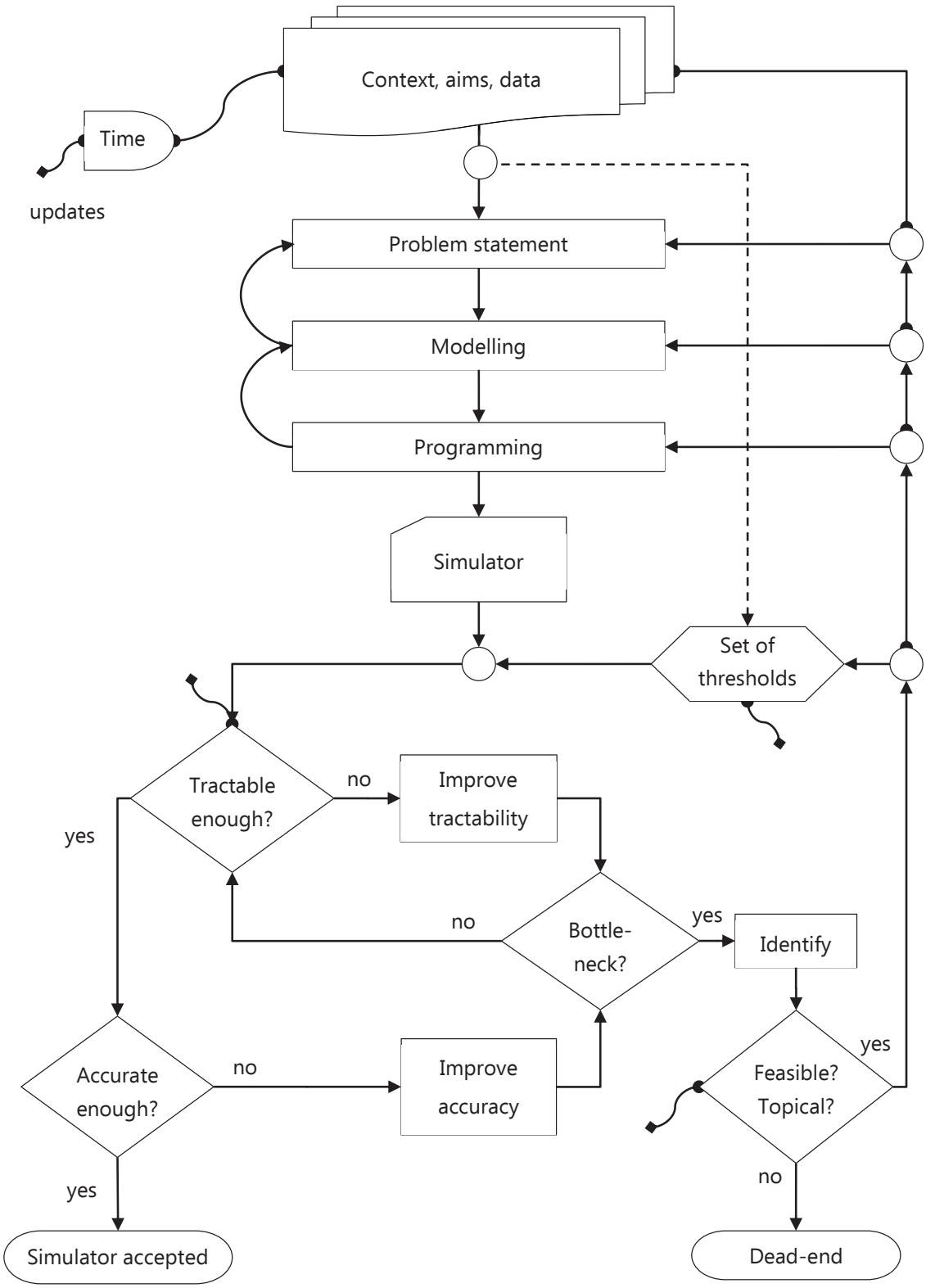

Figure 5.1 Conceptual flowchart used to build an adequate simulator for OUU.

Tractability can be improved in the modelling and programming processes (assuming problem statement is not changed). We suggest the following steps of improvements:

Programming

(1) Improve the code: e.g., pre-allocation of memory, minimize accesses to disc (read-write of files), minimize access to memory which can be avoided.

(2) Implement more efficient algorithms (linked to point 1);

(3) Relax precision: e.g., resolution of discretization, tolerances on residuals.

Modelling

(4) Act on physical models included, assumptions and boundary conditions;

(5) Use surrogate modelling:

  (a) Reduced-order models or;

  (b) Meta-models (approximation or interpolation).

Improve the accuracy of the simulator

The accuracy of the simulator is improved on factors by first acting on those affecting more accuracy than tractability. Before rushing to higher-order models, implementing more detailed physical equations, or using finer discretization, we suggest to start by basic procedures of verification (programming) and calibration & validation (modelling).

Identify the bottleneck

In case a bottleneck seems to be reached to improve either accuracy or tractability, it is useful to identify what is the source of the bottleneck.

- Accuracy: Precision (resolution)? Exactness? About which quantity? At which stage?
- Tractability: CPU-time? Memory? Storage?
- Both: is the methodology and techniques used adequate? (Notably the iterative methods used to improve accuracy or tractability.)

When a bottleneck is identified:

1) Is the corresponding threshold unnecessarily constraining?

  ⇨ Relax threshold until sufficiency.

Otherwise:

2) Are aims still reachable with simplifications of the problem statement? Is it still relevant and topical?

   ⇨ Simplify the statement of the problem ; reduce the scope of the study.

Otherwise:

3) Are better methods available?

   ⇨ Implement and try them.

Otherwise:

4) Potential for fundamental research.

   ⇨ Risk of dead-end, depending on the deadline to keep the subject topical.

5.2 Sensitivity analysis: an example

Figure 5.2 gives an overview of the computing procedure. The CFD model was built with ANSYS FLUENT. The geometry and the mesh were built with GAMBIT. We use MATLAB to manage the sensitivity analysis: the case of reference, previously set up manually on FLUENT, is modified as necessary to launch every new simulation. The results saved after the simulations in FLUENT are then read back with MATLAB, post-treated, and finally saved in a database.

5.2.1 Operating conditions for all cases

Table 5.1 summarizes the operating conditions considered. Atmospheric pressure (1 bar) is set in fluid domains. The fuel entering the anode channel is a mixture of hydrogen, nitrogen, and steam with a composition of respectively 0.60, 0.37, 0.03 in molar fraction. The oxidant entering the cathodic channel is dry air (0.21 O_2, 0.79 N_2). The inlet temperature is 1 000 K for both gaseous mixtures. A current density of $j = 5\,000$ A/m^2 is imposed at the lower face of the MIC, whereas its upper face is imposed an electrical potential of zero volt.

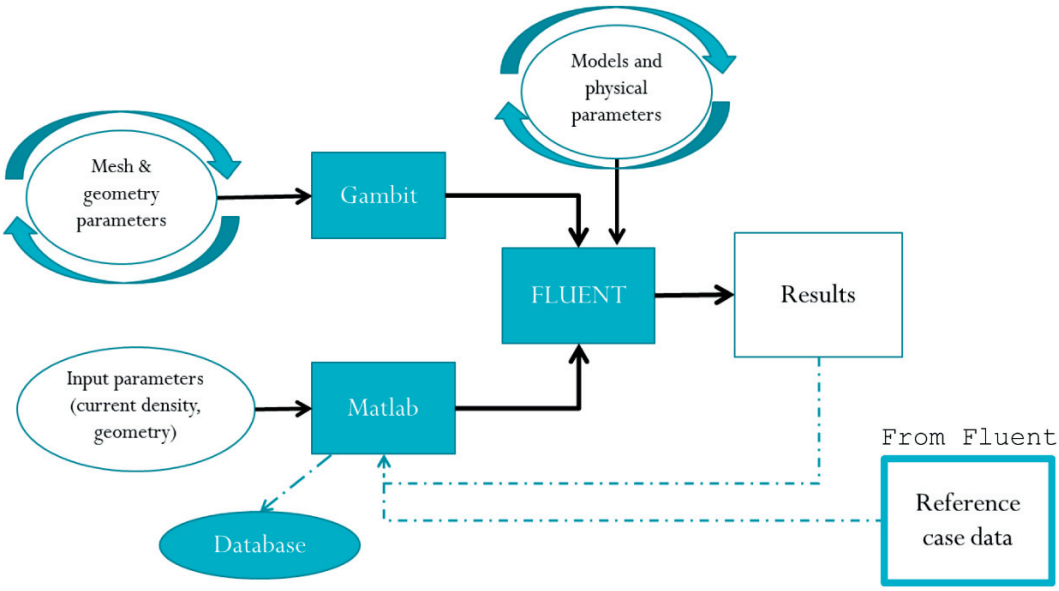

Figure 5.2 Diagram of the computing procedure.

The mass flow rate of fuel at the inlet is computed using Faraday's law and the mixing law, knowing the current density, the fuel utilization $\Upsilon = 0.8$, and the composition of the mixture. The mass flow rate of air at the inlet is then computed knowing the ***air-excess ratio***, which is $\lambda = 4$.

Table 5.1 Operating conditions.

Operating conditions		**Value**	**Unit**
Current density	j	5 000	A/m^2
Fuel utilization	Υ	0.8	—
Air-excess ratio	λ	4	—
Conditions at the inlet			
Temperature of fuel	T_f	1 000	K
Temperature of air	T_a	1 000	K
Pressure of fuel	p_f	1	bar
Pressure of air	p_a	1	bar
Composition of fuel, in mole fraction	x_{H_2}	0.60	—
	x_{H_2O}	0.03	—
	x_{N_2}	0.37	—
Composition of air, in mole fraction	x_{O_2}	0.21	—
	x_{N_2}	0.79	—

5.2.2 Geometry of reference

The geometry considered is a representative "periodic" element (figure 5.3), which is repeated laterally to form a complete fuel cell element. An anode, a cathode, their respective channels, and metallic interconnects compose the element. Table 5.2 gives the dimensions of the geometry.

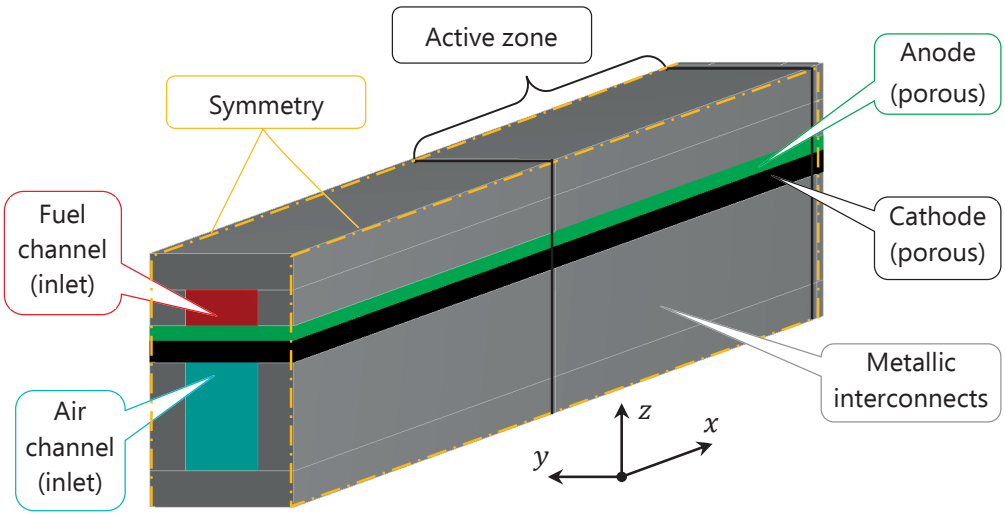

Figure 5.3 Computational domain, with main boundary conditions and type of bodies. The electrolyte is not modelled, as described in the text.

The active zone is surrounded by inactive zones, which are sometimes necessary to get a stable enough CFD simulation. Moreover, it allows to compute the velocity and temperature profiles at the entry of the active zone, without imposing them "arbitrarily". This will be discussed later. The volume of the anode and cathode are porous bodies (porosity of 30 %). The volume of the metallic interconnects is solid, and channels are fluid bodies. All boundary conditions of the domain are walls with no-slip velocity conditions, except for:

- the outlets of the channels: the pressure is imposed;
- the inlets of the channels: the mass flow rate is imposed;
- the sides of the section: symmetry.

Symmetry as a boundary condition implies the hypothesis that the interface is adiabatic. This is usually a simplification, which is fully valid only if the section is in the

middle of an infinitely large cell and infinitely tall stack, or conditions where most of the heat generated is evacuated by the flow of gases.

Table 5.2 Dimensions of the geometry.

Dimension	Value [mm]
Total length in x direction	81.0
Total width in y direction	2.0
Total height in z direction	3.5
Length of the active zone (cell)	40.0
Length of the inactive zone upstream	40.0
Length of the inactive zone downstream	1.0
Height of the anode	0.2
Height of the cathode	0.3
Height of the anodic channel	0.5
Height of the cathodic channel	1.5
Height of MICs, *excluding channels*	0.5
Width of channels	1.0

5.2.3 Indicator of accuracy

The following quantities of interest are extracted from the simulations:

- Velocity profiles at entries (see below);
- Along the electrodes:
  - Mole fractions of species;
  - Temperature;
  - Nernst potential.

These quantities are taken at both the anode and anode, along two lines (four in total) located in suitable zones of the computational domain:

- An horizontal line in the middle of each channel, at the entry of the active zone (rather than at the inlet of the computational domain);
- A longitudinal line along the surface of each electrode (at the width's middle).

The values are taken at the centre of every mesh cells that these lines cross. Voltage values are area-weighted averaged for every mesh cells. We use equation (5.3) to compute a single aggregated indicator of accuracy out of all the values.

5.2.4 Factors: attributes of the simulator

The sensitivity analysis articulates on the following categories of attributes:

(1) Modelling of boundary conditions;

(2) Meshing;

(3) Numerical methods and parameters;

(4) Physical models;

(5) Uncertainty about data.

Table 5.7 summarizes the attributes that we analysed for each category of attribute, and the respective levels that were considered for each attribute. We give further explanations below.

1. Modelling of boundary conditions

We should emphasize that this category of attributes corresponds to *the way the real boundary conditions are modelled* rather than variable values imposed as (real) boundary conditions. For instance, the latter could be different inlet mean velocities, whereas the first could be different ways or hypotheses to model the profile of the inlet velocity. The idea is that simplification of the geometry are often used; however they influence the boundary conditions; or more exactly, simplifying the geometry without adapting the implementation of the boundary conditions can result is significant change in the quantities of interest. Table 5.7 provides a summary of the cases considered, which are described below.

Reference

The geometry used is the one shown in figure 5.3, with the channel prolonged upstream of the active zone. We assume uniform profiles of velocity and temperature at the inlet, as is the case if it is connected to a plenum at inlet temperature (either with flow of same orientation, or with an even larger plenum allowing a homogeneous flow mixing/stabilization). This model has the advantage of computing the development of the flow hydrodynamically and thermally upstream of the active zone. However, cutting this part of the geometry can help to significantly reduce the computation time. Conversely, taking into account a bigger part of the fluid network upstream would allow an even more accurate representation of the reality.

Variations

Three other inlet conditions are considered:

(1) The reference geometry, but with a fully developed velocity profile at the inlet.

(2) A geometry without inactive zone upstream and a uniform velocity profile.

(3) A geometry without inactive zone, but with a fully developed velocity profile at the inlet (which in that case, correspond to the entry of the active zone).

The first boundary condition may be closer to reality if the plenum is not large enough to create uniform flow condition. Also, the flow will be thermally developed quicker. To spare computation time, it may be desirable to remove the part upstream of the active zone. Logically, we should adapt the boundary conditions, especially that of the velocity, which is basically what case (3) implements. We consider situation (4) as a further simplified test-case.

Remark: Obviously, the best would be to solve for the whole domain upstream. This is not usually done due to time constraint. Now, one could wonder why not computing once the profiles and implement them in a reduced geometry. The reason is simply that this would still be an approximation as soon as parameters of the simulation are changed (e.g., flow rate, temperature, …). The goal here is before all to assess the influence of the modelling of the boundary conditions.

2. Meshing

Reference

Since the geometry is simple, we use a mapped mesh to achieve maximum quality. A grading is applied to refine the mesh in the zones where gradients of quantities are expected to be large and to keep a relatively low number of cells elsewhere. In particular, a grading is applied along the longitudinal axis (x), which is especially useful at the interface between the active zone and the zone upstream of it. The total number of mesh cells is around 120 000 (reference).

Variations

We compare meshes with uniform intervals along the x-axis and with a grading instead. For each case, we consider several levels of resolution: 5 levels for the "uniform" mesh and 3 levels for the "gradual" mesh. Table 5.7 provides detail about the levels.

3. Numerical methods and parameters

Reference

Table 5.3 summarizes all the numerical methods and parameters used for the simulator of reference.

Variations

Numerical schemes used for the pressure-velocity coupling:

- *Reference:* `SIMPLE` (Semi-Implicit Method for Pressure-Linked Equations);
- `SIMPLEC` (`SIMPLE` Consistent);
- `Coupled`;
- `PISO` (Pressure Implicit with Splitting of Operator).

Numerical schemes used for the spatial discretization of pressure:

- *Reference:* `Standard`;
- `PRESTO`;
- 2nd order.

Criteria on the residuals used to stop the simulations:

- *Reference:* 10^{-5};
- 10^{-2}; 10^{-4}; 10^{-8}

Table 5.3 Numerical methods and parameters in the case of reference.

Numerical methods and parameters	
Residuals (convergence criteria)	All $< 10^{-5}$
Pressure-velocity coupling schemes	Semi-Implicit Method for Pressure-Linked Equations (`SIMPLE`)
Numerical schemes for spatial discretization of	
Gradients	Least squares cell based
Pressure	Standard
Momentum	2nd order upwind
Species	
Energy	
Electrical potential	

4. Modelling of physics

The electrochemical model is based on the FLUENT add-on for fuel cells. We use the SOFC model, which does not solve for the electrolyte: instead, the production and consumption of species are modelled with respectively sources and sinks of the relevant species at the anode and at the cathode [76].

Reference

Table 5.4 summarizes the parameters of the SOFC model (FLUENT add-on) used as a reference. Table 5.5 gives the models used to compute the properties of fluids in the case of reference.

Variations

We test various models used to calculate the properties of the gaseous mixtures: viscosity, specific heat, and thermal conductivity. Several degrees of approximation are possible, ranging from constant values to kinetic theory. The interested reader will find a good description of the models in the manuals of FLUENT. We tested:

- Constant values for all properties, taken at inlet temperature and pressure [77];
- Sutherland correlation for the viscosity (2 coefficients);
- Polynomial approximation for viscosity;
- Power law for viscosity (3 coefficients);
- Kinetic theory for all properties.

In addition, we tested the impact of disabling the energy sources in the volume and at the surface.

Table 5.4 Parameters of the SOFC model in the case of reference.

Parameters of the SOFC model in FLUENT add-on[1]	Value	Unit
Volumetric energy source	Enabled	
Surface energy source	Enabled	
Species sources	Enabled	
Electrochemistry of CO	Disabled	
Electrolyte conductivity sub-model	Disabled	

[1] In ANSYS FLUENT, the values (or functions) for the tortuosity and the electrical conductivity of materials should also be filled in the panel of the module for SOFC modelling. These properties are reported with the other properties of the solid materials.

Current under-relaxation factor	0.3	—
Total system current	0.4	A
Leakage current density	0	A/m^2
Electrolyte thickness	10^{-6}	m
Electrolyte resistivity	0.1	Ω m
Anode exchange current density	10^{20}	A/m^2
Cathode exchange current density	512	A/m^2

Table 5.5 Models for the properties of fluids in the case of reference.

Property	**Model**
Individual species: H_2, O_2, H_2O, *and* N_2	
Specific heat, $c_{p,i}$	Piecewise polynomial (2 pieces, 4th order)
Thermal conductivity, k_i	Polynomial (4th order)
Dynamic viscosity, μ_i	Sutherland (3 coefficients)
Other constant quantities (e.g., molar mass) left at default values of FLUENT	
Fuel mixture	
Density, ρ	Incompressible ideal-gas law
Specific heat, c_p	Mixing law
Thermal conductivity, k	Ideal-gas mixing law
Dynamic viscosity, μ	Ideal-gas mixing law
Mass diffusivity, D_{ij}	User defined (FLUENT SOFC model)
Thermal diffusion coefficient	Kinetic theory

5. Uncertainty about data

We distinguish this category from the previous (modelling of physics). Indeed, here we do not consider various models, but various constant parameters. Typically, this rather corresponds to uncertainty about available data parameters, or about calibration. Again, we should emphasize that these are attributes of simulators rather than classic variables, because they correspond to *uncertainty about data, impacting how accurately reality can be represented* rather than variable values used as a design purpose. Of course, both overlap in terms of methods and results of a sensitivity analysis; but the goal and conclusions are different. For instance, various materials can be tested to assess how their different properties influence the responses; or, a computation is done considering a particular material, but its properties are not perfectly characterised: measurements uncertainty, natural or manufacturing variability or heterogeneities, deviation with respect to a proper calibration for use in a simulation, etc.

The following properties were considered uncertain for the anode, the cathode, and the MICs:

- Electrical conductivity;
- Thermal conductivity;
- Tortuosity (except MICs, which are not porous).

Reference

Table 5.6 gives the values used as a reference for the properties of the solid materials.

Variations

For each attribute, 2 levels are considered in addition to the reference. An uncertainty of ± 10 % is considered for each, except for the tortuosity and the anodic thermal conductivity, which are changed to a larger extent. Table 5.7 summarizes the variations.

Table 5.6 Properties of the solid materials in the case of reference.

Properties of the solid materials		Value	Unit
Anode (Nickel + Yttria-stabilized Zirconia)			
Electrical conductivity	σ_{A}	134 730	$1/(\Omega\,\mathrm{m})$
Thermal conductivity	κ_{A}	6.23	$\mathrm{W/(K\,m)}$
Porosity	ψ_{A}	0.3	—
Tortuosity	τ_{A}	3	—
Density	ρ_{A}	3 030	$\mathrm{kg/m^3}$
Specific heat (at const. p)	$c_{p,\mathrm{A}}$	595	$\mathrm{J/(kg\,K)}$
Cathode (Lanthanum strontium manganite)			
Electrical conductivity	σ_{C}	6 767.1	$1/(\Omega\,\mathrm{m})$
Thermal conductivity	κ_{C}	1.15	$\mathrm{W/(K\,m)}$
Porosity	ψ_{C}	0.3	—
Tortuosity	τ_{C}	3	—
Density	ρ_{C}	4 375	$\mathrm{kg/m^3}$
Specific heat (at const. p)	$c_{p,\mathrm{C}}$	573	$\mathrm{J/(kg\,K)}$
Metallic interconnects (Stainless steel)			
Electrical conductivity	σ_{MIC}	40	$1/(\Omega\,\mathrm{m})$
Thermal conductivity	κ_{MIC}	72	$\mathrm{W/(K\,m)}$
Density	ρ_{MIC}	8 900	$\mathrm{kg/m^3}$
Specific heat (at const. p)	$c_{p,\mathrm{MIC}}$	446	$\mathrm{J/(kg\,K)}$

Table 5.7 Attributes of the simulator and respective levels that were considered. Bold font indicates for each attribute the level used in the reference case.

Category of attributes	Attribute analysed	Levels considered
Boundary conditions	Profile of velocity at the inlet	**Uniform**; fully developed
	Geometry	**With inactive zone upstream**; without (simplified)
Meshing	Mesh with gradient	Reference [a]; 2× finer; 2× coarser
	Uniform mesh	$\Delta x = \{0.05;\ 0.1;\ 0.25;\ 0.5;\ 1;\ 2\}$ mm
Numerical methods	Pressure-velocity coupling scheme	**`SIMPLE`**; `SIMPLEC`; `Coupled`; `PISO`
	Spatial discretization scheme for pressure	**`Standard`**; `PRESTO`; 2nd order
	Residuals convergence criteria	All $< 10^{-2};\ 10^{-4};\ \mathbf{10^{-5}};\ 10^{-8}$
Physical models	Viscosity of fluid	Constant; **Sutherland** with 2 and **3 coefficients**; polynomial law; power law; kinetic theory
	Thermal conductivity of fluid	Constant; **polynomial**; kinetic theory
	Specific heat of fluid	Constant; **piecewise polynomial**; kinetic theory
	Volumetric reactions	**On**; off
	Surface reactions	**On**; off
Uncertainty of data	Tortuosity of anode and cathode	Reference [b]; +33 %; −33 %
	Electrical conductivity of an., cath., and MIC	Reference [b]; +10 %; −10 %
	Thermal conductivity of cathode and MIC	Reference [b]; +10 %; −10 %
	Thermal conductivity of anode	Reference [b]; × 2; ÷ 2

[a] See text for a description of the mesh.

[b] See table 5.6 for numerical values.

5.3 Results

5.3.1 Boundary conditions modelling

Figure 5.4 shows the impact of the modelling of the boundary conditions (BCs) at the inlet with respect to the reference. Each of the tested BCs model leads to large global RMSD relative to the reference (20 % to 35 %). Even when they lead to rather significant reduction in computation time (e.g., −18 %), the corresponding sacrifice in accuracy (20 %) is clearly unacceptable, and certainly not worth the time spared. Here, it should be emphasized that which of these models of the BCs lead to responses closest to the real situation is *unknown*. Therefore, what we can deduct from these results is not which of these BCs models should be used, but that *the responses are highly sensitive to the modelling of the boundary conditions*. Hence, the conclusions are: 1) lots of care and efforts should be dedicated to gather knowledge and data about BCs; and 2) simplifying assumptions related to BCs should be used only as a last resort and meticulously checked.

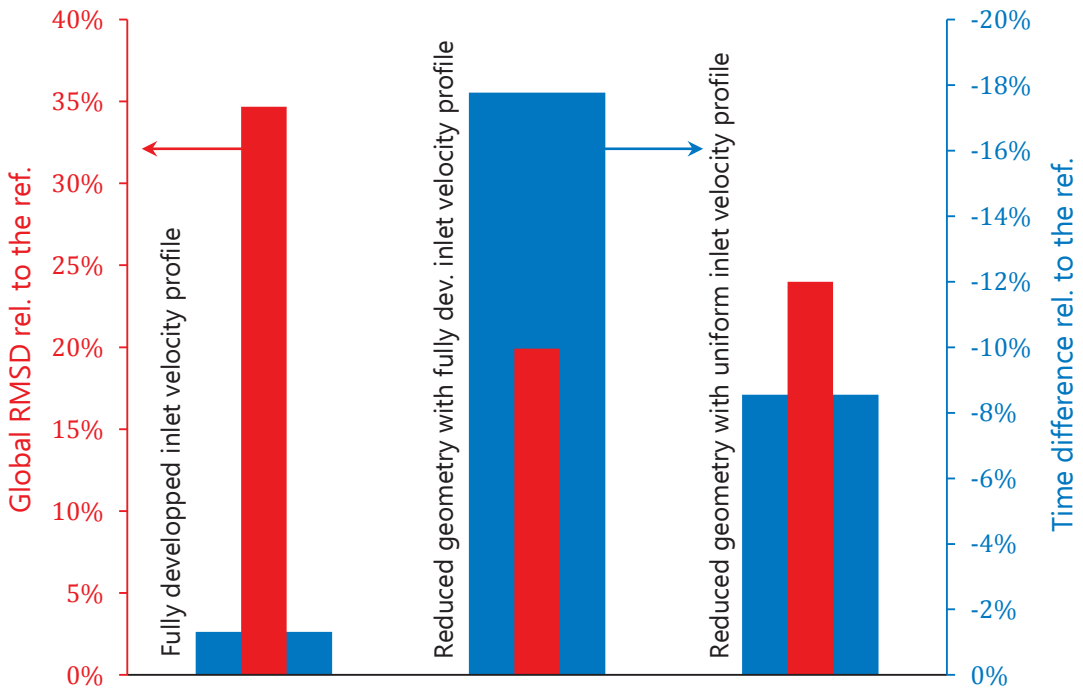

Figure 5.4 Sensitivity to the modelling of the boundary conditions at the inlet with respect to the reference, which has a uniform inlet velocity profile.

5.3.2 Meshes

Figure 5.5 shows the sensitivity to the mesh with respect to the "finest" mesh. The latter is refined twice with respect to the mesh used as a reference in the study of all other categories of attributes. Figure 5.6 includes data labels and illustrates the evolution of the responses for the meshes with uniform intervals, ordered from the coarsest to most refined of the uniform meshes.

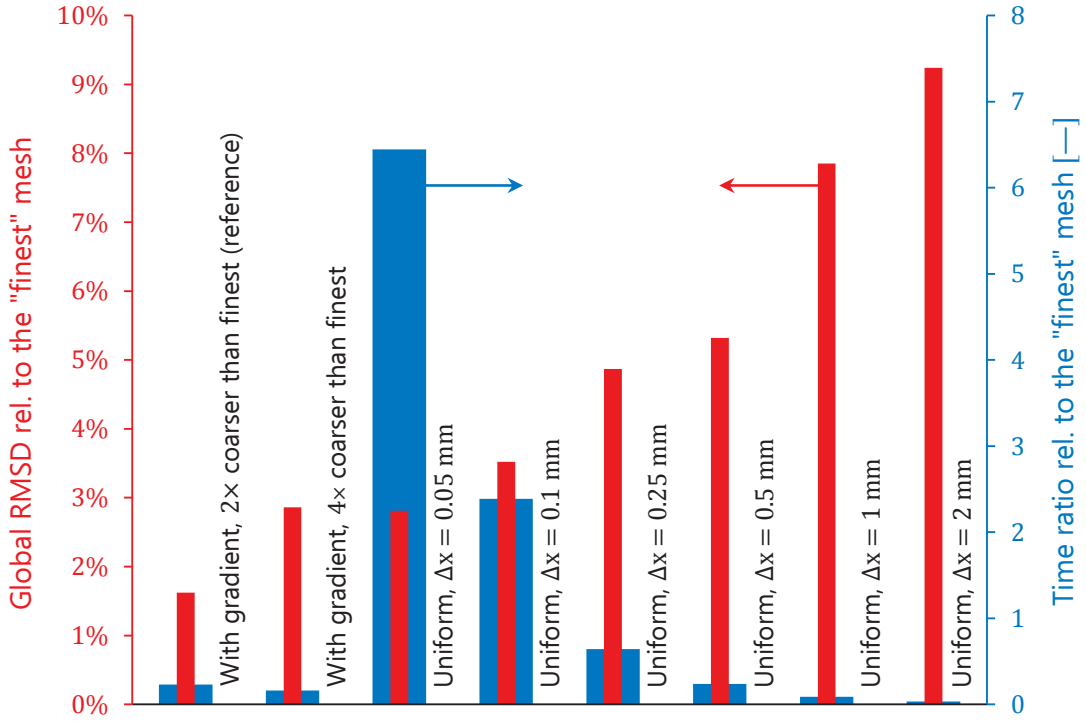

Figure 5.5 Sensitivity to the mesh with respect to the "finest" mesh, which is refined twice with respect to the "reference" mesh.

As could be expected, the global RMSD relative to the finest mesh increases as the resolution of the mesh decreases. The difference is rather significant for the coarsest mesh: ca. 9 %. However, it is 30 times less computer intensive with respect to the finest mesh with gradients. Conversely, the smallest RMSD is 1.6 % for the mesh of reference, i.e. with gradient but *twice coarser* than the finest. The simulation is solved in *less than a quarter of the time*. Interestingly, the finest of the uniform meshes needs more than 6 times longer to be solved (so, 24 × the reference), whereas still displaying a RMSD of 2.8 %. This makes clear that the meshes with gradients offer a much better "efficiency": they are more tractable for a given precision (accuracy).

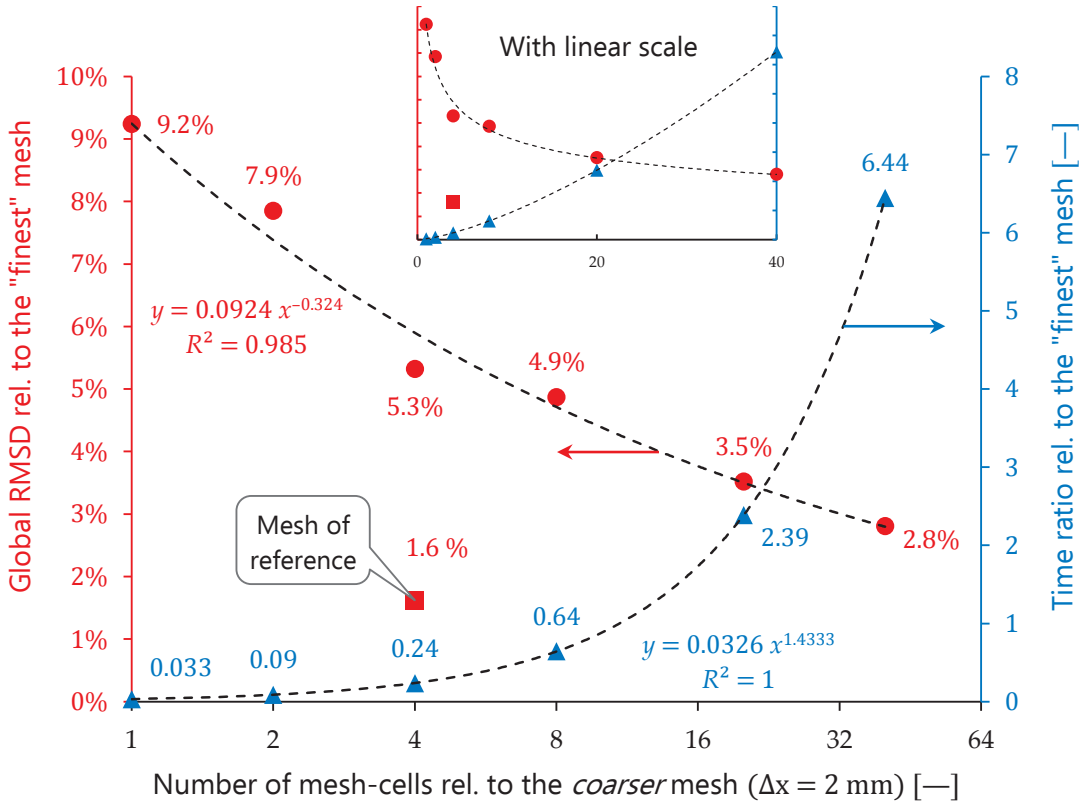

Figure 5.6 Sensitivity to the meshes with uniform intervals. The "finest" mesh is refined twice with respect to the mesh of reference; both use gradients contrary to the uniform meshes. Caution: the abscissa is in $\log_2$ scale.

It is important to realise that the computation time and the accuracy do not scale linearly with the resolution of the mesh. The *time* to solution increases slightly *faster* than the number of mesh-cells, whereas the *accuracy* first increases *faster* than the number of mesh-cells, but then *slower*, reaching a plateau asymptotically.

5.3.3 Numerical methods and parameters

Figure 5.7 shows the effect of the numerical methods and parameters with respect to the reference case. The global RMSD is smaller than 0.6 % for each tested numerical method. Meanwhile, the computation time can be as much as 177 % longer (residuals down to 10^{-8}) and as much as −77 % shorter (residuals down to 10^{-2}). The results show that targeting residuals as low as 10^{-8} is useless and detrimental to tractability. However, it may be risky to reach residuals of 10^{-2} only: 10^{-3} is a safer trade-off. Note

that in other studies, we observed imperfect convergence when the residuals of the energy and species equations where bigger than 10^{-6}.

Results also show that the choice of the numerical scheme to handle the pressure-velocity coupling (`SIMPLE`, `SIMPLEC`, `PISO`, `Coupled`) does not influence much the accuracy. Of course, this is true only as long as the simulation converges, which was not the case with the `Coupled` scheme. We could probably have been able to reach convergence by tuning its numerical parameters. However, in our experience, the `Coupled` scheme is neither the most adequate nor robust enough to handle such multi-physics problems (involving energy and chemistry equations). It is sensitive to small changes in the definition of the problem, so that its numerical parameters must often be adjusted to reach some convergence.

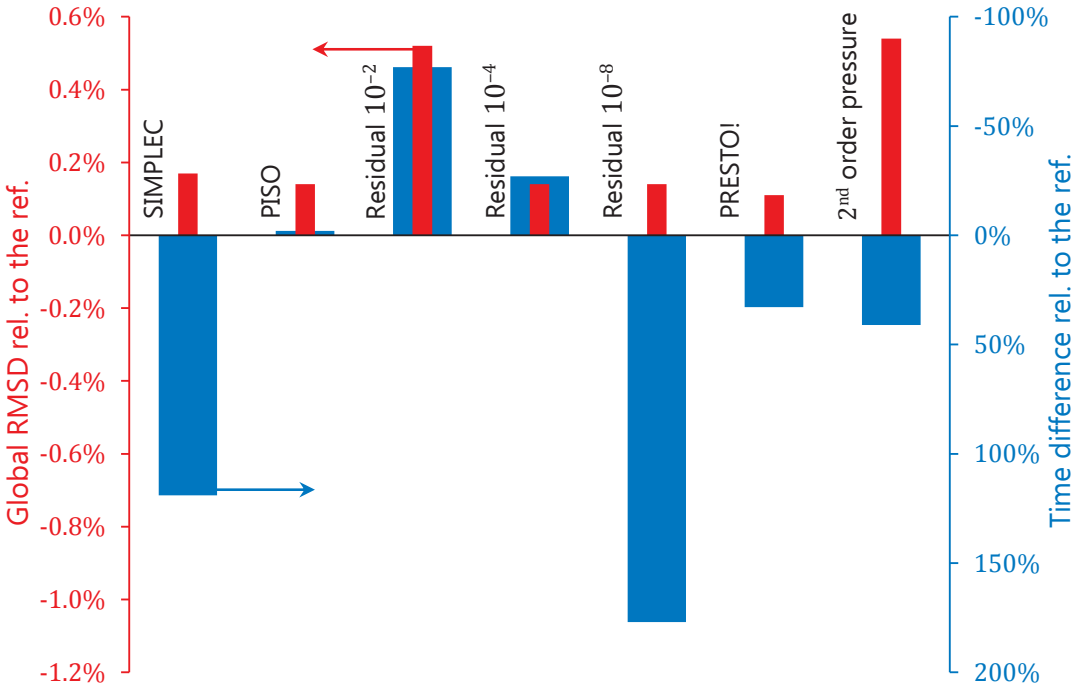

Figure 5.7 Sensitivity to the numerical schemes with respect to the reference.

For the spatial discretization of pressure, `PRESTO` is in principle advised for flows in porous domains [78]. However, in this case, investing more time (30 % for `PRESTO`, 40 % for 2nd order) in a scheme more sophisticated than `Standard` is probably not worth.

Remark: Despite the negligibly low global RMSDs on the responses observed here, these results should not lead to underestimate the importance of using appropriate numerical methods. The numerical schemes available in FLUENT are usually well-behaved and relatively robust, but this is neither true of any numerical implementation, nor in any situation. Only tests and experience will tell whether or not a numerical scheme leads to an accurate enough solution for a given problem.

5.3.4 Physical models

Figure 5.8 shows the influence of the physical models with respect to the reference case. The global RMSD is smaller than 0.5 % for each case except when the energy sources are disabled in the volume (10 %), and at the surface (7 %). Conversely, the time difference is always bigger than 1 %. According to these results, the most efficient modelling for viscosity seems to be Sutherland's correlation (with two coefficients), which allows to reduce the computation time by almost 10 % with respect to the correlation with three coefficients, while conceding only 0.4 % on the responses. Using constant specific heats and constant thermal conductivities for the fluids does not lead to a significant difference in the responses. It should be highlighted, though, that these properties were evaluated at the operating temperature. Depending on the scenario, the validity of this simplification may not hold (e.g., larger temperature difference in the domain). The time spared with constant specific heats is small (−1 %); keeping a polynomial model is therefore preferable (at least for peace of mind). More time is spared with constant thermal conductivities (−8 %), so that such a simplification may be worth.

Impact of viscosity on the evaluation of hydraulic resistances

Conclusions from the previous analysis about models used for the viscosity may be misleading. Indeed, the model used to compute the *viscosity of each particular gas*, and thereby the viscosity of the mixture, has little impact on the final responses. However, the viscosity of the mixture may vary on a bigger range depending on the (local) *composition of the mixture*. For this model of a single channel, composition of the mixture mostly changes in the direction of the flow, so that, on average, the effect of viscosity is small. However, in a complete cell element, with several channels (or paths), the average composition of the mixture along each channel may vary with respect to the

others, i.e., a variation transversal to the flow direction. In that case, the hydraulic resistance of the flow changes correspondingly; so it may lead to less uniform flow distribution.

We therefore conducted a sensitivity analysis with (constant) mixture viscosities at the extreme of the possible interval (according to the composition of the mixture). The maximum possible change of the mixture's viscosity is ca. 15 %. As expected, the effect on the hydraulic resistance is significant and of the same order of magnitude because of the linear relationship between the pressure drop and the viscosity for laminar flows. However, the effect on the global difference is even a bit more significant, with ca. 20 %.

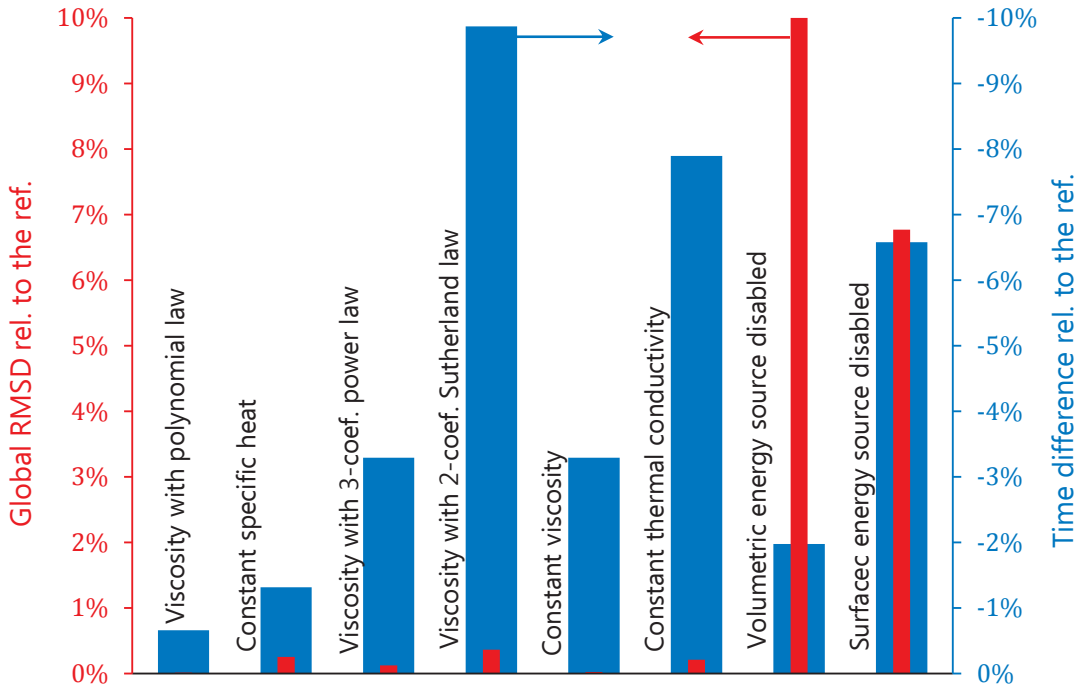

Figure 5.8 Sensitivity to the physical models with respect to the reference.

5.3.5 Uncertainty about data

Figure 5.9 shows the effect of the uncertainty on solid material properties with respect to the reference case. The factors were varied by minimum ± 10 % around the value of reference. The resulting variations of the responses are virtually identical in every direction. So, we do not display them individually, except for the MIC electrical conductivity, for which the global RSMD is slightly bigger for -10 % than for $+10$ %.

The responses are relatively insensitive to the variations of all the tested factors, with a maximum of 1 % global RSMD for a minimum of 10 % variation. The results are particularly insensitive to the thermal conductivities, especially that of the anode (which was varied by +100 %, −50 %). It should be reminded here that similar conclusions were drawn about the thermal conductivities of the fluids. The time difference is small, which is logical, since changing the value of constants should not have a minimal impact on the computation time (as long as the values are in a range where no considerable change occurs in the physics). The measured difference, less than 3 seconds, is most probably noise due to uncontrolled external factors (e.g., computer processes in the background, watch/human precision). It actually *informs us about the margin of error on the computation times* measured. Ideally, the simulations should be re-run several times to eliminate most of this noise.

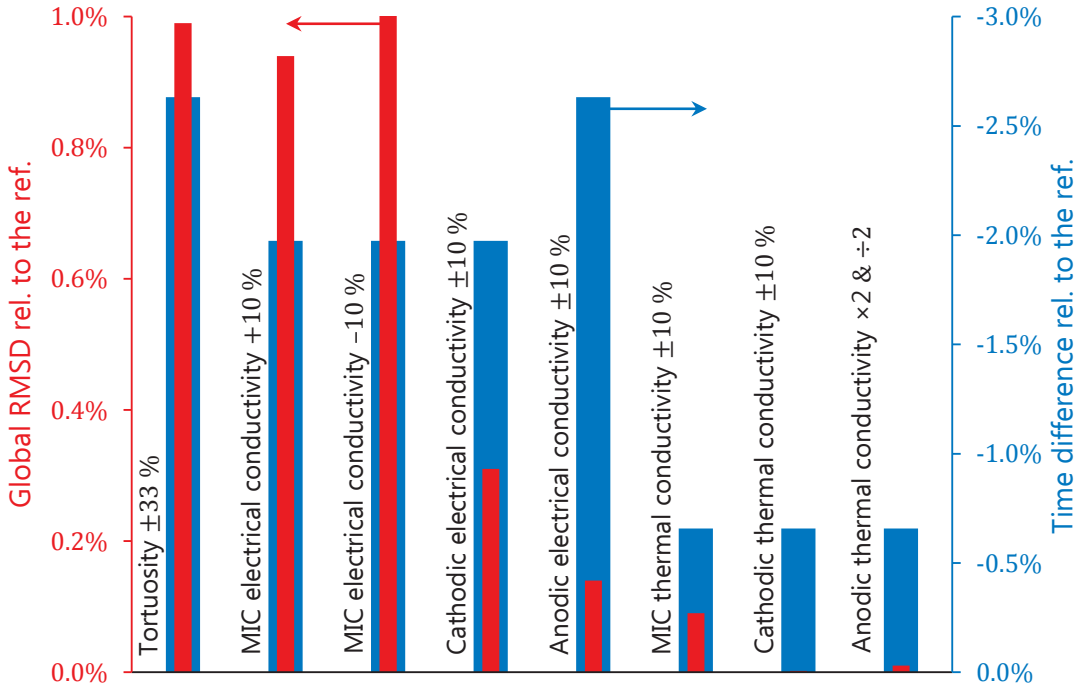

Figure 5.9 Sensitivity to the solid material properties with respect to the reference.

5.4 Conclusions to the chapter

Among the five categories of attributes that we analysed, the uncertainty about data show overall the least amount impact on accuracy and tractability. The numerical methods did not display a strong effect on the accuracy, but the tractability is affected, making such attributes good candidates to choose adequately for getting a more efficient simulator. The meshing usually impacts tractability even more, but their effect on accuracy is also a bit stronger. A compromise need to be done. Nevertheless, it was shown that well-designed meshes can be much more "efficient" than more basic ones. The influence of physical models ranges from negligible (e.g., model of fluid properties)) to significant (sources of energy from reactions). The computation time was only slightly affected in comparison. Finally, it was shown that the modelling choice of the boundary conditions have a significant impact on accuracy, and sometimes also on computation time. It is interesting to note that none of the attributes analysed in our study had an effect at the same time strong on accuracy and negligible on tractability.

"Statistics are like bikinis. What they reveal is suggestive, but what they conceal is vital."
Aaron Levenstein

CHAPTER 6

Sensitivity to decision variables

This chapter presents the application of design and analysis of computer experiments (DACE) to our problem. We used DACE to carry out a sensitivity analysis with a rigorous mathematical approach. Additionally, the purpose was to evaluate the accuracy of the approximate models that can be generated with DACE, and if appropriate, to eventually build and use one such model for the subsequent uncertainty quantifications and optimizations under uncertainty.

This chapter is largely based on our publication *Design and analysis of a computer experiment of the anode-gas-flow distribution in fuel cells* [79].

6.1 Summary

A homogeneous flow distribution into the bipolar plates of fuel cells is known to be important for their proper operation. This study investigates techniques for the design and analysis of computer experiments (DACE) to carry out a sensitivity analysis and generate a meta-model, while optimizing the number of runs needed. Various design variables and operating conditions are considered as factors; namely: (1) topology of manifolds, (2) height of channels, (3) width of manifolds, (4) mole fraction of hydrogen, and (5) electrical current density. A fractional factorial design and a central composite design are chosen in the frame of this study. The responses of interest for which the effect of the factors and their interactions is quantified are (a) flow uniformity and (b) pressure drop. Among the selected factors, the width of the manifolds displays the most significant effect on the flow uniformity.

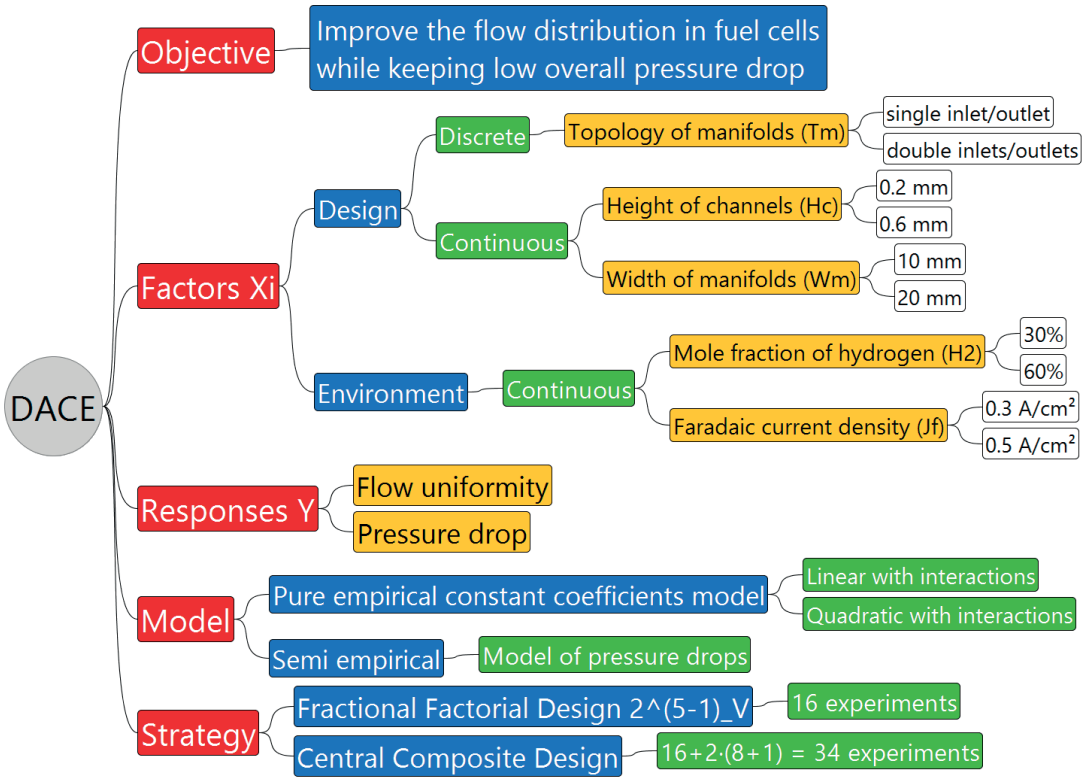

Figure 6.1 Conceptual map of the study, using design and analysis of computer experiments (DACE).

6.2 Introduction

This study will investigate the flow distribution and the pressure drop into the bipolar plate at the anodic side of an SOFC.

A computer experiment is a number of runs of the code (simulation) with different input. Computer experiments are deterministic unless wished stochastic, so that identical outputs can be expected when the code is run with identical inputs. The absence of random error is an important difference between computer experiments and physical experiments [80]. DACE techniques are useful to rationally select the input variables needed for a systematic study of the responses and to minimize the number of simulations. Another goal of DACE is to build an approximate model, often called surrogate model — much simpler and quicker to evaluate than a more exhaustive one, whereas still able to capture the phenomena of interest.

6.3 Problem definition

6.3.1 Computer model

The study focuses on the flow distribution into the bipolar plate at the anodic side of an SOFC fuelled with a mixture of hydrogen, nitrogen, and a constant 3 % mole fraction of water vapour. The flow distribution of fuel mixture into the fuel cell is computed using CFD simulations, carried out with ANSYS FLUENT v14.5.0.

Steady-state and laminar conditions ($Re < 700$) are assumed for the 3D flow model used. To simplify this analysis, the model does not include source terms for species. Indeed, at the anode of SOFCs fuelled with hydrogen, the volumetric flow rate is constant and the maximum possible change of the mixture's viscosity is ca. 15 %. Species transport and energy equations are however activated, to ease the estimation of the fuel-mixture properties. The specific models used to compute these properties are reported in table 6.7, p. 185. It should be noted that in the frame of our study, only density and viscosity are relevant.

The mass flow rate $\dot{M}$ of fuel at the inlet is computed according to gas mixing and Faraday's laws combined in equation (6.1), considering the rate of fuel that would be necessary to provide the specified faradaic current density $j_{\max}$ (i.e., the fuel power that is injected into the fuel cell).

$$\dot{M} = \frac{j_{\max} A_{\mathrm{a}}}{z \mathcal{F} n_{\mathrm{H_2}}} \sum_i \mathcal{M}_i n_i \tag{6.1}$$

where A_{a} is the area of the active zone, z the number of electrons exchanged, $\mathcal{F}$ the Faraday's constant, $\mathcal{M}_i$ the molar mass of species i, and n_i its mole fraction.

The geometry considered and the corresponding computational domain are shown in figure 6.2. The 3D fluidic volume is meshed such as to ensure enough resolution everywhere, while using bi-directional growth ratio to keep a low number of mesh cells (ca. 200 000).

The boundary conditions are as follows: the pressure at the outlet is set with a gauge-pressure relative to atmosphere of 0 Pa; the mass flow rate is set at the inlet according to equation (6.1); inlet and backflow temperature is set at 750 °C; walls are assumed adiabatic and a no-slip velocity condition is imposed on them.

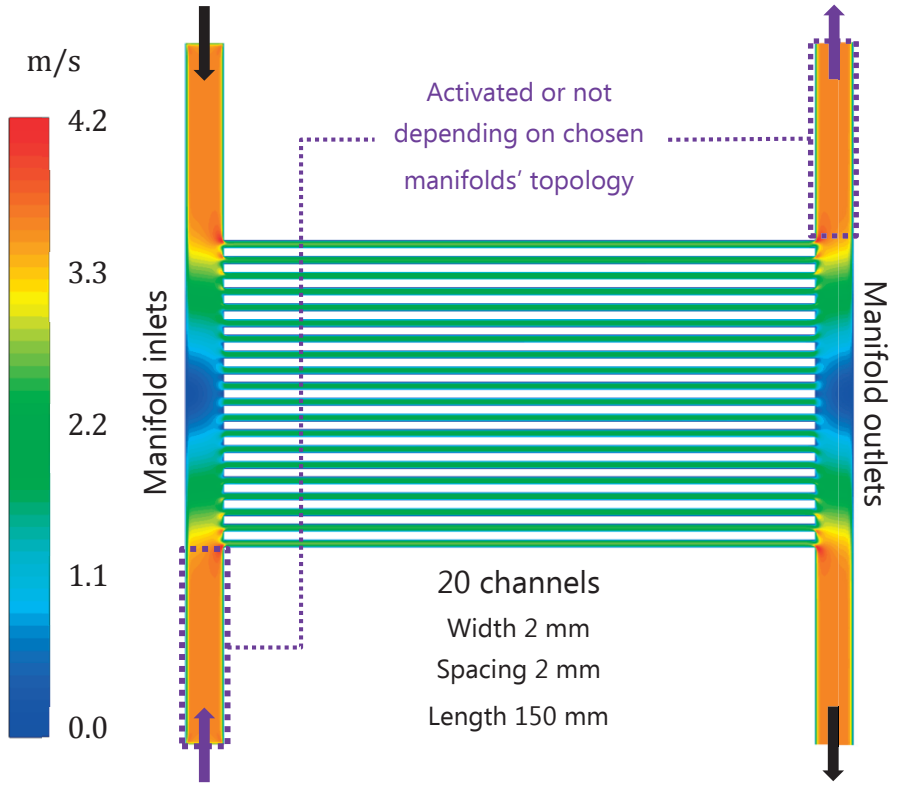

Figure 6.2 Top-view of the studied geometry, with field of velocity magnitude on the middle plane [m/s].

Numerical solver settings

Since the gas-mixture can be assumed incompressible[1], the pressure-based solver is used to solve the subset of the Navier-Stokes equations, using double precision. The Semi-Implicit Method for Pressure-Linked Equations (`SIMPLE`) is used as the pressure-velocity coupling. The chosen discretization scheme is second order upwind for momentum, species, and energy, whereas pressure uses a second order scheme. Relaxation factors and linear solver settings (multi-grid) were left at their default values. The simulations were run for 50 iterations, which was enough to achieve excellent convergence: all residuals $< 10^{-7}$, conservation of mass, convergence of the responses of interest. This is in part due to the high quality of the mesh.

[1] Explanations about situation where a fluid behaves as if it were incompressible are given in the section *Incompressible vs. compressible*, p. 90.

6.3.2 Factors, respective levels, and responses

A total of five factors were considered, with two levels for each. Three factors relate to the design (geometry): topology and width of the manifolds, and height of the channels. Two factors relate to operating conditions: electrical current density (affecting directly flow rate) and mole fraction of hydrogen (affecting directly fuel-mixture properties and flow rate). All factors are continuous variables except for the topology. Two responses are considered: flow uniformity and global pressure drop. Table 6.1 summarizes the chosen factors and their respective levels.

Table 6.1 Factors and levels considered in the DACE.

	Factors	Min values (-1)	Max values $(+1)$
X_1	Topology of manifolds (Tm)	single inlet & outlet	double inlets & outlets
X_2	Height of channels (Hc)	0.2 mm	0.6 mm
X_3	Width of manifolds (Wm)	10 mm	20 mm
X_4	Mole fraction of H_2 (H2)	30 %	60 %
X_5	Faradaic current density (jF)	0.3 A/cm^2	0.5 A/cm^2

6.4 Design and analysis of the computer experiment

6.4.1 First-order model with interactions

Fractional factorial design (FFD)

A fractional factorial design allows building statistical models with a smaller number of runs than a full factorial design.

A "two levels per five factors" experiment is studied in a 2_V^{5-1} design that corresponds to a half fraction of the full 2^5 design. Such a design is built by writing down all possible 24 level[2] combinations for the four factors X_1, X_2, X_3, X_4, and then setting the level of the fifth factor as the product of the first four, so that levels of $X_5 = X_1\, X_2\, X_3\, X_4$. As a consequence, the main effect a_5 is aliased with the fourth order interaction a_{1234}. This means that for this fractional factorial design we can estimate all main effects and all

[2] The number of level is 24 because one factor is discrete.

interactions of two factors independently assuming that higher order interactions are negligible.

The general equation for a first-order model with interaction is:

$$Y = a_0 + \sum_{i=1}^{n} a_i X_i + \sum_{i=1}^{n-1} \sum_{j=i+1}^{n} a_{ij} X_i X_j + \epsilon \tag{6.2}$$

where Y is the set of the responses from the computer experiments, a_i is the coefficient (called effect) associated to the factor X_i, and ϵ the residue.

Evaluation of the model matrix

The covariance- or dispersion-matrix, $(\boldsymbol{X}' \boldsymbol{X})^{-1}$, contains the variances of the variables along the main diagonal and the covariance between each pair of variables in the other matrix positions. This matrix represents the transfer of variance between the factors and the effects [81]. Due to the orthogonality of the fractional factorial design, the dispersion matrix does not contain covariance terms. Moreover, the variance that is transferred from the factors to their respective effect only depends on the numbers N of runs. The dispersion-matrix can hence be written as:

$$\left(\boldsymbol{X}' \boldsymbol{X}\right)^{-1} = \frac{1}{N} \boldsymbol{I_N} \tag{6.3}$$

In this case, 16 runs are computed and the variance for all the diagonal elements is equal to 6.3 %. In classical experiments, the dispersion should be kept as small as possible to avoid amplifying the variance from the factors to the effects. The latter is less important while using deterministic numerical models since by definition no noise (error) is injected through the input factors. Multicollinearity is also not an issue for these designs. The variance inflation factors (VIFs) predict the quality of the estimation of effects a_i and correspond to the diagonal terms of the inverse of the correlation matrix. The terms r_{ij} of the correlation matrix are calculated according to:

$$r_{ij} = \frac{\mathrm{cov}\left[a_{ij}\right]}{\sqrt{\mathrm{var}[a_i]\ \mathrm{var}\left[a_j\right]}} \tag{6.4}$$

The lowest and best value that VIFs can take is 1. A common rule of thumb asserts that multicollinearity is an issue — and a different design should be considered — if $\mathrm{VIF}[a_i] > 10$. In the present case, all VIFs are equal to 1.

Due to the orthogonal property of the dispersion matrix, the coefficients of the model (the effects) can be estimated as:

$$\boldsymbol{E}[\boldsymbol{a}] = \frac{1}{N}\, \boldsymbol{X}'\, \boldsymbol{Y} \tag{6.5}$$

6.4.2 Second-order model

Central composite design

A central composite design (CCD) is used to study the quadratic effects of factors. Central points and "star points" are added to estimate the curvature. The model matrix of the CCD is built by combining a classical FFD matrix with the aforementioned additional points. Figure 6.3 illustrates the graphical domain for a general 2^3 (full) factorial design with one central point and six star points.

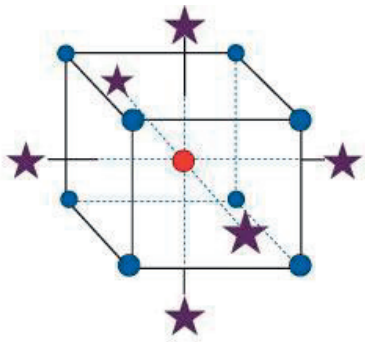

Figure 6.3 Central composite design for 3 factors, each along an axis of the cube.

Discrete factors affect the construction of a CCD model matrix. Figure 6.4 illustrates this with a design composed of one discrete and one continuous factor. As shown, a single common central point cannot be defined for the two factors because the discrete factor admits two levels only (no central point along its axis). For this reason, two central points are necessary — one for each level of the discrete factor — and four "star points" aligned as shown rather than forming a cross (star).

In this study, the design consists of the 2_{V}^{5-1} fractional factorial points, two central points due to the presence of one discrete factor with two levels, and eight star points for each level of the discrete factor (summing to 34 runs). These star points are aligned with each factor's axis on a circle with origin at the central points and a radius equal to 1.607 [for optimality reason, see 80].

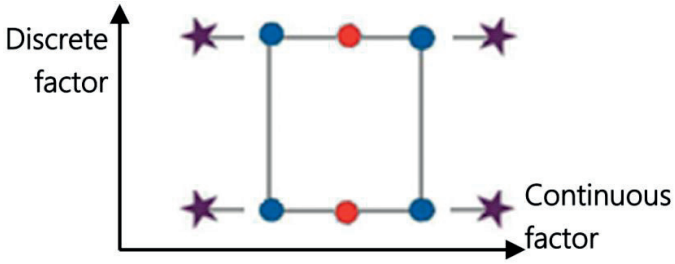

Figure 6.4 Central composite design for 2 factors when 1 factor is discrete.

The CCD allowed the estimation of quadratic terms in addition to the linear terms and interactions of two factors. The coefficients for the quadratic model can be computed from a least-square fit:

$$\boldsymbol{E}[\boldsymbol{a}] = (\boldsymbol{X}'\,\boldsymbol{X})^{-1}\boldsymbol{X}'\,\boldsymbol{Y} \tag{6.6}$$

The quadratic model with interactions of two factors is given by:

$$Y = a_0 + \sum_{i=1}^{5} a_i\,X_i + \sum_{i=1}^{4}\sum_{j=i+1}^{5} a_{ij}\,X_i\,X_j + \sum_{i=2}^{5} a_{ii}\,{X_i}^2 + \epsilon \tag{6.7}$$

Quadratic terms for discrete factors cannot be represented.

Evaluation of the model matrix

The model matrix for CCD is no more orthogonal. Diagonal terms of the dispersion matrix range from 3 % to 30 %. The correlation matrix highlights the influence among the variables. In particular, the second-order model affects the constant a_0 and all second-order coefficients are correlated. The VIFs are reported in table 6.2.

Table 6.2 Variance inflation factors of the coefficients for CCD.

a_0	a_1	a_2	a_3	a_4	a_5	a_{12}	a_{13}	a_{14}	a_{15}
9.95	1.00	1.00	1.00	1.00	1.00	1.00	1.00	1.00	1.00
a_{23}	a_{24}	a_{25}	a_{34}	a_{35}	a_{45}	a_{22}	a_{33}	a_{44}	a_{55}
1.00	1.00	1.00	1.00	1.00	1.00	2.37	2.37	2.37	2.37

Since the VIF of a_0 is almost 10 and those of the second-order terms equal 2.37, the accuracy of the model is not independent on the experimental errors.

6.5 Results and discussion

6.5.1 Pressure drop

The first response analysed is the pressure drop. According to the laws of fluid mechanics, the relationship between the pressure drop and the hydraulic diameter is highly nonlinear. Hence, we expect that at least a second-order model is required.

Linear model with interactions

The coefficients of the first-order model, given in equation (6.2), can be computed using the fractional factorial design. The relative effects, which give an idea about the influences of the factors on the response, are computed by dividing the effects by the constant of the model, a_0. The relative effects are reported in figure 6.5.

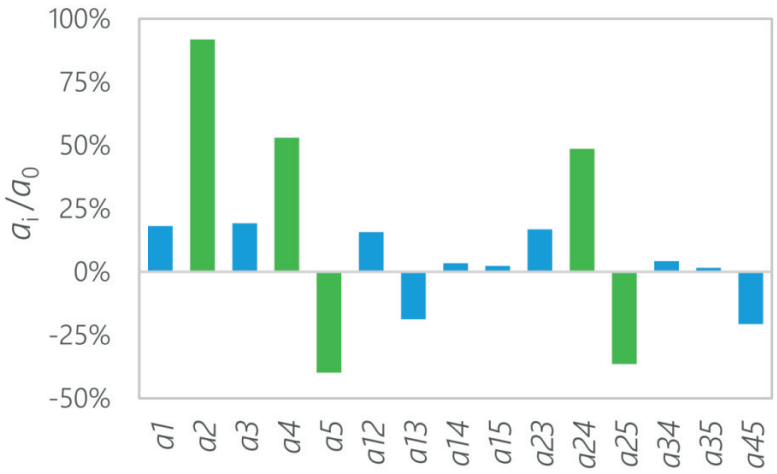

Figure 6.5 Relative effects for Δp^{-1} with the FFD.

Figure 6.5 shows that the coefficients a_2, a_4, a_5, a_{24}, and a_{25} have a large influence on the response. This means that the pressure drop response is mainly dependent on the height of the channel X_2 (affecting the hydraulic diameter), on the mole fraction of hydrogen X_4, and on the current density X_5 as well as on their interactions $X_2\,X_4$ and $X_2\,X_5$.

An analysis of variance (ANOVA) is done to evaluate more accurately the significance of effects. It informs about the degree of variability within a regression model and is the basis for testing statistical significance [81].

Table 6.3 contains the sum of squares (SS) of each factor, its number of degrees of freedom[3] (DF), the mean of the sum of squares (MSS) standardized with respect to DF, the Fisher index (F) of the MSS of the coefficient with respect to the MSS of the residual, and the probability ($\mathcal{P}$) that this ratio and the random variables have the same origin and hence are due to noise. To be able to carry out the ANOVA, it is necessary to have at least one degree of freedom for the residue. In this case, it was necessary to discard one of the smallest relative effects (a_{15}) in figure 6.5.

Table 6.3 shows that the MSS of large relative effects is significantly greater than the MSS of the residual errors, as expected. Considering a threshold of 5 %, the statistically significant effects are the ones already highlighted by the histogram of relative effects. Conversely, the other effects have a higher probability $\mathcal{P}$ to originate from random processes.

However, although the conducted computer experiments certainly do not represent reality with the utmost accuracy, they have the advantage of being marginally affected by random processes, since the sources of noise are minor (convergence was achieved with at least 10^{-7} for all residuals and the mesh was checked for high quality and homogeneity across all design points).

Considering only the significant coefficients highlighted in green in table 6.3, the model is then given by:

$$E(\Delta p^{-1}) = a_0 + a_2\, X_2 + a_4\, X_4 + a_5\, X_5 + a_{24}\, X_2\, X_4 + a_{25}\, X_2\, X_5 \tag{6.8}$$

Results from the simulation are compared with those obtained from the model in figure 6.6. The model reproduces the results in a clear way only for cases with a big pressure drop. As expected, the first-order model is unable to predict a response that is highly nonlinear. A second-order model is then studied to find a better fit.

[3] The number of degrees of freedom equals the number of levels minus one.

Table 6.3 ANOVA of the linear model for Δp^{-1}.

Source	SS	DF	MSS	F	$\mathcal{P}$
a_0	7.68E+5	1	7.68E+5	1.86E+3	1.5 %
a_1	2.52E+4	1	2.52E+4	6.10E+1	8.1%
a_2	6.48E+5	1	6.48E+5	1.57E+3	1.6 %
a_3	2.82E+4	1	2.82E+4	6.84E+1	7.7 %
a_4	2.15E+5	1	2.15E+5	5.22E+2	2.8 %
a_5	1.22E+5	1	1.22E+5	2.95E+2	3.7 %
a_{12}	1.89E+4	1	1.89E+4	4.58E+1	9.3 %
a_{13}	2.71E+4	1	2.71E+4	6.57E+1	7.8 %
a_{14}	8.89E+2	1	8.89E+2	2.16E+0	38.1 %
a_{23}	2.15E+4	1	2.15E+4	5.21E+1	8.8 %
a_{24}	1.81E+5	1	1.81E+5	4.39E+2	3.0 %
a_{25}	1.02E+5	1	1.02E+5	2.47E+2	4.0 %
a_{34}	1.34E+3	1	1.34E+3	3.26E+0	32.2 %
a_{35}	1.82E+2	1	1.82E+2	4.41E−1	62.7 %
a_{45}	3.28E+4	1	3.28E+4	7.94E+1	7.1 %
Residue	4.13E+2	1	4.13E+2		
Total	2.19E+6	16			

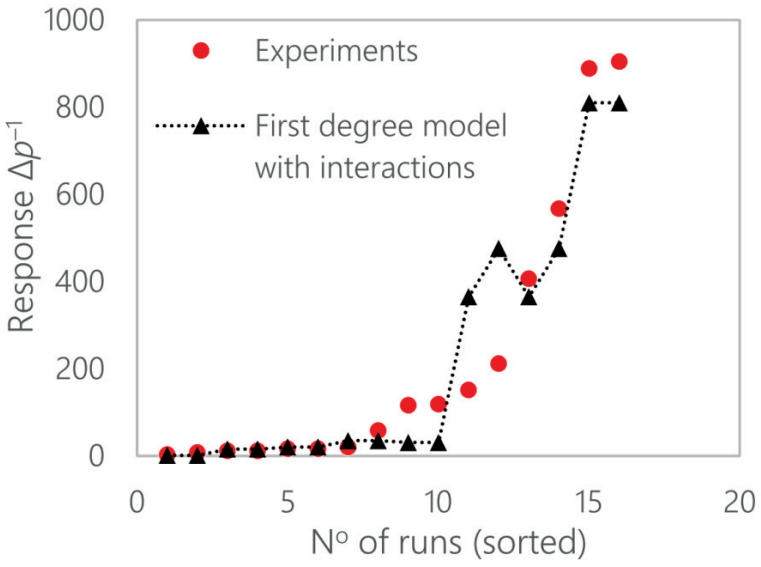

Figure 6.6 Comparison of Δp^{-1} from the simulation and from the linear model with interactions.

Quadratic model with interactions

As described previously, the effect of the factors on the response can be evaluated with various analyses. Figure 6.7 shows the histogram of the relative effects.

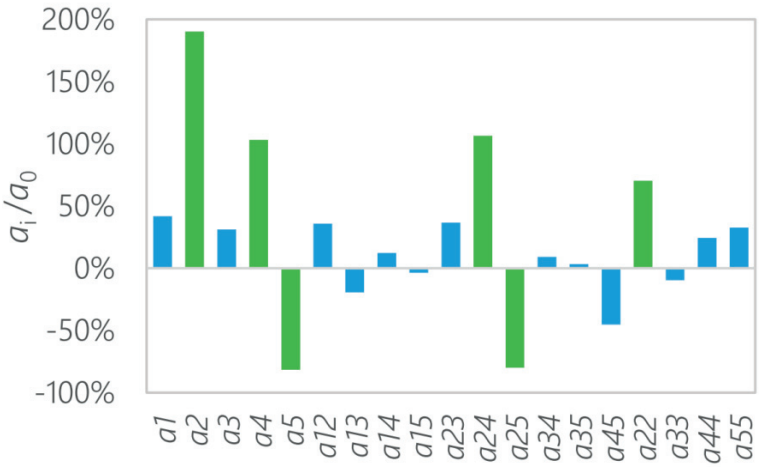

Figure 6.7 Relative effects for Δp^{-1} with the FFD.

The influence of the channel's height X_2 is again evident. The main effects highlighted by the histogram are the same than for the linear model with interactions, with the only difference being the presence in this case of the second-order coefficient related to the channel's height, a_{22}. The central composite design matrix is not orthogonal. As a consequence, to carry out the ANOVA, the design has to be made orthogonal step-by-step, giving the corrected sum of squares (SS^*). It can be observed in

table 6.4 that the effects which have near-zero probability $\mathcal{P}$ to arise from noise are the same as highlighted by the histogram of relative effects. Nevertheless, some other factors with a probability less than 5 % are likely significant, too (in orange).

Considering only the coefficients highlighted in green in

table 6.4, the model becomes:

$$E(\Delta p^{-1}) = a_0 + a_2 X_2 + a_4 X_4 + a_5 X_5 + a_{24} X_2 X_4 + a_{25} X_2 X_5 + a_{22} {X_2}^2 \tag{6.9}$$

Figure 6.8 shows that the quadratic model seems to follow the trend of the simulated responses better than the linear model. Nevertheless, a quadratic model is clearly still

unable to predict accurately the pressure drop. Further analysis could be done considering a fourth-order polynomial model or a more sophisticated model. Among other corrections, the model should not give rise to unphysical responses like here (negative).

Table 6.4 ANOVA of the quadratic model for Δp^{-1}.

Source	SS^*	DF	MSS	F	$\mathcal{P}$
a_0	1.26E+6	1	1.26E+6	4.01E+2	1.0E−11
a_1	5.92E+4	1	5.92E+4	1.88E+1	0.1 %
a_2	9.51E+5	1	9.51E+5	3.03E+2	7.1E−11
a_3	2.56E+4	1	2.56E+4	8.14E+0	1.3 %
a_4	2.80E+5	1	2.80E+5	8.90E+1	1.9E−7
a_5	1.75E+5	1	1.75E+5	5.57E+1	3.1E−6
a_{12}	3.37E+4	1	3.37E+4	1.07E+1	0.6 %
a_{13}	9.86E+3	1	9.86E+3	3.14E+0	9.8 %
a_{14}	3.97E+3	1	3.97E+3	1.26E+0	28.0 %
a_{15}	3.63E+2	1	3.63E+2	1.15E−1	73.9 %
a_{23}	2.15E+4	1	2.15E+4	6.84E+0	2.0 %
a_{24}	1.81E+5	1	1.81E+5	5.77E+1	2.5E−6
a_{25}	1.02E+5	1	1.02E+5	3.25E+1	5.5E−5
a_{34}	1.34E+3	1	1.34E+3	4.28E−1	52.4 %
a_{35}	1.82E+2	1	1.82E+2	5.78E−2	81.3 %
a_{45}	3.28E+4	1	3.28E+4	1.04E+1	0.6 %
a_{22}	8.25E+4	1	8.25E+4	2.63E+1	1.5E−4
a_{33}	1.19E+4	1	1.19E+4	3.80E+0	7.2 %
a_{44}	3.79E+3	1	3.79E+3	1.21E+0	1.7 %
a_{55}	1.92E+4	1	1.92E+4	6.12E+0	2.7 %
residue	4.40E+4	14	3.14E+3		
Total	3.30E+6	34			

6.5.2 Uniformity of flow distribution

The indicator of flow uniformity that we use is γ, defined in equation (3.3).

The aforementioned fractional factorial design is used to identify the main effects in a linear model with interactions. Then, the central composite design is considered to assess curvature and generate a quadratic model.

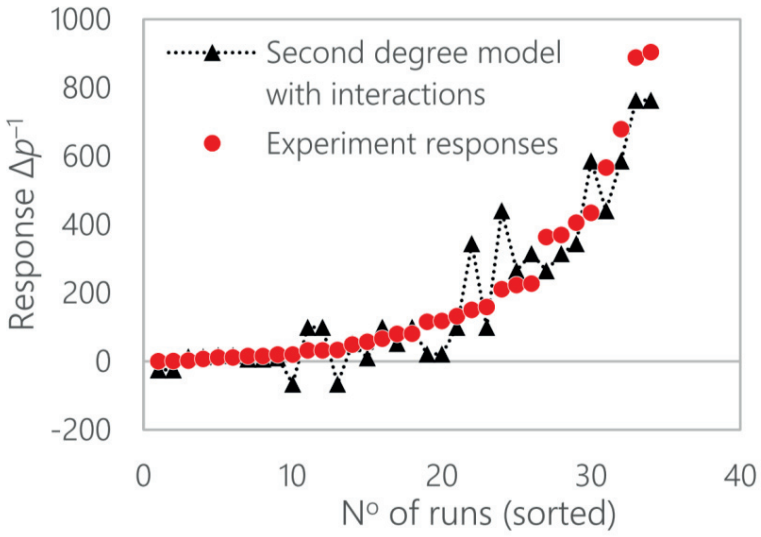

Figure 6.8 Comparison of Δp^{-1} from the simulation and from the quadratic model.

Linear model with interactions

The relative effects are displayed in figure 6.9. Clearly, an increase of the manifolds' width X_3 has a major positive impact on the flow uniformity. The same can be said for the channels' height, although in a lesser extent (1 % instead of 4.2 %). The interaction of both of these factors, X_{23}, is the next main effect. These results correspond overall with expectations, except for the topology of the manifolds' design X_1. It is known to usually influence the flow distribution. The fact that it does not predominate here might be explainable considering that the two topologies analysed have a similar capacity regarding the flow distribution. Besides, interestingly, the relative effects are particularly low with a maximum at around 4 %, suggesting that other effects (or factors) not included in the model are significant. Further findings are presented in the section *Quadratic model with interactions*, p. 182.

An analysis of variance is computed for the factors and displayed in table 6.5. Here again, it was necessary to discard one of the smallest relative effects (a_{45}) to be able to perform the ANOVA. The probability $\mathcal{P}$ that the kept effects are actually random is

close to zero. A linear model with interactions is therefore generated according to these outcomes and is given by:

$$E(\gamma) = a_0 + a_2 X_2 + a_3 X_3 + a_{23} X_2 X_3 \tag{6.10}$$

Figure 6.10 shows how well this model fits with the results from the simulations.

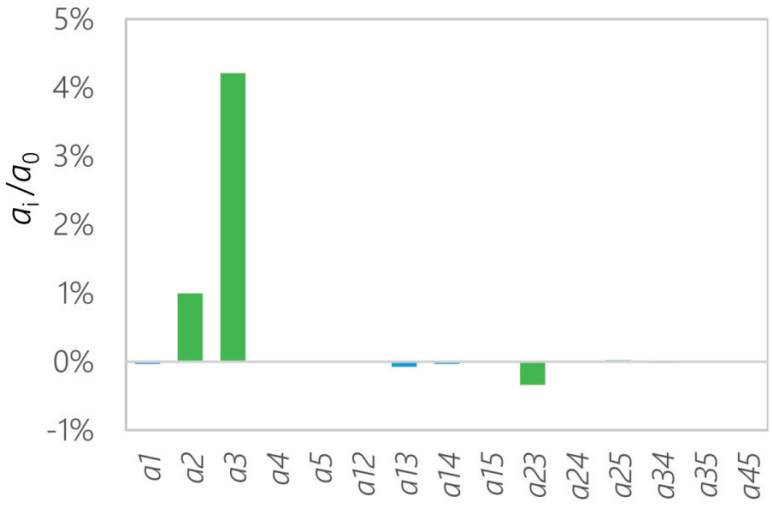

Figure 6.9 Relative half effects for γ with the FFD.

Table 6.5 ANOVA of the linear model for the flow uniformity γ.

Source	SS	DF	MSS	F	$\mathcal{P}$
a_0	1.31E+1	1	1.31E+1	5.27E+6	2.8E−5
a_1	1.53E−6	1	1.53E−6	6.12E+1	8.1 %
a_2	1.30E−3	1	1.30E−3	5.23E+4	0.3 %
a_3	2.33E−2	1	2.33E−2	9.35E+5	0.1 %
a_4	3.22E−7	1	3.22E−7	1.29E+1	17.3 %
a_5	1.52E−8	1	1.52E−8	0.61	57.8 %
a_{12}	2.03E−7	1	2.03E−7	8.14	21.5 %
a_{13}	7.17E−6	1	7.17E−6	2.88E+2	3.8 %
a_{14}	1.37E−6	1	1.37E−6	54.87	8.5 %
a_{15}	2.36E−7	1	2.36E−7	9.49	20.0 %
a_{23}	1.49E−4	1	1.49E−4	6.00E+3	0.8 %
a_{24}	5.10E−8	1	5.10E−8	2.05	38.8 %
a_{25}	6.27E−7	1	6.27E−7	25.16	12.5 %
a_{34}	2.47E−7	1	2.47E−7	9.92	19.6 %

a_{35}	3.34E−9	1	3.34E−9	0.13	77.6 %
residue	2.49E−8	1	2.49E−8		
total	1.32E+1	16			

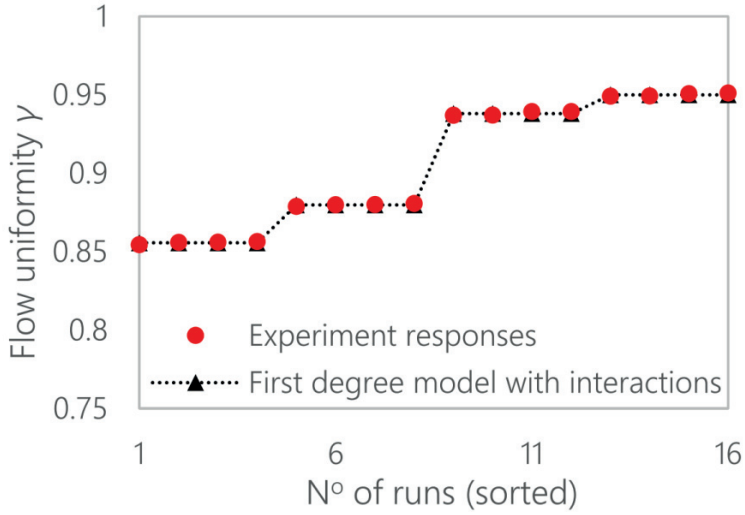

Figure 6.10 Comparison of γ from the simulation and from the linear model with interactions.

Quadratic model with interactions

The relative effects for the quadratic model are displayed in figure 6.11. As can be seen, much more effects seem to be significant. The manifolds' width X_3 and the channels' height X_2 still show the most prominent linear effects. However, in this case, the topology of the manifolds X_1 seems to have some impact. Besides, while the effect of interaction a_{23} stays constant at -0.34 %, the impact of a_{13} now is even larger than a_2. All second-order effects show relatively large values, with a_{33} being by far the most prominent.

It is critical to note here that this change in the outcome regarding the main effects is due to the fact that more data were collected to assess curvature: additional central and "star" points.

The analysis of variance performed for this model is displayed in table 6.6. Since the dispersion matrix is not perfectly orthogonal, a corrected sum of squares (SS^*) is computed. The $\mathcal{P}$ values are now considerably larger than with the FFD.

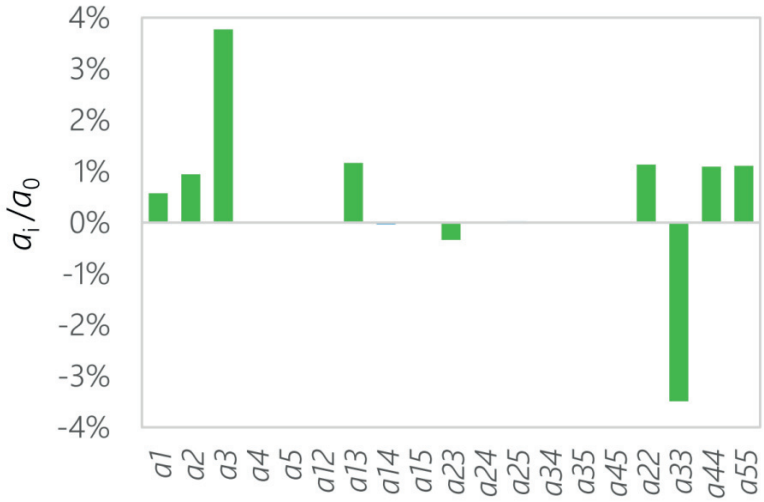

Figure 6.11 Relative effects for γ with the CCD.

Table 6.6 ANOVA of the quadratic model for the flow uniformity γ.

Source	SS^*	DF	MSS	F	$\mathcal{P}$
a_0	2.77E+1	1	2.77E+1	2.55E+4	3.12E−24
a_1	9.00E−4	1	9.00E−4	8.28E−1	37.8 %
a_2	1.91E−3	1	1.91E−3	1.76E+0	20.6 %
a_3	3.06E−2	1	3.06E−2	2.81E+1	0.01 %
a_4	7.47E−7	1	7.47E−7	6.87E−4	98.0 %
a_5	1.04E−8	1	1.04E−8	9.57E−6	99.8 %
a_{12}	4.15E−7	1	4.15E−7	3.82E−4	98.5 %
a_{13}	2.92E−3	1	2.92E−3	2.68E+0	12.4 %
a_{14}	2.66E−6	1	2.66E−6	2.45E−3	96.1 %
a_{15}	2.47E−7	1	2.47E−7	2.28E−4	98.8 %
a_{23}	1.49E−4	1	1.49E−4	1.37E−1	71.6 %
a_{24}	5.10E−8	1	5.10E−8	4.70E−5	99.5 %
a_{25}	6.27E−7	1	6.27E−7	5.77E−4	98.1 %
a_{34}	2.47E−7	1	2.47E−7	2.27E−4	98.8 %
a_{35}	3.34E−9	1	3.34E−9	3.08E−6	99.9 %
a_{45}	2.49E−8	1	2.49E−8	2.29E−5	99.6 %
a_{22}	3.49E−3	1	3.49E−3	3.21E+0	9.5 %
a_{33}	2.84E−2	1	2.84E−2	2.61E+1	0.02 %
a_{44}	8.83E−4	1	8.83E−4	8.12E−1	38.3 %
a_{55}	1.80E−3	1	1.80E−3	1.66E+0	21.9 %
residue	1.52E−2	14	1.09E−3		

Total	2.78E+1	34

A quadratic model with interactions is generated with the most significant effects highlighted in table 6.6 and is given by:

$$E(\gamma) = a_0 + a_1 X_1 + a_2 X_2 + a_3 X_3 + a_{13} X_1 X_3 + a_{23} X_2 X_3 + a_{22} {X_2}^2 + a_{33} {X_3}^2 + a_{44} {X_4}^2 + a_{55} {X_5}^2 \quad (6.11)$$

Figure 6.12 shows that confronted with the additional data points, even the quadratic model is unable to predict accurately the flow uniformity index γ. Furthermore, it also shows that it would not have been wise to discard some of the effects at the "linear" stage, since they were shown to have significant impact when more data is available. The model could be further refined by collecting more data and searching for significant factors which are apparently lacking for a better prediction of the flow uniformity.

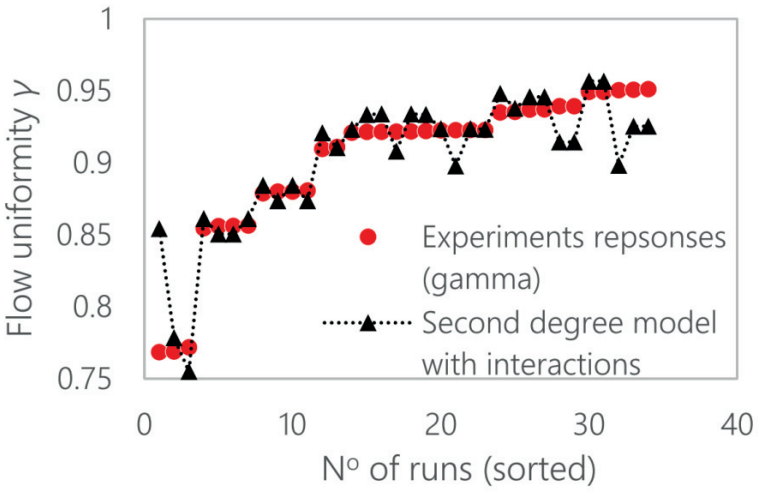

Figure 6.12 Comparison of the flow uniformity γ from the simulation and from the quadratic model with interactions.

6.6 Conclusions to the chapter

The design of experiments methodology is used to design the computer experiment procedure to analyse the effects of five factors on two responses. Specifically, the effects of i) the topology of the manifolds, ii) the height of the channel, iii) the width of the

manifolds, iv) the mole fraction of hydrogen, v) and the current density are investigated with respect to a) the flow uniformity and b) the pressure drop in the bipolar plate at anode.

By applying different techniques such as the relative effect histogram, the half-normal plot and the ANOVA method, it was possible to select, among the analysed effects, the most significant ones for the response considered.

The linear model with interactions was able to predict perfectly the uniformity response by considering as main coefficients the ones related to the channels' height, the manifolds' width, and their interactions. By fitting the same response with a second-order model, the linear coefficient related to the channel's height X_2 seems to have more probability to be a random coefficient compared to its respective second-order coefficient a_{22}. The manifold width is still an important factor to describe the flow uniformity, since the coefficients related to this factor are present as linear and quadratic terms.

The results on the pressure drop response show that the highly nonlinear physics behind this response do not allow predicting its behaviour with a quadratic polynomial model, although the second-order model gives a better representation of the response with respect to a linear model with interactions. In both cases, the main factor is the channels' height, which affects the hydraulic diameter.

It should be highlighted that even if sometimes the model allows perfectly matching the response, it does not mean that the model fits the purpose of predicting the corresponding response accurately in the "actual" computational domain, in terms of both interval and factors considered.

Table 6.7 Models used for gas properties.

Gas property	Model
Individual species H_2, H_2O, and N_2	
Specific heat, C_p	2-pieces-wise quartic polynomial (4th order)
Thermal conductivity, k	Quartic polynomial (4th order)
Dynamic viscosity, μ	Sutherland
Fuel mixture	
Density, ρ	Incompressible ideal-gas law
Specific heat, C_p	Mixing law
Thermal conductivity, k	Ideal-gas mixing law
Dynamic viscosity, μ	Ideal-gas mixing law
Mass diffusivity, D_{ij}	Kinetic theory

Third part

Management of uncertainties

"The purpose of computing is insight, not numbers."
Richard W. Hamming
Introduction to Applied Numerical Analysis (1961)

CHAPTER 7

Characterization of the uncertainties

To characterize the statistical distribution of the dimensions of the channels in a real case, measurements were taken on a stack from SOLIDpower S.p.a after operation. This stack supplied a nominal electrical power of 1 kW. Other data are non-dimensionalised to not disclose proprietary information from our partner. The procedure is described in the next sections.

7.1 Preparation

The main sample was prepared by Yannik Antonetti at HTceramix (SOLIDpower). The stack cannot be dismantled without severely damaging the components whose observation is of interest. Besides, viewing a cross-section is more informative; so it was decided to cut through the stack.

The stack was first filled with epoxy resin (SpeciFix-20 from Struers). It was left aside until complete cool down of the resin (solidification). To get slices, the stack was then sawn with a band-saw (Optimum OptiS275G, with a Rotgen saw-blade from Otelo). The slices were cut along a plane as perpendicular as possible to the channels (i.e., Oyz). Note that the resulting slice (sample) covers the whole height and width of the stack. The slice was then sanded and progressively polished on both sides with a polishing machine (Le Cube from Presi, with reflex NAC type S abrasive papers[1]). This was a time-consuming process (more than a week), due to the rough surface-finish after sawing and due to the large size of the sample (ca. 100 cm^2).

It was decided against cutting it into smaller samples, to preserve the possibility to measure all the channels of a given stack. Otherwise, less measurements of the channels would be available for the stack and it would have been much more difficult to

[1] With grains' sizes P80, P180, P240, P320, P400, P600, P800, P1000, and P1200, in that order.

extract valuable information regarding the potential effect of the spatial position (in both principal directions of the plane), and of the interaction between channels. However, it would probably be useful, though time-consuming, to also take measurements on smaller, better prepared samples, to have a set of more accurate measurements to compare with the others. This way, we could check whether the accuracy is sufficient and hence get more confident with the results.

Some bubbles can be seen in the resin, although care was taken to avoid their formation (see figure 7.1). These bubbles are mostly problematic for the cutting and polishing. Indeed, by weakening the structure, material at the edge tends to be "torn".

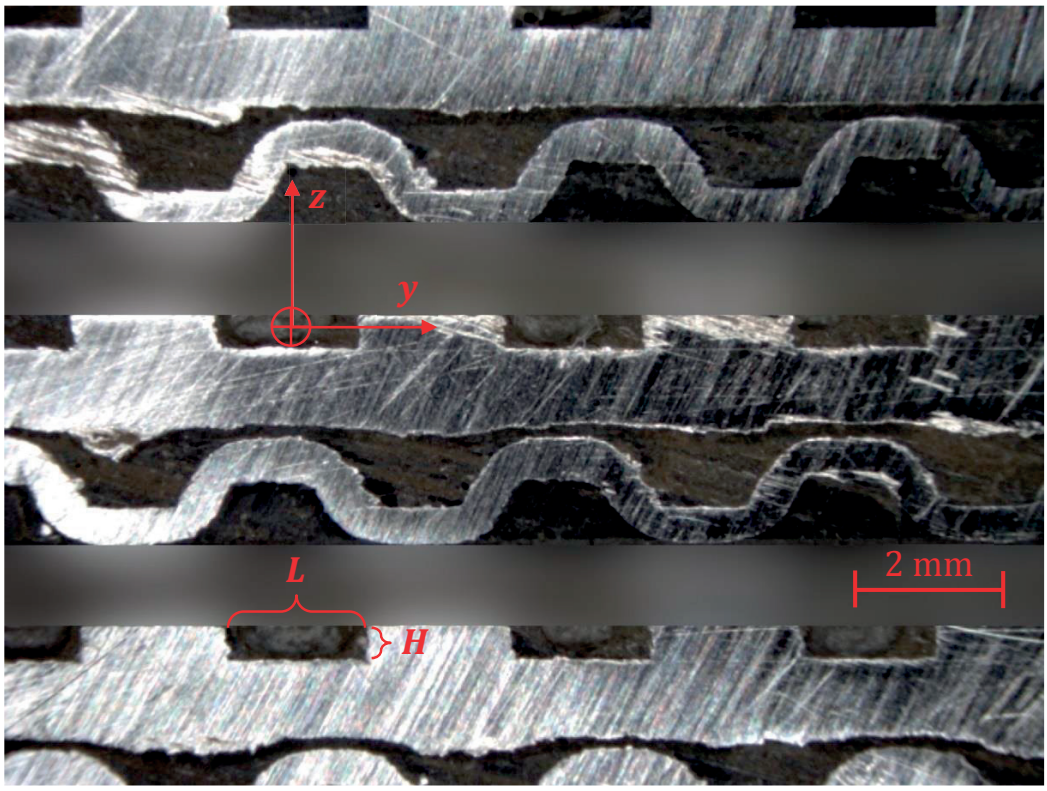

Figure 7.1 Photograph of the MIC, showing the rough surface-finish, despite polishing for several days after sawing. Two bubbles can be seen in the resin, as well as steel being torn (drawn) in the direction of softer materials. This view shows ca. 2% of the slice of the stack used to collect samples.

Possible improvements

- Use a diamond-saw. Such a saw (Discotom-100 from Struers) was bought by HTceramix. Unfortunately, it has a misalignment problem, which could not be fixed in time.
- As written above, also cut smaller samples out of a stack, to get more accurate information, despite less exhaustive / usable.
- Use a fully automated polishing machine.
- Try other cutting and/or finishing techniques (water jets?)

7.2 Measurements

We took measurements with a Nikon measuring microscope MM-400/S, coupled to the software M3 Metrology Readout v1.50.07 from Ryf AG.

For each channel, the coordinate of the centre, the average length, and the average width were recorded. This was achieved by placing points on the perimeter of the channel, from which a rectangle is interpolated by the aforementioned software. A total of 12 points per channel were placed: 1 point at each corner and 2 additional intermediate points on each edge.

7.2.1 Sources of errors

In summary, the sources of errors are:

- Precision of the measuring chain
- User error: visual and personal assessment (random or systematic)
- Contamination left by preparation (abrasion, non-planarity)
- Post-treatment approximations (mostly rotation)
- Statistical approximation; finite number of samples

The maximum precision of the measuring chain (measuring table, microscope, and software) is 1 µm. However, we estimated that the random error when visually placing a point is closer to 5 µm or even 10 µm. This is due from one part to the fact that the contours of the channels, even when regular in shape, are often not razor-sharp; a zone of "blur" around the features is present even when focus is well adjusted. Another part was a constraint of time to collect the data.

Remark: The software offers possibilities to automate or semi-automate the selection of points. They were tried. They clearly did not provide accurate enough results with respect to manual selection; certainly primarily because the shape, contrast, and maybe colour, were not regular enough.

In addition to the aforementioned visual error, the data is "contaminated" by the cutting and polishing procedure. The shape of the channels were often clearly impacted. In the best case, no trace of "contamination" could be identified visually. But it was sometimes even impossible to place a point without "guessing", judging by where it *should* be. To track how much effect this contamination has on the measurements, a *qualitative rating* was written down for each channel, counting how many edges were significantly affected (0 to 4).

Despite the care taken to align the elements with the axis of the measuring table, a slight rotation was noticeable during post-processing. It was decided to take the average of the span-wise (y) positions as a reference to be aligned with the vertical axis (z). The necessary rotation was computed and applied to the data.

Knowing the travel per revolution of the focus knob, the planarity of the sample's surface was evaluated by adjusting the focus on 9 points, each time on the interconnects (steel). Figure 7.2 shows the tendency. Basically, the plane is slightly inclined around an axis going in diagonal from top left to bottom right. The maximum difference of height (along x) is 1.04 mm, giving a tilt-angle of ca. 0.44°.

This top surface is not necessarily perpendicular to the average axis of the channels. So, these measurements are only indicative of the planarity of this surface with respect to the surface on the other side of the sample, which was also cut through and polished.

Statistical approximation due to the finite number of samples

For a bilateral confidence interval, the margin of error d around the mean μ is given by:

$$d = t[1 - \alpha/2\,]\frac{\sigma}{\sqrt{n}} \tag{7.1}$$

with n the minimum number of samples, t the parameter (t-Student) corresponding to the reduced centred normal law, and σ a first estimation of the standard deviation. The interval of confidence is $[\mu - d\,;\mu + d]$. The corresponding level of confidence is $\beta = 1 - \alpha$.

In total, 342 channels were measured; this is the number of samples. Hence, we can calculate the theoretical margin of error corresponding to a chosen level of confidence.

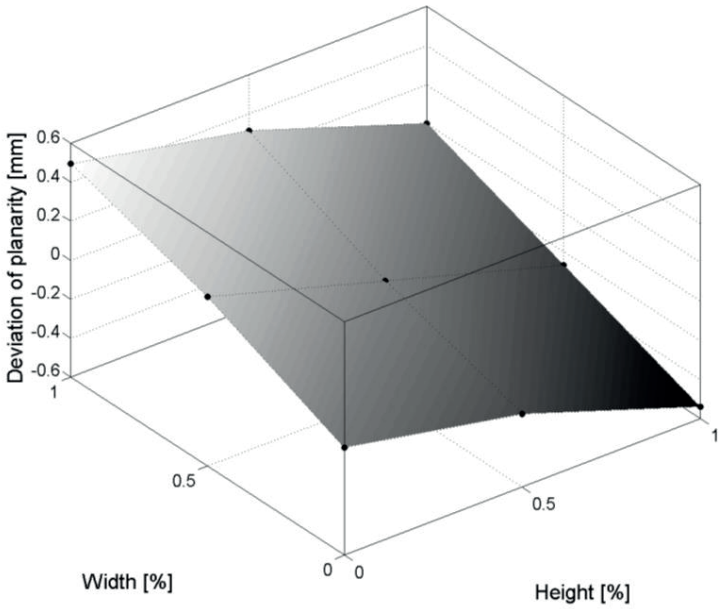

Figure 7.2 Deviation of planarity.
Uncertainty on each data point: ± 0.023 mm ($1/8^{\text{th}}$ revolution of the precision-knob for focus).

The following example is for the mean. The number of samples is $n = 342$. Choosing a level of confidence of 95 % (for instance): $\alpha = 1 - 0.95 = 0.05$. Hence, according to the table of t-Student (reduced centred normal law) for $n = 342$, the parameter $t \cong 1.96$. Using a *first* estimation of the standard deviation (e.g., $\sigma = 10$ µm), the margin of error d is hence $d = t\frac{\sigma}{\sqrt{n}} \cong 1.06$ µm (it would be $\cong 1.39$ µm for 99 % level of confidence).

Let's assume that the estimator for the mean is $\overline{H} = 500$ µm. Then, the probability that the interval of confidence $[\overline{H} - d; \overline{H} + d] \cong [499;\ 501]$ µm contains the true mean is around 95 %, when the standard deviation is $\sigma = 10$ µm and the number of samples is $n = 342$. Note that the error margin d is around 10 times smaller than the standard deviation σ in this case (0.2 % of the mean rather than 2 %). Also, to reduce again this margin of error by a factor 10, then 100 times more samples would be necessary (ca. 40 000 samples). Around $n = 6$ samples are necessary (at 0.95) to get $d \equiv \sigma$.

Remark: The previous calculation is correct when all samples are used to compute the mean. If instead a plot is made to display the mean for each cell element, then only 18 samples (channels) are used to compute each of these mean, so that the result is different.

Conversely, using equation (7.2) serves to estimate the minimum number of samples necessary to achieve a desired confidence interval (error margin) at a chosen level of confidence. A first estimation of the standard deviation is used. The estimation is then adjusted and if necessary, more samples are taken.

$$n = \left(\frac{t\,\sigma}{d}\right)^2 \tag{7.2}$$

The confidence interval for a sampled standard deviation, with a level of confidence of 95 %, is:

n	Lower bound	Upper bound
2	0.45 σ	31.9 σ
10	0.69 σ	1.83 σ
100	0.88 σ	1.16 σ

7.2.2 Imputation of the data

Due to the "contamination" of the results discussed before, it was decided to censure the most probably wrong data. For this, we decided to use ***imputation*** rather than *trimming* of the data. The imputation is based on the 2nd and 98th percentiles. Note that among the possibilities, replacing incorrect measurements by the sample average would have been a bad idea.

Since a lot of data are available, these points could also have been eliminated. On the other side, given the number of samples, getting more extreme values than these percentiles is reasonably probable. These values were nonetheless chosen, since it was observed during the measurements that the risk of inconsistencies is high. 21 measured values were imputed on H and L, which out of 2×342 samples, correspond to 3 % of the data. The effect of the imputation is negligible on the mean (< 0.05 %). The effect is stronger on the standard deviations, since the data is "compacted": $\sigma[H]$ is reduced by 12 % and $\sigma[L]$ by 7 %.

Also, without imputation, the kurtosis for H and L are respectively 6.7 and 6.1, which is much bigger than the kurtosis of a normal distribution (i.e., 3). After imputation, the kurtosis is closer to that of a normal distribution with 2.6 and 3.3 respectively[2].

[2] This was however not the goal of the imputation.

7.3 Results

7.3.1 Treatment

All variables are made non-dimensional; e.g., the lengths become:

$$L = \frac{L_{\mathbb{M}}}{L_{\mathbb{N}}} \tag{7.3}$$

with $L_{\mathbb{M}}$ a measured length and $L_{\mathbb{N}}$ the nominal (design) value of the length of the channels.

A rotation is calculated and applied to the data, to correct for a global misalignment of the sample when taking measurements.

Apart from the raw data (H, L, y, z), the main quantities of interest for the channels are their area $A = L\,H$, their perimeter $P = 2\,(L + H)$, their hydraulic diameter $D_{\mathrm{h}} = \frac{4\,A}{P}$, and the geometric factor associated with their hydraulic resistance[3], $R_{\mathrm{h,\ geo}} = \frac{P^2}{A^3}$.

7.3.2 Outcomes

1. Global

First, we present statistics based on all samples measured. Caution, after imputation at the 2nd and 98th percentiles.

Remark: Since the measurements are made non-dimensional with the nominal values of each characteristic length, the standard deviation is equivalent to "coefficients of variation" but with respect to the respective nominal value instead of the mean, which slightly deviates from the nominal values.

The mean of the height is significantly smaller (6.2 %) than its nominal (design) value (corresponding to 1.000). The dimensional tolerance of the manufactured parts cannot be the sole explanation for such a large discrepancy. The cutting (and polishing) procedure is probably part of the explanation. However, we suspect that it is not the only factor either, since all measurements are below the nominal value, whereas a few channels show no visible contamination. The mean of the length is slightly bigger (0.6 %) than its nominal value.

[3] This expression corresponds to the simple case of laminar flow in a channel.

Table 7.1 Statistics with 342 samples (non-dimensional quantities).

	$\boldsymbol{\mu}[\cdot]$	$\boldsymbol{\sigma}[\cdot]$	kurtosis	skewness
$\boldsymbol{H}$	0.938	0.017	2.594	− 0.406
$\boldsymbol{L}$	1.006	0.022	3.313	− 0.842
$\boldsymbol{A}$	0.944	0.032	2.190	− 0.369
$\boldsymbol{P}$	0.993	0.020	2.795	− 0.638
$\boldsymbol{D_{\mathrm{h}}}$	0.951	0.016	2.264	− 0.426
$\boldsymbol{R_{\mathrm{h,\,geo}}}$	1.174	0.080	2.334	+ 0.520

All values of kurtosis are relatively close to that of a normal distribution (i.e., 3). The skewness of H and L are negative, which means that the mass of the distribution is concentrated above the mean. The skewness might be an artefact due to the measuring procedure.

Note that even the maximum measured value of the height, 0.973, is still smaller than the nominal value by 2.7 %. In table 7.2, $\Delta_{\max}[\cdot] = \max[\cdot] - \min[\cdot]$ indicates the maximum difference of the quantity in brackets. It always equates about 4.5 $\sigma[\cdot]$.

It is also interesting that the geometric component of the hydraulic resistance $R_{\mathrm{h,\,geo}}$ is always bigger than its nominal value. By 2.7 % at the minimum and up to 40.6 % at the maximum. Moreover, its standard deviation is roughly equal to four times that of the height and the length (average of both). This is consistent with the theory, taking the derivative of the expression of $R_{\mathrm{h,\,geo}}$ for a small variation.

Table 7.2 Statistics for H, L, and $R_{\mathrm{h,geo}}$, 342 samples (non-dimensional quantities).

	$\boldsymbol{\min}[\cdot]$	$\boldsymbol{\max}[\cdot]$	$\boldsymbol{\Delta_{\max}}[\cdot]$	$\boldsymbol{6\,\sigma}[\cdot]$
$\boldsymbol{H}$	0.897	0.973	0.076	0.102
$\boldsymbol{L}$	0.944	1.041	0.097	0.132
$\boldsymbol{R_{\mathrm{h,\,geo}}}$	1.027	1.406	0.379	0.480

2. Variations along y (channels) and z (elements)

Statistics are plotted for the height and length of the channels, respectively their mean along y (figure 7.3) and along z (figure 7.4) and their standard deviation along y (figure 7.5) and along z (figure 7.6).

The variations along y for both the height and width of the channels display no particular tendency apart from an apparent kind of periodicity (3 channels), especially visible for the mean. This is further discussed in § 7.3.3.

It is striking that this variation is bigger than the variation along z (elements), despite our observation that measuring the channel dimensions accurately became more difficult when getting to the "top" (bigger z values).

When looking at $\mu[H]$ along the elements (z), we observe that it slightly increases. We suspect that this is due to an evolution of personal assessment when placing the points. $\mu[L]$ varies a bit more, but such a tendency is not observed towards larger or smaller values.

We observe an increase of the standard deviation for both H and L. It was clear, while doing the measurements, that the top elements were much more "damaged" by the cutting/polishing procedure than the bottom ones. In consequence, it was more difficult to measure them consistently. This increase of the standard deviation is therefore not surprising.

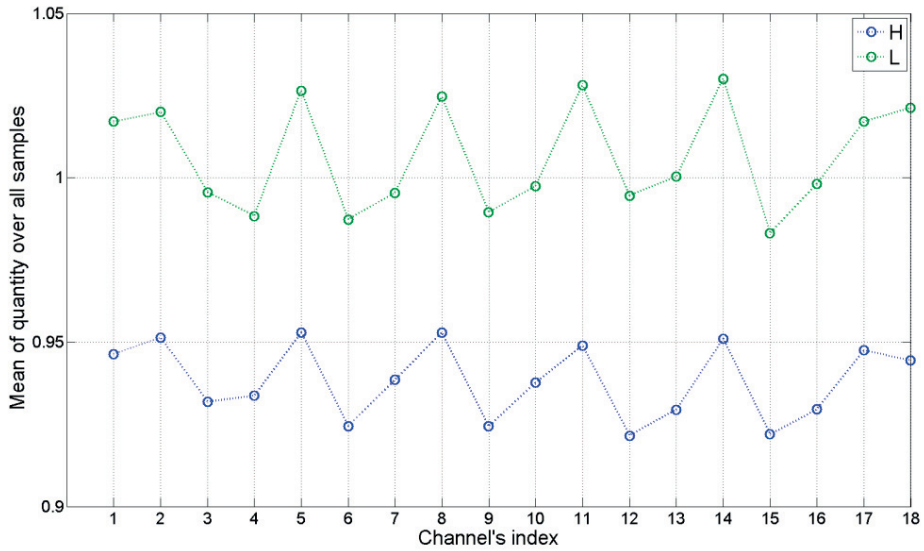

Figure 7.3 Mean of the height and length for each channel (along y).

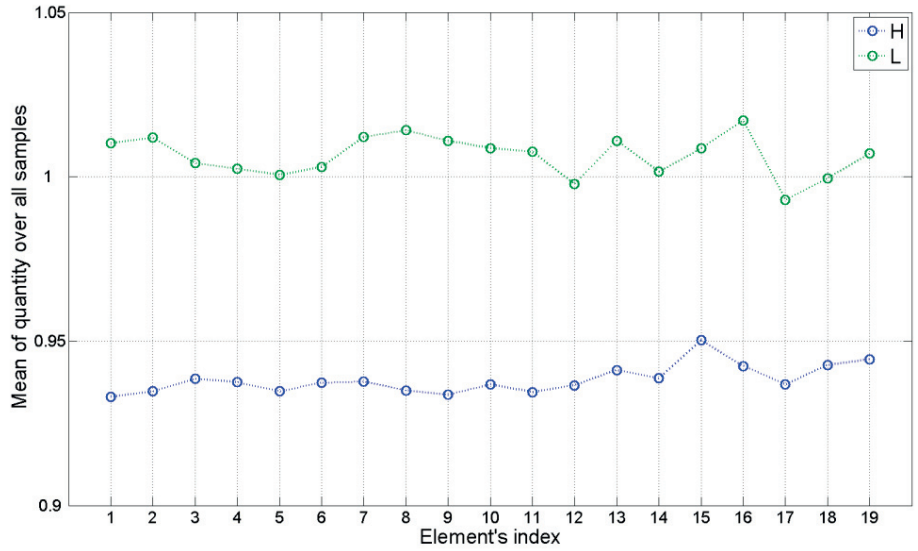

Figure 7.4 Mean of height and length for each element (along z).

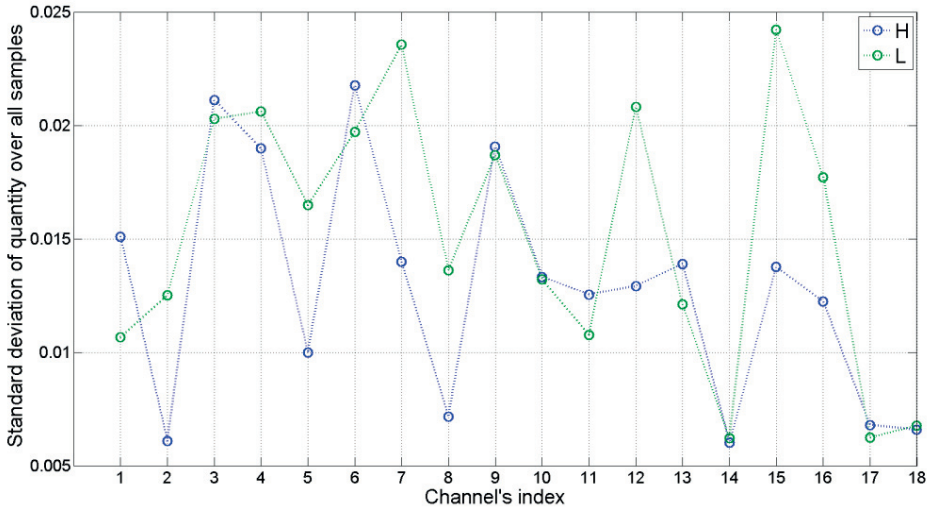

Figure 7.5 Standard deviation of height and length for each channel (along y).

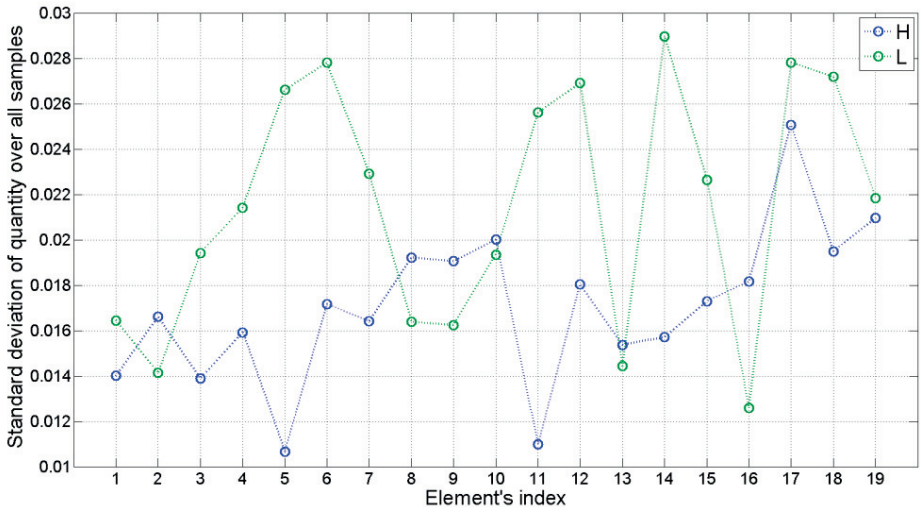

Figure 7.6 Standard deviation of height and length for each element (along z).

3. Hydraulic resistance of the channels

Overall, as expected from theory, the standard deviation is ca. 4 times the standard deviation of the channels' dimension. About the variations along y and z: a compound of the previous trends can be observed since the hydraulic resistance is based on width and height of the channels: we see a periodicity along y and an increase of the standard deviation along z.

4. Position of the channels

Regarding the span-wise variations (y), the elements are systematically bent "down". It is related to the structure and manufacturing, including assembly (which are confidential). Concerning the vertical variations (z), the elements are tilted towards one side and progressively towards the other side between first and last element. A bending of the elements is also observed.

From the first to the last element, a deviation of +0.4 mm was measured on the right with respect to the left, which is ca. 0.4 % of one side. The statistical data are consistent with this global measurement.

Contamination of the results by the cutting/polishing procedure

To assess the effect of cutting/polishing procedure on the results, we looked for a possible correlation between the quantities measured or derived from them, and the qualitative rating of the measurements (described in § 7.2.1). The effect seems to be minor on the positions of the channels, which is logical. However, it is strong on the height and width, and on the values that depend on them (area, hydraulic diameter …). For instance, the coefficient of linear correlation between the qualitative rating of the measurements and the hydraulic resistance is $\varrho_{\mathrm{l}} = 0.63$ with a $\mathcal{P}$-value of 0.51%. When looking at the evolution of the standard deviation of the height along the elements (z), it jumps to $\varrho_{\mathrm{l}} = 0.81$ with a $\mathcal{P}$-value of only 0.006%.

7.3.3 Correlation

Test of dependence of the dimensions on the position of the channels

A key aspect to choosing an appropriate method of optimization under uncertainty is to assess whether the random variables are independent or not.

Intuitively, we thought that the width of the channels, and possibly also their height, may depend on their absolute position, and/or on their position relative to one another. Indeed, several potential reasons for a variability of these dimensions are linked to the position. Here is a non-exhaustive list:

(a) Regular wear of the tool along its path if the parts are machined (material removal);

(b) Global, systematic deviation if the parts are formed with a pressure-based process (e.g., stamped, hydro-formed, etc.);

(c) Sinking of the membrane at specific locations, depending on the underlying structure;

(d) Systematic deviation due to the responses of the structure to stress during assembly and operation;

(e) Propagation of a deviation from one channel (or element) to others.

Three main situations can arise that we illustrate as follows: given a nominal dimension $d_{\mathbb{N}}$, if a channel measures $d_1 = d_{\mathbb{N}} + \Delta d_1$, we can imagine that the dimension of an adjacent channel:

(i) measures $d_1 \pm \epsilon$ with a high probability (ϵ small);

(ii) measures $d_{\mathbb{N}} - \Delta d_1$ with a high probability (the middle rib is not centred);

(iii) is independent of d_1 (and possibly all others).

Hypothesis: systematic deviation dependent on the absolute position

All statistical tests on this hypothesis were inconclusive. Our eyes could not either decipher some dependence.

Hypothesis: dependence on the relative position (closeness of channels)

A clear periodicity can be seen in the results, notably in figure 7.3. It is straightforward to draw a parallel between this periodicity and the details of the geometry of the FDP, when knowing them. However, it is not clear whether this is representative of actual values in operation, or if this is an artefact due to cutting through such a geometry, or both. We cannot give more insights without risking to disclose confidential information.

7.3.4 Conclusions about this characterization

The contamination of the results is judged too large to afford to use them with confidence as inputs to an uncertainty quantification or an optimization under uncertainty. In other words, the (epistemic) uncertainty on the aleatory uncertainties that we wish to characterize is larger than desirable.

More specifically, quantitatively, the results do not seem representative of the values actually expected, i.e., inferring from the nominal values, the manufacturing tolerance, and the additional variations induced by assembly and operation which seem reasonable. According to our observations of the sample under the microscope, the most plausible explanation is that a large part of the discrepancy is due to the contamination of the results by the intrusive measuring procedure.

However, qualitatively, the results seem to confirm our expectations. In particular, the fact that height and width conform well to a normal distribution supports the assumption of a normal-like distribution.

Aside from that it is interesting that the underlying structure of the pattern “appears” in the results, although it is not clear, whether this is an artefact of the cutting/polishing procedure induced by the pattern, or if such variance would appear even with a perfect slice.

A more accurate measuring procedure is needed (e.g., using a diamond saw, or measuring the dimensions of single channels). In the absence of such characterizations, it is questionable what is more reasonable: using the current data, knowing that they are contaminated, or using data based on manufacturer's specifications, experience, and intuition?

7.4 Data from another design

Another design allowed us to get data with a less destructive approach. This design was basically formed by parallel channels at cathode and at anode. Both patterns were obtained by stamping. A laser-distance-measuring instrument was used to characterize the profile of the pattern. The local height was measured along the width of the cathode and anode patterns. Data points were taken by steps of 0.080 mm ($\sigma =$ 0.005 mm). For the anode, the characterization was done after stamping and after sintering (but before operation). No post-operation data are available because the pattern suffered too much from the disassembly. For the cathode, three states were characterized: stamped, sintered, and post-operation. It should be reminded that disassembly likely affected the pattern.

In the following, although it is the complete profile of the channels that determine the flow distribution, we will mostly discuss the height of the channels. Indeed, it is the predominant dimension, because it is at the same time the smallest dimension and the most subject to variability.

1. Anode

Figure 7.7 shows the profile of height along the width of the pattern at anode, in stamped and sintered state. Table 7.3 shows the main corresponding statistics.

The stamped profile is quite regular: the standard deviation is only 1 % of the mean value of the height, whereas the maximum and the minimum stand 4 % above and below the mean. Besides, the profile is almost flat. The mean height is 5 % larger than the nominal targeted value, but such a larger value is desirable, because the material shrinks during sintering.

The sintered profile is much less regular. First, we can observe that the profile is bent in a concave shape. Fortunately, the whole profile is subject to this curvature, so that the distance between the top and bottom of the channels is more constant than other-

wise. Still, this curvature implies that the contact with the cell may not be homogeneous, leading to differential electrical contact-resistances. In the worst case, it could even lead to a loss of contact and create a by-pass from one channel to another for the flow. Although in this case, the flexibility of the materials can most probably compensate for this variation, which is at least progressive rather than randomly distributed.

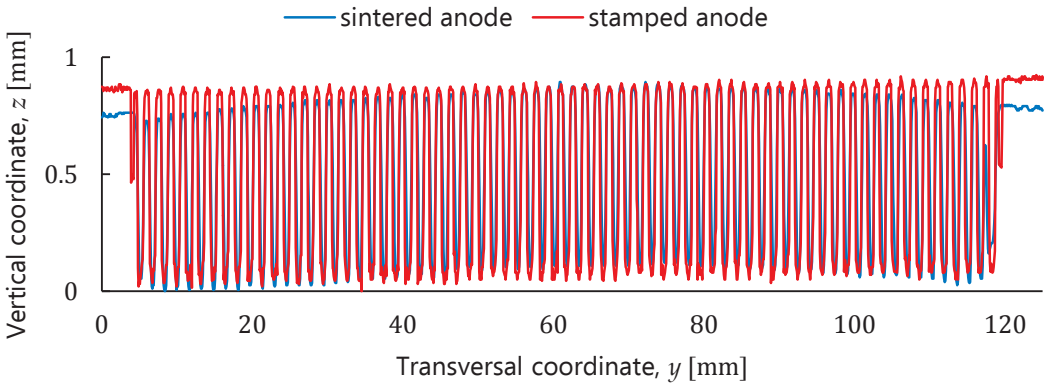

Figure 7.7 Profile of height along the width of the anodic pattern.

Quantitatively, looking at statistics, the standard deviation of the height for the sintered profile is 3 % of the mean, which, however being three times bigger than for the stamped profile, still seems reasonably low. The maximum is besides only 3 % larger than the mean. In contrast, the minimum is 26 % below the mean, which is troublesome and will ultimately limit the achievable global fuel utilization. This matter is further discussed in § 7.4.3, p. 209. Additionally, the mean height is 4 % smaller than the nominal targeted value: hence, the stamped design is not over-dimensioned enough to fully compensate for shrinkage. Moreover, it would lead to larger resistance to flow (so pressure drops) in the channels; this is in principle beneficial for a homogeneous *nominal* flow distribution, but also makes the design more sensitive to variabilities, potentially leading to a worse *effective* flow distribution.

Table 7.3 Statistics of the height of the anodic channels, corresponding to the profile in figure 7.7.

Height of channel	Stamped	Sintered
Mean/nominal	105 %	96 %
Median/mean	100 %	101 %
Min/mean	96 %	74 %
Max/mean	104 %	103 %
Std/mean	1 %	3 %

2. Cathode

Figure 7.8 shows the profile of height along the width of the pattern at cathode, in stamped, sintered, and post-operation state. Table 7.4 shows the main corresponding statistics.

Like for the anode, the stamped profile is quite regular: the standard deviation is again only 1 % of the mean, whereas the maximum and the minimum stand 2 % above and below the mean. The mean height is 11 % larger than the nominal targeted value. We will see whether this is enough to compensate for shrinkage.

The sintered profile is much less regular. This time, the profile is bent in a convex shape. The mean height is still 6 % larger than the nominal targeted value, suggesting that the cathode-material shrinks less than the anode-material. It is however interesting that after operation, the mean height is 3 % larger than the nominal targeted value, suggesting that the pattern is further compressed by a relatively large amount. If a similar outcome can be extrapolated to the anode, it would then imply much lower channels-height than targeted. We should however note that disassembly may have damaged the pattern.

In figure 7.8, we can also see that the first and last channel are basically non-existent after sintering and after operation. Looking at figure 7.9, we observe that the sealing material overflew into those channels. This issue will be further discussed in the next section.

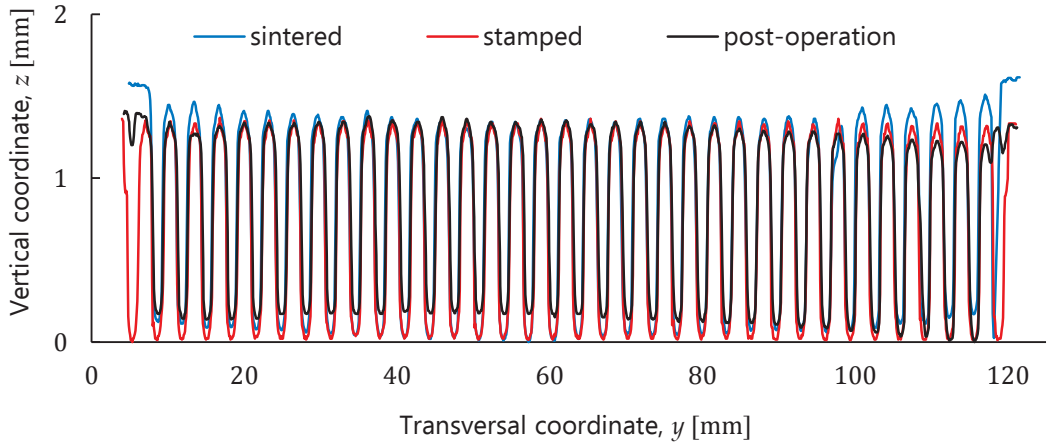

Figure 7.8 Profile of height along the width of the cathodic pattern.

The standard deviation of the height for the sintered profile is 9 % of the mean, which is considerable. It is almost the same after operation (10 %). The maximum is 5 % larger than the mean for both cases. Like for the anode, the minimum height is much

lower than the mean: respectively 43 % and 40 % smaller after sintering and after operation.

Table 7.4 Statistics of the height of the channels at cathode, corresponding to the profile in figure 7.8.

Height of channel	Stamped	Sintered	Post-operation
Mean/nominal	111 %	106 %	97 %
Median/mean	100 %	102 %	102 %
Min/mean	98 %	57 %	60 %
Max/mean	102 %	105 %	105 %
Std/mean	1 %	9 %	10 %

7.4.2 Distribution of air flow

By observing the cathode pattern after disassembly, we discovered an unexpected way of getting insight about the flow distribution: in that particular situation, grey traces can be seen at the bottom of the channels (see figure 7.9). These traces are essentially due to the formation of strontium chromate ($SrCrO_4$). Strontium is a compound of the cathode, while chromium comes from the stainless steel. According to fluid-mechanics, the intensity and length of these traces are likely to be indicative of the flow rate.

Figure 7.9 Traces left by the air flow at the bottom of the channels, giving insight on the flow distribution.

Qualitatively, the "bar-graph" formed by these traces (figure 7.9) shows that the air flow was likely rather homogeneous, apart from the lateral channels. This seems coherent with what is often observed in similar situations (either experimentally or computationally). Lateral channels are usually less fed, at least partly because of the boundary-layer that forms in the manifold. Additionally, it can be seen here that the most extreme channels were partially blocked by the sealing material.

To get a quantitative insight, we measured the length of each of these traces. Since they are fuzzy[4], and to avoid a personal bias, three persons including myself measured them independently. Figure 7.10 shows the average and standard deviation corresponding to these measurements.

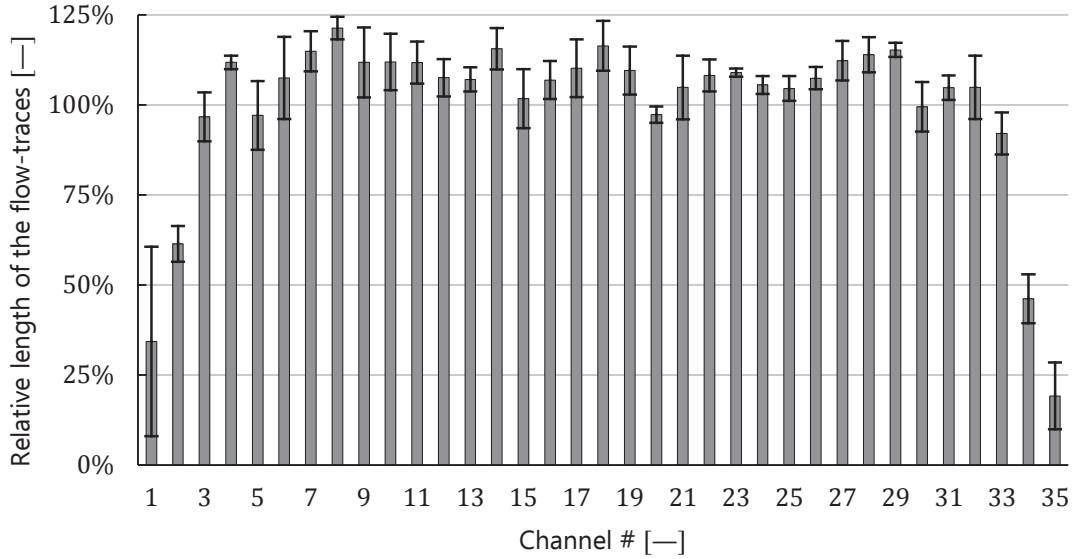

Figure 7.10 Relative lengths of the traces of strontium chromate at the bottom of the cathodic channels. Reference is the average.
The error bars show the standard deviation among three independent evaluations (different persons).

The median of this distribution is bigger than the average by 7 %. So, more channels are overfed than underfed; but it also means that to compensate for this, the deviations with respect to the ideal flow rate is larger for underfed channels than for overfed ones. This is clear in figure 7.10. It is not a desirable situation, because limitation in fuel utilization is caused by the minimum flow rate (without accounting for averaging effects due to diffusion in the porous electrodes). In principle, it would be preferable to have many channels underfed by as small a margin as possible, than only a few by a large margin.

[4] Even more so because the part was no more available, so the measurements were taken from this archived photograph, corrected for rotations and perspective.

Correlation between airflow traces and channels profile at cathode

It is interesting to look whether the profile of the channels at the cathode side are correlated with the traces of strontium chromate left by the air flow.

From the profile of the channels, we computed for each channel the flow resistive term corresponding to the geometry of the channels[5] for a fully-developed laminar flow: P^2/A^3. Then, the coefficient of linear correlation ϱ_l was computed between the relative length of the flow traces (indicator of flow rate) and the inverse of the aforementioned resistive term. This way, if all underlying hypothesis are perfectly verified, we should get $\varrho_l = 1.0$. The coefficient of correlation is displayed in table 7.5 for each characterized state.

Table 7.5 Coefficient of correlation between the relative length of the traces left by the air flow in the channels and A^3/P^2.

State	ϱ_l
Stamped	0.19
Sintered	0.76
Post-operation	0.74

It can be seen that the linear correlation is particularly weak for the stamped profile. It is however reasonably high in both other states. Given all the (epistemic) uncertainties that remain with the available data, this relatively high score gives confidence in the observations we made, relationships we tried to establish, and outcomes we can draw.

This case is a good illustrative example of a crucial point: *(pre-)manufactured conditions are not necessarily representative of operating conditions.* Therefore, it may not be wise to use their characterization to predict products' performance, nor to rely on them to take design decisions.

7.4.3 Consistency with the characterization of the fuel cell

According to the report of operation, the fuel cell was limited by concentration polarization for fuel utilization larger than 70 % (for all gas inputs). This seems coherent with the insight available about the flow distribution: lateral channels, which are fed

[5] The coefficient of shape (c_s) is neglected; its effect is insignificant, especially since the shape of the channels is mostly unchanged.

by less than 70 % of their nominal flow, are correspondingly subject to a *local* fuel utilization of 100 % (or even over, numerically) when the *global* fuel utilization is set at 70 %. Moreover, limitations appear before the theoretical limit of 100 % fuel utilization even for perfectly uniform flow distributions. Therefore, it is clear that these 4 lateral channels are largely contributing to severely limit the performance and durability of the fuel cell. Note that they correspond to more than 10 % of the cell area.

This 2-cells stack achieved a maximum electrical power of 145 W for a flow rate of hydrogen equal to 6 $ml/(min \cdot cm^2)$ and an electrical efficiency of ca. 41 % for a flow rate of hydrogen equal to 4 $ml/(min \cdot cm^2)$.

Words of caution and potential for improvements

The characterization of the channels-profile was done on a single cell and at a single location along the length of the cell. Therefore, it may not be representative of the average manufacturing, assembling, and operating scenario. Similarly, the extracted profile may not be an accurate representation of the average profile over the full length of the channels.

"The purpose of computing numbers is not yet in sight."
Richard W. Hamming
Introduction to Applied Numerical Analysis (1997)

CHAPTER 8

Propagation of the uncertainties

The purpose of this chapter is to apply uncertainty quantification, i.e. propagate input uncertainties in the form of probability distribution functions through the model of the fuel cell to quantify the output uncertainties.

The beginning of this chapter is largely based on our publication *Impact of Random Geometric Distortions on the Performance and Reliability of an SOFC* [82].

8.1 Summary

A method based on Monte Carlo simulations (MCS) is developed to assess the impact of manufacturing tolerances on the durability of performance and on the reliability of solid oxide fuel cells (SOFCs). Computational fluid dynamics (CFD) simulations of the fluid distribution pattern (FDP) at the anode are carried out for a set of deformed geometries. An automated code allows generating standardized deformations in a random manner on the original meshed geometry taken as input. In the scope of this study, the fuel flow uniformity is taken as the indicator of the performance and uniformity is taken as the indicator of the performance and reliability of SOFCs. Statistical uncertainty quantification analyses are carried out to assess the impact of dimensional tolerances on repeat elements both taken individually and stacked together. The implemented method is evaluated with two FDPs from the literature. Results show that the sensitivity to variability in thickness is predominant on the sensitivity to in-plane deformations of channels. Besides, the magnitude of sensitivity largely depends on the FDP and on the extent of the deformation, too. In addition, negative effects of deformations are shown to be exacerbated in stack situation. The method proved successful in getting relatively quick insights on the quality of FDPs with respect to dimensional tolerances.

8.2 Introduction

The scope of the following study is limited to standardized distortions and to a simple model of the FDP, confined to the computation of the flow distribution at the anode, without electrochemical reactions, and assuming isothermal conditions. Besides, only FDPs with straight channels are considered and a maximum of two deformations is applied per sample.

The methodology is based on Monte Carlo simulations (MCS) using computational fluid dynamics (CFD) tools. The idea is to compute quality indicators for a set of randomly deformed FDPs. From that point, several uncertainty quantification analyses are done to forecast the quality of the gas distribution and to highlight the best FDP geometries for given dimensional tolerances.

The methodology and routines developed for this study can be used as a decisional tool to conduct the design optimization phase of FDPs and manifolds.

8.3 Description of the problem

8.3.1 Influence of flow uniformity on channels' fuel utilization

As stated before, the flow uniformity is of major importance for the performance and reliability of fuel cells [12,13,18,27–29]. This is explainable schematically by the fact that the possible fuel conversion a channel is limited by the mass flow rate of fuel available. As a consequence, if a channel is not supplied with enough fuel, degradation may occur by fuel depletion, re-oxidation of the cell, or even breakage. From the point of view of the airflow, heterogeneous distribution may lead to temperature gradients, themselves being potentially responsible for structural stresses and for gradients of reaction rate (fuel consumption).

Besides, the fact that the fuel utilization for each channel may be different from the apparent — i.e., average — fuel utilization of the repeat element makes it really difficult to have a reliable measurement feedback on possible issues in the stack during operation [30].

8.3.2 Modelling of defects

To approach the reality, different levels of modelling can be considered. The following concepts are illustrated in figure 8.1 and are explained below. The highlighted green arrow is intended to show the channel with the minimum mass flow rate, which will be considered as the limiting channel-zone for performance and reliability.

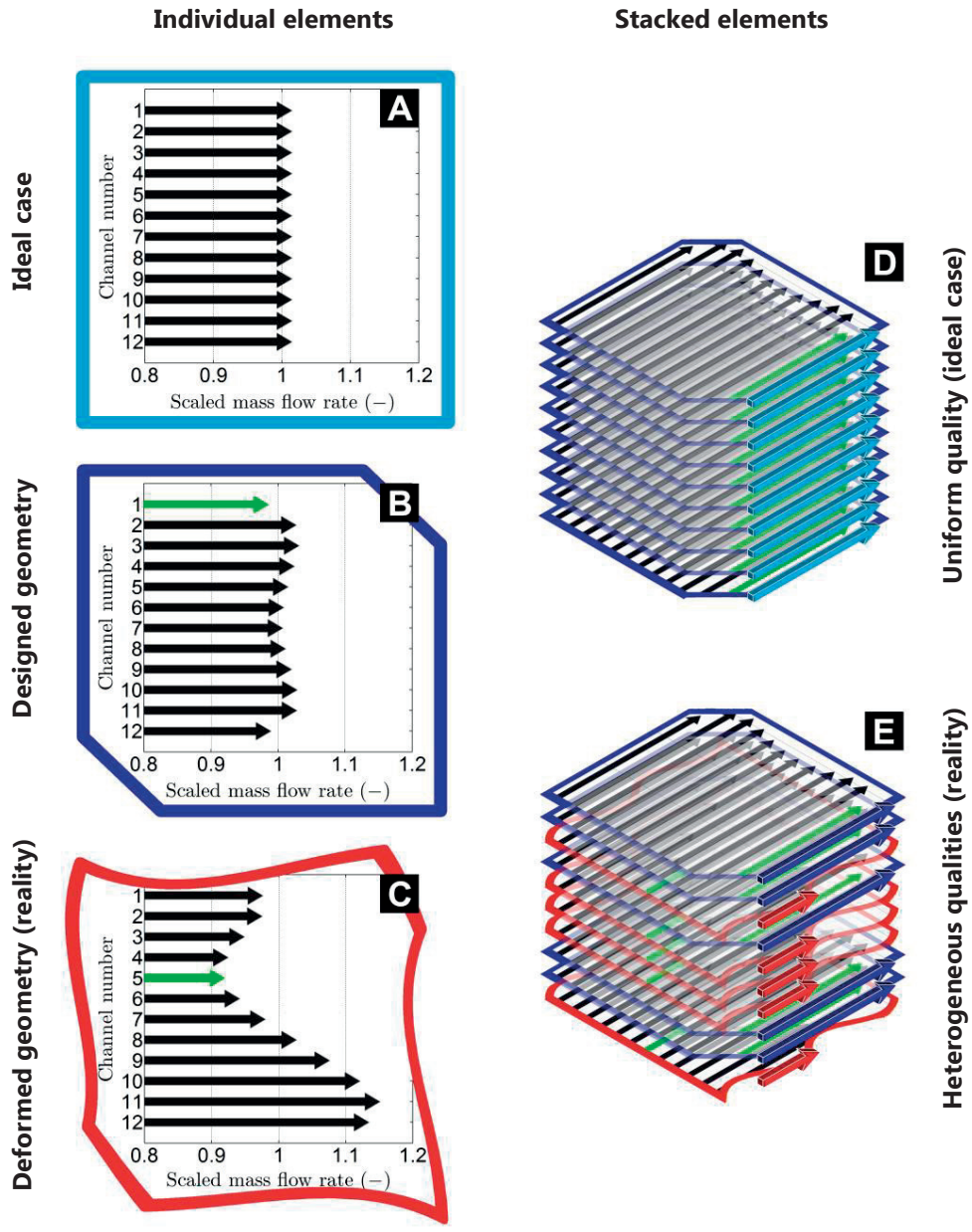

Figure 8.1 Concepts of the methodology.
Left: Individual element. A: Ideal. B: Designed. C: Deformed geometries.
Right: Stacked elements. D: Uniform quality. E: Heterogeneous quality.

1. Effects of defects on individual elements

To evaluate repeat elements individually, the mass flow rate that enters each element is kept constant; this is the mass flow rate imposed at the inlet for the simulation: $\dot{M}_{\mathrm{el}}^{\mathrm{ie}} = \dot{M}_{\mathrm{el}}^{\mathrm{simu}}$. Taken individually, the quality of a repeat element may be defined by the deviation of mass flow rate across its channels.

In an *ideal case,* the fuel would be perfectly uniformly distributed among the channels, as shown in figure 8.1A. Hence, performance and reliability issues would not arise from the flow distribution. Unfortunately, as soon as a *designed geometry* — even free from distortions — is considered, the flow distribution will present some deviations, e.g., as illustrated in figure 8.1B. Of course, as a matter of fact, the *real geometry* is likely to be more or less a *deformed geometry* due to manufacturing tolerances. As shown in figure 8.1C, the flow distribution will be affected by the deformation, with possible critical consequences (even if in some rare cases an improvement of the homogeneity may be observed).

Finally, the resulting pressure drop corresponding to the imposed nominal flow $\Delta P_{\mathrm{el}}^{\mathrm{IE}}$ differs for each element, in accordance with the geometrical deformations.

2. Impact of defects at stack level

When considering a stack of repeat elements as a whole, the pressure drop is assumed to be constant for each element (stacked in parallel). As a result, the mass flow rate varies *among the repeat elements* in accordance to the aforementioned distribution of pressure drops at nominal flow, i.e., of deformations among them.

In an *ideal case,* the stack would be made of repeat elements with a *uniform quality,* as shown in figure 8.1D. Thus, in this idealized situation, the stack performance would be only limited by the quality of the design, i.e., by the minimal flow rate in the channels, which would be identical for each individual element. However, *in reality,* the elements are more likely to be distributed with *heterogeneous qualities* among the stack, as shown in figure 8.1E. Consequently, the flow rates may differ from one element to the other: if some elements are underfed compared to the ideal case, the flow rate in the limiting channels will be even lower than when considering the elements individually. As repeat elements are electrically connected in series, the local (actual) fuel utilization differs among the different elements [30]; hence, the channel with the lowest flow rate will reach the highest channel's fuel utilization among the whole stack. This channel is thus decisive for the stack performance and reliability.

8.4 Methodology

8.4.1 Steps of the computation process

The methodology is based on MCS by using a CFD model. MCS are carried out for typical geometric deformations. Then, data extracted from the simulations are analysed statistically to quantify the uncertainties. From these analyses, the effect of stacking can be evaluated, as well as different geometries of the FDP.

As also detailed in figure 8.2, the computation process for the MCS is as follows:

- Meshing the geometry of reference;
- Generating parameters of deformations in a random manner;
- Deforming the mesh;
- Running CFD simulations (ANSYS FLUENT);
- Post-processing data (MATHWORKS MATLAB).

The entire process is automated with a home-made MATLAB routine. In particular, the random geometric distortions are generally directly on the original mesh free from distortions by post-processing it. To cover a representative collection of possible cases with the random parameters, the *Latin hypercube sampling* (LHS) algorithm implemented in MATLAB is used (versions for both normal and uniform distributions) [20].

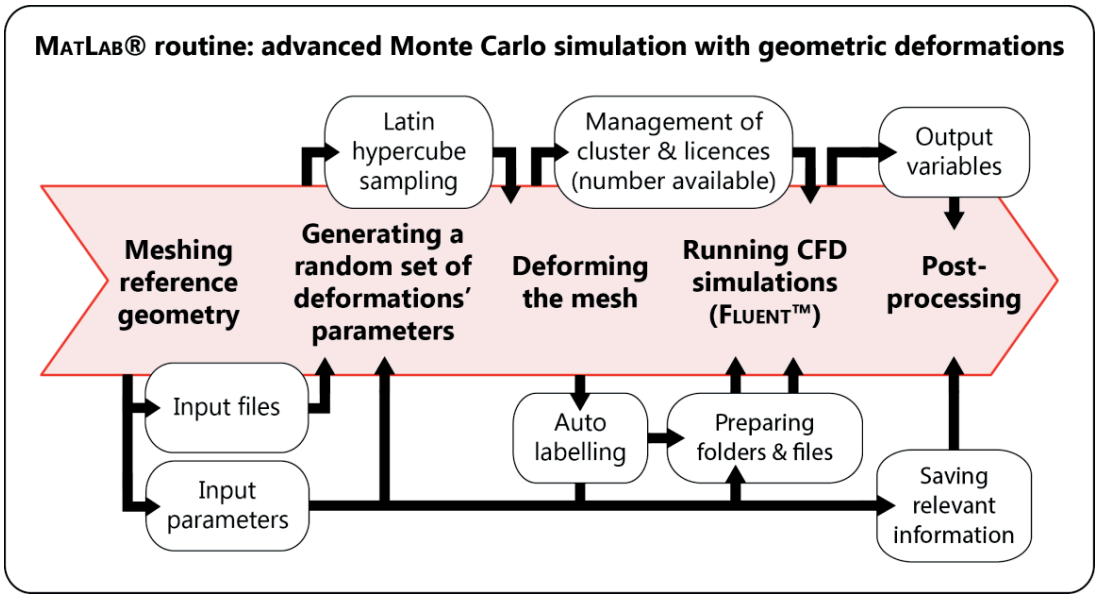

Figure 8.2 Main steps of the computation process for the MCS.

8.4.2 Automated generation of standardized deformations

To systematize the tasks and allow both an automatic treatment and meaningful statistical analyses, some typical deformations are chosen to be applied to the geometries. Typical curves of the deformations are shown in figure 8.3. Three-dimensional representations of exaggerated deformations on meshed geometries are shown in figure 8.4 to clarify the purpose.

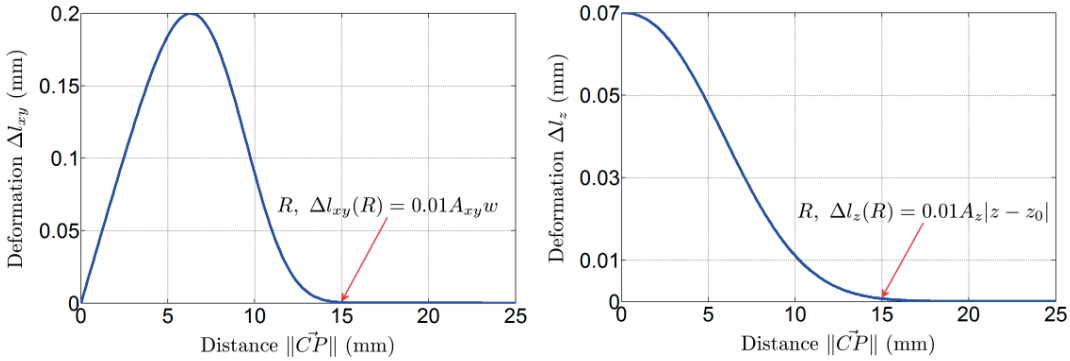

Figure 8.3 Typical variation in function of the distance from the centre.
Left: In-plane deformation. Right: Thickness deformation with respect to the designed thickness (0.7 mm), at $z = z_{\max}$.

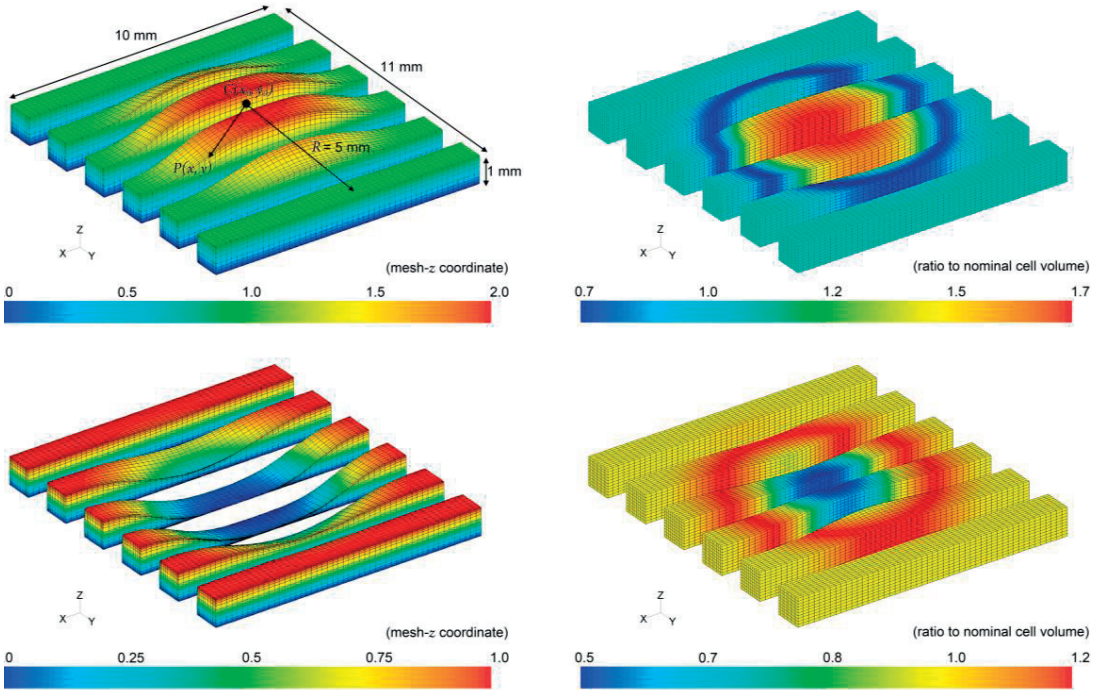

Figure 8.4 Fragment of the FDP showing the standard deformations applied (exaggerated for the purpose of illustration).
Left: Thickness variations; $A_z = \pm 100$ %.
Right: In-plane deformations; $A_{xy} = \pm 50$ %.

The functions to compute these deformations at mesh point P are defined by the following equations:

1. In-plane (xy) deformation

The shape of the in-plane deformation is determined by the function s_{xy} (mm), defined as:

$$s_{xy} = l_0 \, \mathrm{e}^{\left[-\frac{1}{2}\left(\frac{l_0}{M_{xy}\,R}\right)^{n_{xy}}\right]} \tag{8.1}$$

This function allows translating mesh points toward or away from a point defined as the centre of the deformation. In this function, $l_0 = \|\boldsymbol{CP}\|$ is the in-plane distance of any mesh point $P[x, y]$ from the centre of the deformation $C[x_0, y_0]$. M_{xy} is a dimensionless factor that controls the position of the maximum of the deformation with respect to the

range of influence R of the deformation (in mm). The exponent n_{xy} is defined in equation (8.1) such that the residual deformation at radius R is below a given threshold of the nominal amplitude.

$$n_{xy} = -\frac{\ln\left[-2\ \ln\left[\frac{\alpha_R}{R}\right]\right]}{\ln\left[M_{xy}\right]} \quad \text{such that} \quad \Delta l_{xy}[R] = \alpha_R\ A_{xy}\ w, \tag{8.2}$$

where α_R is the residual fraction of the amplitude of the deformation at the distance R from the centre of the deformation.

The absolute deformation Δl_{xy} is then obtained by normalizing the shape s_{xy} and by multiplying it with the desired amplitude of the deformation. The latter is defined as the product of the relative amplitude of the deformation A_{xy} and the width of the channel w (in mm):

$$\Delta l_{xy} = A_{xy}\ w\ \frac{s_{xy}}{\max\left[s_{xy}\right]} \tag{8.3}$$

Finally, the new coordinate P' of any mesh point P is computed with:

$$\boldsymbol{OP'} = \boldsymbol{OP} + \frac{\boldsymbol{OP}}{\|\boldsymbol{OP}\|}\ \Delta l_{xy} \tag{8.4}$$

2. Vertical (z) deformation

The thickness variation of the FDP is obtained in a similar manner. The absolute vertical deformation $\Delta l_z = z' - z$, which allows computing each new vertical coordinate z', is defined as:

$$\Delta l_z = A_z\ |z - z_0|\ \mathrm{e}^{\left[-\frac{l_0{}^{n_z}}{M_z}\right]}, \tag{8.5}$$

where A_z is the relative amplitude of the deformation and z_0 is the vertical coordinate at the baseline of the FDP. M_z is a factor that controls the steepness of the deformation. Finally, n_z is defined as:

$$n_z = \frac{\ln[-M_z\ \ln[\alpha_R]]}{\ln[R]} \quad \text{such that} \quad \Delta l_z[R] = \alpha_R\ A_z\ |z - z_0|, \tag{8.6}$$

where α_R is again the residual fraction of the amplitude of the deformation at the distance R from the centre of the deformation.

In the current study, the parameters M_{xy}, M_z, and α_R are kept constant and, respectively, equal to 0.5, 100, and 0.01.

Figure 8.4 is an illustration of the exaggerated deformations on a fragment of the FDP obtained with preceding equations implemented in a MATLAB routine.

Both in-plane deformations and thickness variations are modelled and can be applied alone or in conjunction to the geometries. The model is intrinsically coded such as several deformations can be superposed. In this study, however, with a view to analyse the statistical sensitivity to various parameters, a maximum of one deformation of each type is applied per sample, with for both a common centre $C[x_0, y_0]$ for the functions of deformations.

The parameters that are randomly varied in the MCS are the point of control (centre) C of the deformation functions, the amplitudes A_{xy} and A_z, and the range of influence R. These parameters are summarized in table 8.1 together with their assumed statistical law of distribution.

While the amplitudes are supposed to follow a normal distribution, the range of influence R and the point of control C are assumed uniformly distributed on given intervals. For the range of influence R, the bounds are related to the width W, and the length L of the cell.

Table 8.1 Parameters of the Monte Carlo simulations.

Deformations' parameters	Statistical law assumed
Amplitude A	Normal distribution (μ, σ)
Range of influence (radius) R	Uniformly distributed in $[W/8 \dots \sqrt{W^2 + L^2}]$
Point of control (centre) C	Uniformly distributed in the domain of the cell: $\{40 \times 40\}$ mm

8.5 Results and discussion

8.5.1 Fluid distribution patterns under study

To have a reliable basis, it was decided to consider two "standard" FDPs for which a study of the flow uniformity can be found in literature [18,53,83]. The first pattern is "asymmetric" with a single-inlet/single-outlet design, proposed by Yakabe et al. [84]. The second pattern is "symmetric" with a double-inlet/single-outlet design, proposed by de Haart et al. [85] and modified by Huang et al. [53]. Both patterns have identical cell geometries. These measure 40 mm × 40 mm and are divided by 12 channels with

a height of 0.7 mm and a width of 1.74 mm. The symmetric pattern includes in addition 10 equally spaced guide-vanes.

Figure 8.5 shows the studied FDPs with computed contours of static pressure and velocity magnitude, illustrating the different concepts for the distribution of gases.

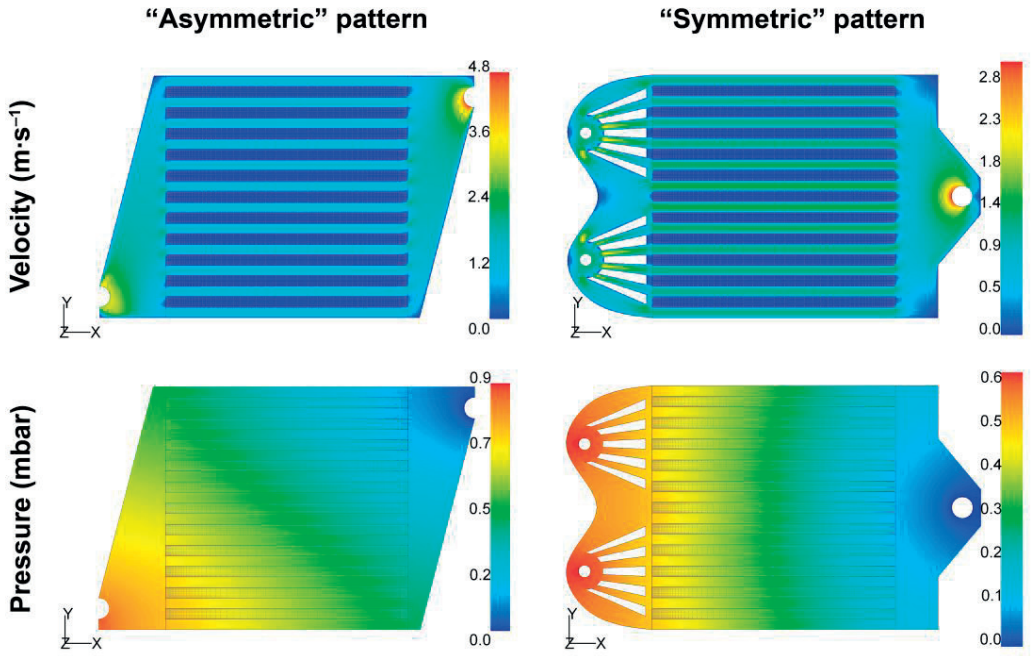

Figure 8.5 Selected standard configuration of FDPs [53].
Respectively the "asymmetric" (left) and "symmetric" (right) patterns. Top: Contours of velocity magnitude [m/s]. Bottom: Contours of static pressure [mbar].

8.5.2 Variations of parameters

For both FDP, sets of 1 500 samples were simulated for each combination of parameters as given in table 8.2. The amplitudes of deformation were always considered to follow centred Gaussian distributions ($\mu = 0$ µm). For the sets where a superposition of vertical and in-plane deformations was simulated (both amplitudes varied), two situations were studied: first with the ranges of influence R set constant and then with R varying. Besides, R and C were unchanged between both types of deformation in this study. For each other case, R was kept constant and equal to 10 mm. The centre of the deformation C was always uniformly distributed on the cell's surface. In total, 16 MCS' sets of 1 500 samples were computed, which are summarized in table 8.2.

In the following, relative amplitudes are expressed as the ratio of the absolute amplitude over the characteristic length, i.e., the height and the width of the channel, respectively, for vertical and in-plane deformations.

Table 8.2 Parameters varied for the deformations.

		$\sigma[A_{xy}]$			
		0 %	6 %	12 %	24 %
$\sigma[A_z]$	0 %	ref.	×	×	×
	5 %	×			
	10 %	×		×, ◊	
	15 %	×			
	C uniformly distributed for all cases. $R = 10$ mm, except for the case "◊" (see text).				

8.5.3 Sensitivity of individual repeat elements to dimensional tolerances

1. Flawless geometries (references)

To allow relevant comparisons of cases, the flawless geometries are simulated first to have references. Besides, mass flow rates within channels are scaled with the averaged channel mass flow rate, which corresponds to an "ideal," homogeneous distribution:

$$\dot{M}_{\mathrm{ch}}^{\mathrm{mean}} = \frac{1}{\mathcal{N}_{\mathrm{ch}}} \sum_{ch=1}^{\mathcal{N}_{\mathrm{ch}}} \dot{M}_{ch}^{\mathrm{IE}} = \frac{\dot{M}_{\mathrm{el}}^{\mathrm{IE}}}{\mathcal{N}_{\mathrm{ch}}} = \frac{\dot{M}_{\mathrm{el}}^{\mathrm{simu}}}{\mathcal{N}_{\mathrm{ch}}} \tag{8.7}$$

$$\dot{M}_{ch}^{\mathrm{IE,\,scaled}} = \frac{\dot{M}_{ch}^{\mathrm{IE}}}{\dot{M}_{\mathrm{ch}}^{\mathrm{mean}}} \tag{8.8}$$

The flow distributions obtained for the geometries of reference are presented *on top* of figure 8.6. It clearly stresses out that the flow is more uniform for the asymmetric pattern.[1] The minimum channel flow rate is 98 % of the ideal mass flow rate, whereas, it reaches only 95 % for the symmetric pattern. For both patterns, the minimal flow is found on the sides of the element. In these non-deformed cases, a slight diminution of

[1] This difference with respect to the results obtained by Huang et al. [53] is essentially due to slight differences between geometries, especially the position and shapes of the guide-vanes. Indeed, we reproduced the geometries based on the drawing in their article.

the maximal safe fuel utilization can, therefore, already be expected from the simulated deviation of fuel distribution.

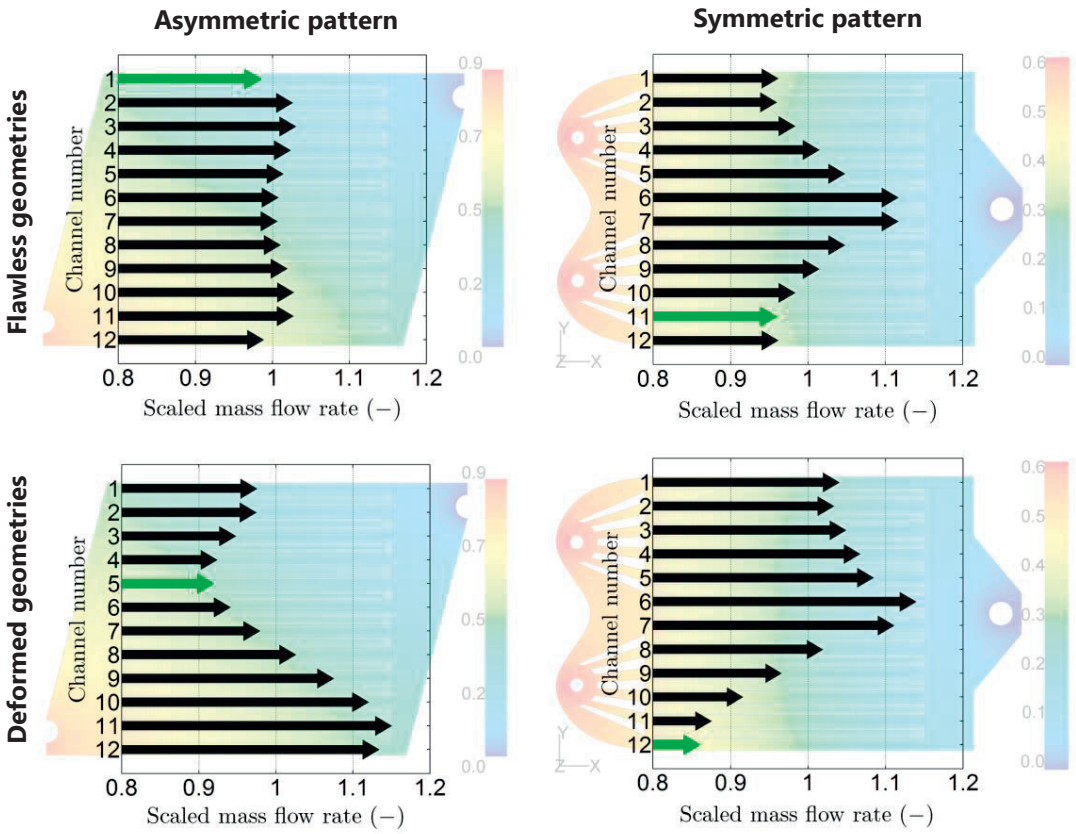

Figure 8.6 Distribution of flow rate within channels.
Top: flawless geometries. Bottom: example of deformed geometries. Left: asymmetric pattern. Right: symmetric pattern.

2. Deformed geometries

Examples

Bottom of figure 8.6 shows examples of flow distributions for deformed FDPs, extracted from a set of MCS samples. It illustrates that the minimum flow rate within a channel can be significantly lower than within the flawless geometries (references). For these samples, the minima are, respectively, 91 % and 85 % for the asymmetric and symmetric patterns. In addition, it is visible that the deformation of the FDP induces a depletion of fuel on about half of the element, showing that the risk of degradation or

damages at high fuel utilization may affect a large part of the cell. Finally, by the law of mass conservation, some channels present an important increase of fuel flow when compared with the non-deformed case.

Statistical distribution for a set of samples

Figure 8.7 shows the statistical distribution of the scaled flow rates obtained with MCS of a set of 1 500 samples. The histograms show the distribution for the reference geometries. Bullets are the averages $\mu = \mu\left[\dot{M}_{ch}^{\text{scaled}}\right]$ over all MCS. "Error bars" corresponds to standard deviations $\sigma = \sigma\left[\dot{M}_{ch}^{\text{scaled}}\right]$ around μ. The MCS parameters of the deformations are as follows: the standard deviations of amplitudes for z and xy directions are, respectively, $\sigma[\mathrm{A}_z] = 10\ \%$ (70 µm) and $\sigma\left[A_{xy}\right] = 12\ \%$ (200 µm). The range of influence R and the point of control C of the deformations are uniformly distributed according to table 8.1.

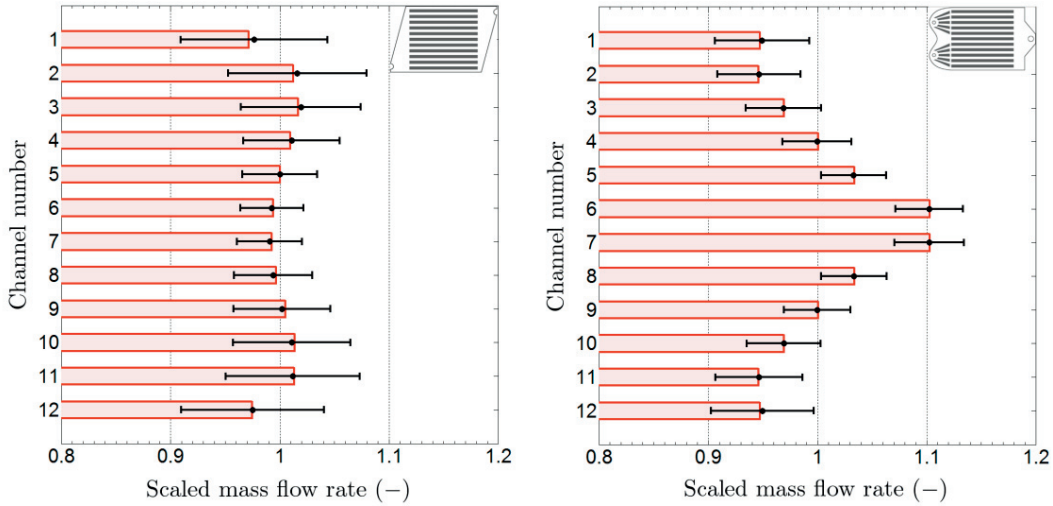

Figure 8.7 Statistical distribution of the scaled mass flow rate within the channels. Histograms: distribution for flawless geometries. Bullets $= \mu$ and "error bars" $= [\mu - \sigma\ ;\ \mu + \sigma]$, computed from the MCS results with parameters: $\sigma[A_z] = 10\ \%$ (70 µm), $\sigma\left[A_{xy}\right] = 12\ \%$ (200 µm), R and C uniformly distributed according to table 8.1.
Left: asymmetric pattern. Right: symmetric pattern.

First, it can be seen that the average values are not much different from the reference patterns. *On average* the deformed geometries have similar quality of flow uniformity than the reference geometries. However, the standard deviations of flow rates within channels are important. Therefore, the *dispersion of quality is large* and the probability

to be in the presence of a really worse geometry is correspondingly high. Moreover, the sensitivity to deformations is larger along the sides for both patterns: for the asymmetric pattern $\sigma_{\text{side}} = 6.0$ % and $\sigma_{\text{centre}} = 2.9$ %, and for the symmetric pattern $\sigma_{\text{side}} = 4.7$ % and $\sigma_{\text{centre}} = 3.0$ %. Besides, it is worth to stress that the asymmetric pattern is globally more sensitive, even if it shows better distribution on average. Nevertheless, the minimum bounds of error bars are about equal for both patterns and reach ca. 91 % of the ideal flow rate.

Finally, it should be mentioned that these outcomes are largely due to the choice of the deformation parameters. In fact, when a case of small defects only is considered (fixed range $R = 10$ mm for instance), the results show lower dispersion of flow rates within the FDP and also a lower difference between sides and centre: from $\sigma_{\min} = 2.1$ % to $\sigma_{\max} = 2.6$ % for the asymmetric pattern and from $\sigma_{\min} = 1.7$ % to $\sigma_{\max} = 2.2$ % for the symmetric pattern.

Sensitivity to the type of deformation

To investigate the sensitivity specific to the direction of the deformation, series of MCS were run once for each direction, with all parameters kept constant except the point of control C and the amplitude A in the specified direction. In other words, no deformation was allowed in the other direction ($A = 0$ %) and the range of influence R was taken constant and set to 10 mm.

Sets of MCS were computed for thickness variations with standard deviations of the amplitude, $\sigma[A_z]$, equal to 5 %, 10 %, and 15 % of the nominal thickness of the FDP. Regarding the sensitivity to in-plane deformations, $\sigma\left[A_{xy}\right]$ equal to 6 %, 12 %, and 24 % of the channels' width. In absolute magnitude, those values correspond, respectively, to $\{35, 70, 105, 100, 200, \text{and } 400\}$ µm.

Considering thickness variations, data in figure 8.8 represent for each channel the lower bounds of error bars for scaled mass flow rates, i.e., $\mu\left[\dot{M}_{ch}^{\text{scaled}}\right] - \sigma\left[\dot{M}_{ch}^{\text{scaled}}\right]$. Here again, each value that is below 1 — stating the average — is limiting the performance and the reliability of the fuel cell. Actually, it is important to notice that by mass conservation, those values cannot be obtained all simultaneously for an element: 10 % lack in one channel must be compensated by an excess in other ones. Once more, the asymmetric pattern is globally more sensitive to thickness variations. However, extreme values are worse for the symmetric pattern.

It is now important to remember that the interval between the boundaries of error bars corresponds to only a fraction of all reachable situations (ca. 68 % for a normal distribution). Hence, a non-negligible number of cases are still worse. Evidence of this and

its consequences will be discussed later on in the section *Statistical distribution of the flow deviation* (p. 230) and shown in particular in figure 8.10.

Figure 8.9 is the counterpart of figure 8.8 for in-plane deformations. By comparing these two figures, it is clear that the tolerance along the z-direction is more critical than along the xy-plane. Even with a standard deviation of the amplitude as large as 400 µm in xy-direction (24 % of the characteristic length), the flow uniformity is statistically still better than with "only" 70 µm (10 %) along z and is similar to the flow uniformity obtained with 35 µm (5 %) along z. Nevertheless, these statements should not hide the fact that the geometry of the FDP is one of the most preponderant factors, as the results also show.

8.5.4 Impact of tolerances on a stack

1. Mathematical transition to stack situation

To assess the impact of stacking elements produced with a given tightness on tolerances, the results obtained in MCS series for individual elements are post-treated to correspond to a stack situation.

In the studied case, the hypothesis is made that the deformation on one element has no link with the deformations on other elements (no macroscopic deformation applied to the entire stack). In other words, each element is deformed, and then, they are (virtually) staked together. Hence, the data issued from the MCS are used to compute the "corrected" data specific to the stack situation. The laws of mass conservation and fluid mechanics (pressure drop) are used to move from one situation to the other. The development is as follows.

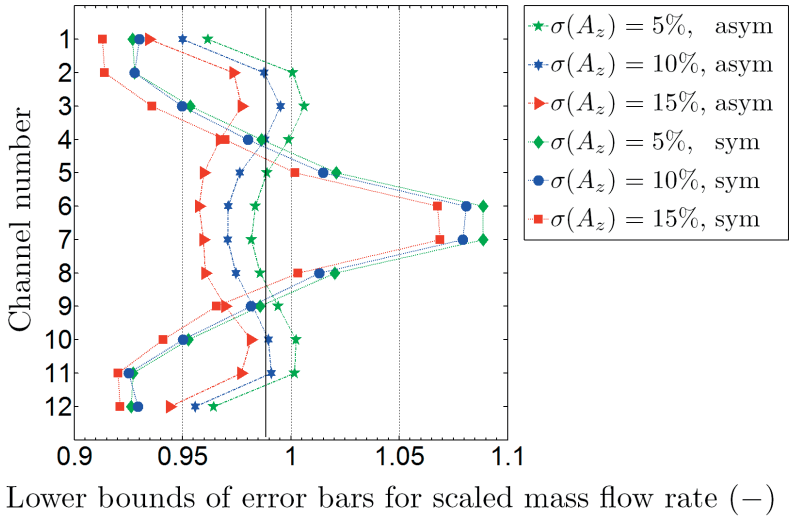

Figure 8.8 Sensitivity to thickness variations.

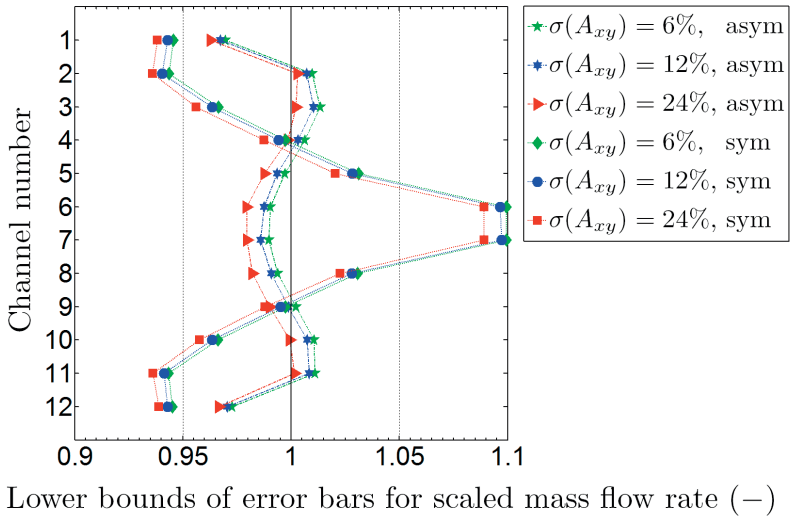

Figure 8.9 Sensitivity to in-plane deformations.

Considering the elements individually (IE)

The mass flow rate that enters the element, $\dot{M}_{\mathrm{el}}^{\mathrm{IE}}$, is imposed and is the same for each simulation, whereas, the pressure drop for the element, $\Delta P_{el}^{\mathrm{IE}}$, depends on the deformation and is part of the data extracted for each simulation. For each channel of each element, the mass flow rate $\dot{M}_{ch}^{\mathrm{IE}}$ is also extracted and by the law of mass conservation they are linked to the mass flow rate of the element by:

$$\dot{M}_{\mathrm{el}}^{\mathrm{IE}} = \sum_{ch=1}^{\mathcal{N}_{\mathrm{ch}}} \dot{M}_{ch}^{\mathrm{IE}} = \mathcal{N}_{\mathrm{ch}}\ \dot{M}_{\mathrm{ch}}^{\mathrm{mean}} \tag{8.9}$$

Considering a stacking of all those elements (ST)

In this situation, it is the pressure drop for each element that is constant:[2] $\Delta P_{\mathrm{el}}^{\mathrm{ST}} = \mathrm{cst}$. This is a consequence of the stacking of the elements (hydrodynamically in parallel). That pressure drop is obtained with the equilibrium of all pressure drops of the individual elements, i.e.:

$$\Delta P_{\mathrm{el}}^{\mathrm{ST}} = \mathcal{N}_{\mathrm{el}} \left(\sum_{el=1}^{\mathcal{N}_{\mathrm{el}}} \frac{1}{\Delta P_{el}^{\mathrm{IE}}} \right)^{-1} \tag{8.10}$$

Assuming a laminar flow within the channels, the pressure drop is proportional to the mass flow rate; hence, for a given fluid and a given geometry, the pressure drops and the mass flow rates for the stacked and the individual elements are linked according to:

$$\frac{\dot{M}_{el}^{\mathrm{ST}}}{\Delta P_{\mathrm{el}}^{\mathrm{ST}}} = \frac{\dot{M}_{\mathrm{el}}^{\mathrm{IE}}}{\Delta P_{el}^{\mathrm{IE}}} \tag{8.11}$$

As a consequence, the mass flow rate that enters a given element in the stack is computed as:

$$\dot{M}_{el}^{\mathrm{ST}} = \dot{M}_{el}^{\mathrm{IE}}\ \frac{\Delta P_{\mathrm{el}}^{\mathrm{ST}}}{\Delta P_{el}^{\mathrm{IE}}} \tag{8.12}$$

Implicitly and with previous hypotheses, the deformation is identical for an element taken individually than for the same element when stacked. As a result, the flow distribution will have the same *shape* qualitatively, but with a global shift of the amplitudes quantitatively; hence, the mass flow rate that enters a given channel for a given element in the stacked situation is computed the same way:

$$\dot{M}_{ch}^{\mathrm{ST}} = \dot{M}_{ch}^{\mathrm{IE}}\ \frac{\Delta P_{\mathrm{el}}^{\mathrm{ST}}}{\Delta P_{el}^{\mathrm{IE}}} \tag{8.13}$$

Finally, the stack pressure drop is defined such as to obtain an average flow per element equal to the nominal flow imposed in the MCS runs $\left(\dot{M}_{\mathrm{el}}^{\mathrm{simu}}\right)$. It is defined here as

[2] Neglecting the effect of gravity and considering perfect manifold.

$\Delta P_{\mathrm{el}}^{\mathrm{ST}} = \overline{\Delta P}_{\mathrm{MCS}}$ the stack pressure drop for the considered set of simulations. This corresponds to a stack with a large number of elements. Here, it is not considered the case of smaller stacks, where the stack pressure drop obtained for the average fuel flow may differ from $\overline{\Delta P}_{\mathrm{MCS}}$ ($\mathcal{N}_{\mathrm{el}} < \mathcal{N}_{\mathrm{MCS}}$). This case is considered later in § 8.6 *Statistics for practical combinatorial cases*, p. 232.

We use the indicator of flow uniformity δ_{min}, as defined in equation (3.4). The statistical distributions of δ_{min} are shown in figure 8.10 and are discussed in the following paragraphs.

2. Statistical distribution of the flow deviation

The results presented hereinafter were obtained with MCS of a set of 1 500 samples deformed with one vertical distortion and one in-plane distortion, whose parameters are as follows: standard deviation of amplitudes for z and xy directions are, respectively, $\sigma[A_z] = 10\ \%\ (70\ \mu\mathrm{m})$ and $\sigma\left[A_{xy}\right] = 12\ \%\ (200\ \mu\mathrm{m})$. The range of influence R and the point of control C of the deformations are uniformly distributed according to table 8.1.

With equation (3.5), it is possible to obtain the statistical distribution of the flow rate deviation in the stack situation, which can be compared to its counterpart of elements considered individually, equation (3.4). These statistics are shown in figure 8.9 for both FDPs in the form of probability distribution functions. The green dashed line represents the deviation δ_{min} for the reference — flawless — geometries, while the red dash-dot line represents the average of the deviation indicator $\mu[\delta_{\mathrm{min}}]$ computed over the whole set of 1 500 deformed samples. The two blue surrounding lines show the standard deviation of δ_{min}, i.e., $\sigma[\delta_{\mathrm{min}}]$.

Firstly, the statistical distribution for individual elements can be found *on top* of figure 8.10. It points out that the deviation is, *on average* over all sampled deformations, worse than the deviation for the geometries of reference, free from deformation. For instance for the asymmetric pattern of individual elements, $\delta_{\mathrm{min,\ ref}} = -3\ \%$ and $\mu\left[\delta_{\mathrm{min}}^{\mathrm{IE}}\right] = -7\ \%$. Moreover, the cumulative probability of being worse than the reference is ca. 80 % for both FDPs. These results also show that, again, the symmetric pattern proves to be less sensitive to deformations than the asymmetric pattern, by about 1 % to 2 %. Furthermore, these statistics bring to light that a small number of individual elements ($< 1\ \%$) leads to a deviation worse than $-20\ \%$. In other words, those elements will limit the range of safe fuel utilizations to a large extent, without any additional considerations.

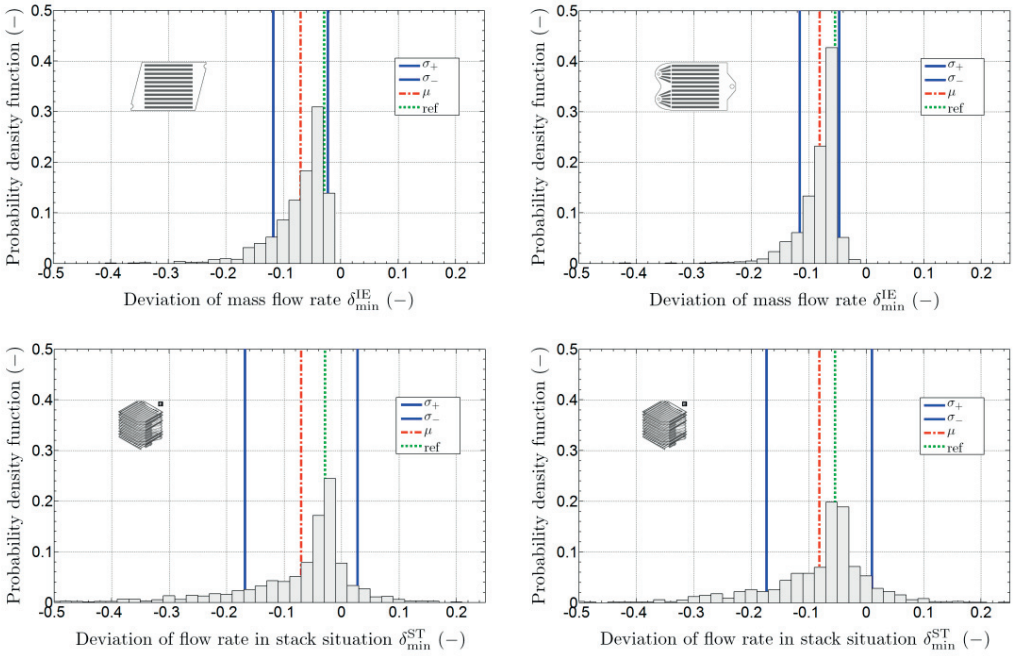

Figure 8.10 Statistical distribution of the flow rate deviation.
Top: elements taken individually. Bottom: whole stack.
Left: asymmetric pattern. Right: symmetric pattern.

Secondly, looking at the statistical distribution for the stack situation (*bottom* of figure 8.10), the deduction is straightforward: stacking the elements leads to a critical increase of the statistical dispersion of the flow deviation and thus an increase of the risk of failure. Although it is interesting to notice that some channels are better fed (excess of fuel at the level of the element), it should be reminded that it is the worst channel, which is decisive for the destiny of the entire stack. Quantitatively, the *average* $\mu\left[\delta_{\min}^{\mathrm{ST}}\right]$ is almost equal to $\mu\left[\delta_{\min}^{\mathrm{IE}}\right]$, which is smaller by less than 0.5 ‰. However, the standard deviation $\sigma\left[\delta_{\min}^{\mathrm{ST}}\right]$ is about twice to three times as large as $\sigma\left[\delta_{\min}^{\mathrm{IE}}\right]$: respectively, 10 % instead of 5 % and 9.5 % instead of 3.5 % for symmetric and asymmetric patterns. As a consequence, when stacked, some elements lead to a deviation worse than −40 %, limiting the range of safe fuel utilizations to a considerable extent for the corresponding elements, and, therefore, also *for the whole stack*. In stack situation, the cumulative probability to get a deviation worse than −20 % *for any elements* amounts to 9.5 % and 10 % for the asymmetric and symmetric patterns, respectively. Hence, when stacking 1 500 elements manufactured with the given dimensional tolerances, ca. 150 elements are expected to have one channel underfed by at least 20 %. In addition, it should be

emphasized that since those values are only due to geometrical considerations, other factors adding to them will contribute to even lower reachable fuel utilizations.

This case study — based on real stack dimensions and dimensional tolerances — shows in this example how strongly the performance and reliability of an SOFC stack are affected by dimensional tolerances. Indeed, with vertical and in-plane dimensional tolerances of, respectively, 10 % and 12 %, the minimum channel flow rate in stack situation may be lowered by not less than 40 % with respect to the ideal flow rate.

8.6 Statistics for practical combinatorial cases

The statistical analysis performed in § 8.5.4, p. 227 is only valid for stacks composed of all the same elements that correspond to all the realizations (samples) which were simulated. This implies that $\mathcal{N}_{\text{cells}} = \mathcal{N}_{\text{samples}}$. For the statistical quantification of the uncertainties, it is useful to have as many realizations (samples) as possible. However, in reality, a stack contains a limited number of repeat elements, typically around 100. As a consequence, a stack will be assembled out of a subset of a manufactured "population" of repeat elements. Statistically, this corresponds to doing a "combinatorial draw."

8.6.1 Stack of 60 elements drawn from batch of 1 500

Let k be the number of repeat element per stack and n the total number of samples (realizations), corresponding to a batch of production. Then, the number of possible combinations $\mathcal{C}$ is:

$$\mathcal{C}[n,k] = \frac{n!}{k!\,(n-k)!} = \frac{n(n-1)\cdots(n-k+1)}{k!}$$

$$\mathcal{C}\big[1\,500, 60\big] \approx 10^{108}$$

Assuming $t = 1$ ms is the time to assess the performance of one of these combinations (i.e., one realization of a stack) on one contemporary computer-core, and that we would have access to the current 1st supercomputer in the world (3.12×10^6 cores), the time to get an exhaustive statistical description would still be:

$$t > 10^{90} \text{ years}$$

Therefore[3], only an estimator of the statistics (mean, variance) of these combinations can be computed.

Estimation procedure

The estimation was done with 100 000 draws. To speed up the computation procedure, we used "logical indexing" in MATLAB, which is an efficient way of randomly drawing k elements of a vector of length n. The indexes are randomly generated with a pseudorandom number generator. It is not even necessary to reorder the indexes.

Example for $\mathcal{C}[\mathbf{9},\mathbf{3}]$ in MATLAB notation

Let $A = [1, 4, 9, 16, 25, 36, 49, 64, 81]$ be a vector of 9 elements in which we want to draw 3 random elements. B is a vector randomly generated with indexes between 1 and number of items in A. For the following, we assume that one realization of B is equal to $[3, 7, 1]$. Then, using B we can construct the Boolean vector C with:

$$C(B) = \text{logical}(1) \rightarrow C = [1, 0, 1, 0, 0, 0, 1]$$

C has the same length as A and contains 1 at every index corresponding to the 3 elements to be drawn in A and 0 at every other. Using the vector C, we can now build one particular realization (draw) of all the possible combinations $\mathcal{C}[\mathbf{9},\mathbf{3}]$:

$$D = A(C) \rightarrow D = [1, 9, 49]$$

We repeat this process as many times as wished ($\mathcal{N}_{\text{samples}}$).

Additional remark

For such a large number of draws, it is worth fine-tuning the computation of even the most basic mathematical functions and to pre-allocate space in memory to hold the variables. The overall time to run the code can be reduced significantly.

Examples: In MATLAB `(sum((x-μk(c)).^2)/(n-1)).^0.5` is faster than `std(x)` and `sum(x)/n` is faster than `mean(x)`.

[3] 10^{90} years is obviously an enormous amount of time. But to give a sense of perspective: the current model for the Big Bang suggests that the age of the Universe is of the order of 10^{10} years. Put otherwise, $10^{90} = 10^{10} \cdot 10^{80}$, the latter being the approximate number of atoms in the observable Universe.

Results

Figure 8.11 shows the statistical distribution of the flow-rate deviation *in the most limiting channel* in a stack of 60 elements drawn randomly from a manufactured population of 1 500 elements. We observe that the worst channel in the stack is always much below the worst channel of the reference geometry. Instead of −3 %, it takes values in the interval $[-60\ \%\ ;\ -15\ \%]$, with an average of ca. −40 %. Note that when not taking into account the variability, the worst element is always at −3 %, disregarding if elements are stacked and how many are (in both reasoning, the effect of the stack-manifolds is neglected). Hence, when stacking 60 elements taken from a batch of 1 500 elements manufactured with the given dimensional tolerances, it is almost certain that the most limiting channel is underfed by at least 20 %.

Figure 8.12 shows the statistical distribution of the flow-rate deviation in channels at one standard deviation from the mean in a stack of 60 elements drawn randomly from a manufactured population of 1 500 elements. The range of dispersion is around three times lower for the standard deviation than for the minimum (both being random variables here).

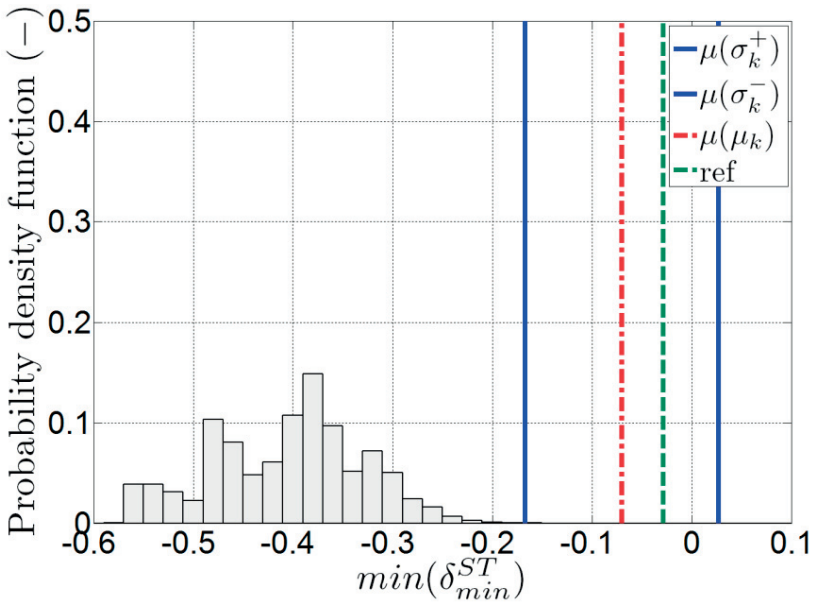

Figure 8.11 Statistical distribution of the flow-rate deviation in the most limiting channel in a stack of 60 elements drawn randomly from a manufactured population of 1 500 elements.

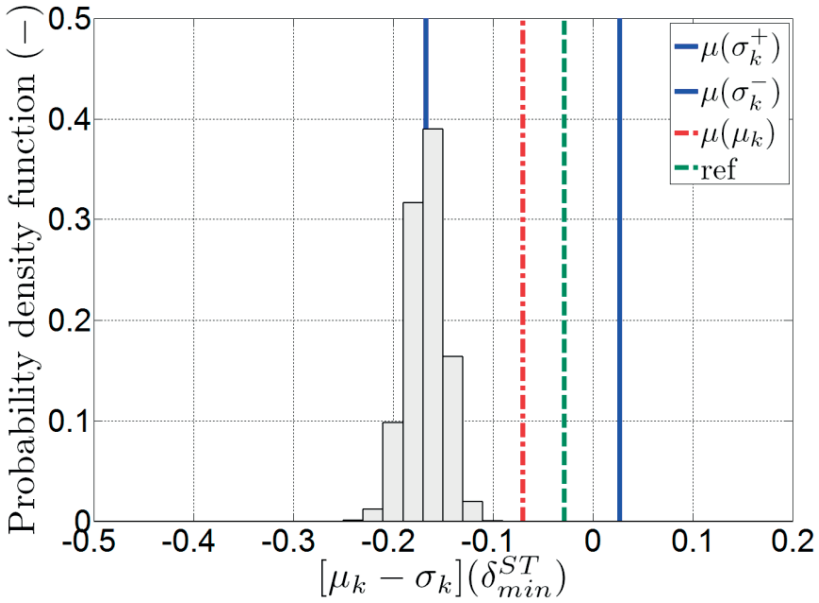

Figure 8.12 Statistical distribution of the flow-rate deviation in channels at one standard deviation from the mean in a stack of 60 elements drawn randomly from a manufactured population of 1 500 elements.

8.7 Limitations of the method

This first study clearly reveals the impact of dimensional tolerances on possible issues for the planar SOFC technology, which corresponds well to typical performance limitations and failures observed in the laboratory. Therefore, it shows the interest of the presented approach for design purposes and for the definition of quality requirements.

The main fields of potential improvements are:

(1) Additional types of deformations and defaults.

(2) Coupling to electro-chemistry and heat transfer for a better assessment of performance limitations.

(3) Introduction of reliability indicators for determining the domain of safe operation [12,13,28].

(4) Coupling between CFD and thermo-mechanical models to simulate possible interactions.

Another limitation is inherent to the basics of Monte Carlo methods, i.e., the heavy computing load, both in terms of time and of resources. However, for a limited number of cases, the load is reasonable regarding the useful information that can be obtained. Moreover, a comparison of the results with 400 or 1 500 samples shows a *relative difference* of less than 2 % for the principal statistic indicators (μ, σ). Hence, the computing effort can be tailored in the context of an industrial design phase, for instance.

8.8 Computer resources

The MCS were ran on the high-power computing (HPC) cluster *Pleiades*, at EPFL. The EPFL's community has access to 50 *shared* ANSYS software licences. Relevant data are given in table 8.3 to give an insight of the computing effort. The portion of the server that was used has the following characteristics [86]:

- 120 Dell PowerEdge SC1425 processors:
  Intel Xeon mono-processor, 2.8 GHz; 5.6 Gflop/s at peak; 1 Mo of L2 cache.
- 4 GB dual access DDR memory (6.4 GB/s at peak).

Table 8.3 Computing effort for *one* set of samples (16 sets in total).
The values in this table do not account for post-processing the results.

Indicators of the computing effort	Values
Samples per set of MCS	1 500 samples / set
Cells of mesh per sample	ca. 500 000 cells / sample
Size of raw data per sample	ca. 150 MB / sample
Size of optimized data per set	ca. 150 MB / set
Cores (mono) per simulated sample	≤ 16 | 8 cores / sample
Simultaneously simulated samples	≤ 7 | 14 samples
Duration for generating 1 deformed mesh	ca. 1 to 4 min / sample
Duration for solving 1 sample with 1 CPU	ca. 50 min / sample
Duration for solving 1 sample with 8 | 16 CPU	ca. 12 | 8 min / sample
Cumulated duration per set (16 CPU)	ca. 200 h / set
Sun-clock duration for running 16 sets of MCS	ca. 640 h (4 weeks)

8.9 Conclusions to the chapter

A method based on MCS of deformed FDPs, modelled using CFD, has been developed, implemented, and assessed. The methodology proved successful in effectively getting insights on the quality of FDPs with respect to dimensional tolerances.

The results of the statistical analyses processed on data from the MCS bring to light four major outcomes:

(1) The planar SOFC technology is highly sensitive to the geometrical quality of the FDP at the anode, both in terms of performance limitations or possible risk of degradations and damages.

(2) The sensitivity to thickness variations of the FDP at the anode is preponderant when compared to in-plane deformations. Regarding manufacturing processes and real designs, this implies strong criteria of quality for the choice of appropriate production methods.

(3) In stack situation, the negative effects of deformations are exacerbated by the deviation of flow among the elements.

(4) Some geometries of the FDP are more favourable than others, revealing that the design of the FDP can restrain to a certain extent the sensitivity to manufacturing tolerances, i.e., allow better durability of performance and reliability for the same dimensional accuracy.

Briefly, the results highlight the importance of dimensional tolerances, i.e., of the appropriate choice of the FDP geometry and manufacturing processes. Thus, the method implemented in this custom-made automated tool also helps to take decisions by giving quantified indications on tolerance requirements.

« Les grandes personnes aiment les chiffres. »
Antoine de Saint-Exupéry
Le Petit Prince

CHAPTER 9

Optimization under uncertainty

The purpose of this chapter is firstly to concretely show the usefulness of an optimization under uncertainty to design fluid distribution patterns for fuel cells. Secondly, it gives quantitative insights of what are the most adequate geometries to get a robust design, and specific solutions under the particular situation as represented by the model, fixed parameters, and optimization problem. Thirdly, it shows how the chosen methods help to make the problem tractable, but also shows the remaining challenges and dilemma, opening perspectives for further research.

9.1 Formulation of the optimization problem

The general formulation of an optimization problem is:

$$\begin{aligned} &\min_{\boldsymbol{x}} f[\boldsymbol{x}] \\ \text{satisfying:} \quad &\\ &\boldsymbol{h}[\boldsymbol{x}] = 0 \\ &\boldsymbol{g}[\boldsymbol{x}] \leq 0 \end{aligned} \tag{9.1}$$

where $f: \mathbb{R}^n \to \mathbb{R}$ is the objective function, $\boldsymbol{x} \in \mathbb{R}^n$ the n decision variables, $\boldsymbol{h}$ the equality constraints and $\boldsymbol{g}$ the inequality constraints. Note that in our case, the model forms the equality constraints; in the context of our optimization, we only set inequality constraints. Also, the most basic inequality constraints are constituted of bounds on the decision variables: $\boldsymbol{x}_{\text{low}} \leq \boldsymbol{x} < \boldsymbol{x}_{\text{up}}$.

9.1.1 Objectives of the optimization

The objective of an optimization problem is written as an objective function. Yet, most real problems involve multiple objectives $\boldsymbol{f} = (f_1 \dots f_m)'$. A first convenient approach,

when applicable, is to regroup the objectives by (generalized) multiplication: e.g., power density may be used as a replacement for power and compactness. A solution that is often considered is to cast several objectives into a single objective function by weighting them in a linear combination: $f = w_1 f_1 + w_2 f_2 + \cdots + w_m f_m$. The main drawbacks of this approach is that the solution depends on the weights and it is typically subjective. A multi-objective algorithm can also be used, with the advantage of keeping the objectives distinct to compare various combination in a Pareto graph. We used a multi-objective genetic algorithm to distinguish two objectives (compactness and efficiency). Last but not least, it is sometimes interesting to reformulate some objectives as constraints: e.g., efficiency can be wished to be at least 50 % instead of maximal.

9.1.2 Tolerances as objective or as constraint

In our study, dimensional tolerances play an important role. Two different approaches were looked after to consider them:

- Find the maximum manufacturing tolerances under which the model satisfies the constraints (notably, lower bounds on efficiency to guaranty a minimal efficiency).
- Or find the maximum efficiency achievable — and how to achieve it by choosing the design variables adequately — under given tolerances (parameters).

Both are interesting approaches. The more adequate depends on how the company who designs the parts plans to manufacture them. For instance, one of our partners cannot really get reduction of cost from their manufacturer by requesting less tight tolerances [87], whereas it is a lever for the other. It is also a question what is the priority for the company: e.g., from a marketing point of view, if efficiency is a key asset or if it is acceptable to sacrifice a bit of efficiency to lower the cost and/or increase the lifetime. The first formulation is a bit less convenient, since an equivalent deterministic formulation does not exist (to get a starting point for the stochastic optimization).

9.1.3 Nonlinear inequality constraints

As noted above, equality constraints are constituted of the model equations; we have no others to add. About inequality constraints, we provided bounds for the decision variables, which are given in table 9.2. Other inequality constraints are non-linear and are discussed here.

Although the goal of the thesis is not to optimize operating conditions, it was necessary to pay attention that the base case is chosen meaningfully in accordance to the simple designs considered. So, in a first step, we used the following constraints to explore possible operating conditions, aside from the "true" decision variables. The power density should not be trivially low, so that $P_{\mathrm{d}} > 0.15\ \mathrm{W/cm^2}$ is imposed. Also, a minimum cell voltage of $U_{\mathrm{cell}} > 0.7\ \mathrm{V}$ in order to avoid degradation from other sources than mentioned below. Similarly, $j_{\mathrm{cell,avg}} < 0.6\ \mathrm{A/cm^2}$, because too high current densities also favour degradation. Given our focus on very high fuel utilization, hence at a low current density, those constraints were not activated in the last optimization runs and could be omitted. Lastly, we imposed a minimum flow uniformity $\gamma > 0.8$ in the deterministic case to help the optimization solver to converge.

The other and main inequality constraints concern directly the degradations which are typically sensitive to the flow distribution. We used two indicators for the re-oxidation of nickel at the anode (with oxygen and with water vapour), and one aggregated indicator for the formation of zirconate at the cathode. Details for the computation of these indicators are provided in the next section. According to their definition, the related degradation occurs when they are positive, so that the inequality constraints are:

$$\begin{aligned} &\zeta_{\mathrm{NiO|O_2}} < 0 \\ &\zeta_{\mathrm{NiO|H_2O}} < 0 \\ &\zeta_{\mathrm{LZO,SZO}} < 0 \end{aligned} \tag{9.2}$$

Remark:

Here, we write constraints in a natural way. In the code, all the constraints are reformulated in the standard way requested by the algorithm, i.e., $\boldsymbol{g}[\boldsymbol{x}] < 0$.

Initially, we used indicators of degradation (ζ) in a Boolean form (1 = degradation, 0 = no degradation) with equality constraints applied to them. We now use them in a continuous form with inequality constraints, as defined above. It is advantageous for the convergence of the optimization algorithm. Moreover, it is more in line with the fact that the risk and severity of degradation varies in magnitude (rather than as an on/off process). Also, in a stochastic framework, it allows to define a statistical criterion (e.g., probability) by retaining precision, otherwise lost in the truncation to form a Boolean indicator.

Degradation of the electrodes

Rather than arbitrarily imposing a maximum fuel utilization, we assess the risk for degradation of the electrodes. The optimization solver can then choose an optimum value for the fuel utilization.

Special acknowledgements are due to Arata Nakajo for providing the relevant data.

Re-oxidation of nickel at anode

We use the approach of Diego Larrain [88], which we briefly report here.

The *oxidation of nickel with oxygen* corresponds to the reaction:

$$\mathrm{Ni(s)} + 0.5\mathrm{O_2} \leftrightarrow \mathrm{NiO(s)}$$

The corresponding indicator of degradation is computed with:

$$\zeta_{\mathrm{NiO|O_2}} = p^{\mathrm{A}}_{\mathrm{TPB}}[\mathrm{O_2}] - p_{\mathrm{eq}}[\mathrm{O_2}] \tag{9.3}$$

We estimate the molar fraction of oxygen at the *anode* side with:

$$p^{\mathrm{A}}_{\mathrm{TPB}}[\mathrm{O_2}] = p^{\mathrm{C}}_{\mathrm{TPB}}[\mathrm{O_2}] \exp\left[\frac{-U_{\mathrm{Nernst}}\, 4\, \mathcal{F}}{\mathcal{R}\, T}\right] \tag{9.4}$$

We compute the partial pressure of oxygen at equilibrium with:

$$p_{\mathrm{eq}}[\mathrm{O_2}] = \exp\left[\frac{2\, \Delta_{\mathrm{f}}\tilde{g}^{o}[\mathrm{NiO}]|_{\mathrm{O_2}}}{\mathcal{R}\, T}\right] \tag{9.5}$$

with the Gibbs free enthalpy for the formation of nickel oxide by reaction of nickel with oxygen computed with the data in table 9.1 as:

$$\Delta_{\mathrm{f}}\tilde{g}^{o}[\mathrm{NiO}]|_{\mathrm{O_2}} = \Delta_{\mathrm{f}}\tilde{h}[\mathrm{NiO}] - T\,(\Delta\tilde{s}^{o}[\mathrm{NiO}] - 0.5\,\Delta\tilde{s}^{o}[\mathrm{O_2}] - \Delta\tilde{s}^{o}[\mathrm{Ni}]) \tag{9.6}$$

Table 9.1 Thermodynamic data used to compute the Ni/NiO equilibrium.

$\boldsymbol{\Delta_{\mathrm{f}}\tilde{h}[\mathrm{NiO}]}$	$\boldsymbol{\Delta\tilde{s}^{o}[\mathrm{O_2}]}$	$\boldsymbol{\Delta\tilde{s}^{o}[\mathrm{Ni}]}$	$\boldsymbol{\Delta\tilde{s}^{o}[\mathrm{NiO}]}$
J/mol	J/(mol K)	J/(mol K)	J/(mol K)
$-244 \cdot 10^3$	205	30.14496	38.602296

So, the indicator in equation (9.3) depends on the temperature T, the molar fraction of $\mathrm{O_2}$ at the TPB, and the Nernst voltage, but it does not depend on the molar fractions of $\mathrm{H_2O}$ and $\mathrm{H_2}$. A positive value indicates a degradation.

The *oxidation of nickel with water vapour* corresponds to the reaction:

$$\mathrm{Ni(s)} + \mathrm{H_2O} \leftrightarrow \mathrm{NiO(s)} + \mathrm{H_2}$$

The corresponding indicator of degradation is computed with:

$$\zeta_{\mathrm{NiO|H_2O}} = \exp\left[\frac{-\Delta_\mathrm{f}\tilde{g}^o[\mathrm{NiO}]|_{\mathrm{H_2O}}}{\mathcal{R}\,T}\right] p^{\mathrm{A}}_{\mathrm{TPB}}[\mathrm{H_2O}] - p^{\mathrm{A}}_{\mathrm{TPB}}[\mathrm{H_2}] \tag{9.7}$$

with the Gibbs free enthalpy for the formation of nickel oxide by reaction of nickel with water vapour computed with the following fit of data [68]:

$$\Delta_\mathrm{f}\tilde{g}^o[\mathrm{NiO}]|_{\mathrm{H_2O}} = -4 \cdot 10^{-3}\,T^2 + 38.7\,T + 8742.8 \tag{9.8}$$

This indicator depends on the temperature T and the molar fractions of $\mathrm{H_2O}$ and $\mathrm{H_2}$ at the TPB, but it does not depend on the Nernst voltage, nor on the molar fraction of $\mathrm{O_2}$. It only activates for very low amount of $\mathrm{H_2}$, relatively high amount of $\mathrm{H_2O}$, and high temperature. A positive value indicates a degradation.

Formation of zirconate at cathode

The performance of cathodes made of LSM-YSZ[1] can be degraded by the formation of an insulating layer of zirconate, namely lanthanum zirconate (LZO) and strontium zirconate (SZO). The interested reader will find details about zirconate in [68] and further references in it.

The indicator for the formation of LZO and SZO is computed with:

$$\zeta_{\mathrm{LZO,SZO}} = \log_{10}\left[p^{\mathrm{eq}}_{\mathrm{O_2}}\right] - \log_{10}\left[p_{\mathrm{O_2}}\mathrm{TPB}\right] \tag{9.9}$$

with the partial pressure of oxygen at the TPB computed from:

$$p_{\mathrm{O_2}}\mathrm{TPB} = p^{\mathrm{C}}_{\mathrm{TPB}}[\mathrm{O_2(g)}] \exp\left[\frac{-\eta_\mathrm{C}\,4\,\mathcal{F}}{\mathcal{R}\,T}\right] \tag{9.10}$$

and the value of $\log_{10}\left[p^{\mathrm{eq}}_{\mathrm{O_2}}\right]$ is computed at a given temperature with a linear interpolation of the data from [68], shown in figure 9.1.

[1] Lanthanum strontium manganite (LSM), Yttria-stabilized zirconia (YSZ).

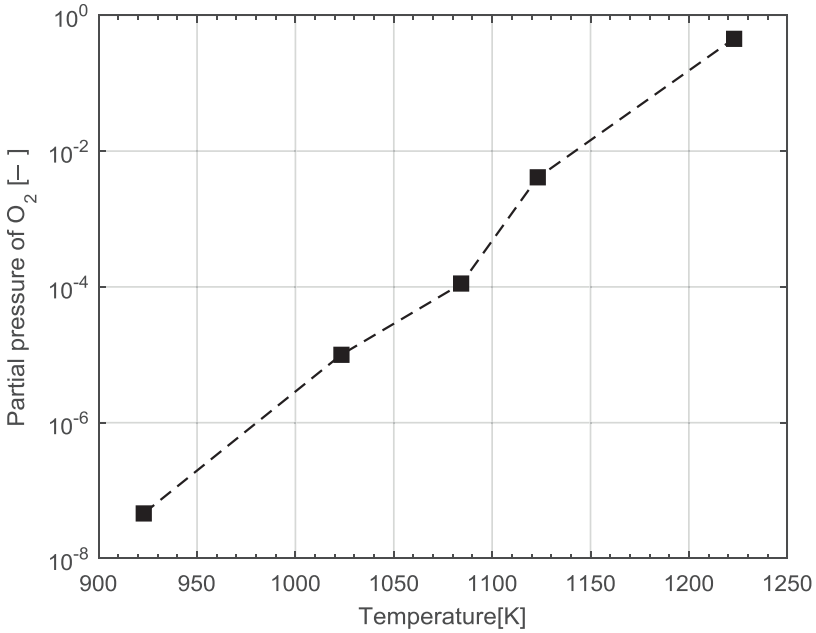

Figure 9.1 Partial pressure of oxygen at the equilibrium of the formation of LZO, SZO. Data from [68]. Dashed lines represent the linear interpolation.

9.1.4 Remark regarding stochastic aspects

1. Algorithm of optimization

We remind here that the objective function of a stochastic problem is often "noisy", non-smooth, due to the variability of the uncertain variables. This characteristic gives difficulty to gradient-based solvers, which are likely to get stuck in a local optimum. Indeed, they rely on the information of the gradients, which are often imprecise or unreliable in such situations. We used the genetic algorithm of MatLab to deal with multi-objective optimization and also pattern search.

2. Decoupling with principle of superposition

The idea is to treat separately variables a) which have a strong effect on the flow uniformity deterministically but less stochastically, versus variables b) which have a strong effect stochastically but less deterministically (e.g., width of the manifolds vs. hydraulic diameter of the channels).

Following this idea, a deterministic optimization would be carried out with all decision variables, with variables (a) having priority. In a second stage, a stochastic optimization would be carried out with only variables (b).

By pushing the reasoning further: variables (b) are considered by fixing values of (a) to their respective ideal: e.g., "infinitely" big manifolds corresponding to no constraints on compactness. So, for instance, the variance of the response to PDF of (b) with ideal (a) is superposed (added) to the response when (b) are nominal (towards optimal) and (a) optimal. This assumes that the interactions between variables (a) and (b) are negligible around the actual values with respect to other effects.

Note that by using the principle of superposition, one assumes that the physics is mainly linear where the principle is applied. Therefore, we decided not to apply it in the following. We however strongly believe that it could be worth to investigate this possibility in more detail.

9.2 Application to straight channels

9.2.1 Model used

Initially, we simplified the problem by setting the maximum achievable fuel utilization with the minimum flow uniformity at the anode and cathode sides:

$$u_\mathrm{f} = \min[\gamma_\mathrm{A}, \gamma_\mathrm{C}] \tag{9.11}$$

However, degradation starts before the species are lacking. So, in the current model, fuel utilization is also a decision variable and indicators of degradation are used as constraints: re-oxidation of the anode and formation of LZO/SZO at the cathode.

9.2.2 Definition of the optimization problem

The heights of the channels at the anode and at the cathode are simultaneously uncertain variables and decision variables.

The ***objectives*** are the *system efficiency* and a measure of *compactness*. Note that compactness can also be seen as a kind of alias for *specific power* and *specific cost*. Indeed, here we consider a constant number of cells, having a constant area, with which we desire to achieve optimal performance, while making sure the design is robust to manufacturing tolerances. We therefore look for a trade-off depending on the heights of the

channels. We define an indicator of compactness such that it takes values in [0 1], 1 being best:

$$\zeta_{\text{compactness}} = \frac{H_{\text{total}} - H_{\text{A}} - H_{\text{C}}}{H_{\text{total}}} \tag{9.12}$$

The main ***decision variables*** are the heights of the channels at the anode $H_{\text{A}}^{\mathbb{N}}$ and at the cathode $H_{\text{C}}^{\mathbb{N}}$. We impose the same nominal value for every channel of one side. We could also imagine to let the algorithm decide which nominal value is ideal for each channel. However, it would make the problem longer to run, especially for a large number of channels. Besides, it is cheaper to manufacture, and notably much easier to control the quality of a uniform design. The fuel utilization[2] is also chosen by the optimization algorithm, because it should be large for performance but is in principle constrained by the flow uniformity.

The ***constraints*** are defined as described in § 9.3.1. In addition, the decision variables are bounded as shown in table 9.2, such as to limit the search space.

Table 9.2 Initial values and bounds of the decision variables.

Quantity	x_0	$x_{\min}$	$x_{\max}$
H_{A} [mm]	0.5	3.3 σ ‡	2
H_{C} [mm]	1	3.3 σ ‡	2
u_{f}	0.8	0.7	1

‡ close to zero but bigger than 3 σ

The ***uncertain variables*** are the heights of the channels c at anode $H_{\text{A}}^{\mathbb{U}}[c_{\text{A}}]$ and at cathode $H_{\text{C}}^{\mathbb{U}}[c_{\text{C}}]$, i.e., two *vectors*. We make the following assumptions for all random variables:

(5) They are independent and identically distributed (IID) random variables.

(6) They follow a truncated normal distribution:

(a) $\boldsymbol{H}^{\mathbb{U}} \sim N(\mu, \sigma)$, with $\mu[\boldsymbol{H}^{\mathbb{U}}] \coloneqq H^{\mathbb{N}}$ and $\sigma[\boldsymbol{H}^{\mathbb{U}}] \coloneqq 7$ µm,
$\forall\, c \text{ of } \boldsymbol{H}^{\mathbb{U}} \in \left\{H_{\text{A}}^{\mathbb{U}}[c_{\text{A}}], H_{\text{C}}^{\mathbb{U}}[c_{\text{C}}]\right\}$

(b) Truncation at $\pm\, 3\,\sigma = 21$ µm (yield 99.7 %)

[2] Without recirculation.

A few points should be highlighted here. The value returned by the optimization algorithm for the nominal design height is assigned to the mean of the distribution (for each electrode). So, the distribution may change every iteration. The recessed part is fundamental: each channel is attributed an IID random variables, so that their values are typically different. Figure 9.2 is a schematization of the variability of the height of the channels, emphasizing that each channel is attributed a random variable (IID). This may seem trivial, but is actually at the core of the problem: first, it is especially under such circumstances that the flow uniformity can be severely impacted even with small variations. Second, in all tools tested, no option is available to implement this characteristic, or at least not in a practical way for our context. It was hence necessary to write our own program in MATLAB. Last but not least, this characteristic leads to ***combinatorial explosion***, as discussed. The latter may explain its absence in tools I tested.

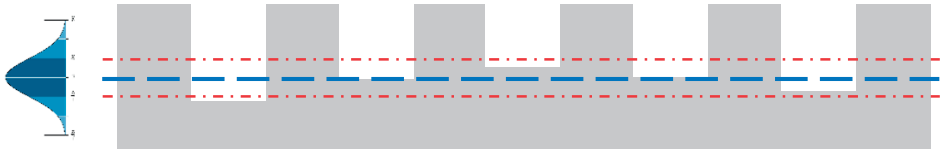

Figure 9.2 Schematization of the variability of the height of the channels, as *independent* and *identically distributed* random variables, following a truncated normal distribution.

The blue dashed line is the mean μ. The red dot-dashed lines is the standard deviation σ to the mean. The distribution is truncated at 3 σ.

We use a truncated distribution for two reasons: It is an easy way to avoid the occurrence of unphysical situations (e.g., negative height) or other unexpected behaviour that the program cannot handle (limit crashes). It may also better model the real-world, where the control of quality should eliminate any part beyond six sigma (when this criterion is used).

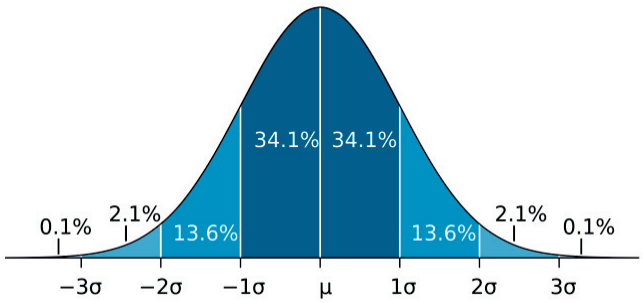

Figure 9.3 Scheme of the normal distribution, showing its properties.
Centred mean = median, symmetric, skewness = 0 ; 6σ covering ca. 99.7 %.

We rely on *Latin hypercube sampling* (LHS) to draw samples. It is however adapted to a truncated normal distribution. The statistics are monitored to check their convergence. The number of samples are adjusted as necessary. It was found that 100 samples already provided a fair estimation in this case.

The following procedure is useful to shorten the optimization under uncertainty: 1) start with a deterministic optimization, 2) use a rough estimation of the statistics (low number of samples), 3) refine the solution with more samples when progressing towards the solution.

9.2.3 Parameters and case studied

Table 9.3 provides the operating conditions, figure 9.4 shows the efficiencies of system components and basic geometry features, and table 9.5 give the thermodynamic and electrochemical properties of materials.

Table 9.3 Operating conditions.

Quantity	Value	Unit
$n^{\mathrm{in}}[\mathrm{O_2}]$	0.21	—
$\widetilde{m}[\mathrm{air}]$	28.89	kg/kmol
p_0	101 325	Pa
T_{stack}	750	°C
λ	7	—
$j_{\mathcal{F}}$	0.3	$\mathrm{A/cm^2}$
u_{f}	Decided by algorithm	—

Non-ideal flow distribution puts a limit on the maximum achievable fuel utilization. Besides, maximization of fuel utilization is wished at low input of fuel flow rate (i.e., low achievable current densities). Otherwise, fuel utilization is not maximized because ohmic and polarization losses are the limiting factors. Therefore, we considered as a basis a low faradaic current $j_{\mathcal{F}}$. The fuel is hydrogen humidified with 3 % of steam (molar).

Table 9.4 Efficiencies of system components and basic geometry features.

Quantity	Value	Unit
$\mathcal{N}_{\text{cells}}$	1	—
A_{active}	32	cm^2
$\varepsilon_{\text{blower}}$	0.4	—
$\varepsilon_{\text{ACDC}}$	0.97	—

Table 9.5 Thermodynamic and electrochemical properties of materials [62,63].

Quantity	Value	Unit
$E_{\text{C}}^{\text{act}}$	$1.533 \cdot 10^5$	J/mol
$E_{\text{C}}^{\text{diss}}$	$1.489 \cdot 10^5$	J/mol
E_{E}	$7.622 \cdot 10^4$	J/mol
h_{E}	$1 \cdot 10^{-6}$	m
$R_{0,\,\text{C}}$	$9.225 \cdot 10^{-14}$	$\Omega\,\text{m}^2$
$k_{0,\,\text{C}}$	$4.103 \cdot 10^{11}$	$1/(\Omega\,\text{m}^2)$
$\sigma_{0,\,\text{E}}$	$1.63 \cdot 10^4$	$1/(\Omega\,\text{m}^2)$
R_{mic1}	$9.872 \cdot 10^{-3}$	Ω
R_{mic2}	$9.872 \cdot 10^{-3}$	Ω

9.2.4 Results

1. Deterministic solution

It is first interesting to look at the trade-off between system efficiency and compactness in figure 9.4. As can be seen, the compactness becomes “incompressible” with a sharp drop of the system efficiency, due in large part to the pressure drop increasing at the fourth power of the inverse of the hydraulic diameter, which is not compensated by a

potential betterment of the flow distribution (which would allow higher fuel utilization).

Since the channels are particularly short (8 cm) in this example, the height of the channels can be very small (retaining a reasonable pressure drop). The deterministic optimization solver hence converges to low values of H to increase the flow uniformity. For this set of solutions, the values of the height of the anodic channels are close to the lower bound imposed: $H_{\mathrm{A}} \in [0.022\,;0.045]$ mm. The height of the cathodic channels are a bit bigger due to a larger influence of pressure drops: $H_{\mathrm{C}} \in [0.09\,;0.39]$ mm. It is obvious that these heights are smaller than the values used in practice. In fact, the heights found for the anodic channels are so small that a designer would probably discard them for un-manufacturability reasons (thereby accounting "naturally" for dimensional tolerances).

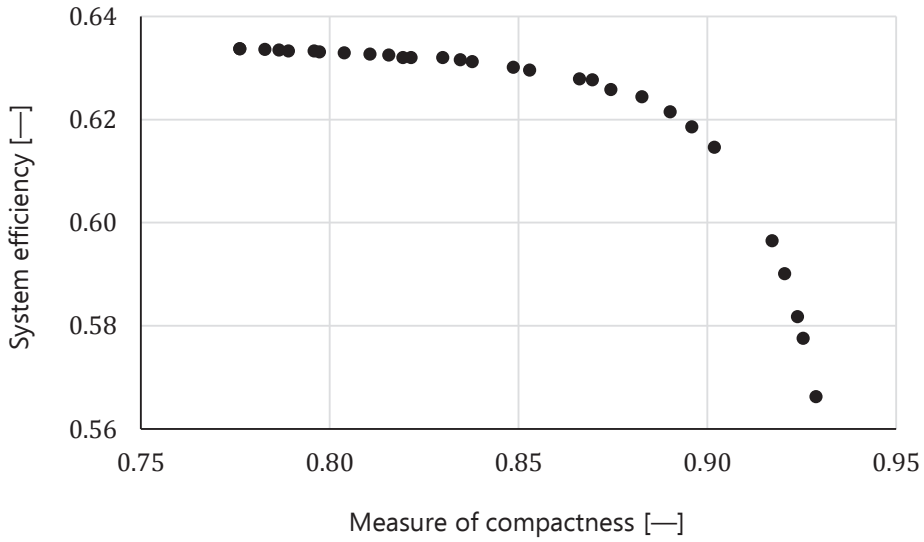

Figure 9.4 Pareto front showing the best couples of system efficiency and compactness (1 = best) found with the genetic algorithm.

The fuel utilization chosen to maximize the system efficiency while satisfying the constraints always lies close to $u_{\mathrm{f}} = 0.97 \pm 0.004$. This particularly high value is only theoretically possible because of the almost perfect flow uniformity obtained thanks to the tiny deterministic heights.

Synthesis for the deterministic solution

The optimal height of the channels is a trade-off between flow uniformity (thereby, achievable fuel utilization) and the penalty that pressure drop imposes on system efficiency. Note however that in this case, flow uniformity is only affected by the nominal, assumed constant, heights of the channels, since they are deterministic. As expected, the solution is more sensitive to the height of cathodic channels than to that of anodic ones (higher penalty due to pressure drop).

2. Stochastic solution

An optimization procedure accounting for the many possibilities corresponding to the trade-off between compactness and system efficiency would have been too long. Instead, we decided to focus on one point: the objective is to maximize the minimum system efficiency, while satisfying the constraints.

As expected, the optimal nominal heights of the channel are much bigger in this case, with $H_{\mathrm{A}}^{\mathbb{N}} \cong 0.44\,\mathrm{mm}$ and $H_{\mathrm{C}}^{\mathbb{N}} \cong 0.85\,\mathrm{mm}$. The compactness indicator therefore fall down to 0.54. According to figure 9.4, the corresponding system efficiency would be at least $\varepsilon_{\mathrm{sys}} = 0.63$ under the deterministic assumption. In the stochastic case, it is "only" $\varepsilon_{\mathrm{sys}} \cong 0.58$, which is by the way a more realistic value. Also, the reachable fuel utilization is lower with $u_{\mathrm{f}} \cong 0.95$. It however remains high. Furthermore, using the design of the deterministic solution in reality would certainly not allow to reach as high a value without risking severe degradation. This will be shown below.

Synthesis for the stochastic solution

The maximum efficiency is limited by the fuel utilization that is judged permissible without risking to severely degrade or even break the fuel cell, rather than by the penalty on efficiency induced by increasing the pressure drop. Actually, the resulting pressure drop (of the stochastic optimal solution) is smaller than it is for the deterministic optimum, since higher heights are requested to compensate for the dimensional tolerances. It is however important to note that, even without consideration of compactness, heights of the channels are limited for a given size of the manifolds[3]. Otherwise, a bad flow distribution is obtained regardless of the stochastic aspect.

[3] Indeed, the upper bounds imposed to the heights were not reached (constraint not activated).

1. Non-robustness of the deterministic solution

In reality, the solution (design) provided by the deterministic optimization is also subject to uncertainty. We therefore performed a post-quantification of the uncertainty from such a solution. For comparison reason, we chose a point on the Pareto curve with the same efficiency than obtained with the stochastic solution: so, $H_{\mathrm{A}}^{\mathbb{N}} = 0.022$, $H_{\mathrm{C}}^{\mathbb{N}} = 0.102$, and $u_{\mathrm{f}} \cong 0.973$, which gave $\varepsilon_{\mathrm{sys}} \cong 0.58$ and a compactness $= 0.92$ under the deterministic assumption.

When propagating the uncertainties without changing the fuel utilization, two constraints regarding degradation are violated to a large margin: $\zeta_{\mathrm{LZO,SZO}} = 2.38$ and $\zeta_{\mathrm{NiO|H_2O}} = 1350$. Furthermore, the index of flow uniformity is extremely low: $\gamma = 0.14$. This explains the activation of degradation. So, to keep a safe operating condition with this design, the actual fuel utilization must be lowered to around $u_{\mathrm{f}} \approx 0.1$, obviously lowering the reachable electrical efficiency. Interestingly, in this situation, the system efficiency actually becomes negative, meaning that electrical power must be supplied to the compressor to compensate for the pressure drops, since the power produced by the fuel cell is not enough anymore.

2. Further comparison between deterministic and stochastic cases

In the light of the results above, we think that it is interesting and easier to illustrate a situation from an angle where the deterministic solution is obtained with less aggressively low bounds on the height of the channels. One can see it as a case where an experienced designer chose bounds he believes are more reasonable. So we reuse here results from previous optimization runs.

The results in figure 9.5 show that, at the optima, the deterministic efficiency is higher than the average from the stochastic result, and compactness is better, too. However, when doing a post-quantification of uncertainty for the deterministic optimal solution, the efficiency is now lower, because it is limited by the fuel utilization achievable without risking to severely degrade or even break the fuel cell. Therefore, under such manufacturing variability — which is obviously identical, since it represents one reality — the trade-off is the following: is it worth sacrificing e.g. 10 % of *actual* efficiency to have a fuel cell e.g. 10 % more compact? The answer to this question depends on the particular industrial scenario (marketing strategy, resulting total cost of ownership, etc.). Note that this trade-off also has implications in terms of lifetime, since the rate of degradation and risks increase when reaching higher fuel utilization with respect to the nominally "safe" determined one (which is not an on/off limit).

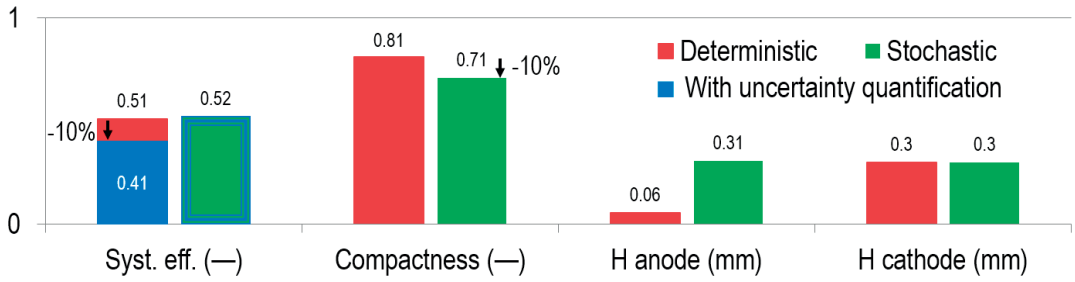

Figure 9.5 Synthetic comparison of deterministic and stochastic solutions.

9.2.5 Perspective for improvements

Some possible ways of improvements are:

- Apply RDO to a more detailed model and complex geometry;
- Study the optimization of the topology: use discrete Boolean decision variables or a scenario-based approach.
- Study epistemic and model-related uncertainties more closely;
- Use discrete decision variables may be useful for manufacturability.

9.3 Study of the effect of constrictions

9.3.1 Introduction

The following study was inspired by a technique used to stabilize and homogenize the flow field in heat sinks involving biphasic flows (e.g. at the laboratory of Prof. John Thome, LTCM at EPFL). The principle is to implement ***constrictions*** at the inlet of the channels [89,90]. The idea is depicted in figure 9.6.

Its effectiveness was demonstrated in the context of boiling flows, where the resulting quick expansion of volume is likely to happen asynchronously in channels. The consequence is instability of the flow (oscillations): bubbles of gases tend to flow back upstream towards the manifold or plenum (i.e., where resistance is lower). With the constrictions, a large resistance is created upstream of the boiling flow, preventing backflow.

Moreover, the large singular pressure drop that they create help to distribute uniformly even single-phase flows, as discussed before. Therefore, constrictions could be

useful in fuel cells, too. In the case of PEFC, they should probably be implemented at the outlet of the channels since the water vapour is condensing: we want to prevent backflows into the channels from the *outlet* manifold. Last but not least, the case of fuel cells is particular: in addition to possible changes of phase, a net sink (or source) of mass or mole exist depending on the type of fuel cells.

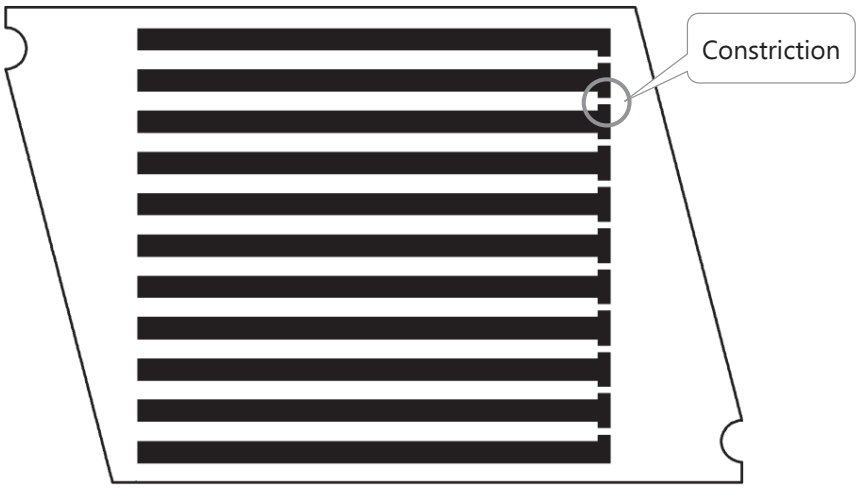

Figure 9.6 Scheme of a FDP implementing constrictions at one extremity of the channels.

As already discussed, in a deterministic framework, the uniformity of the flow distribution in the active zone typically increases along with the ratio of the resistance to flow in this zone over that in the manifolds. The resistance is lower with larger cross-sections. However, too big manifolds are not desirable, because the size (and the cost) of the product must be kept reasonable. Conversely, too narrow internal geometries are not desirable in the active zones, for at least three reasons:

- The global pressure drop should be kept as low as possible, to increase the efficiency at the level of the system (i.e., to reduce the energy that the compressor or the fan must supply).
- The geometry should be relatively cheap to manufacture. For given dimensional tolerances, smaller details typically increase the manufacturing cost[4].
- The negative effect of dimensional tolerances on flow uniformity increases rapidly with the reduction of the cross-section.

[4] Even when the manufacturing process is not based on the removal of material by machining.

The idea to implement constrictions then arises from the following observations: the resistance increases linearly with the length of a (long) channel, whereas it increases with about the fourth power of the inverse of the hydraulic diameter. Therefore, it is possible to obtain an adequate resistance by combining a long and relatively wide channel with a shorter and narrower channel. Besides, when a flow passes through a constriction, a singular pressure drop is created (energy is lost during the irreversible contraction/expansion phenomenon).

Such constrictions could be useful under the following scenario (assumptions):

(1) Manufacturing costs are lower for wider (long) channels with *looser tolerances* (because tolerances on wider channels can be slightly loosened without reducing flow uniformity);

(2) It is manageable, and cost-effective, to manufacture accurate constrictions (i.e., narrower channels with tighter tolerances, but short);

(3) The quality control is cheaper when only a local item is checked (higher quality required on a small part rather than lower quality required on a large part).

The questions studied below are then:

(1) How tight the tolerances on the constrictions can be? (What restrictions?)

(2) Is there an optimal size (width, height, length) of the restrictions?

(3) How loose the tolerances on the long channels can be? (What gain?)

Indeed, constrictions have a positive effect on the flow uniformity under a deterministic assumption. But what happens when accounting for stochastic processes, e.g., dimensional tolerances?

9.3.2 Example of application

This study involved five main steps:

(1) Creation of a parameterized 3D geometry of a Z-type design;

(2) Computation of the solution for a baseline design;

(3) Deterministic optimization (flow uniformity ; width of constrictions);

(4) Uncertainty quantification of the deterministic optimum to assess the sensitivity of flow uniformity to the dimensional tolerances (Six Sigma Analysis).

(5) Based on the results, look for an optimal trade-off.

We used ANSYS FLUENT as a flow solver and a mix of MATLAB and ANSYS DESIGNXPLORER for the analyses.

9.3.3 Deterministic solution

Results show that the flow uniformity, under a deterministic assumption, would increase monotonically with narrower constrictions. In that case, the only constraints would be 1) the also monotonically increasing pressure drop, and 2) the manufacturability of such small width. This last point raises the question: "what accuracy is implied under the notion of *manufacturability*?" It naturally questions the deterministic assumption; in other words, what happens when accounting for stochasticity?

9.3.4 Stochastic solution

As in § 9.2, we use a truncated normal distribution, with a standard deviation $\sigma = 10$ µm on the dimensions.

When considering stochastic processes, results show that the flow uniformity does not increase monotonically with the reduction of the constriction's width. It increases and then decreases after some maximum. The increase of pressure drop may be limiting before reaching this optimum, depending on the particular fuel cell, so that the optimum width to the global problem may be larger than the value at which flow uniformity is maximum.

Remark: The sum of independent normally distributed random variables is again a normally distributed random variable, with the following properties:

$$X \sim \mathcal{N}[\mu_X, \sigma_X]\,; \qquad Y \sim \mathcal{N}[\mu_Y, \sigma_Y]\,; \qquad Z = X + Y\,; \qquad Z \sim \mathcal{N}[\mu_X + \mu_Y, \sigma_{X+Y}]$$

$$\sigma_{X+Y} = \sqrt{{\sigma_X}^2 + {\sigma_Y}^2 + 2\,\varrho_l\,\sigma_X\,\sigma_X} \tag{9.13}$$

where ϱ_l is the coefficient of (linear) correlation. The covariance matrix is used when there is more than two variables.

Equation (9.13) shows interesting properties. When the random variables are *uncorrelated*, the total variance equals the sum of the variances. Also, the resulting variance is smaller than the sum of the variances when $\varrho_l < 0$. It shows a way to reduce the variance: make the variables negatively correlated.

9.3.5 Summary about constrictions

Under deterministic conditions, constrictions increase flow uniformity. When accounting for variability of their dimensions, we observe that they may actually decrease flow uniformity. The point where the tendency inverses depends on the specific case: topology, dimensions, and tolerances of the whole design, as well as flow conditions. However, for a given case, the optimal flow uniformity corresponds to a finite size of the constrictions.

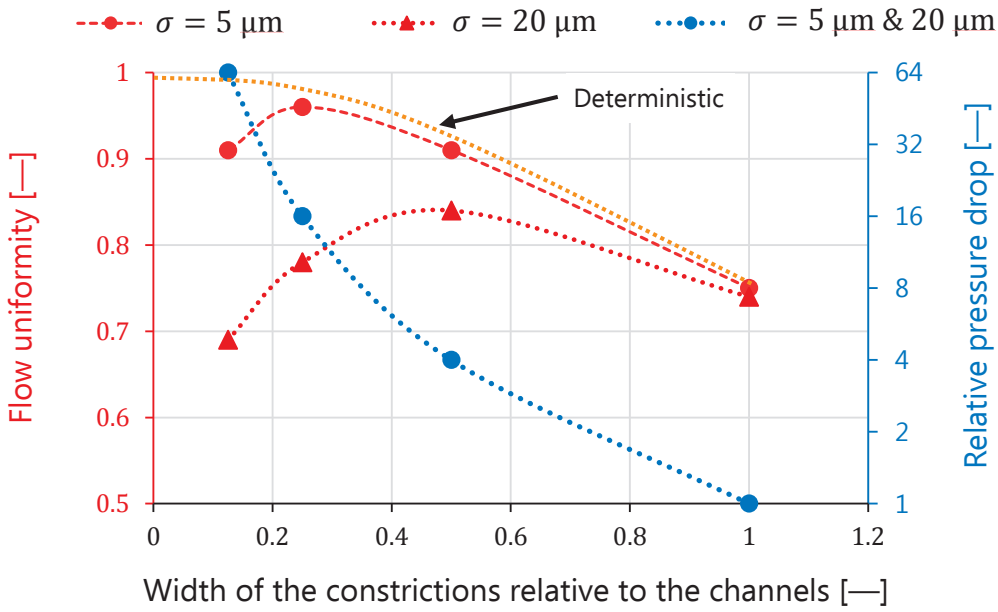

Figure 9.7 Flow uniformity and pressure drop in function of the width of the constrictions, with absolute tolerance in parameter.

It emphasizes that pressure drop may become excessive before the optimal uniformity is reached.

Note that the pressure drop due to constrictions may become excessive before reaching that optimum, especially if tolerances are tight. In summary, constrictions is a good solution if certain conditions are met (scenario in § 9.3.1).

Usually, the guideline to get uniform distribution is to design big manifolds with respect to channels. However, when tolerances on narrow channels are loose, to a certain point, enlarging manifolds becomes useless: having a perfect distribution under a deterministic assumption is not a guarantee to get a good distribution when accounting for variabilities.

« La confiance est souvent une des formes
de la paresse, car ajouter foi donne
moins de peine que de contrôler. »
Alfred Capus
Les Pensées

CHAPTER 10

Conclusions

10.1 Overview

All along these years of research, we have had the opportunity to witness in many respects how big a role uncertainties play. The focus of our study was on dimensional tolerances. It was a first occasion to test and show the usefulness of uncertainty quantification in the context of fuel cells, and to apply robust design optimization. However, from the beginning, we believed that it could be applied more generally for the development of robust fuel cell products. Meanwhile, other people get convinced, too. The involvement of SOLIDpower and EPFL (FUELMAT) in the PROSOFC[1] European project [91] is certainly not a coincidence, and I am glad to see that fuel cell companies and research groups will continue to use UQ, OUU and similar tools with hopefully great successes.

10.2 Methodological aspects

10.2.1 Quantification of the uncertainty

1. Inputs

The characterization of the uncertainties proved to be challenging (get knowledge about the unknown). A sufficient number of samples were available to characterize with a good precision the statistical distribution of the dimensions of the channels of a used SOFC stack. However, according to us, the samples were not of sufficient quality to get accurate estimates. Unfortunately, the equipment available did not allow a better

[1] Production and reliability oriented SOFC cell and stack design.

quality when preparing these samples. A large diamond saw and an automated professional polishing machine should provide for more reliable statistics in the future.

Despite this issue, some valuable information could nonetheless be extracted. For instance, the macroscopic bended and slanted shape of the elements in the stack was highlighted and quantified. Also, we could reasonably conclude that the dimensions of the channels are normally distributed, rather than significantly skewed, for instance. We therefore took the decision to keep on with this assumption, and to consider a range of possible manufacturing tolerances to generalize the approach.

2. Outputs

Similarly, no direct experimental measurement procedure was identified as able to provide accurate enough quantification of the flow distribution in the micro-channels in a stochastic framework (for validation).

Nevertheless, we unexpectedly discovered an interesting way to relate the variability and the flow distribution in the channels. It consisted in measuring the length of fine layers of pollutants which have reacted at the bottom of the channels and to compare that distribution with the profile of the channels measured with a laser in various conditions (stamped, sintered, post-operation). The correlation between the profiles was significant. The method has several limits, though: a) it is intrusive, since the stack must be disassembled; b) it is indirect, since the pollutants may not accurately represent "tracers" of the flow rate. The advantage of the method is its simplicity and the potential for automation (laser and image recognition), which is crucial to collect many samples.

10.2.2 Tractability and accuracy

1. Modelling physics

We have shown that reduced-order modelling such as 2D CFD does not seem a practical approach to carry out an optimization of the design (under uncertainty) spanning a large number of geometrical variables. Depending on the implementation, it is either intractable, or inaccurate.

Using 1D porous-jump is very effective to reduce the computational time of long channels. As a downside, the electrochemistry and heat transfer cannot then be solved simultaneously, hindering an accurate local prediction.

2. Modelling uncertainties

Under laminar conditions and for parallel channels, it is more efficient and as accurate to model dimensional variability by averaging it over the length of the channel.

3. Uncertainty quantification

Bootstrapping is helpful to reduce the number of samples drawn by providing a better estimate of the MSE, online, which can be used as a stopping criteria. This information can be used to avoid naively choosing an arbitrarily large number of samples. Sampling with LHS proved to be efficient. However, using control variates is also a smart way to reduce the number of samples drawn, for a given accuracy. It is particularly useful in a context where the response is smooth over an interval of the random variables, and non-smooth elsewhere.

4. Optimization

Despite many trials, we observed that gradient-based solvers usually fail to converge to a reasonable optimum when uncertainty quantification is active (OUU). It suggests that the response is not smooth enough, with lots of small "waves" and as many random local optima, also preventing the solver to get an accurate estimation of the gradients. *Patternsearch* was more successful thanks to its derivative free solver. Probably due to its deterministic iterates, it was also faster than the multi-objective genetic algorithm (stochastic iterates). However, it is troublesome to carry out a multi-objective optimization with a mono-objective solver. Weighing the objectives basically "drowns" useful information. Otherwise, Pareto fronts can also be constructed "manually" by considering one objective at a time, but such an approach is less convenient.

Compared to a "random" initialization, it was usually efficient to use a gradient-based solver such as *fmincon* to first find a deterministic optimum, then used as a starting point for the optimization under uncertainty (using then a derivative free solver). However, we realized that the deterministic optimal values were sometimes far from the robust ones, and our intuition could often provide for initial points closer to the solution.

10.2.3 Applicability to industrial context

The current model used to solve the robust optimization problem is fast enough to give relatively quick answers in an industrial context. However, the model is probably not complete enough yet to provide optimal points which can be used confidently. For

instance, the geometry considered for our OUU is simple in comparison to industrial cases. It is therefore more prudent to use it as an insight and guidelines giving tool.

The issue is that a more complete problem would require too much time to provide for a solution in a fast-paced industry. Conversely, methods for uncertainty quantification which are more efficient, but intrusive and sophisticated, do not seem ready yet to be used as a standard/common practice in an industrial context (and vice-versa).

A middle-ground should be looked for. Maybe OPTISLANG offers such a compromise. (Unfortunately, I have not yet had the chance to test this software.)

10.3 General technical outcomes

Guidelines for robust design are suggested in § 10.3.5. We expose here some general observations.

10.3.1 Interaction between manifolds and active zone

It is known that large manifolds with respect to the flow path in the active zone is beneficial. However, when accounting for tolerances, we observe that big manifolds — while not using space efficiently — is not either a sufficient condition. Indeed, if the tolerance is too large with respect to the smallest cross-section in the active zone, the real flow distribution will be severely impacted, irrespective of a perfect distribution in a deterministic case.

Conversely, it is useless to target a near-zero tolerance if the manifolds are not designed appropriately, since they provide the "baseline" flow distribution.

10.3.2 Implementation of constrictions

As already shown by other authors, we indeed observe that constrictions in parallel channels are effective to improve the flow uniformity, even with single phase flows. However, when accounting for uncertainties, we observe that flow uniformity degrades again when the constrictions become too thin with respect to its tolerance. A maximum can therefore be found. Of course, depending on the design, it is also probable that the extra pressure drop caused by the constrictions becomes limiting for the system efficiency (compressor) before actually reaching that maximum.

Alternatively, designers could take advantage of the extra pressure drops to increase the cross-section of the channels, thereby keeping a reasonable pressure drop, and decreasing the sensitivity of the channels to tolerances (or allow less tight tolerances). Yet, this is not necessarily feasible in practice. Indeed, compared to the singular pressure drop created by the constriction, the necessary increase of the cross-section may be so big that the limiting factor becomes ohmic losses or diffusion losses (or both).

In conclusion, whether constrictions are beneficial is design specific. When it is a good option, it is worth looking for a robust optimum.

10.3.3 Redundancy – alternative pathways

Like for transportation networks, it is helpful to provide alternative pathways in case a blockage occurs (a channel is obstructed, or smaller than designed). Regarding fuel cells, such solutions were implemented by many companies and research groups. It typically consists in a pattern of interrupted channels, or staggered ribs, or honeycomb pins, etc. The difficulty is to produce these patterns in a reproducible and cost-effective way. The tolerances that can be achieved when manufacturing such patterns are often poor (e.g., by stamping or 3D printing). Moreover, the shape and position of such small bits of interconnect are highly subject to variability and to heterogeneous compression (crushing). Lastly, while intersections upstream and downstream of an obstruction help to redistribute the flow, it cannot correct for a region fully obstructed (e.g., one interrupted channel narrower along its full length compared to others).

Redundancy is nevertheless a desirable feature to help homogenize the flow, so that investigation should continue.

10.3.4 Inertial effects

We observed that inertial effects, such as jets, are particularly unfavourable to a homogeneous distribution of the flow. Jets upstream of several inlets of channels are especially problematic and should be avoided by enlarging parts of the distributor provoking such jets. Besides, such a measure is beneficial in many ways: a) it reduces the pressure drops in the distributor, b) thereby distributes the flow more homogeneously, c) lowers the overall pressure drop, and last but not least, d) reduces the sensitivity of that area to tolerances. A word of caution, though: enlarging such a zone too much may cause in turn sensitivity problems in case the “ceiling” of the cavity is not rigid enough and risk to make the height vary (e.g., GDL or membrane of a PEFC).

10.3.5 Summary of guidelines to design robust FDP

Some of the following guidelines may already be known, especially by engineers who design FDP. We write all of them nonetheless, to give a reference as exhaustive as possible.

(1) Make sure that the ratio of flow resistance is large between the manifolds and the lower-level branches of the distributors. A rule of thumb is a ratio of at least 10. Similarly, isobars should usually be as perpendicular as possible to the main flow direction.

(2) Make sure that the variability of the cross-sections to flow is small relatively to their nominal dimensions. Either by acting on the variability, or by acting on the nominal dimensions.

(3) Favour a design with "redundancy", i.e., with alternative paths allowing flow to change of main paths. This should however not compromise the achievement of a repeatable, high-quality manufacture (low enough variability).

(4) Avoid the formation of a jet upstream of a flow division, i.e., minimize the bulk velocity at the inlet of flow divisions. This point relates to (1).

(5) A good compromise must be found for the width of the channels and for their spacing. Generally speaking, the spacing should be as thin as manufacture and mechanical strength allow[2], to minimize diffusion losses. Channels should be narrow as well, to minimize ohmic losses and to take part in getting a resistance to flow adequate for point (1); however, channels should be kept large enough to:

   (a) keep a low relative variability;

   (b) avoid higher resistance to flow than is beneficial (lower system efficiency not compensated by the gain on the flow distribution, or worse: flow distribution deteriorates due to variability);

(6) The smallest dimension of a cross-section is the limiting one for the flow resistance *and thereby* also the most susceptible to be problematic regarding its variability.

   (a) It is the first dimension which a designer should increase when no other factors dictate otherwise.

[2] In principle, too thin ribs acting as electrical connectors increase the ohmic losses. However, in our experience, manufacturability, cost, and strength, are problematic before such a limit is reached.

(b) The height of flow paths in fuel cells is generally subject to a greater variability than other dimensions (of paths), because it is determined by the assembly with the GDL, or contacting layer, and the cell (i.e., different materials, flexibility, etc.). Besides, this height also depends on the force applied to the stack and on the resulting distribution of the contacting pressure. Last but not least, it is also often smaller than the width for various reasons (compactness of stacks, cost of material, diffusion of species along gradients of concentration formed vertically, …). Hence, the height often has the largest relative variability, making it a key factor.

(7) The flow paths lateral to the cell are often critical; they are closest to sealing material, are subject to less supply because of the boundary-layer forming in the manifolds and sometimes also because of configuration of the latter. Moreover, they are also closest to the external environment; they are therefore subject to heterogeneous fields "coming" from the boundary conditions.

(8) *End-of-pipe actions to correct for bad flow distribution should be avoided as much as possible*. In particular:

(a) Tiny, punctual solid parts should be avoided. They increase pressure drops and are often subject to high relative variability, making the design less robust, while also more complex and potentially more costly to manufacture.

(9) A large aspect-ratio (length/width) of the active zone helps to get a uniform flow distribution for a given size of the manifolds, because the length of the manifolds (i.e., width of the cell) is reduced in comparison to the length of the channels (cell). From the viewpoint of compactness, this makes the design of manifolds more "efficient". Besides, this also helps to get an adequate ratio of resistances to flow, without needing extremely narrow channels (more sensitive to variability)

(10) In accordance with point (9), it is beneficial to supply and evacuate fluid from *each* "lateral" side of the active zone ("H" configuration) when inlet or outlet cannot directly face the width of the cell. Indeed, this is equivalent to virtually split the flow rate into two "C" configurations, each having an effective aspect-ratio twice as big as the real one.

(a) For identical dimensions, the configurations which enable the best flow distribution are usually in order: I > T > H > Z > L > C.

(11) Some geometrical elements, such as "tabs", should be implemented to guaranty the best alignment of parts as possible.

(12) Make sure that the cavities where the fluid flows are kept free from any other material. In particular, grooves are advised to contain the sealing material, especially if it is subject to spread.

(13) Although a fuel cell stack may be seen as essentially a pile of quasi bidimensional elements, designers should not forget that their "playground" are composed of three dimensions, even when leeway is narrow in one or another.

(14) Since the main manifolds are most often directly formed by stacking the elements, their internal surface is potentially extremely rough. This should be taken into account because it dictates the flow regime into them.

(15) From a modelling point of view, designers should be extremely careful when considering usage of 2D simulations. They can provide accurate enough results when tailored to a specific design (with 3D or experimental information), but hide lots of pitfalls when trying to generalize their application to explore different designs.

10.4 Limitations and perspectives

Although general conceptually, the scope of our research was narrowed down to make it tractable. The main limitations are then in the investigated cases (variables, geometries) and in the level of detail and physical phenomena captured by the models. However, it should be noted that these improvements would be demanding in terms of computing resources, despite the efforts to find solutions for a better ratio "tractability over accuracy".

The recommended future directions of research are the following. Some of them are in line with the topics that the project PROSOFC will address.

Methodology

- In an academic context, use existing implementation of algorithms which build and validate a reduced model (meta-model) out of an original detailed model prior to the optimization, allowing minimal update calls to the original detailed model during optimization (e.g., see [92]).

- Investigate usability of OPTISLANG software, especially when interfacing other codes with ANSYS creates lots of overhead development. Consider using DAKOTA if the number of proprietary licences is a bottleneck.
- Concerning projects joining academic research and industry, it seems crucial to have a tighter collaboration to exchange necessary information.[3] Notably, to better characterize the uncertain inputs, and reduce ambiguities and vagueness.
  - The manufacturer is in better position to provide the statistical data extracted from many manufactured parts and products. To use a systematic, well documented, and traceable approach is crucial, but not trivial.
- Take advantage of increasing parallel capabilities and HPC resources. Monitor the advancement in the fields of computing with general purpose GPU. In principle, it should be particularly efficient to solve combinatorial problems.

Technology

- UQ and OUU should be applied to the design of cells (material) and investigations should be conducted about the thermo-mechanics. From a fluidic point of view, a special interest would be the interactions between the fluid distribution pattern and the top surfaces. It would be useful to model the variability (e.g., due to creep, GDL crushing, etc.) in a predictive manner rather than a descriptive one.
- Investigate in more detail the role of (forced) turbulent regime: its effect on the sensitivity to geometric variability on flow uniformity.
- Pursue investigations about the statistical (in)dependence of the uncertain input variables. In particular, look at the effect of positively and negatively correlated variables, notably at the level of the stack. Depending on the results, look for particular manufacturing and assembly procedures which may reduce the sensitivity thanks to such a property (well-chosen dependence).

[3] To achieve a successful "campaign" using UQ and OUU, I believe it is crucial that the company trusts the usefulness of such approach, has a desire to involve itself in the process, and allocates resources to it. Academic research cannot effectively solve these problems for industry if this condition is not met.

10.5 Original contributions

The main original contributions of this research is the application, for the first time to our best knowledge, of an optimization under uncertainty of the (geometric) design of the fluid distribution pattern of fuel cell stacks. The OUU for the constrictions in flow channels may also be a first-of-a-kind.

Although CFD software companies have now implemented tools to apply and manage such kind of procedures, *at the level of the geometry and mesh*, such features were inexistent when we started our research, or at least not in a convincing way regarding ANSYS for instance — in terms of reliability, reproducibility, speed, etc. (these issues did not completely disappear). When in September 2014 I attended the Lecture Series of the Von Kármán Institute on UQ in CFD, developers at NUMECA (3rd CFD company) were still finalizing their implementation and presented their progress about automatic (hexa) mesh adaptation in the context of OUU [93].

10.6 Direct improvement and transfer to the industry

Part of the efforts in this research were focused on finding ways to solve the many challenges faced for performing an OUU of the design of fuel cells. So, we needed simple cases to develop and test our ideas, models and codes. Nevertheless, with simulations and general knowledge acquired during our investigations, we managed to provide direct improvements and inputs for the industrial designs of our partners.

The flow uniformity in the bipolar plates of a PEFC stack was improved by ca. 200 %. The flow uniformity of the distribution pattern of a predecessor SOFC design was improved by ca. 100 %. In both cases, we strived to improve the flow distribution with robustness in mind. For instance, “end-of-pipe” measures were eliminated and we took advantage of as much of the space available (restricted by external constraints) to enlarge flow paths in distributor zones.

Last but not least, a new SOFC design took birth, partly thanks to the insights provided by our studies of dimensional tolerances (notably [82]) and by numerous simulations and incremental improvements of a new concept. The qualities of this design are highlighted by a research paper, which can be found in Appendix A: *High-performance SOFC stacks tested under different reformate compositions*. To our best knowledge, a world-record may have been broken with this concept (see text), and it is still giving regular pleasant “surprise”.

10.7 Afterword

Certainly, my interest in uncertainties and my decision to study them in a thesis did not happen by chance. Like many people, and despite being very curious, I naturally tend to avoid uncertainties and "the unknown"; because as Rory Sutherland said: *"We don't like uncertainty."* [1] (see Foreword). The fact that I involved myself in such a thesis may then look paradoxical. A wish to better understand how to get control over uncertainties, or get rid of them, is probably part of the explanation.

Yet, I made an interesting discovery when growing with this thesis: to accept uncertainties, to get to learn them, to be able to better "play" with them, *is often more productive* than to forcibly reduce potentially irreducible uncertainties at all cost, without looking more "pacific" means. According to Abraham Lincoln, *"the best way to destroy an enemy is to make him a friend."* This advice certainly applies to uncertainties, too. I cannot say (yet) that uncertainties became my buddies… But I happen to present them or speak about them to my acquaintances. So now I'm confused: I certainly don't like uncertainties, but I surely got fond of them!

Appendix A

Outcome from industrial stack tests

This appendix serves to give better insights about the improvements which were made on the *lifetime*[1], the *performance*, and the *cost*[2] of fuel cell stacks, by applying some of the methods and recommendations described in this document. As we discussed in early chapters, to our knowledge, no direct and effective means exists to validate without doubt the influence of decisions for robust design on the flow distribution, in a stochastic framework. However, we believe that the following material is a fair proof that "it actually works".

This material is from a paper published as co-author at the European Fuel Cell Forum in Lucerne, 2014; the lead author is Zacharie Wuillemin [7].

Credits for the text and images are essentially due to Zacharie Wuillemin. Many thanks Zacharie! Any mistake in the reproduction is mine. Some adaptations were made for consistency with the rest of the document.

A.1 High-performance SOFC stacks tested under different reformate compositions

Abstract

In the past years, HTceramix SA – SOFCpower has developed with its partners an innovative stack design, optimized for high electrical efficiencies and low manufacturing costs. Using CFD models coupled with an optimization algorithm based on Monte-

[1] High fuel utilization stress-test, durability test, and thermal cycling allowed to assess the improvements of the lifetime.

[2] We apologize that we cannot disclose actual number. As stated in the article, our partner could reduce production cost by using a design robust to dimensional uncertainties. Also, since more products pass the controls of quality, the yield is increased, reducing the effective manufacturing cost.

Carlo simulations, the quality of different fuel distribution patterns was tested ab initio, allowing developing a design having an excellent distribution of gases, compatible with the manufacturing tolerances of low-cost, mass-production fabrication methods.

Testing short stacks, electrical efficiencies as high as 74 % (LHV) have been demonstrated using steam-reformed methane as fuel, while converting more than 90 % of the fuel in a single-pass. With hydrogen, efficiencies slightly above 60 % (LHV) have been attained at 94 % of fuel utilization, almost reaching the theoretical maximum efficiency for single-pass flows. Not only short stacks, but also complete units have been shown to operate at over 90 % of fuel utilization for an electrical power of 1 kW, hence proving the quality of the internal gas distribution and the validity of the concept.

In this paper, performance maps are presented for this new family of stacks, for different fuels, reformate compositions, and pre-reforming ratios.

Introduction

Since 2007, SOFCpower develops and manufactures SOFC-based stacks and (co)- generators based on its proprietary Gen-II anode supported cells. The company includes in its product portfolio 1 and 2.5 kW electric micro-CHP appliances designed for the residential and commercial market and is capable of providing also stack modules of different sizes for other applications, including High Temperature Electrolysers, off-grid generators and biogas/syngas fuelled systems. To cover this wide range of potential products having each different constraints, the stack has to offer excellent characteristics in terms of electrical efficiency and reliability of operation, as well as in terms of cost.

As it is strongly dependent on the homogeneity of the fuel distribution in the stack, a high electrical efficiency is most often synonym of severe production tolerances for the fuel distribution channels, and therefore of high manufacturing costs. Unless a way can be found to reduce the tolerance requirements, but without compromise on the quality of the fuel distribution.

Using a Design for Manufacturing (DFM) approach and with the help of advanced modelling tools, HTceramix SA – SOFCpower has developed a completely new stack concept that demonstrates today higher performance and reliability, as well as the potential for a drastic reduction of production costs.

In early 2013 the stack has been transferred to the pilot production and has been integrated in the EnGen-2500™ cogenerators to be installed in field tests.

Stack design

The stack is based on metallic cassettes including a proprietary fuel distribution structure enabling a very homogenous distribution of fuel inside and among the repeat elements, and therefore reliable operation of the stack at high fuel utilization (FU). This structure was optimized by modelling the effect of random geometric deformations — corresponding to typical fabrication tolerances — on the flow distribution [82]. The cassettes are made of coated, low-cost ferritic alloy shaped by standard sheet metal forming processes.

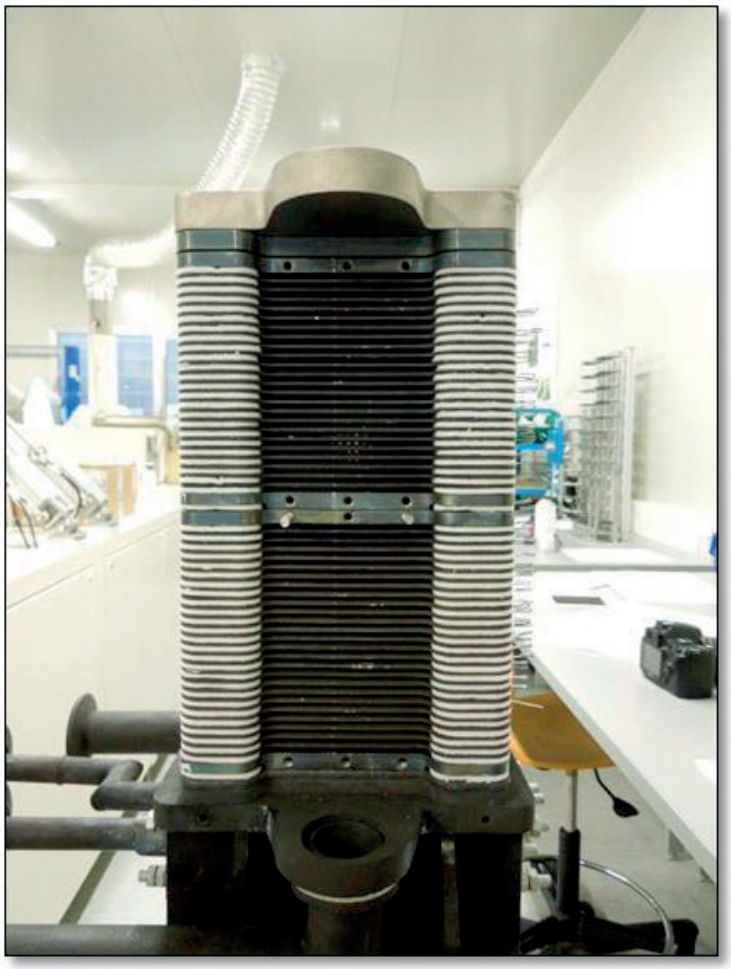

Figure A.1 Stack of 50 elements. (Courtesy of Z. Wuillemin.)

The number of repeat elements can be varied from 50 to 70 depending on the final application. Two stack platforms have been developed, one with an active area of 48 cm^2 in replacement of previous products, and a new one with an increased active area of

80 cm^2 that serves as basis for the new products. Standard Ni/YSZ anode-supported cells are used, on which a barrier layer and a LSCF composite cathode are deposited and sintered.

Stack performance

Hydrogen fuel

A typical performance map for a stack of 6 elements is shown in Figure A.2. The map synthesizes the experimental results obtained in a series of IV curves performed at different fuel flow rates, for constant thermal boundary conditions.

Operated with a mixture of 60 % H_2 and 40 % N_2 to simulate CPOX conditions, the stack is able to convert more than 90 % of the fuel in a wide range of fuel flow rates. With a stack outlet temperature fixed at 800 °C, the maximum electrical efficiency achieved in such conditions is slightly above 60 % (LHV) for a power density of 0.17 W/cm^2 and a fuel utilization of 94 %. The specific fuel flow rate for such conditions is 1.5 $SMLPM/cm^2$ (standard millilitre per minute and per cm^2).

At a nominal power density of 0.32 W/cm^2, the maximum achievable electrical efficiency is 55 % using hydrogen as fuel (LHV), 51 % for a fuel utilization of 80 % that corresponds to the nominal case for SOFCpower's micro-CHP applications.

Comparable results are obtained on full-scale stacks, with in particular the capability to operate at high fuel utilization, as depicted in Figure A.2. The marks (★) represent points tested with stacks having between 48 and 66 elements. The large stacks are tested with 360 l/min of air and the same mixture as above (60 % H_2 and 40 % N_2), in a furnace heated at 750 °C. The air outlet temperature is fixed at 800 °C. At 1.8 $SMLPM/cm^2$ of H_2 and 92 % FU, the tested stack achieved a power density of 0.19 W/cm^2 and an electrical efficiency of 58 %. At 2.6 $SMLPM/cm^2$ and 90 % FU, it was 0.26 W/cm^2 for 56 % efficiency. Finally, at 3.6 $SMLPM/cm^2$ of H_2 and 87 % FU, an efficiency of 53 % was reached at 0.34 W/cm^2. A corresponding typical IV curve is shown in Figure A.3, obtained on a stack of 66 elements. At 87 % of fuel utilization, the potentials remain well grouped. The onset of the potential inflexion at high fuel utilization is homogenous among the 66 elements, indicating the absence of any significant deviation of fuel supply.

For the three different cases mentioned here, the efficiencies and power densities are the same as in short stack configuration (see Figure A.2).

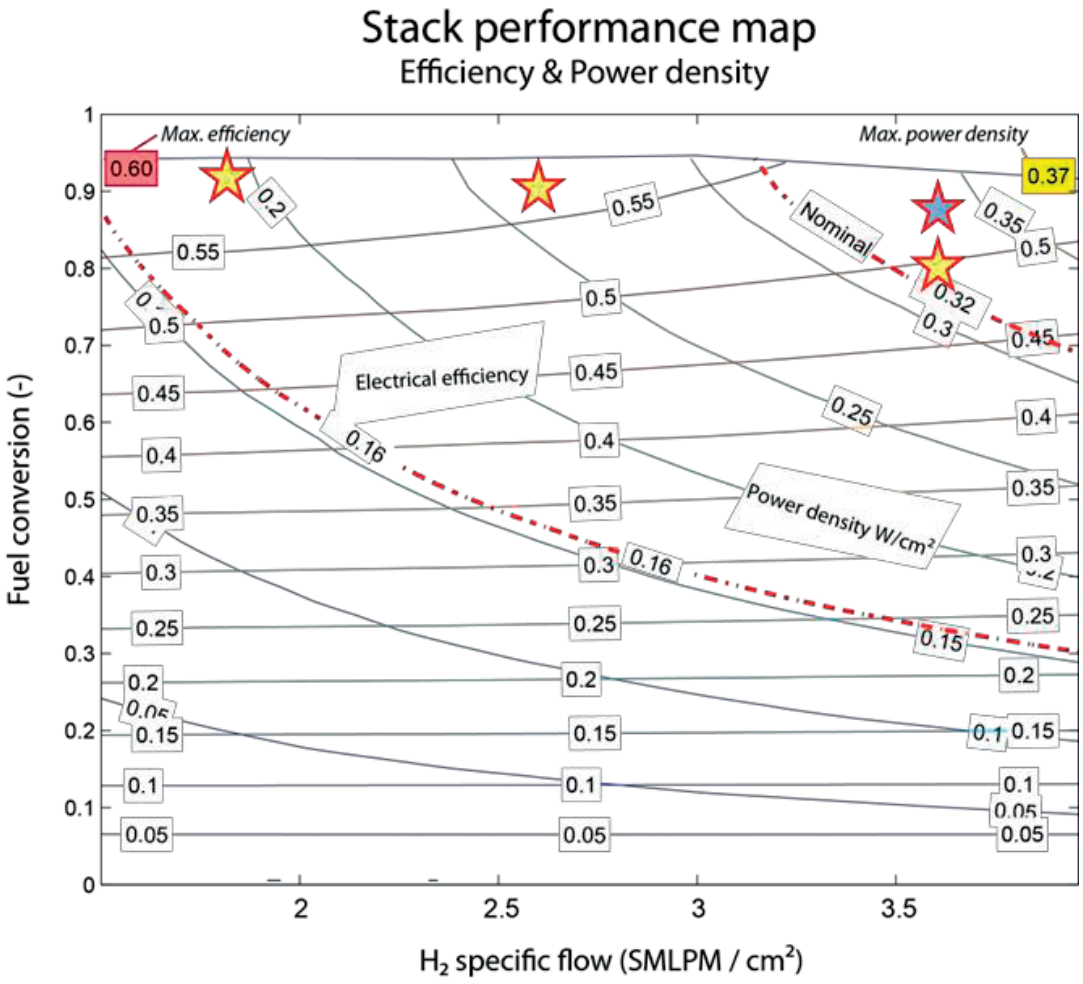

Figure A.2 Typical performance map of a short stack: power density and efficiency as function of fuel flow rate and fuel utilization. (★) Performance validation with full-scale stacks. (Courtesy of Z. Wuillemin.)

Single-pass conversion efficiency

The 60 % electrical efficiency measured at part load with short stacks is very close to the maximum achievable electrical efficiency for this fuel mixture and when operating in single pass fuel flow, i.e. if the cell potential would equal the fuel outlet's Nernst potential of an ideally-constructed repeat element (Nernst potential pinch).

This situation can be found in Figure A.4, for a short stack supplied with 1.8 SMLPM/cm^2 hydrogen. The Nernst potential of the gas mixture leaving the stack is computed as function of the fuel utilization and temperature. At 800 °C, the maximum electrical efficiency reachable in such conditions would be 60.8 % (air-excess ratio of 17). The measured cell voltage follows closely the Nernst potential, without increasing

difference towards high fuel utilizations, depicting a Nernst potential pinch situation. At a fuel utilization of 94 %, a maximum efficiency of 59.3 % was reached, for a cell voltage of 791 mV and a theoretical Nernst potential of 811 mV (pinch of 20 mV).

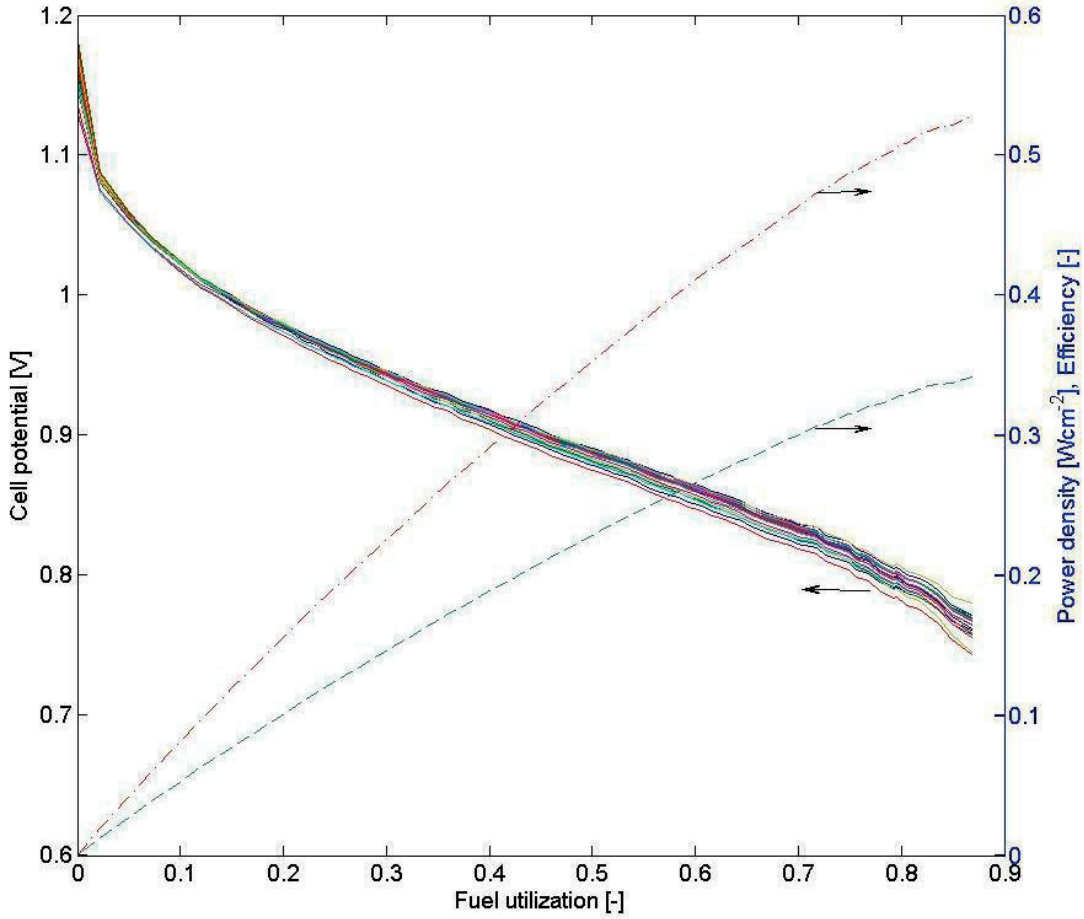

Figure A.3 Qualification IV curve obtained on a stack of 66 elements, and corresponding efficiency and power density. (Courtesy of Z. Wuillemin.) Flow of H_2, N_2, and air are respectively of 3.6, 2.4, and 68 SMLPM/cm^2.

For any stack, this indicator is a function of the maximum achievable fuel utilization — hence of the homogeneity of the reactant supply — and of the ohmic and polarization losses.

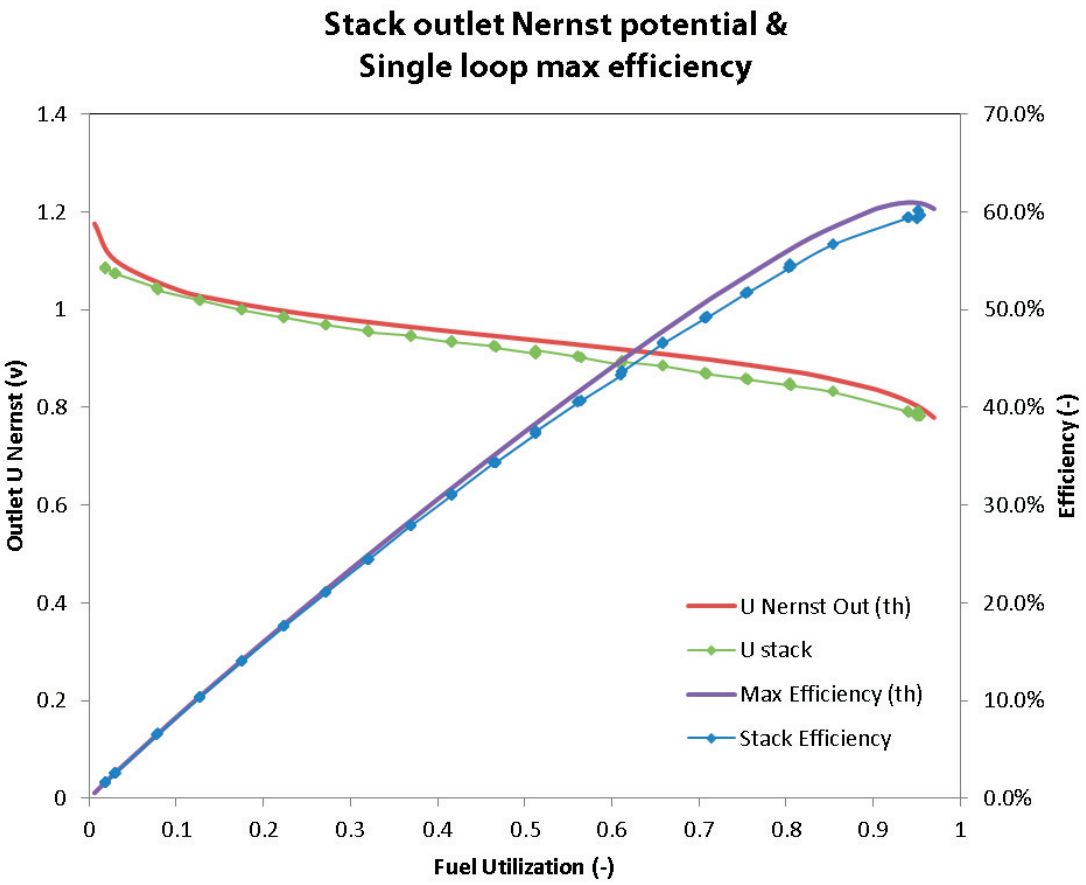

Figure A.4 Nernst potential at the stack outlet and measured stack voltage. Comparison between achieved and maximum theoretical efficiency. $T_{\text{out}} = 800\,°\text{C}$. Specific flow rate of H_2 1.8 SMLPM/cm^2. (Courtesy of Z. Wuillemin.)

With a value of 97.5 %, the stack performance is therefore not any more limited by the ohmic and polarization losses, but solely by the decrease of Nernst potential along the fuel flow. With a pinch of 20 mV at a fuel utilization of 94 % percent, the homogeneity of the fuel flow among and within the repeat elements can therefore be estimated to be excellent.

For higher power densities and lower temperatures, the maximum single-pass conversion efficiency decreases, as shown in Figure A.5. In each case, the maximum stack efficiency was measured above 90 % of fuel utilization. At the lowest fuel flow rates, the conversion efficiency tends to a common value higher than 95 % independently of the temperature, hence showing the presence of the Nernst potential pinch. At higher fuel

flow rates, the single-pass conversion efficiency becomes limited by the ohmic and polarization losses.

The large stacks, whose results are summarized above, present similar results. At specific flow rates of H_2 of {1.8, 2.6, and 3.6} SMLPM/cm^2, the recorded maximum single-pass conversion efficiencies are respectively 95 %, 92 % and 87 %. In that case, the stacks were operated at slightly lower fuel utilizations (> 87 %) to prevent any potential damage to the costly prototypes. Nevertheless, the 95 % achieved at part load for a fuel utilization of 92 % indicate that the fuel distribution among the repeat elements is good.

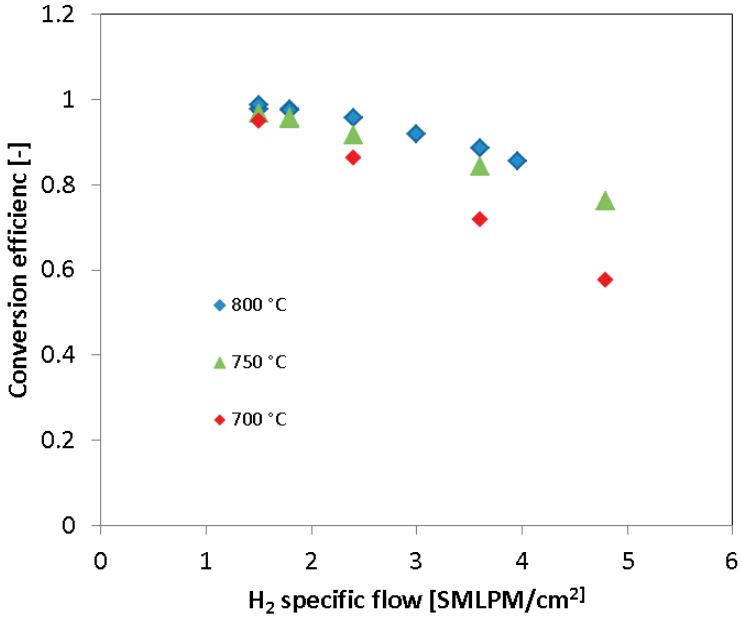

Figure A.5 Single-pass conversion efficiency measured under different conditions in a short stack. (Courtesy of Z. Wuillemin.)

Steam-reformed methane

Using steam-reformed natural gas as fuel, correspondingly high electrical efficiencies can be achieved, as shown in Figure A.6. The data is obtained from short stack tested in a furnace at 750 °C. Part of the reforming reaction was performed upstream of the stack in a reformer. The ratio of stack-internal to total reforming was varied in a range from 10 % to 70 % by controlling the temperature of the reactor.

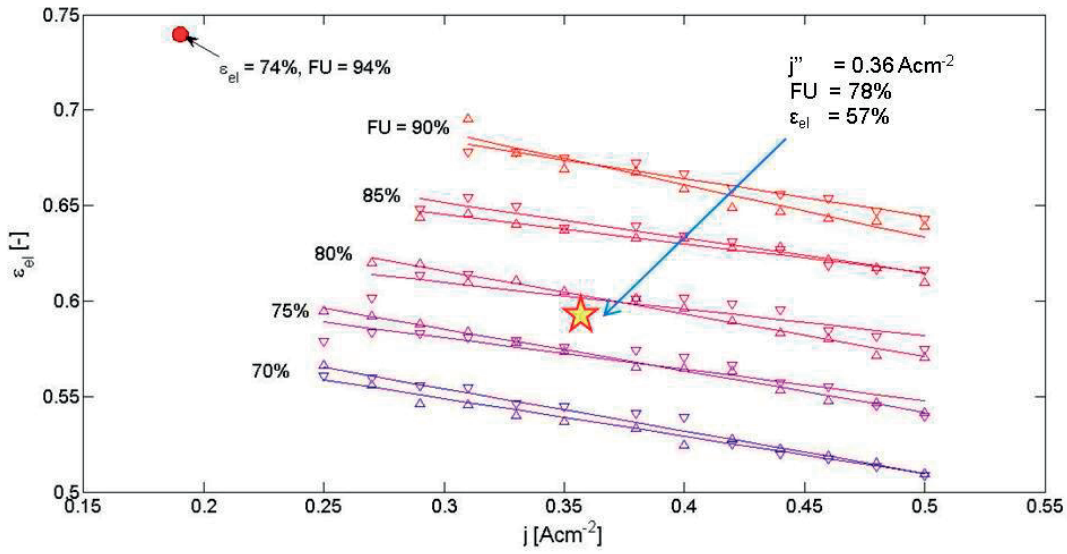

Figure A.6 Electrical efficiency at different fuel utilizations and current densities. $T = 750$ °C. Internal reforming ratio of 10 % (▼) vs. 70 % (▲). Maximum efficiency reached at 10 % internal reforming (●). Validation of performance with full-scale stacks in micro-CHP system (★). (Courtesy of Z. Wuillemin.)

Contrarily to the results shown for hydrogen, the stack was operated here in counter-flow arrangement, the air inlet temperature being 690 °C and its outlet around 760 °C. The steam-to-carbon ratio was 2.2.

A maximum electrical efficiency of 74 % was reached at 94 % of fuel utilization, for a current density of 0.19 A/cm^2 and a power density of 0.16 A/cm^2. To our best knowledge, such high efficiency for single pass operation has not been reported so far. With a maximum theoretical single-pass efficiency of 76 % for these testing conditions, the stack reached again a max. single-loop conversion efficiency of 97.4 %, similarly to the hydrogen case reported above.

In this short stack configuration, the impact of the internal reforming reaction remains noticeably limited, the difference in efficiency being in the range of 1 % for an internal reforming varied from 10 % to 70 %. This is of interest for systems where a large ratio of internal reforming is advantageous. At a nominal current density of 0.4 A/cm^2, the electrical efficiency is 60 % for 80 % of fuel utilization, and up to 67 % at 90 % FU.

Similarly to the hydrogen case, the scale-up to full-scale stack doesn't add much limitation. Tested in a 2.5 kW micro-CHP system, the two stacks operated in parallel reached 1434 W, respectively 1435 W at 28.5 A each (together 2869 W, 57 A total), their efficiency being 57.6 % and 57.7 %. This corresponds to a current density of

0.36 A/cm^2 and a fuel utilization of 78 %. The homogeneity of performance among the two stacks operated with a common air and fuel supply is an encouraging result. At the corresponding operating point (see Figure A.6), the short stack attained an efficiency of 59 %, however for different thermal boundary conditions.

Durability and stress tests

High fuel utilization stress-test

The capability to operate at high fuel utilization is of interest only if such conditions can be maintained for long periods without damage to the stack. In the frame of the European Project DESIGN, stress tests were performed up to 90 % fuel utilization.

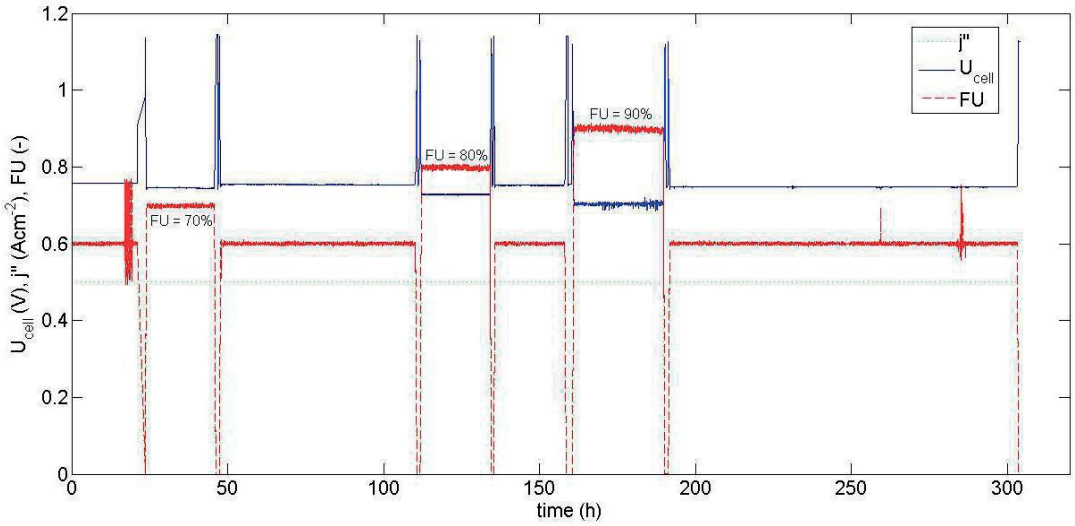

Figure A.7 High fuel utilization stress test at constant current density (single repeat unit). (Courtesy of Z. Wuillemin.)

The result of such an experiment, performed at EPFL, is shown in Figure A.7. A single repeat unit was submitted for periods of more than 24 hours to increasing fuel utilizations, at a constant current density of 0.5 A/cm^2. A fuel utilization of 90 % was maintained for 30 hours without damage. Some oscillations of potential were recorded, resulting from condensing off-gas in the piping. Returning back to a fuel utilization of 60 %, the element recovered its earlier performance (−4 mV). This test will be repeated at full-scale in near future.

Durability tests

With the introduction of this new stack technology, new degradation tests were started for validation. The results of an ongoing test are shown in Figure A.8, operated at a fuel utilization of 80 % with a fuel mixture of 60 % H_2 and 40 % N_2. In the initial 2 000 h, the average degradation rate was less than 0.05 % per thousand hours. After an unwanted thermal cycle, during which the stack lost 1 % of performance, the degradation rate increased to an average of 0.3 %/kh.

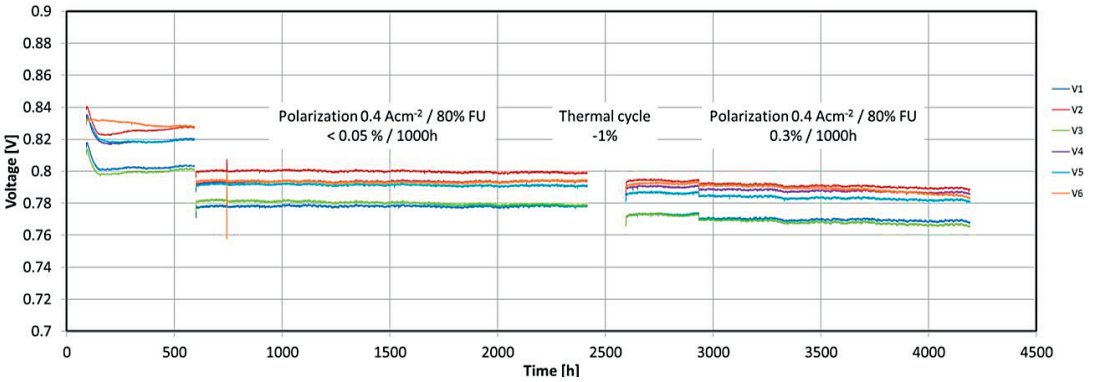

Figure A.8 Long-term tests on a short stack. Fuel: hydrogen/nitrogen. $T = 750$ °C. (Courtesy of Z. Wuillemin.)

The objective being to maintain degradation rates below 0.5 %/kh, more detailed studies are ongoing to investigate the principal degradation mechanisms. These studies are mainly based on localized measurements made in a segmented repeat element that give spatial information about the degradation of the individual electrochemical processes. Details can be found in [12,94,95].

Thermal cycling

Thermal cycling tests are currently ongoing in simulated system start-up/shut-down conditions. An example is given below for a stack of 6 elements (active area of 48 cm^2) operated with steam-reformed methane. The thermal cycles are performed between 220 °C and 750 °C, without use of protective gas. The effect on the stack OCV and full-load voltage are shown in Figure A.9, up to now for 51 thermal cycles.

In average, the OCV decreases by 0.4 mV per thermal cycle, indicating that the seals do not suffer too much from cycling. Similarly, the potential recorded here at 0.54 A/cm^2 (82 % FU) decreases in average by 0.6 mV per cycle, which corresponds to less than 0.1 % of performance loss per cycle. As shown in Figure A.10, the initial efficiency of 58 % decreased after the 51 cycles to 55 % (average 56.5 %), for corresponding power

densities of 0.40 and 0.38 W/cm^2 (116 to 110 W). This is in line with the expectation for system operation, even if it needs to be reproduced for the more complex thermos-mechanics of a full-scale stack.

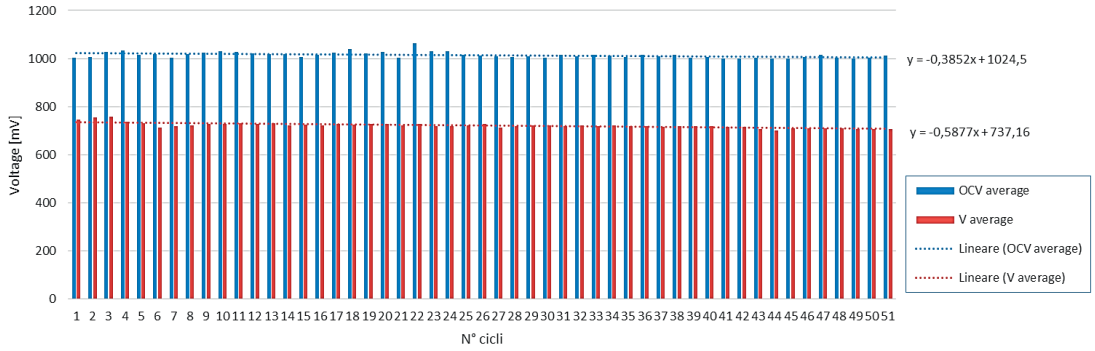

Figure A.9 Evolution of the OCV and full-load stack voltage (0.54 A cm^{-2}) upon thermal cycling in short-stack configuration. Fuel: steam-reformed natural gas. (Courtesy of Z. Wuillemin.)

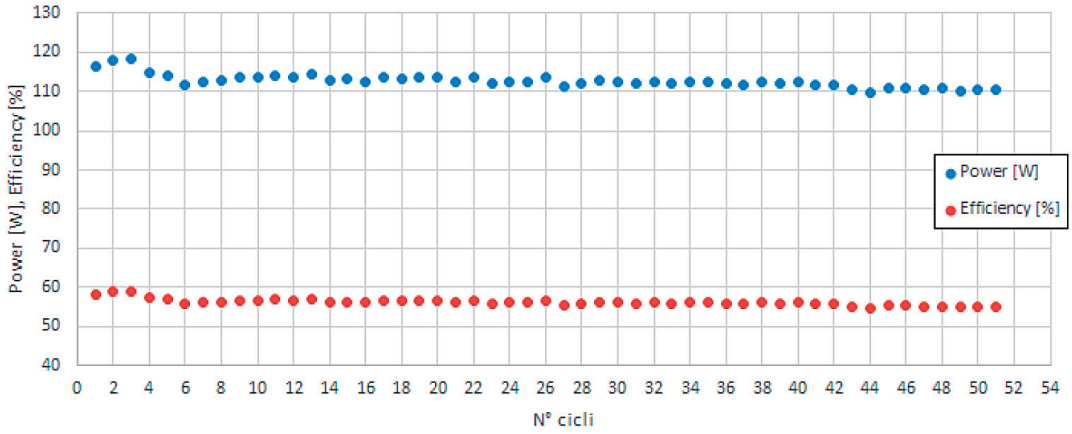

Figure A.10 Evolution of the stack power and efficiency upon thermal cycling. Fuel: steam-reformed natural gas. (Courtesy of Z. Wuillemin.)

Conclusion

With this new stack technology, SOFCpower – HTceramix SA has developed a platform suitable for a wide range of applications. The very high maximum single-loop conversion efficiency demonstrated for different fuels, and possibly reaching one record in electrical efficiency, opens today new perspectives of application.

With its low cost and the possibility for further scale-up, this technology seems to be well adapted for the emerging SOFC market.

Appendix B

Additional formulas

B.1 Generalities and definitions

Law of ideal-gas:

$$N = \frac{p\,V}{\mathcal{R}\,T} \tag{10.1}$$

The molar flow rate of fuel for one cell can be derived from **Faraday's law of electrolysis**:

$$I = \nu_{\mathrm{e}}\,\mathcal{F}\,\dot{N} \tag{10.2}$$

$$\dot{N}_{\mathrm{fuel}} = \dot{N}_{\mathrm{H_2}} = \frac{I\,\mathcal{N}_{\mathrm{cells}}}{\nu_{\mathrm{e}}\,\mathcal{F}} \tag{10.3}$$

Definition of the **molar mass** for species k:

$$M_k = \widetilde{m}_k\,N_k$$

Definition of fuel utilization:

$$\Upsilon_{\mathrm{f}} = \frac{I_{\mathrm{actual}}}{I_{\mathrm{max}}} = \frac{\dot{N}^{\mathrm{c}}_{\mathrm{fuel}}}{\dot{N}^{\mathrm{in}}_{\mathrm{fuel}}} = \frac{1}{\lambda_{\mathrm{f}}} \tag{10.4}$$

The fuel-excess ratio λ_{f} is simply the inverse of the fuel utilization:

Definition of **air-excess ratio** ($\lambda = 1$ corresponds to stoichiometry):

In SOFC, typical values of λ are in the interval [4 ; 8] to evacuate the heat generated in the stack, thereby smoothing thermal gradients. Homogeneous temperature is desirable for thermo-structural reason and because local performance of the fuel cell is highly dependent on the temperature.

The following relations will be used in the next developments:

Stoichiometric (st) and consumed (c) are not interchangeable terms.

$\dot{N}_k^{\text{out}} = \dot{N}_k^{\text{in}} - \dot{N}_k^{\text{c}} + \dot{N}_k^{\text{p}}$, with c for consumed and p for produced species k

Fuel utilization Y_f: $\dot{N}_{H_2}^{\text{c}} = Y_f \, \dot{N}_{H_2}^{\text{in}}$

Air-excess ratio λ_a: $\dot{N}_{O_2}^{\text{in}} = \lambda_a \, \dot{N}_{O_2}^{\text{st}}$

Molar fractions $\tilde{c}_k$: $\dot{N}_k^{\boldsymbol{x}} = \tilde{c}_k^{\boldsymbol{x}} \, \dot{N}_{\text{mix}}^{\boldsymbol{x}}$ and $\sum_k \tilde{c}_k = 1$, $\forall\, k \in \text{mix, at location } \boldsymbol{x}$

$\tilde{c}_k = \frac{N_k}{N_{\text{mix}}} = \frac{\dot{N}_k}{\dot{N}_{\text{mix}}}$

$$\dot{N}_{O_2}^{\text{c}} = 0.5 \, \dot{N}_{H_2}^{\text{c}} \;;\; \dot{N}_{H_2O}^{\text{p}} = \dot{N}_{H_2}^{\text{c}} \;;\; \dot{N}_{H_2}^{\text{c}} = Y_f \, \dot{N}_{H_2}^{\text{in}} \;;\; \dot{N}_{\text{cat}}^{\text{in}} = \frac{\dot{N}_{O_2}^{\text{in}}}{\tilde{c}_{O_2}^{\text{in}}} \tag{10.5}$$

The air flow rate is linked to the fuel flow rate through the stoichiometry of the oxidation reaction. Since $H_2 + ½\, O_2 \rightarrow H_2O$, the *stoichiometric molar* flow rate of *oxygen* is:

$$\dot{N}_{O_2}^{\text{st}} = 0.5 \, \dot{N}_{H_2}^{\text{in}} \tag{10.6}$$

$$\dot{N}_{\text{air}}^{\text{in}} = \frac{\dot{N}_{O_2}^{\text{in}}}{\tilde{c}_{O_2}} = \frac{\lambda \, \dot{N}_{O_2}^{\text{st}}}{\tilde{c}_{O_2}} \tag{10.7}$$

Mass flow rate of air:

$$\dot{M}_{\text{air}} = \tilde{m}_{\text{air}} \, \dot{N}_{\text{air}}^{\text{in}} = \tilde{m}_{\text{air}} \frac{\lambda \, \dot{N}_{H_2}^{\text{in}}}{2 \, \tilde{c}_{O_2}} \tag{10.8}$$

$$\tilde{m}_{\text{mix}} = \sum_k \tilde{c}_k \, \tilde{m}_k \tag{10.9}$$

Reactions

The stoichiometric coefficients are determined by writing the redox reactions:

The number of electrons that are exchanged are determined by writing the half-reactions. For the case of methane, they are:

$CH_4 \rightarrow C + 4\, H^+ + 4\, e^-$ and $2\, O_2 + 8\, e^- \rightarrow 4\, O^{2-}$

- "Water-gas-shift": $CO + H_2O \leftrightarrow H_2 + CO_2$
- Methane steam reforming: $CH_4 + 2\, H_2O \leftrightarrow 4\, H_2 + CO_2$

The reforming of 1 mole of methane with 2 mole of steam produces 4 moles of hydrogen and 1 mole of carbon dioxide. Therefore, even a small molar fraction of methane

can modify sensibly the resulting molar fractions of steam and hydrogen. Assuming these reactions are at equilibrium, the resulting values can be computed using the equilibrium-constant (depending on temperature).

Heating power contained in (or conveyed by) the fuel flow rate:

$$\dot{Q}^{\mathrm{in}} = \dot{N}^{\mathrm{in}}_{\mathrm{fuel}}\,\Delta\tilde{h}^{\ominus}_{\mathrm{fuel}} = \dot{N}^{\mathrm{in}}_{\mathrm{H_2}}\,\Delta\tilde{h}^{\ominus}_{\mathrm{H_2}} \tag{10.10}$$

Standard redox potential

Standard redox potential $E^{\ominus}_{(T)}$ = potential difference between both electrodes where each chemical participating in the reaction is considered at its reference *standard state* ($\ominus$).[1] Therefore, it does not account for specific concentrations, which typically occur when the fuel cell works (net external electrical current).

The *standard* redox potential *does not take into account the concentration of gases*, since it is determined for unit concentration.

Standard redox potential as function of temperature:

$$E^{\ominus}(T) = -\frac{\Delta_{\mathrm{r}}\tilde{g}^{\ominus}(T)}{\nu_{\mathrm{e}}\,\mathcal{F}} \tag{10.11}$$

The relation between the standard redox potential $E^{\ominus}$ and thermodynamics is:[2]

$$\Delta_{\mathrm{r}}\tilde{g}^{\ominus}_{(T)} = -\nu_{\mathrm{e}}\,\mathcal{F}\,E^{\ominus}_{(T)} \tag{10.12}$$

Gibbs free enthalpy-change

The standard molar Gibbs free enthalpy-change of reaction $\Delta_{\mathrm{r}}\tilde{g}^{\ominus}$ is given by the fundamental relation:

$$\Delta_{\mathrm{r}}\tilde{g}^{\ominus}(T) = \Delta_{\mathrm{r}}\tilde{h}^{\ominus}(T) - T\,\Delta_{\mathrm{r}}\tilde{s}^{\ominus}(T) \tag{10.13}$$

[1] Although standard state is often marked with (^{0}) for convenience, the original symbol $\ominus$ is purposefully used here to highlight the non-zero nature of standard state.

[2] This relation holds in non-standard conditions, too: $\Delta_{\mathrm{r}}\tilde{g} = -\nu_{\mathrm{e}}\,\mathcal{F}\,E = \Delta_{\mathrm{r}}\tilde{g}^{\ominus} + \mathcal{R}\,T\,\ln(Q)$.

The enthalpies ($\Delta_\mathrm{r}\tilde{h}$) and entropies ($\Delta_\mathrm{r}\tilde{s}$) of a reaction are determined thanks to the Hess' law, using the enthalpies of formation, $\Delta_\mathrm{f}\tilde{h}_k$, respectively entropies ($\tilde{s}_k$), of the k reactants and products. This law holds true for standard or non-standard states, as long as state is consistent.

Hess' law (to compute enthalpies and entropies of reaction)

$$\Delta_\mathrm{r}\tilde{h} = \sum_j \nu_j \, \Delta_\mathrm{f}\tilde{h}_j - \sum_i \nu_i \, \Delta_\mathrm{f}\tilde{h}_i \tag{10.14}$$

for a reaction such as:

$$\sum_i \nu_i \, \mathrm{Reactant}_i \Leftrightarrow \sum_j \nu_j \, \mathrm{Product}_j \tag{10.15}$$

The validity of this law extends to both $\Delta_\mathrm{r}\tilde{s}$ and $\Delta_\mathrm{r}\tilde{g}$.

As long as no phase change occurs, the dependence of $\Delta_\mathrm{r}\tilde{h}^\ominus$ and $\Delta_\mathrm{r}\tilde{s}^\ominus$ with temperature is usually relatively low compared to the (direct) linear dependence of $\Delta_\mathrm{r}\tilde{g}^\ominus$ with temperature. Hence, a good approximation is:

$$\frac{\partial \Delta_\mathrm{r}\tilde{g}^\ominus(T)}{\partial T} \cong -\Delta_\mathrm{r}\tilde{s}^\ominus \tag{10.16}$$

It follows:

$$\frac{\partial E^\ominus(T)}{\partial T} \cong \frac{\Delta_\mathrm{r}\tilde{s}^\ominus}{\nu_\mathrm{e}\,\mathcal{F}} \tag{10.17}$$

Integrating this relation gives:

$$E^\ominus(T) \cong E^\ominus_{T_\mathrm{ref}} + \left.\frac{\partial E^\ominus(T)}{\partial T}\right|_{\mathrm{T}_{ref}} (T - T_\mathrm{ref}) = \frac{\Delta_\mathrm{r}\tilde{g}^\ominus_{T_\mathrm{ref}} + \Delta_\mathrm{r}\tilde{s}^\ominus_{T_\mathrm{ref}}\,(T - T_\mathrm{ref})}{\nu_\mathrm{e}\,\mathcal{F}} \tag{10.18}$$

In case more exact values are necessary, we use **Kirchoff's law:**

$$\frac{\partial \Delta_\mathrm{r}\tilde{h}^\ominus(T)}{\partial T} = \Delta\tilde{c}_p\ (T) \tag{10.19}$$

It can be decomposed to integrate the heat-capacities for individual compounds. $\Delta\tilde{c}_p\ (T)$ from tables of reference [NIST] (polynomials).

Over the interval [25 ; 1000] °C, both methane- and hydrogen-oxidations are exothermic, since $\Delta_\mathrm{r}\tilde{h} < 0$. Both oxidations are also spontaneous over this interval, though the

spontaneity decreases for H_2 as temperature increases. This corresponds to the decrease of standard redox potential.

Standard state

Basically, the *standard state* ($^\ominus$) of any chemical is defined as the (hypothetical) state it would have at the *standard pressure* $p^\ominus$ or unit concentration (1 bar or 1 mol/L or 1 mol/kg, though conceptually, any value could be used). The standard state should not be confused with standard temperature and pressure for gases, even though the operating conditions under which data are tabulated for standard state may correspond to them.

Indeed, *standard state apply to any temperature*. Hence, the sign for standard ($^\ominus$) should not be confused with a degree sign or 0 °C. It should also be noted that the standard state of a substance may not exist in nature.

Non-standard state

Since a standard state is defined under specific conditions, related properties are usually invalid when concentrations are non-standard (or partial pressures for gases). A function of the reaction's quotient Q_r is used to treat these cases.

In case reactants are diluted, then they are not any more at standard state. As a consequence, there exist a gradient of concentration. In that case, the electrochemical potential of the reaction is a function of the concentration, through the term $\mathcal{R}\,T\ln[Q_\mathrm{r}]\,/\,(\nu_\mathrm{e}\,\mathcal{F})$.

Redox potential: the equation of Nernst

$$E(T,p_k) = E^\ominus(T) - \Delta E_\mathrm{composition} = E^\ominus(T) - \frac{\mathcal{R}\,T}{\nu_\mathrm{e}\,\mathcal{F}}\ln(Q_\mathrm{r}) \tag{10.20}$$

The redox potential is computed thanks to Nernst's equation, which account for the gases' composition and pressure.

Quotient of a reaction:

$$Q_\mathrm{r} = \frac{\prod_j a_j^{\nu_j}}{\prod_i a_i^{\nu_i}} \cong \frac{\prod_j \left(\frac{p_j}{p^\ominus}\right)^{\nu_j}}{\prod_i \left(\frac{p_i}{p^\ominus}\right)^{\nu_i}} = \frac{\prod_j \left(\tilde{c}_j \frac{p_{\mathrm{mix}\ni j}}{p^\ominus}\right)^{\nu_j}}{\prod_i \left(\tilde{c}_i \frac{p_{\mathrm{mix}\ni i}}{p^\ominus}\right)^{\nu_i}} \tag{10.21}$$

With j and i the index of respectively the products and reactants, a their activity, ν their stoichiometric coefficient, and $p_{\mathrm{mix}\ni k}$ the pressure of the mixture to which species k belongs, so that $\tilde{c}_k = p_k/p_{\mathrm{mix}\ni k}$. For gases, activities are equivalent to the partial pressures with respect to the standard pressure, which in their turn can be written in function of molar fractions.

B.2 Solid-oxide fuel cell (SOFC)

The operating pressure p_o in both the anodic and cathodic compartments is atmospheric pressure $(1\ \mathrm{atm})$ in our case. Furthermore, the effect of the relatively small change of pressure along the cell on the thermodynamic properties may be assumed negligible, so that they can be evaluated at a constant pressure. The standard pressure $p^\ominus$ corresponding to the data is[3] 1 bar ≃ 1 atm. Therefore, the pressure of the mixes has no additional effect with respect to the standard pressure. Only the molar fractions (partial pressures) enter into considerations.

The quotient of the reaction for SOFCs is then:

$$Q_\mathrm{r} = \frac{\prod_j \tilde{c}_j^{\,\nu_\mathrm{j}}}{\prod_i \tilde{c}_i^{\,\nu_i}} = \frac{\tilde{c}^{\mathrm{an}}_{\mathrm{H_2O}}}{\tilde{c}^{\mathrm{an}}_{\mathrm{H_2}} \left(\tilde{c}^{\mathrm{cat}}_{\mathrm{O_2}}\right)^{1/2}} = \frac{\Upsilon_\mathrm{f}}{(1-\Upsilon_\mathrm{f}) \left(\frac{\tilde{c}_{\mathrm{O_2}}\,(\lambda-\Upsilon_\mathrm{f})}{\lambda - \tilde{c}_{\mathrm{O_2}}\,\Upsilon_\mathrm{f}}\right)^{1/2}} \tag{10.22}$$

This quotient of the reaction is defined according to the local concentrations. The molar fraction of oxygen was computed assuming that its consumption is "synchronous" with that of hydrogen, i.e., air and fuel flow in the same direction (co-flow configuration).

The expression of the redox potential can therefore be computed as a function of the fuel utilization.

$$E(T, p_k) = E^\ominus(T) - \frac{\mathcal{R}\,T}{\nu_\mathrm{e}\,\mathcal{F}} \ln\left(\frac{\Upsilon_\mathrm{f}}{(1-\Upsilon_\mathrm{f}) \left(\frac{\tilde{c}_{\mathrm{O_2}}\,(\lambda-\Upsilon_\mathrm{f})}{\lambda - \tilde{c}_{\mathrm{O_2}}\,\Upsilon_\mathrm{f}}\right)^{1/2}}\right) \tag{10.23}$$

$$E^\ominus(T) = -\frac{\Delta_\mathrm{r}\tilde{g}^\ominus(T)}{\nu_\mathrm{e}\,\mathcal{F}} = \frac{-\Delta_\mathrm{r}\tilde{h}^\ominus(T) + T\,\Delta_\mathrm{r}\tilde{s}^\ominus(T)}{\nu_\mathrm{e}\,\mathcal{F}} \tag{10.24}$$

[3] From 1982, IUPAC recommends using a standard pressure of 1 bar. The previous value of 1 atm is however still used by several other organisms (e.g., NIST). In practice, this makes little difference.

Molar fraction at anode

Numerators and denominators can be expressed in function of the hydrogen injected, so that it cancels. This quantity will therefore be considered known (constant) in the next reasoning.

Generally speaking, the molar fractions of hydrogen and steam are, respectively:

$\tilde{c}_{\mathrm{H_2}}^{\mathrm{an}} = \frac{\dot{N}_{\mathrm{H_2}}}{\dot{N}_{\mathrm{an}}}$ and $\tilde{c}_{\mathrm{H_2O}}^{\mathrm{an}} = \frac{\dot{N}_{\mathrm{H_2O}}}{\dot{N}_{\mathrm{an}}}$ with $\dot{N}_{\mathrm{an}} = \dot{N}_{\mathrm{H_2}} + \dot{N}_{\mathrm{H_2O}} + \dot{N}_{\mathrm{N_2}} = \mathrm{cst} = \frac{\dot{N}_{\mathrm{H_2}}^{\mathrm{in}}}{\tilde{c}_{\mathrm{H_2}}^{\mathrm{in}}}$

According to the electrochemical reaction, for 1 mole of hydrogen consumed, 1 mole of steam is produced; besides, steam is generated at the anode for SOFCs. So, *the molar rate at anode remains constant in SOFCs*.

In addition, the molar fraction of steam can be obtained knowing that of hydrogen, since both must sum to unity. It is therefore only necessary to express the flow rate of hydrogen as a function of the fuel utilization, which is simply the amount of hydrogen injected minus the hydrogen that is consumed at (or up to) that fuel utilization:

$$\dot{N}_{\mathrm{H_2}}[\Upsilon_{\mathrm{f}}] = \dot{N}_{\mathrm{H_2}}^{\mathrm{in}} - \dot{N}_{\mathrm{H_2}}^{\mathrm{c}}[\Upsilon_{\mathrm{f}}] = \dot{N}_{\mathrm{H_2}}^{\mathrm{in}} - \Upsilon_{\mathrm{f}}\,\dot{N}_{\mathrm{H_2}}^{\mathrm{in}}$$

Finally, the molar fractions at anode in function of the fuel utilization are simply given by:

$$\tilde{c}_{\mathrm{H_2}}^{\mathrm{an}}[\Upsilon_{\mathrm{f}}] = \frac{\dot{N}_{\mathrm{H_2}}[\Upsilon_{\mathrm{f}}]}{\dot{N}_{\mathrm{an}}} = \frac{\tilde{c}_{\mathrm{H_2}}^{\mathrm{in}}\left(\dot{N}_{\mathrm{H_2}}^{\mathrm{in}} - \Upsilon_{\mathrm{f}}\,\dot{N}_{\mathrm{H_2}}^{\mathrm{in}}\right)}{\dot{N}_{\mathrm{H_2}}^{\mathrm{in}}} = \frac{\tilde{c}_{\mathrm{H_2}}^{\mathrm{in}}\,\dot{N}_{\mathrm{H_2}}^{\mathrm{in}}\,(1-\Upsilon_{\mathrm{f}})}{\dot{N}_{\mathrm{H_2}}^{\mathrm{in}}} = \tilde{c}_{\mathrm{H_2}}^{\mathrm{in}}\,(1-\Upsilon_{\mathrm{f}})$$

$$\tilde{c}_{\mathrm{H_2O}}^{\mathrm{an.}}[\Upsilon_{\mathrm{f}}] = \frac{\dot{N}_{\mathrm{H_2O}}[\Upsilon_{\mathrm{f}}]}{\dot{N}_{\mathrm{an}}} = \frac{\dot{N}_{\mathrm{H_2O}}^{\mathrm{in}} + \Upsilon_{\mathrm{f}}\,\dot{N}_{\mathrm{H_2}}^{\mathrm{in}}}{\dot{N}_{\mathrm{an}}} = \tilde{c}_{\mathrm{H_2O}}^{\mathrm{in}} + \tilde{c}_{\mathrm{H_2}}^{\mathrm{in}}\,\Upsilon_{\mathrm{f}}$$

$$\tilde{c}_{\mathrm{N_2}}^{\mathrm{an}} = \tilde{c}_{\mathrm{N_2}}^{\mathrm{in}} = \mathrm{cst}$$

Molar fractions at cathode

At cathode, only the molar fraction of oxygen enters in the computation of the reaction-quotient:

$\tilde{c}_{\mathrm{O_2}}^{\mathrm{cat}} = \frac{\dot{N}_{\mathrm{O_2}}}{\dot{N}_{\mathrm{cat}}}$ with $\dot{N}_{\mathrm{O_2}} = \dot{N}_{\mathrm{O_2}}^{\mathrm{in}} - \dot{N}_{\mathrm{O_2}}^{\mathrm{c}}$ and $\dot{N}_{\mathrm{cat}} = \dot{N}_{\mathrm{air}}^{\mathrm{in}} - \dot{N}_{\mathrm{O_2}}^{\mathrm{c}} \neq \mathrm{cst}$

The molar rate at cathode decreases in SOFCs since steam is produced at anode. It however decreases at a relatively slow rate, since: a) only 1 mole of 0_2 is consumed for 2 mole of H_20; b) 0_2 is diluted around five-fold in air; and c) the air-excess ratio is usually large in SOFCs ($\lambda \in [3\,;8]$).

Using the previous expressions, the molar flow rate of oxygen for a given fuel utilization becomes:

$$\dot{N}_{\mathrm{O}_2}[Y_\mathrm{f}] = 0.5\,\lambda\,\dot{N}^{\mathrm{in}}_{\mathrm{H}_2} - 0.5\,Y_\mathrm{f}\,\dot{N}^{\mathrm{in}}_{\mathrm{H}_2} = 0.5\,\dot{N}^{\mathrm{in}}_{\mathrm{H}_2}\,(\lambda - Y_\mathrm{f})$$

The molar flow rate of air injected can be expressed as:

$$\dot{N}^{\mathrm{in}}_{\mathrm{air}} = \frac{\dot{N}^{\mathrm{in}}_{\mathrm{O}_2}}{\tilde{c}_{\mathrm{O}_2}} = \frac{\lambda\,\dot{N}^{\mathrm{st}}_{\mathrm{O}_2}}{\tilde{c}_{\mathrm{O}_2}} = \frac{0.5\,\lambda\,\dot{N}^{\mathrm{in}}_{\mathrm{H}_2}}{\tilde{c}_{\mathrm{O}_2}}$$

So that the total (i.e., of mix) molar flow rate at the cathode for a given fuel utilization becomes:

$$\dot{N}_{\mathrm{cat}} = \dot{N}^{\mathrm{in}}_{\mathrm{air}} - \dot{N}^{\mathrm{c}}_{\mathrm{O}_2} = \frac{0.5\,\lambda\,\dot{N}^{\mathrm{in}}_{\mathrm{H}_2}}{\tilde{c}_{\mathrm{O}_2}} - 0.5\,Y_\mathrm{f}\,\dot{N}^{\mathrm{in}}_{\mathrm{H}_2} = \frac{0.5\,\dot{N}^{\mathrm{in}}_{\mathrm{H}_2}\,(\lambda - \tilde{c}_{\mathrm{O}_2}\,Y_\mathrm{f})}{\tilde{c}_{\mathrm{O}_2}}$$

Finally, an expression independent of flow rate is found for the molar fraction of oxygen:

$$\tilde{c}^{\mathrm{cat}}_{\mathrm{O}_2}[Y_\mathrm{f}] = \frac{0.5\,\dot{N}^{\mathrm{in}}_{\mathrm{H}_2}\,\tilde{c}_{\mathrm{O}_2}\,(\lambda - Y_\mathrm{f})}{0.5\,\dot{N}^{\mathrm{in}}_{\mathrm{H}_2}\,(\lambda - \tilde{c}_{\mathrm{O}_2}\,Y_\mathrm{f})} = \frac{\tilde{c}_{\mathrm{O}_2}\,(\lambda - Y_\mathrm{f})}{\lambda - \tilde{c}_{\mathrm{O}_2}\,Y_\mathrm{f}}$$

If the consumption of oxygen is neglected in the expression of $\dot{N}_{\mathrm{cat}}$ then it becomes:

$$\tilde{c}^{\mathrm{cat}}_{\mathrm{O}_2}[Y_\mathrm{f}] = \frac{\tilde{c}_{\mathrm{O}_2}\,(\lambda - Y_\mathrm{f})}{\lambda} = \tilde{c}_{\mathrm{O}_2}\left(1 - \frac{Y_\mathrm{f}}{\lambda}\right)$$

Remark:

At low fuel utilization and/or high air-excess ratio, the consumption of oxygen is negligible relative to the amount injected. But for, e.g., $Y_\mathrm{f} = 0.9$ and $\lambda = 3$, the residual oxygen is 15.7 % from an initial 21 % (the approximation above gives 14.7 %).

Observations:

- The changes in the molar fraction of oxygen is small with respect to the changes in the molar fractions of hydrogen and steam (Y_f).
- At high fuel utilization, the (Nernst) redox potential is significantly lower than the standard redox potential (e.g., 18 % at $Y_\mathrm{f} = 95$ %)

- However, the redox potential can actually also take bigger values than the standard redox potential.

Nernst's equation as expressed above is valid for any physical value of its terms, except for $\lambda < 1$. It shows limit at extreme values ($\lambda = 0$, $\lambda = 1$, $Y_\mathrm{f} = 0$, $Y_\mathrm{f} = 1$, $\tilde{c}_{\mathrm{O}_2} = 0$), though these are actual physical limits. It is indefinite for $Q_\mathrm{r} < 1$.

B.3 Performance

Local Nernst (redox) potential

The redox potential E computed above is in fact not exactly E_cell; since it corresponds to the *concentrations at inlet*, it is the redox potential of the electrode *at inlet*.

Nernst potential of the cell

A better estimation of the Nernst potential *of the cell*, E_cell, can be approximated as the average of E between inlet and outlet (linear approximation):

$$E_\mathrm{cell} = \frac{E_\mathrm{inlet} + E_\mathrm{outlet}}{2}$$

This approximation is equivalent to assuming the current density (so the rates of mass-transfer) is constant along the cell. The best is to compute the integral over the cell.

Cell voltage

Nernst's equation is *not* valid (sufficient) to compute the cell voltage. The cell voltage equals the redox potential E when no electrical current is drawn from the cell (open circuit voltage, OCV). As soon as an electrical current is drawn from the cell, various losses of potential arise (e.g., ohmic loss $R\,I^2$), lowering the cell voltage.

Operating voltage of the cell

The operating voltage of the cell corresponds to the (Nernst) redox potential of the cell, E_cell, minus the ohmic and non-ohmic losses (i.e., voltage drops, or overpotentials):

$$U_\mathrm{cell} = E_\mathrm{cell} - \eta_\mathrm{ohmic} - \eta_\mathrm{non-ohmic}$$

$$\Delta V_\mathrm{cell} = E - \text{overpotentials}$$

Overpotential (losses)

Losses of potential increase sharply at high fuel utilization, leading to lower power and efficiency. Besides, a fuel cell product is not an ideal reactor with homogeneous reactions: locally, the fuel utilization can be bigger than the average fuel utilization, leading as a consequence to local fuel starvation and re-oxidation (i.e., degradation) of the cell.

Concentration overpotential account for drop of potential due to concentration-gradients and related effects (dilution, diffusion …). At a given location, the term $\mathcal{R}\,T\ln[Q_\mathrm{r}]\,/(\nu_\mathrm{e}\,\mathcal{F})$ allows to estimate the difference of potential due to concentration. Yet, in practice, the knowledge of the species-concentration at the triple-phase boundary depends on several factors not taken into consideration here. They relate to mass transfers by diffusion in porous media and by advection-diffusion in the bulk media.

Ohmic losses of potential

Thermal power dissipated by Joule effect = dissipation rate of ohmic losses: $(R\,I)\,I$

The ohmic loss *within the electrolyte* depends on its resistance to electrical current (flow of charge). The electrical resistance [ohm, Ω] is the inverse of electrical conductance [siemens, $\mathrm{S} = 1/\Omega$]. Similarly, resistivity $\rho\ \left[\Omega\,\mathrm{cm}\right]$ is the inverse of conductivity σ [S/cm]. The electrical resistance R of a conductor (or resistor) of resistivity ρ, length l, and cross-surface S, is given by $R = \rho\,l/\mathrm{S}$.

For a unit surface, the electrical resistance of the electrolyte is then $\rho\,l = l/\sigma\ \left[\Omega\,\mathrm{cm}^2\right]$. Here, the length l corresponds to the thickness of the electrolyte.

Voltage and current of the stack

Cells are connected in series. Therefore, the voltage of the stack is the sum of each cell's voltage, whereas the current is the same for every cell (which is also the current of the stack). The average voltage of one cell is hence $\Delta V_\mathrm{cell} = \Delta V_\mathrm{stack}/\mathcal{N}$

Electrical power

The electrical power delivered by the stack: $\dot{E}_{\mathrm{el,\,stack}} = \Delta V_\mathrm{stack}\,I = \mathcal{N}_\mathrm{cells}\,U_\mathrm{cell}\,I$

Current density: $j = I/A_\mathrm{cell}$

Power density: $\dot{E}'' = \dot{E}_\mathrm{stack}/A_\mathrm{stack} \equiv \dot{E}_\mathrm{cell}/A_\mathrm{cell} \equiv j\,\Delta V_\mathrm{cell}$

Electrical efficiency (LHV-based)

$$\varepsilon_{\mathrm{el}} = \frac{\text{FC ouput power}}{\text{fuel input power}} = \frac{\dot{E}_{\mathrm{el}}}{\dot{Q}_{\mathrm{th}}} = \frac{U_{\mathrm{cell}}\, I}{\dot{N}_{\mathrm{H_2}}^{\mathrm{in}}\, \Delta_{\mathrm{r}} \tilde{h}^{\ominus}_{25°\mathrm{C}\,(g)}} \tag{10.25}$$

$$\varepsilon_{\mathrm{el}} = \varepsilon_{\mathrm{th}}\, \varepsilon_{\mathrm{E}}\, \varepsilon_{\mathrm{I}} \quad \text{with: } \varepsilon_{\mathrm{th}} = \frac{\Delta_{\mathrm{r}} \tilde{g}^{\ominus}_{T_{\mathrm{op}}}}{\Delta_{\mathrm{r}} \tilde{h}^{\ominus}_{25°\mathrm{C}\,(g)}}\ ; \quad \varepsilon_{\mathrm{E}} = \frac{U_{\mathrm{cell}}}{E_{T_{\mathrm{op}}}}\ ; \quad \varepsilon_{\mathrm{I}} = Y_{\mathrm{f}} = \frac{I}{I_{\mathrm{max}}} \tag{10.26}$$

$$\varepsilon_{\mathrm{el}} = \frac{\Delta_{\mathrm{r}}^{\ominus} \tilde{g}\{T_{\mathrm{op}}\}}{\Delta_{\mathrm{r}}^{\ominus} \tilde{h}\{25°\mathrm{C}\,(g)\}}\, \frac{U_{\mathrm{cell}}}{E\{T_{\mathrm{op}}\}}\, \frac{I}{I_{\mathrm{max}}} \tag{10.27}$$

List of figures

List of tables

Glossary & index

This thesis deals with uncertainties. Those arising from (mis)communication obviously also propagate in the knowledge acquisition, and hence in research & development based on it. So, it seems important and appropriate to make a particular effort in this document to specify the definition associated to words of jargon and to use them as consistently as possible.

Unfortunately, some of these words are often used with loose, different, or even conflicting definitions in the scientific community. Sometimes, a consensus is not even reached about their meaning in a specific field: e.g., what is robust optimization in the context of operational research? A particular method, or any optimization to improve some measure of robustness? *Robust* has slightly different meanings when used in the following contexts, although they are all technical/scientific: [Wiktionary].

- (Systems engineering) Designed or evolved in such a way as to be resistant to total failure despite partial damage.
- (Software engineering) Resistant or impervious to failure regardless of user input or unexpected conditions.
- (Statistics) Not greatly influenced by errors in assumptions about the distribution of sample errors.

An example which can lead to unfortunate ambiguity is *independent variables*, which may mean statistically independent or "input variables to a function/experiment" (as opposed to dependent variables, computed from the input). We use the first meaning.

Since this document covers various fields, it was not possible to find all definitions in a single reference. We therefore combined several references. However, most of the definitions were adopted or inspired from the *Encyclopaedia of operations research and management science* (EORMS, [96]) and from the *International vocabulary of metrology* (IVM, [97]). We did not find a reference with the same consistency and authority as the IVM for the context of computerized experiments. So, we "extended" some of their definitions, with the modifications that we judged necessary. Most of the adopted definitions are given here without their justifications (apart from the reference where appropriate). Since the process of creating a consistent *vocabulary* goes beyond the purpose of this thesis, there certainly remain some inconsistencies.

A word or phrase in ***bold italics*** is defined in this *Glossary*. It serves at the same time as an *Index* for some terms. Pages in *italics* refer to pages, in this document, which are most relevant to these terms. Pages to bibliographic references are given in squared brackets: [ ]. Some subjects, which are developed more thoroughly in the *Encyclopaedia of operations research and management science* [96], are referenced when judged of potential interest to the reader.

Links: A B C D E F G H I J K L M N O P Q R S T U V W X Y Z

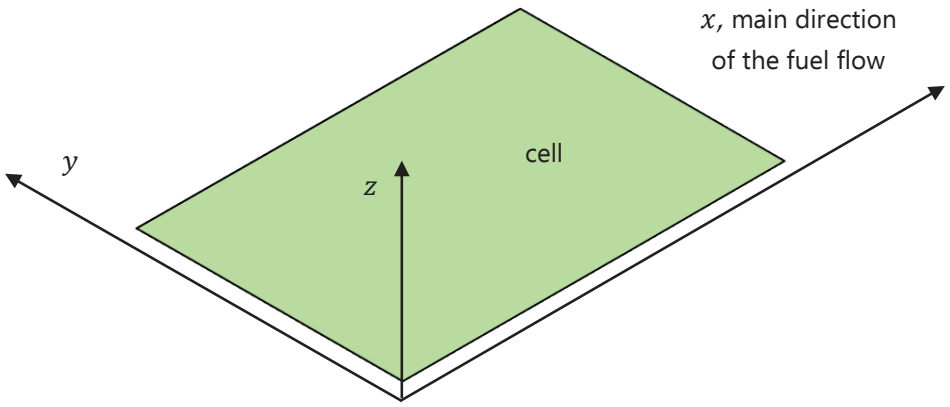

Figure 10.1 Standard referential used in this document unless otherwise specified.
The cell is in the plane Oxy. The fuel flows in the direction of x along the cell. In the main inlet manifold supplying the cells, the fuel flows in the direction of z.

A

Accuracy *of a measurement [computation], accurate(ly).* "Closeness of agreement between a measured [computed] quantity value and a true [exact] quantity value of a measurand". [IVM]
We use the definition encouraged by the IVM and ISO 5727, rather than the common usage, which associate accuracy to systematic errors only. We also extend the usage of the IVM to computation (i.e., "measurement" on a computerized experiment).
See also ***trueness***, ***exactness***, and ***precision***.

Active constraint. "A constraint in an optimization problem that is satisfied exactly by the solution [i.e., equality is reached]." [EORMS, 1]
See also ***inactive constraint***.

Air-excess ratio. The ratio of the air that is injected (into the fuel cell), with respect to the amount of air strictly needed (i.e., stoichiometric) for the complete electrochemical oxidation of the fuel that is injected.

Aleatory uncertainty. An uncertainty which does not arise from a lack of knowledge, but is rather inherent to the random nature — acknowledged as such in the context — of the quantity to which it is associated. An aleatory uncertainty is therefore an *irreducible uncertainty* and is sometimes called a *random uncertainty*, due to the closeness to the concept of a ***random error***.
See also ***epistemic uncertainty***.

Algorithm. "A computational procedure whose application yields a solution to an associated class of problems." [EORMS, 51]

Ambiguity, *ambiguous*. Similar concept as ***vagueness***, with the difference that an ambiguous statement lead to hesitating between a finite ensemble of possible "conclusions", often of opposite nature, whereas a vague statement does not imply a countable number of alternatives.

Attribute. In the context of this document, an attribute is a property (parameter) defining a software simulator. It may be a built-in feature, but often needs an input, on which the outputs depend. But it is most often *not* an input of interest for the user regarding real-world quantities. As such, attributes can be seen as the constituents of simulators, defining a transfer function between the "true" inputs and the outputs. An attribute consists of a "name" (or key) and a "value". It may be a quantity but is often a more complex object.
Example : simulator S_1 uses a fine *mesh* (quantifiable) and uses Sutherland's correlation to *model viscosity*'s dependence on temperature, whereas S_2 uses a coarser mesh and viscosity is assumed constant.
S_1 and S_2 can both be used to run $\mathcal{N}$ simulations with, e.g., inlet velocities and temperatures (inputs) varying from U_1 to $U_\mathcal{N}$ and T_1 to $T_\mathcal{N}$ to compute pressure drops (output) Δp_1 to $\Delta p_\mathcal{N}$. The simulators are de facto two transfer functions S_1 and S_2, such that $\Delta p_i = S_k\left[U_i, T_i\right]$, with $S_k = S[mesh_k, viscosity\_model_k]$.

B

Bootstrapping. "In forecasting, the term bootstrapping refers to models that have been developed by regressing an individual's (or group's) forecasts against the inputs that the individual used to make the forecasts." [EORMS, 127]

Bounded rationality. "The concept that a decision maker lacks both the knowledge and computational skill required to make choices in a manner compatible with economic notions of rational behaviour." [EORMS, 130]

Bounded variable. "A variable x_j in a linear-programming problem that is required to satisfy a constraint of the form $0 \leq x_j \leq b$, $-b \leq x_j \leq 0$, or $b_1 \leq x_j \leq b_2$, where b is some positive constant and $b_1 \leq b_2$." [EORMS, 131]

C

Certainty factor. "A numeric measure of the degree of certainty about the goodness, correctness, or likelihood of a variable value, an expression (e.g., premise) value, or conclusion." [EORMS, 160]

Coefficient of variation (CV). "The ratio of the standard deviation to the mean of a random variable." [EORMS, 180]
Also known as relative standard deviation, RSD, as used in this document.

Combinatorial explosion. "The phenomenon associated with optimization problems whose computational difficulty increases exponentially with the size of the problem. One common paradigm is the traveling salesman problem." [EORMS, 192]
See also ***curse of dimensionality***.

Computational complexity. "The term computational complexity has two usages which must be distinguished. On the one hand, it refers to an algorithm for solving instances of a problem: broadly stated, the computational complexity of an algorithm is a measure of how many steps the algorithm will require in the worst case for an instance or input of a given size. The number of steps is measured as a function of that size. The term's second, more important use is in reference to a problem itself. The theory of computational complexity involves classifying problems according to their inherent tractability or intractability — that is, whether they are easy or hard to solve. This classification scheme includes the well-known classes P and NP; the terms NP-complete and NP-hard are related to the class NP." [EORMS, 238]

Computational resource. "A resource needed by some computational models in the solution of computational problems" [Wikipedia]
This term refers and includes resources such as computation time, iterations, memory (RAM), and storage ; by extension, also refers to hardware and software required (or available) for computing.

Concave function. "A function that is never below its linear interpolation. Mathematically, a function $f[x]$ is concave over a convex set S, if for any two points, x_1 and x_2 in S and for any $0 \leq \alpha \leq 1$, $f[\alpha\, x_1 + (1-\alpha)\, x_2] \geq \alpha\, f[x_1] + (1-\alpha)\, f[x_2]$." [EORMS, 257]

Constrained optimization problem. "A problem in which a function $f[X]$ is to be optimized (minimized or maximized), where the possible solutions X lie in a defined solution subspace S, which is usually determined by a set of linear and/or nonlinear constraints." [EORMS, 267]

Constraint. "An equation or inequality relating the variables in an optimization problem; a restriction on the permissible values of the decision variables of a given problem." [EORMS, 267]

Constriction. A narrower region in the geometry where a fluid flows (inverse of an aneurysm).

Control variates. "In stochastic or Monte Carlo simulation, a variance reduction technique whereby a simulated random variable with known expectation (the control variate) is used to construct a more precise estimator by combining it (usually linearly) with another more standard estimator." [EORMS, 280]

Controllable variables. "In a decision problem, variables whose values are determined by the decision process and/or decision maker. Such variables are also called ***decision variables***." [EORMS, 280]

Convex function. "A function that is never above its linear interpolation. Mathematically, a function $f[x]$ is a convex over a convex set S, if or any two points x_1 and x_2 in S for any $0 \leq \alpha \leq 1$, $f[\alpha\, x_1 + (1-\alpha)\, x_2] \leq \alpha\, f[x_1] + (1-\alpha)\, f[x_2]$." [EORMS, 280]

Cost of production. In the cost of production, we include the *cost of raw materials*, the *cost of manufacture* (i.e., production of elementary parts), the *cost of treatment* (e.g., thermal or chemical), the *cost of assembly* of the parts, the *cost of quality control*, and the *cost of discarding* (i.e., non-ideal yield) . We exclude the cost of R&D and of storage in this definition.

Curse of dimensionality. "The situation that arises in such areas as dynamic programming, control theory, integer programming, combinatorial problems, and, in general, time-dependent problems in which the number of states and/or data storage requirements increases exponentially with small increases in the problems' parameters or dimensions; sometimes referred to as ***combinatorial explosion***." [EORMS, 333]

D

Decision analysis. See [EORMS, 367]

Decision problem. "The basic decision problem is as follows: Given a set of r alternative actions $A = \{a_1, \ldots, a_r\}$, a set of q states of nature $S = \{s_1, \ldots, s_q\}$, a set of rq outcomes $O = \{o_1, \ldots, o_{rq}\}$, a corresponding set of rq payoffs $P = \{p_1, \ldots, p_{rq}\}$, and a decision criterion to be optimized, $f[a_j]$, where f is a real-valued function defined on A, choose an alternative action a_j that optimizes the decision criterion $f[a_j]$." [EORMS, 386]

Decision variables. "The variables in a given model that are subject to manipulation by the specified decision rule." [EORMS, 395]
The input variables that are changed by the optimization algorithm to find a feasible optimal solution to the problem.
See also ***controllable variables***.

Deep uncertainty. See [EORMS 396]

Degradation *of performance*. Lowering of the performance due to wear of the product, but which does not prevent its operability, in contrast to ***failure***. Without failure, the lifetime is determined by the rate of degradation and the minimal (guaranteed) specifications.

Design variables. Variables describing the design of a product. They must be chosen *before* the final manufacture of the product. By opposition to operating variables, they cannot be changed once the product is in operation. The designer has a direct influence

on them, although they may be interdependent. Typically hardware as opposed to software. Example: geometry, material, chemical treatment, etc. of a component.

Deterministic algorithm. An algorithm that does not employ probabilistic elements (as opposed to a ***probabilistic algorithm***).

Deterministic model. "A mathematical model in which it is assumed that all input data and parameters are known with certainty [i.e., they are not random variables, as opposed to a ***stochastic model***]." [EORMS, 409]

Deterministic optimization. Optimization that does not involve random variables, neither in the objective function, nor in the constraint functions. The search process (algorithm) *may* however introduce randomness. For differentiation, the latter kind of optimization are sometimes called *stochastic optimization*; but not in this thesis.
See also ***stochastic optimization***.

Deterministic programming. A mathematical programming problem in which not any of the data are random variables, as opposed to ***probabilistic programming***.

Deviation variables. "Variables used in goal programming models to represent deviation from desired goals or resource target levels." [EORMS, 412]

Distributor. Part of a ***manifold*** which is inside each cell element (xy-plane).

Durability *of performance*. Property (quality) of the product regarding its ability to maintain performance with time, which means low degradation of performance.

E

Efficient solution (**non-dominated** or **Pareto-optimal solutions**). See [EORMS, 476]

Epistemic uncertainty. An uncertainty arising from a lack of knowledge in a given context, whether this lack is "chosen" or not. An epistemic uncertainty is therefore a *reducible uncertainty* and is sometimes called a *systematic uncertainty*, due to the closeness to the concept of a ***systematic error***.
See also ***aleatory uncertainty***.

Exactness *of a computation / model (formulation), exact(ly)*. Closeness of agreement between the (average of an infinite number of replicate) computed value and a reference value. [inspired from the IVM, trueness of a measurement]
The IVM defines *true value* and *trueness of measurement*. In this document, we extend the usage of *exact value* to the model itself — *exact model* — because we wish to emphasize where the uncertainties are formed, in addition to where they are contained, and appear.
We chose to use *exactness* instead of *trueness* in the context of computerized experiment for essentially two reasons: 1) because the notion of an "exact" mathematical model seems more self-explanatory to us than one of a "true" model ; and 2) to mark the distinction between experimental (physical) model and computerized (mathematical) model, where the latter is usually deterministic — leading to cancellation of the phrase in parenthesis, since the average reduces to any realization of the model

in a deterministic context.
See also ***accuracy***, ***trueness***, and ***precision***.

Explanatory modelling and analysis. See [EORMS, 532]

F

Failure. Any reason which makes the product completely inoperable (i.e., cannot satisfy minimal specifications), so that it requires a repair or a replacement.

Failure-rate function. See [EORMS, 552]

Feasible region. "The set of points that satisfy prescribed restrictions (constraints) on a solution." [EORMS, 533]

Feasible solution. "A solution to an optimization problem that satisfies its constraints. In linear programming, these are the conditions $\boldsymbol{A}\,\boldsymbol{x} = \boldsymbol{b}$ and $\boldsymbol{x} \geq \boldsymbol{0}$." [EORMS, 534]

Flop/s. Floating-point operations per second are a measure of the performance of a computer. The maximum theoretical number of flop/s achievable on common computer architecture is given by: FLOPS = sockets × cores/socket × cycles/s × FLOPs/cycle. In real application, the maximum is much lower because of all sources of limitations such as memory bandwidth. [Wikipedia]

Fuel utilization.
Ratio of the fuel that is consumed by the electrochemical reactions into the fuel cells, with respect of the fuel that is injected into it. So the fuel utilization is the ratio between the *actual* current and the theoretical current (maximal), which could be obtained if the total fuel flow were converted into electricity. The fuel utilization can be thought of as the current-efficiency, part of the electrical efficiency.

Framing. "Refers to how a problem is presented to decision makers, or how they formulate it in their minds." [EORMS, 609]

G

Global maximum (minimum). "For an optimization problem, the largest (smallest) value that the objective function can achieve over the feasible region." [EORMS, 649]

Gradient vector. [EORMS, 661]

H

Heavy-tailed distribution. "A probability distribution that has more probability in its tail than exponentially decaying densities such as the normal (Gaussian) and exponential distributions. Sometimes also called fat-tailed distribution, particularly in the finance community. The detailed technical definition may differ in the literature, but a commonly used one is the following: The cumulative distribution function F is heavy-tailed if there exists a $\gamma > 0$ such that

$$\lim_{x \to \infty} e^{\gamma\, x}\, F^{\mathrm{c}}[x] = \infty$$

where the superscript c denotes the complement. Special cases include long-tailed

distributions and sub-exponential distributions. The most commonly known heavy-tailed distributions are also long-tailed and sub-exponential, including the lognormal, Pareto, and Weibull with certain shape parameter values (one-tailed), and the student-t, Cauc[h]y, and family of stable distributions (two-tailed)." [EORMS,662]

Hessian matrix. See [EORMS, 694]

Heuristic procedure. "For a given problem, a collection of rules or steps that guide one to a solution that may or may not be optimal. The rules are usually based on the problem's characteristics, intuition, hunches, good ideas, or reasonable processes for searching." [EORMS, 695]

I

Importance sampling. "In stochastic or Monte Carlo simulation, a variance reduction technique whereby the underlying probability distribution is altered to increase the probability of (1) simulating events of highest interest, such as rare events, or (2) sampling from regions that have a larger effect on the quantity being estimated, such as a high-dimensional integral." [EORMS, 750]

Imputation of data. Imputation, also known as Winsorisation, is a method of censoring data. Ideally, only aberrant, obviously wrong data, are imputed, not outliers. "Note that Winsorising [imputing] is not equivalent to simply excluding data, which is a simpler procedure, called trimming or truncation. In a trimmed estimator, the extreme values are discarded; in a Winsorized [imputed] estimator, the extreme values are instead replaced by certain percentiles (the trimmed minimum and maximum)." [Wikipedia]

Inactive constraint. "An inequality constraint of an optimization problem that is satisfied as a strict inequality." [EORMS, 750]
See also ***active constraint***.

(In)dependent variables. Variables that are *statistically* (in)dependent.
Also often used in literature as meaning input (output) variables of a function (or system, model, …), although input variables are not necessarily statistically independent. For this reason, we prefer to use "input variables" in that case.
If X and Y are independent random variables, then the expectation operator has the property $E[X\,Y] = E[X]\,E[Y]$ and the covariance $\mathrm{cov}[X, Y] = 0$. However, a null covariance (no linear correlation) does not imply independence. [Wikipedia]

Integer and combinatorial optimization. See [EORMS, 771]

Interval of confidence. The interval of confidence is defined as $[m - d\,; m + d]$, with m the variable of interest and d the ***margin of error***. An interval of confidence is computed for a chosen ***level of confidence*** $(1 - \alpha)$.

Inverse transform method. "In stochastic or Monte Carlo simulation, a method for sampling from a given probability distribution by using random numbers transformed by the inverse of the cumulative distribution function." [EORMS, 815]

J

K

Karush-Kuhn-Tucker (KKT) conditions. "The KKT conditions are necessary conditions that a solution to a general nonlinear-programming problem must satisfy, provided that the problem constraints satisfy a regularity condition called constraint qualification. If the problem is one in which the constraint set (i.e., solution space) is convex and the maximizing (minimizing) objective function is concave (convex), the KKT conditions are sufficient. Applied to a linear-programming problem, the KKT conditions yield the complementary slackness conditions of the primal and dual problems." [EORMS, 833]

L

Lagrange multipliers. "The multiplicative, linear-combination constants that appear in the Lagrangian of a mathematical programming problem. They are generally dual variables if the dual exists, so-called shadow prices in linear programming, giving the rate of change of the optimal value with constraint changes, under appropriate conditions." [EORMS, 845]

Level of confidence. $(1 - \alpha)$.
See also ***interval of confidence***.

Lifetime. The time during which the product can work under acceptable conditions. These acceptable conditions may vary, but typically, it means for a fuel-cell that it should be able to supply for instance ca. 80 % of its nominal (rated) power.

Likelihood ratio method. "A method for gradient estimation in simulation used for sensitivity analysis and optimization; also known as the score function method." [EORMS, 880]

Linear programming. See [EORMS, 882]

Local maximum. "A function $f[\boldsymbol{x}]$ defined over a set of points S is said to have a local maximum at a point $\boldsymbol{x}_0$ in S if $f[\boldsymbol{x}_0] \geq f[\boldsymbol{x}]$ for all $\boldsymbol{x}$ in a neighbourhood of $\boldsymbol{x}_0$ in S. The point $\boldsymbol{x}_0$ is referred to as a local optimum (maximum)." [EORMS, 891] For a local minimum, replace $\geq$ by $\leq$.

Lower-bounded variables. See [EORMS, 908]

M

Manifold. A mechanical part whose geometry is such that fluid is split or combined.
In this document, *distribution columns* refers specifically to the part of manifolds, which supply to and collect from each cell element of the stack (principal flow direction in z). We use *distributor* to refer to the part of the manifold which is inside each cell element (xy-plane), and *performance.* in this document, performance usually relates to all quantities of interest which describe the "output" of the (fuel cell) product

at a given time. that is, mainly, electrical power and efficiency. sometimes, *performance* is used more broadly, referring to the "selling specifications" or "qualities" of a product, such as lifetime, size, and cost.

plenum chamber to refer to a part of the distributor which is a stabilization/mixing chamber, when these parts exist.

Markov Chain Monte Carlo (MCMC). See [EORMS, 925]

Mathematical model. "An idealized — abstract and simplified — [mathematical] representation of a real-world situation that is to be studied and/or analysed. Models can be classified in many ways. […] a symbolic or mathematical model represents a symbolic representation of the process under investigation, e.g., Einstein's equation $E = m\,c^2$, a linear-programming model, or a computer simulation model. […] In operations research/management science, mathematical models take on varied forms (e.g., linear programming, queueing, Markovian systems), many of which can be applied across application areas. The basic OR/MS mathematical model can be described as the decision problem of finding the maximum (or minimum) of a measure of effectiveness (objective function) $E = F[X, Y]$, where X represents the set of possible solutions (alternative decisions) and Y the given conditions of the problem. Although a rather simple model in its concept, especially since it involves the optimization of a single objective, this mathematical decision model underlies most of the problems that have been successfully formulated and solved by OR/MS methodologies." [EORMS, 949, 983]
Numerical model is usually understood as the implementation of a mathematical model in a computer code.

Maximum. A function $f[x]$ is said to have a maximum on a set S when the least upper bound of $f[x]$ on S is assumed by $f[x]$ for some x^0 in S. Thus, $f[x^0] \geq f[x]$ for all x in S. [Minimum: *lower* instead of *upper* and $\leq$ instead of $\geq$] [EORMS, 958]

Measurand. "Quantity intended to be measured (computed)" [We may suggest *computand* as an equivalent in computational context; otherwise, measurand extends to it]. [IVM]

Measured [computed] value. "value of a measured [computed] quantity". [IVM]

Measure of effectiveness (MOE). "In a decision problem, the single objective that is to be optimized is called the measure of effectiveness (MOE). In a linear-programming problem, the MOE is the objective function." [EORMS, 959]

Metaheuristics. See [EORMS, 960]

Metamodeling. "For simulation models, the objective is to provide an explicit input-output relationship through a fitted mathematical function, e.g., using statistical regression, splines, neural networks, or kriging. Differs from the use of the term in computer science." [EORMS, 970]

Minimum (maximum) feasible solution. "In a mathematical-programming problem, the solution that both satisfies the constraints of the problem and minimizes (maximizes) the objective function is a minimum (maximum) feasible solution. Such solutions may not be unique." [EORMS, 981]

Model evaluation. See [EORMS, 984]

Monte Carlo methods. "General term used to refer to the use of random numbers in a particular methodology, e.g., evaluating a high-dimensional deterministic integral or carrying out a randomized algorithm or simulation of a stochastic system, all based on statistical sampling techniques. The term "Monte Carlo" signifies the random or uncertain component that characterizes the method and was coined in the 1940s by physicists working on the Manhattan nuclear weapons project, an allusion to gambling in Monte Carlo casinos.
One of the strengths of the Monte Carlo method is that in many applications its computational burden grows only linearly in the dimension of problems where other methods suffer from an exponential (geometric) growth in computation." [EORMS, 991]

Monte Carlo simulations. "Simulation of systems modelled using random variables and/or stochastic processes. The underlying inputs are generally random numbers, sequences of independent and identically distributed random variables uniformly distributed on the unit interval.. Monte Carlo simulation is one of the most widely used tools in operations research and management science (OR/MS) and can be used to provide detailed models of complex systems arising in various OR/MS fields from manufacturing to transportation to computer/communications networks to financial engineering. […]" [EORMS, 992]

Multi-objective programming. See [EORMS, 996]

Multiple criteria decision making. See [EORMS, 1007]

Multivariate quality control. See [EORMS, 1014]

N

Near-optimal solution. "For an optimization problem, a near-optimal solution is a feasible solution with an objective function value within a specified range from the (usually unknown) optimal objective function value." [EORMS, 1025]

Network optimization. See [EORMS, 1026]

Neural networks. See [EORMS, 1042]

Nominal value (of a quantity). "Rounded or approximate value of a characterizing quantity of a (measuring instrument or measuring) system that provides guidance for its appropriate use." Should not be confused with *nominal property* of a phenomenon, body, or substance, where the property has no magnitude (but a "name"). [IVM]

Nonlinear programming. See [EORMS, 1053]

Numerical analysis. See [EORMS, 1064]

O

Objective function. "The mathematical expression that is to be optimized (maximized or minimized) in an optimization problem." [EORMS, 1069]

Open-source software (for OR). See [EORMS, 1070]

Operating variables. Variables that can change after the manufacture of the product, and which determine its state. They are either controlled (e.g., flow rates) or not (e.g., ambient temperature surrounding the system). Other examples: Fuel composition, inlet air temperature, level of pressure.

Opportunity cost. "The cost associated with forgoing an opportunity; the money or other value sacrificed by choosing a non-optimal course of action. In linear programming, the opportunity cost is the reduced cost of a variable not in the optimal basic solution. If a unit of a non-basic variable is introduced into the solution, the optimal value of the objective function would decrease by an amount equal to the associated reduced cost." [EORMS, 1091]

Optimal computing budget allocation. See [EORMS, 1091]

Optimal feasible solution. "For an optimization problem, an optimal feasible solution is a solution that satisfies all the constraints of the problem and optimizes the objective function." [EORMS, 1091]

Optimal value. "The best value that can be realized or attained; for a mathematical programming problem, the minimum or maximum value of the objective function over the feasible region." [EORMS, 1092]

Optimal value function. "The optimal value of a mathematical programming problem as a function of problem parameters, such as objective function coefficients. Also the name given to the function satisfying the Bellman optimality equation in a Markov decision process or dynamic program, especially in a revenue/profit maximization problem; otherwise sometimes known as the optimal cost-to-go function for a cost minimization problem." [EORMS, 1092]

Optimality criteria. "Mathematical conditions used to test whether or not a given feasible solution is optimal in an optimization problem. Examples include the Karush-Kuhn-Tucker conditions for some nonlinear-programming problems; the simplex algorithm test applied to the reduced costs of the non-basic variables for linear-programming problems; the Bellman optimality equation for dynamic programming, and the Hamilton-Jacobi-Bellman equation for optimal control." [EORMS, 1092]

Optimization. "The process of searching for the best value that can be realized or attained. In mathematical programming, this [best value] is the minimum or maximum value of the objective over the feasible region." [EORMS, 1092]
Usually, the term *optimization* is used in this thesis with the meaning of using an algorithm (mathematical programming). In contrast, *improvement* does not involve an algorithm. Although *optimization* is the process of searching for the best (optimal) value, we may decide to stop the process when satisfied with the current best value.

Optimizer (minimizer, maximizer). Value of the decision variables corresponding to a (local) optimum of the objective function.

Optimum. Optimal value (of the objective function over the feasible region).

Ordinal optimization. "In the simulation optimization setting, an approach that exploits the property that it is easier to select the correct order among noisy measurements than to obtain precise estimates, i.e., ordering converges faster (exponentially) than estimation." [EORMS, 1093]

Output quantities (in a measurement [computational] model). "Quantity, the measured [computed] value of which is calculated using the values of *input quantities* in a measurement [computational] model. [IVM]

P

Parallel computing. See [EORMS, 1103]

Parameter. "A quantity appearing in a mathematical model that is subject to controls beyond those affecting the ***decision variables***." [EORMS, 1107] Parameters are not variables *stricto sensu* , i.e. they are constant in a realization of a model. Caution: "parameter" is also used in the statistical framework to describe a *population* (its distribution) with a numerical characteristic.

Pareto-optimal solution. "If a feasible deviation from a solution to a multi-objective problem causes one of the objectives to improve while some other objective degrades, the solution is termed a Pareto-optimal. Such a solution is also called an *efficient or non-dominated solution*." [EORMS, 1112]

Performance. In this document, performance usually relates to all quantities of interest which describe the "output" of the (fuel cell) product at a given time. That is, mainly, electrical power and efficiency. Sometimes, *performance* is used more broadly, referring to the "selling specifications" or "qualities" of a product, such as lifetime, size, and cost.

Plenum chamber. Part of a ***distributor*** which is a stabilization/mixing chamber.

Post-optimal analysis. "The study of how a solution changes with respect to (usually) small changes in the problem's data. In particular, this term is applied to the *sensitivity analysis* and parametric analysis of a solution to a linear-programming problem." [EORMS, 1148]

Precision, *precise(ly);*

of a measurement. "Closeness of agreement between indications or measured quantity values obtained by replicate measurements on the same or similar objects under specified conditions." [IVM]

of a computation. Resolution of the representation, depending typically on the number of significant digits, on the discretization, and other similar characteristics of numerical implementation of a mathematical model. [adapted from Wikipedia]
See also ***accuracy***, ***exactness***, and ***trueness***.

Practice of OR and MS. See [EORMS, 1148]

Predictive model. "A model used to predict the future course of events and as an aid to decision making." [EORMS, 1156]

Prescriptive model. "A model that attempts to describe the best or optimal solution of a man/machine system. For a decision problem, such a model is used as an aid in selecting the best alternative solution." [EORMS, 1159]

Probabilistic algorithm. "An algorithm that employs probabilistic elements (as opposed to a ***deterministic algorithm***)." [EORMS, 1161]

Probabilistic programming. "A mathematical programming problem in which some or all of the data are random variables [as opposed to ***deterministic programming***]." [EORMS, 1161]

Probability density function (PDF). Derivative $f(x)$ of a cumulative probability distribution function $F(x)$, when it exists." [EORMS, 1161]

Probability distribution. "Term used (loosely) to refer to a function describing the probabilistic behaviour of a random variable; could refer to the probability measure, the cumulative distribution function (CDF), the probability mass function (PMF) for discrete random variables, or the probability density function (PDF) for continuous-valued random variables." [EORMS, 1162]

Q

Quadratic programming. See [EORMS, 1207]

Quality. Quality is a fuzzy concept. Although, by definition, a quality is not a quantity — and therefore cannot be expressed with numbers nor units, or may not even have a magnitude — *to quantify the quality of a product (or a service) is often desirable*. Quantifiable indicators of quality can be estimated for that purpose. For instance, lifetime is quantifiable and can be associated to "one particular quality" of a product.

Quality control. See [EORMS, 1215]

Quantity. "Property of a phenomenon, body, or substance, where the property has a magnitude that can be expressed as a number and a reference." [IVM, 2]

Quantity of interest (QOI). Any quantity (variable) whose value is important to take a decision. It can be both input and output, it often appears explicitly in the objective function or in the constraints of an optimization problem.

R

Random error. "Component of measurement error that in replicate measurements varies in an unpredictable manner." [IVM]
See also ***systematic error*** and ***aleatory uncertainty.***

Random field. "A ***stochastic process*** with a multi-dimensional index set; for example, $\{R[x,y],\ -\infty < x,y < \infty\}$, where $R[x,y]$ equals the amount of rain falling during a given day at location (x,y)." [EORMS, 1256]

Random search. "A search algorithm that uses probabilistic sampling to select search points from a neighbourhood of the current solution(s)." [EORMS, 1263]

Random variates. "Random values generated according to a specified probability distribution, corresponding to the outcomes of a random variable. Generally, this is realized on a computer through a transformation from IID pseudorandom numbers. The most commonly used procedures are the inverse transform method (inversion) and acceptance-rejection (rejection methods)." [EORMS, 1263]

Randomized algorithm. "An algorithm that employs a probabilistic element in its procedure, as in Monte Carlo sampling implemented using a random number generator. Thus the performance of the algorithm, in terms of results returned and computation time, will be random variables. Examples include random search, evolutionary algorithms, model-based algorithms, and algorithms based on swarm intelligence." [EORMS, 1264]

Reasoning. "A problem-solving process. Two paradigms are logical and analogical reasoning. *Logical reasoning* includes deductive and inductive. *Deductive reasoning* is arriving at a conclusion from premises and rules of inference. *Inductive reasoning* is forming a general conclusion that explains multiple observations. *Analogical reasoning* uses analogy of a current situation to familiar ones from previous experiences. One paradigm for analogical reasoning is a neural network." [EORMS, 1280]

Redundancy. See [EORMS, 1280]

Redundant constraint. "An inequality or equation of a mathematical programming problem that does not define part of the solution space. An equivalent problem can be formed by removing redundant constraints." [EORMS, 1282]

Regression analysis. See [EORMS, 1289]

Reliability, *reliable.* "The ability of a component or system to be operable when called upon to do its intended job. Reliability is most often quantified as the probability that the component or system has not failed (is alive) at a particular time: $R[t] = \Pr\{\text{ lifetime} > t\ \} = 1 - F[t]$, where F is the cumulative distribution function of the lifetime of the component or system. This reliability function is often also called the survival function." [EORMS, 1292]

Reliability is a quality of a product characterizing its ability to work without ***failure*** during a specified *duration* (time). This definition is somehow overlapped with that of ***robustness***, but with emphasizes on the notion of *duration* rather than that of *insensitivity*.

Reliability of stochastic systems. See [EORMS, 1292]

Research and development. See[EORMS, 1298]

Response surface methodology. See [EORMS, 1307]

Risk assessment. See [EORMS, 1331]

Robust optimization. See [EORMS, 1346]

Robustness, *robust.* Quality of the product regarding its ability to *maintain performance under uncertainty*, which means that its sensitivity to them is low. This definition is somehow overlapped with that of ***reliability***, but with emphasizes on the notion of *insensitivity* rather than that of *duration*. Durach [98] suggested that robustness has two dimensions: resistance and avoidance.

Robustness analysis. See [EORMS, 1346]

Round-off error. "The computational error due to the significant-digit arithmetic inherent in digital calculations." [EORMS, 1347]

S

Sample average approximation. See [EORMS, 1350]

Satisficing. "In a decision problem, the selection by the decision maker (DM) of a satisfactory alternative as opposed to the selection of an "optimal" alternative. Here, the DM sets aspiration levels or acceptable levels on the outcomes and chooses the (first) alternative that satisfies these levels. This compromise selection is due to the DM's inability to encompass all the complexities of the decision problem and/or lack of a method that can determine an optimal solution [in an acceptable time and budget]. The concept is due to Herb Simon (1955, 1957)." [EORMS, 1355]

Scaling. "The pre-solution transformation of the data of a problem that attempts to make the magnitudes of all the data as close as possible. Such scaling is important for mathematical- and linear-programming problems as it helps to reduce ***round-off error***. Most mathematical-programming systems have a SCALE command that automatically adjusts the magnitudes of the data in the rows and columns. This can be done by multiplying the technological coefficient matrix $\boldsymbol{A}$ by suitable row and column transformation matrices. A frequently used scaling algorithm is to divide each row by the largest absolute element in it, and then divide each resulting column by the largest absolute element in it. This ensures that the largest absolute value in the matrix is 1.0 and that each column and row has at least one element equal to 1.0." [EORMS, 1356]

Scenario. "The set of conditions and characteristics that define the situation or environment under which a system or policy has to perform. There is often a *baseline scenario* (what will happen if trends continue) and an *ideal scenario* (what future one would like to have). In ***stochastic programming***, a scenario represents a possible future uncertain outcome (or sample path)." [EORMS, 1356]

Sensitivity, sensitive. "Quotient of the change in an indication of a measuring system and the corresponding change in a value of a quantity being measured." [IVM]
More generality, the sensitivity of y to x is the ratio of the change of an output quantity y when an input quantity x is changed. At a point x_0, the local sensitivity is the partial derivative $\partial y/\partial x|_{x_0}$.

Sensitivity analysis. See [EORMS, 1379]

Simulated annealing. See [EORMS, 1395]

Simulation metamodeling. See [EORMS, 1404]

Simulation of stochastic discrete-event systems. See [EORMS, 1410]

Simulation optimization. See [EORMS, 1418]

Simulator. An artificial means used to represent the functioning of a real-world system, generally falling into two categories: *physical simulator* (e.g., a bench to test a single-cell element of a fuel-cell system, a scaled dam) and *computer simulator*. The latter is made of a *computer code* (software), which is an *implementation* of a ***mathematical model*** of the system, and is run on some computer(s) (hardware). [adapted to the context of this document from EORMS, 1423]
Deterministic computer models are sometimes excluded from this definition. Besides, in this document, a particular simulator is defined by ***attributes*** having a particular set of values, whereas such a *single* simulator may be used to carry out *N simulations* with *N* deterministic sets of values of "real-world" quantities.

Slack variable. See [EORMS, 1424]

Solution. "A set of values for the variables of a problem that satisfy all the constraints of the problem." [EORMS, 1437]

Solution space. "For a constrained mathematical programming problem, the solution space is a portion of Euclidean space defined by all the constraints of the problem. For a linear-programming problem, the solution space is defined by the intersection of the nonnegative portion of Euclidean space and the constraints of the problem." [EORMS, 1437]

Splines. See [EORMS, 1443]

Stationary stochastic process. "A stochastic process in which the state probability distributions are invariant over time"

Statistic. A quantity characterizing (statistical) data, calculated from *sample* data. For instance, the arithmetic mean and the standard deviation are two different statistics. When calculated from a *population*, the term (statistical) *parameter* is sometimes used instead. Of course, statistics (always plural) is also "the study of the collection, analysis, interpretation, presentation, and organization of data" [99].

Stochastic approximation. See [EORMS, 1470]

Stochastic input model selection. See [EORMS, EORMS, 1476]

Stochastic model. "A mathematical model in which some data and parameters are random variables." [EORMS, 1486]

Stochastic optimization. "Optimization in which the objective function and/or constraint functions are "noisy," i.e., involve random variables (e.g., expected values) that cannot be evaluated analytically and thus require estimation, such as through simulation of a stochastic system. Sometimes the term is also used to refer to deterministic optimization problems that introduce randomness in the search process, i.e., the resulting procedures are randomized algorithms for optimization." [EORMS, 1486]
See also s***imulation optimization***.

Stochastic process. "A set of random variables indexed over a parameter set that is either discrete or continuous and often represents some concept of time." [EORMS, 1486]

Stochastic programming. See [EORMS, 1486]

Structural variables. "The original variables of a linear-programming problem as differentiated from *slack*, *surplus* and *artificial variables*. Structural variables are usually the variables of interest and have a physical interpretation such as production or shipments. They appear in the original defining inequalities or equations prior to the conversion of the problem to all equations." [EORMS, 1499]

Subjective probability. See [EORMS, 1504]

Sub-optimization. "The finding of a solution to an optimization problem by a procedure that does not guarantee that the solution will be optimal. The procedure usually includes heuristic rules that help eliminate the generation of poor solutions." [EORMS, 1504]

System. "A set of related elements organized to achieve a purpose." [EORMS, 1519]

Systematic error. "Component of measurement error that in replicate measurements remains constant or varies in a predictable manner." [IVM]
See also ***random error*** and ***epistemic uncertainty*.**

T

Tabu search. See [EORMS, 1537]

Theory of constraints. See [EORMS, 1545]

Tolerance, dimensional. Tolerance about the angular and linear dimensions.

Tolerance, geometric. Tolerance about property of the geometry but not directly to dimensions. Property such as perpendicularity, parallelism, planarity, concentricity.

Total quality management. See [EORMS, 1556] (also Taguchi loss function)

Total cost of ownership. The cost of using a product, until (but not including) its disposal. This includes the *fixed costs of investment* for the owner (including all components constituting the price at which the seller agrees to sell: R&D, production, marketing, storage, margin, etc.) and the *operating cost* (resources consumed in operation, maintenance, etc.).
See also ***cost of production***.

Tractability, *tractable*. Characteristic of how easily an action can be done. In our case, solving a problem by using computer means, such as simulations, uncertainty quantification, optimizations, etc. A measure of it (typically including CPU-time and RAM). We do not use here the definition specific to the theory of computational complexity (i.e., that a tractable problem can be solved in polynomial time).

Trueness. "Closeness of agreement between the average of an infinite number of replicate measured value and a reference value." [IVM]
See also ***accuracy***, ***exactness***, and ***precision***.

U

Uncertain variables. Variables whose value is not known with certainty; which is stochastic and considered as such, rather than deterministic *or* assumed as such.

Uncertainty (o**f** a measurement [computation]). "non-negative parameter characterizing the dispersion of the values of the quantity being attributed to a measurand, based on the information used." [IVM]

Uncertainty quantification (UQ). Uncertainty quantification is an elaborated version of sensitivity analysis. Whereas sensitivity analysis usually looks at a small set of input variations around a nominal value (e.g., extreme cases, or $\pm$ 10 %), the purpose of UQ is to characterize the statistical distribution of the random variable. Besides, uncertainty quantification involves the characterization of both input and output variables.

Uncontrollable variables. "In a decision problem, variables and other elements of a decision problem that are not under the control of the decision maker." [EORMS, 1587]

Unrestricted variable. "A variable that can take on any value." [EORMS, 1588]

Utility theory. See [EORMS, 1593]

V

Vagueness. Lack of knowledge to conclude.
See also ***ambiguity***.

Validation. "The process of determining how well a mathematical model of a real-world system conforms to reality for the purposes of the study being undertaken. Two key aspects of validity are face validity and predictive validity. *Face validity* is based on an examination of the assumptions and data going into the model for logical consistency and the review of the results by experts knowledgeable in the real-world situation. *Predictive validity* is based on examining the model's predictions for events that were not used in building the model." [EORMS, 1597]
To distinguish validation from verification, this mnemonic expression is often used: "Solve the right equations (validation), versus solve the equations right (verification)."

Value function. "In a decision problem, let a be a feasible alternative from the set of all feasible alternatives A. Each alternative is measured against n attributes $\{X_1, \ldots, X_n\}$. The decision maker's (DM) problem is to choose an alternative $a \in A$ that maximizes the payoff vector of scores $\{X_1[a], \ldots, X_n[a]\} = \boldsymbol{X}[a]$. The value function is a real-valued, scalar function $v[\cdot]$ with the property that $v\big[\boldsymbol{X}[a]\big] > v\big[\boldsymbol{X}[b]\big]$ if and only if the DM prefers alternative a to alternative b; and $v\big[\boldsymbol{X}[a]\big] = v\big[\boldsymbol{X}[b]\big]$ if and only if the DM is indifferent between alternative a and alternative b. A similar concept can be found in dynamic programming and Markov decision processes." See [EORMS, 1598]

Variability. In this document, variability is used as a shorthand synonym for ***aleatory uncertainty***, or more precisely, as the variation of the values of an aleatory uncertain quantity (random variable).

Variables. See ***design v.***, ***decision v.***, ***controllable v.***, ***random v.***, ***uncertain v.***, ***uncontrollable v.***, and ***parameters***.

Variance reduction techniques in Monte Carlo methods. See [EORMS, 1598]

Verification. "For a mathematical model, especially a computer-based one such as a simulation model, verification is the process by which the computational procedure (computer program or software) is checked to determine if it is error free (debugged) and the determination that the model, as represented by the calculations or software, does what the analyst intended. A model is said to be verified if it (the computation) correctly executes the intended calculations." [EORMS, 1618]
To distinguish verification from validation, this mnemonic expression is often used: "Solve the equations right (verification), versus solve the right equations (validation)."

Verification, validation, and testing of models. See [EORMS, 1618]

Visualisation. See [EORMS, 1627]

W

Worst-case analysis. "For an algorithm and associated problem, the determination of an upper bound on the number of steps that the algorithm can take on any instance of the problem. For an optimization problem and an associated heuristic or suboptimal algorithm, worst-case analysis may include a statement regarding bounds on how far the objective function value for the solution returned by the algorithm can be from the true optimal value." [EORMS, 1641]

X

Y

Yield. In the context of industrial production, the number of units that satisfy the criteria of a quality-control divided by the total number of units controlled.
Yield = accepted units over controlled units.

Z

Bibliographic references

[1] Sutherland, R., 2014, "This Thing For Which We Have No Name," Edge.org [Online]. Available: http://edge.org/conversation/rory_sutherland-this-thing-for-which-we-have-no-name. [Accessed: 15-Oct-2015].

[2] Bertoldi, M., Bucheli, O., Ravagni, A., Autissier, N., Signorini, M., and Modena, S., 2009, "Status Report of SOFC Development and Pilot Manufacturing at SOFCpower Srl," ECS, pp. 105–114.

[3] Du, B., Guo, Q., Pollard, R., Rodriguez, D., Smith, C., and Elter, J., 2006, "PEM fuel cells: status and challenges for commercial stationary power applications," JOM J. Miner. Met. Mater. Soc., **58**(8), pp. 45–49.

[4] Ellis, M. W., Gunes, M. B., Thompkins, D., and Uselton, R., 2002, "Status of fuel cell systems for combined heat and power applications in buildings," ASHRAE Trans., **108 PART 1**, pp. 1032–1044.

[5] Sasaki, H., and Takasu, K., 1997, "Status of SOFC development in Japan," Proc. Fifth Int. Symp. Solid Oxide Fuel Cells Sofc-V, **97**(40), pp. 12–19 1398.

[6] Larsen, P. H., Bagger, C., Linderoth, S., Mogensen, M., Primdahl, S., Jorgensen, M. J., Hendriksen, P. V., Kindl, B., Bonanos, N., Poulsen, F. W., and Maegaard, K. A., 2001, "Status of the Danish SOFC program," Solid Oxide Fuel Cells Vii Sofc Vii, **2001**(16), pp. 28–37 1104.

[7] Wuillemin, Z., Ceschini, S., Antonetti, Y., Beetschen, C., Modena, S., Montinaro, D., Cornu, T., Bucheli, O., and Bertoldi, M., 2014, "High-performance SOFC stacks tested under different reformate compositions," Proceedings of the 11th European SOFC and SOE Forum, Lucerne, Switzerland, pp. 1–10.

[8] SOLIDpower, 2015, "Solidpower," Solidpower [Online]. Available: http://www.solidpower.com/en/home/. [Accessed: 10-Dec-2015].

[9] Bacon, F. T., 1969, "Fuel cells, past, present and future," Electrochimica Acta, **14**(7), pp. 569–585.

[10] SwissHydrogen SA, 2015, "Fuel Cell Range Extender for Electric Vehicle."

[11] PROSOFC collaborators, 2015, "Production and Reliability Oriented SOFC Cell and Stack Design (PROSOFC)."

[12] Wuillemin, Z., 2009, "Experimental and modeling investigations on local performance and local degradation in solid oxide fuel cells," Ecole Polytechnique Fédérale de Lausanne (EPFL).

[13] Wuillemin, Z., Autissier, N., Nakajo, A., Luong, M., Van herle, J., and Favrat, D., 2008, "Modeling and Study of the Influence of Sealing on a Solid Oxide Fuel Cell," J. Fuel Cell Sci. Technol., **5**(1), pp. 011016–9.

[14] Nakajo, A., Wuillemin, Z., Van herle, J., and Favrat, D., 2009, "Simulation of thermal stresses in anode-supported solid oxide fuel cell stacks. Part II: Loss of gas-tightness, electrical contact and thermal buckling," J. Power Sources, **193**(1), pp. 216–226.

[15] Nakajo, A., Wuillemin, Z., Van herle, J., and Favrat, D., 2009, "Simulation of thermal stresses in anode-supported solid oxide fuel cell stacks. Part I: Probability of failure of the cells," J. Power Sources, **193**(1), pp. 203–215.

[16] Haga, K., Adachi, S., Shiratori, Y., Itoh, K., and Sasaki, K., 2008, "Poisoning of SOFC anodes by various fuel impurities," Solid State Ion., **179**(27-32), pp. 1427–1431.

[17] Hilpert, K., Das, D., Miller, M., Peck, D. H., and Weiss, R., 1996, "Chromium vapor species over solid oxide fuel cell interconnect materials and their potential for degradation processes," J. Electrochem. Soc., **143**(11), pp. 3642–3647.

[18] Huang, C. M., Shy, S. S., and Lee, C. H., 2008, "On flow uniformity in various interconnects and its influence to cell performance of planar SOFC," J. Power Sources, **183**(1), pp. 205–213.

[19] Costamagna, P., Arato, E., Achenbach, E., and Reus, U., 1994, "Fluid dynamic study of fuel cell devices: simulation and experimental validation," J. Power Sources, **52**(2), pp. 243–249.

[20] Liu, D. 'an, Peng, L., and Lai, X., 2009, "Effect of dimensional error of metallic bipolar plate on the GDL pressure distribution in the PEM fuel cell," Int. J. Hydrog. Energy, **34**(2), pp. 990–997.

[21] Nelson, G. J., Peracchio, A. A., and Chiu, W. K. S., 2011, "Analytical investigations of varying cross section microstructures on charge transfer in solid oxide fuel cell electrodes," J. Power Sources, **196**(10), pp. 4695–4704.

[22] Cassenti, B. N., Nelson, G. J., DeGostin, M. B., Peracchio, A. A., and Chiu, W. K. S., 2014, "Analytical solutions for extended surface electrochemical fin models," J. Power Sources, **265**, pp. 282–290.

[23] Nelson, G. J., Nakajo, A., Cassenti, B. N., DeGostin, M. B., Bagshaw, K. R., Peracchio, A. A., Xiao, G., Wang, S., Chen, F., and Chiu, W. K. S., 2014, "A rapid analytical assessment tool for three dimensional electrode microstructural networks with geometric sensitivity," J. Power Sources, **246**, pp. 322–334.

[24] Jeon, D. H., 2009, "A comprehensive CFD model of anode-supported solid oxide fuel cells," Electrochimica Acta, **54**(10), pp. 2727–2736.

[25] Bi, W., Chen, D., and Lin, Z., 2009, "A key geometric parameter for the flow uniformity in planar solid oxide fuel cell stacks," Int. J. Hydrog. Energy, **34**(9), pp. 3873–3884.

[26] Lee, J.-H., Kim, H., Kim, H.-R., Son, J.-W., Kim, J., Lee, H.-W., and Song, H., 2007, "Performance and Reliability Improvement of Planar SOFC Stack with Advanced Design of Unit Cell and Sealing," ECS Transactions, ECS, Nara, Japan, pp. 295–300.

[27] Larrain, D., Van herle, J., and Favrat, D., 2006, "Simulation of SOFC stack and repeat elements including interconnect degradation and anode reoxidation risk," J. Power Sources, **161**(1), pp. 392–403.

[28] Wuillemin, Z., Faes, A., Diethelm, S., Nakajo, A., Autissier, N., Van herle, J., and Favrat, D., 2008, "Modeling of Local Cell Degradation in Solid Oxide Fuel Cells: Cumulative Effect of Critical Operating Points," 8th European Fuel Cell Forum 2008, Lucerne, Switzerland, pp. 1–12.

[29] Huang, C. M., Shy, S. S., Li, H. H., and Lee, C. H., 2010, "The impact of flow distributors on the performance of planar solid oxide fuel cell," J. Power Sources, **195**(19), pp. 6280–6286.

[30] Reinert, A., and Strohbach, T., 2009, "Determination of Global/local Fuel Utilization via Variation of Fuel Utilization," ECS Trans., **25**(2), pp. 811–814.

[31] Ramousse, S., Menon, M., Brodersen, K., Knudsen, J., Rahbek, U., and Larsen, P. H., 2007, "Manufacturing of Anode-Supported SOFC's: Processing Parameters and their Influence," ECS Transactions, ECS, Nara, Japan, pp. 317–327.

[32] Sun, X., Tartakovsky, A. M., and Khaleel, M. A., 2009, "Probabilistic-Based Design Methodology for Solid Oxide Fuel Cell Stacks," J. Fuel Cell Sci. Technol., **6**(2), pp. 021004–10.

[33] Wu, S. J., Shiah, S. W., and Yu, W. L., 2009, "Parametric analysis of proton exchange membrane fuel cell performance by using the Taguchi method and a neural network," Renew. Energy, **34**(1), pp. 135–144.

[34] Chen, Q., Zeng, M., Zhang, J., and Wang, Q., 2010, "Optimal design of bi-layer interconnector for SOFC based on CFD-Taguchi method," Int. J. Hydrog. Energy, **35**(9), pp. 4292–4300.

[35] Peng, L., Lai, X., Liu, D., Hu, P., and Ni, J., 2008, "Flow channel shape optimum design for hydroformed metal bipolar plate in PEM fuel cell," J. Power Sources, **178**(1), pp. 223–230.

[36] Peng, L., Liu, D., Hu, P., Lai, X., and Ni, J., 2010, "Fabrication of Metallic Bipolar Plates for Proton Exchange Membrane Fuel Cell by Flexible Forming Process-Numerical Simulations and Experiments," J. Fuel Cell Sci. Technol., **7**(3), p. 031009.

[37] Pornprasertsuk, R., Cheng, J., Huang, H., and Prinz, F. B., 2007, "Electrochemical impedance analysis of solid oxide fuel cell electrolyte using kinetic Monte Carlo technique," Solid State Ion., **178**(3-4), pp. 195–205.

[38] Seidenberger, K., Wilhelm, F., Schmitt, T., Lehnert, W., and Scholta, J., 2011, "Estimation of water distribution and degradation mechanisms in polymer electrolyte membrane fuel cell gas diffusion layers using a 3D Monte Carlo model," J. Power Sources, **196**(12), pp. 5317–5324.

[39] Subramanyan, K., Diwekar, U. M., and Goyal, A., 2004, "Multi-objective optimization for hybrid fuel cells power system under uncertainty," J. Power Sources, **132**(1–2), pp. 99–112.

[40] Subramanyan, K., and Diwekar, U. M., 2005, "Characterization and quantification of uncertainty in solid oxide fuel cell hybrid power plants," J. Power Sources, **142**(1-2), pp. 103–116.

[41] Zhao, D., and Xue, D., 2010, "Parametric design with neural network relationships and fuzzy relationships considering uncertainties," Comput. Ind., **61**(3), pp. 287–296.

[42] Hernandez, A., Hissel, D., and Outbib, R., 2006, "Fuel cell fault diagnosis: A stochastic approach," Industrial Electronics, 2006 IEEE International Symposium on, pp. 1984–1989.

[43] Gazzarri, J. I., and Kesler, O., 2008, "Short stack modeling of degradation in solid oxide fuel cells: Part II. Sensitivity and interaction analysis," J. Power Sources, **176**(1), pp. 155–166.

[44] Momma, A., Takano, K., Tanaka, Y., and Kato, T., 2009, "Uncertainty Analysis in SOFC Performance Testing," ECS Transactions, ECS, Vienna, Austria, pp. 369–376.

[45] Oliveira, S. P., Rocha, A. C., Couto, P. R. G., and others, 2009, "Uncertainty of measurement by Monte-Carlo simulation and metrological reliability in the evaluation of electric variables of PEMFC and SOFC fuel cells," Measurement, **42**(10), pp. 1497–1501.

[46] Putko, M. M., Taylor, A. C., Newman, P. A., and Green, L. L., 2002, "Approach for Input Uncertainty Propagation and Robust Design in CFD Using Sensitivity Derivatives," J. Fluids Eng., **124**(1), p. 60.

[47] Crossland, R., Williams, J. H. S., and McMahon, C. A., 2003, "An object-oriented modeling framework for representing uncertainty in early variant design," Res. Eng. Des., **14**(3), pp. 173–183.

[48] Huang, S. H., Liu, Q., and Musa, R., 2004, "Tolerance-based process plan evaluation using Monte Carlo simulation," Int. J. Prod. Res., **42**(23), pp. 4871–4891.

[49] Kumar, A., Nair, P. B., Keane, A. J., and Shahpar, S., 2008, "Robust design using Bayesian Monte Carlo," Int. J. Numer. Methods Eng., **73**(11), pp. 1497–1517.

[50] Witteveen, J. A. S., and Bijl, H., 2008, "A Monomial Chaos Approach for Efficient Uncertainty Quantification in Nonlinear Problems," SIAM J. Sci. Comput., **30**(3), p. 1296.

[51] Bowman, R. A., 2009, "Efficient Gradient-Based Tolerance Optimization Using Monte Carlo Simulation," J. Manuf. Sci. Eng., **131**(3), p. 031005.

[52] Huang, C. M., Shy, S. S., Huang, S. C., and Lee, C. H., 2009, "Performance Measurements of a Single-cell Stack Using Various Designs of Flow Distributors for Planar SOFC," ECS Trans., **25**(2), pp. 221–230.

[53] Huang, C. M., Shy, S. S., and Lee, C. H., 2007, "Experimental and Numerical Studies on Flow Uniformity in Interconnects and Its Influence on a Single Planar Solid Oxide Fuel Cell," 10th International Symposium on Solid Oxide Fuel Cells (SOFC-X), Electrochemical Society Inc, Nara, Japan, pp. 1849–1858 2646.

[54] Oliver, T. A., 2014, "Introduction to Epistemic Uncertainty," VKI lectures series on UQ in CFD, Von Kármán Institute, Waterloo, Belgium.

[55] Oberkampf, W. L., and Trucano, T. G., 2002, "Verification and validation in computational fluid dynamics," Prog. Aerosp. Sci., **38**(3), pp. 209–272.

[56] O'Hagan, A., and Oakley, J. E., 2004, "Probability is perfect, but we can't elicit it perfectly," Reliab. Eng. Syst. Saf., **85**(1–3), pp. 239–248.

[57] Cornu, T., 2009, "Optimization of the anode flow field for a solid oxide fuel cell stack," Master thesis, Ecole Polytechnique Fédérale de Lausanne (EPFL).

[58] Borhani, N., 2013, "Meeting at LTCM: discussion about available means to get experimental results of the flow distribution for the PEMFC of Belenos."

[59] Peschke, P., 2011, "Discussion about available techniques for the measurements of flow-rate in multiple microchannels."

[60] Schmal, P., 2014, "Discussion about the fuel-cell module of gPROMS."

[61] Incropera, F. P., 2011, Fundamentals of heat and mass transfer, John Wiley & Sons.

[62] Marchetti, A., Gopalakrishnan, A., Chachuat, B., Bonvin, D., Tsikonis, L., Nakajo, A., Wuillemin, Z., and Van herle, J., 2011, "Robust Real-Time Optimization of a Solid Oxide Fuel Cell Stack," J. Fuel Cell Sci. Technol., **8**(5), p. 051001.

[63] Bunin, G. A., Wuillemin, Z., François, G., Nakajo, A., Tsikonis, L., and Bonvin, D., 2012, "Experimental real-time optimization of a solid oxide fuel cell stack via constraint adaptation," Energy, **39**(1), pp. 54–62.

[64] Diethelm, S., Van herle, J., Wuillemin, Z., Nakajo, A., Autissier, N., and Molinelli, M., 2008, "Impact of materials and design on solid oxide fuel cell stack operation," J. Fuel Cell Sci. Technol., **5**(3), p. -.

[65] Chan, S. H., Khor, K. A., and Xia, Z. T., 2001, "A complete polarization model of a solid oxide fuel cell and its sensitivity to the change of cell component thickness," J. Power Sources, **93**(1–2), pp. 130–140.

[66] Park, J.-H., and Blumenthal, R. N., 1989, "Electronic transport in 8 mole percent Y2O3-ZrO2," J. Electrochem. Soc., **136**(10), pp. 2867–2876.

[67] Berger, C. (ed. ., 1968, Handbook of fuel cell technology, Prentice Hall, Englewood Cliffs.

[68] Nakajo, A., 2011, "Thermomechanical and Electrochemical Degradation in Anode-Supported Solid Oxide Fuel Cell Stacks," PhD, Ecole Polytechnique Fédérale de Lausanne (EPFL).

[69] Dujc, J., 2014, "Personal communication: Model reduction from 3D to 2D."

[70] Schumacher, J. O., Eller, J., Sartoris, G., Colinart, T., and Seyfang, B. C., 2012, "2+1D modelling of a polymer electrolyte fuel cell with glassy-carbon microstructures," Math. Comput. Model. Dyn. Syst., **18**(4), pp. 355–377.

[71] Lee, P.-S., and Garimella, S. V., 2006, "Thermally developing flow and heat transfer in rectangular microchannels of different aspect ratios," Int. J. Heat Mass Transf., **49**(17–18), pp. 3060–3067.

[72] Holmes, D. B., and Vermeulen, J. R., 1968, "Velocity profiles in ducts with rectangular cross sections," Chem. Eng. Sci., **23**(7), pp. 717–722.

[73] The MathWorks Inc, ed., 2015, MatLab documentation, The MathWorks Inc, Natik, MA.

[74] Knuth, D. E., 1998, Art of Computer Programming, Volume 2: Seminumerical Algorithms, Addison Wesley, Reading, Mass.

[75] McKay, M. D., Beckman, R. J., and Conover, W. J., 1979, "A Comparison of Three Methods for Selecting Values of Input Variables in the Analysis of Output from a Computer Code," Technometrics, **21**(2), pp. 239–245.

[76] Ansys Inc, 2013, Ansys Fluent Fuel Cell Modules Manual v13.0, Ansys Inc, Canonsburg, PA.

[77] Linstrom, P., and Mallard, W., 2001, NIST Chemistry WebBook; NIST Standard Reference Database No. 69.

[78] Ansys Inc, 2013, Ansys 15.0 Documentation, Fluent, Ansys Inc, Canonsburg, PA.

[79] Cornu, T. M., Caliandro, P., Nakajo, A., and Van herle, J., 2014, "Design and analysis of a computer experiment of the anode-gas-flow distribution in fuel cells," Proceedings of the 11th European SOFC and SOE Forum, Lucerne, Switzerland, pp. 1–10.

[80] Sacks, J., Welch, W. J., Mitchell, T. J., and Wynn, H. P., 1989, "Design and Analysis of Computer Experiments," Stat. Sci., **4**(4), pp. 409–423.

[81] Montgomery, D. C., 2013, Design and analysis of experiments, John Wiley & Sons, Hoboken, NJ.

[82] Cornu, T. M., and Wuillemin, Z., 2011, "Impact of Random Geometric Distortions on the Performance and Reliability of an SOFC," Fuel Cells, **11**(4), pp. 553–564.

[83] Huang, C. M., Shy, S. S., Chien, C. W., and Lee, C. H., 2010, "Parametric study of anodic microstructures to cell performance of planar solid oxide fuel cell using measured porous transport properties," J. Power Sources, **195**(8), pp. 2260–2265.

[84] Yakabe, H., Ogiwara, T., Hishinuma, M., and Yasuda, I., 2001, "3-D model calculation for planar SOFC," J. Power Sources, **102**(1-2), pp. 144–154.

[85] de Haart, L. G. J., Vinke, I. C., Janke, A., Ringel, H., and Tietz, F., 2001, "New developments in stack technology for anode substrate based SOFC," 7th International Symposium on Solid Oxide Fuel Cells (SOFC VII), H. Yokokawa, and S.C. Singhal, eds., Electrochemical Society Inc., Tsukuba, Japan, pp. 111–119.

[86] 2009, "The Pleiades Cluster" [Online]. Available: http://pleiades.epfl.ch.

[87] Hannesen, U., "Personal communication."

[88] Larrain, D., 2005, "Solid oxide fuel cell stack simulation and optimization, including experimental validation and transient behavior," Ecole Polytechnique Fédérale de Lausanne (EPFL).

[89] Park, J. E., Thome, J. R., and Michel, B., 2009, "Effect of inlet orifice on saturated CHF and flow visualization in multi-microchannel heat sinks," Semiconductor Thermal Measurement and Management Symposium, 2009. SEMI-THERM 2009. 25th Annual IEEE, IEEE, pp. 1–8.

[90] Szczukiewicz, S., 2012, "Thermal and visual operational characteristics of multi-microchannel evaporators using refrigerants," Ecole Polytechnique Fédérale de Lausanne (EPFL).

[91] "PROSOFC, European project" [Online]. Available: http://www.prosofc-project.eu/. [Accessed: 10-Dec-2015].

[92] Biegler, L. T., Lang, Y., and Lin, W., 2014, "Multi-scale optimization for process systems engineering," Comput. Chem. Eng., **60**, pp. 17–30.

[93] Wunsch, D., 2014, "Personal communication about the current implementation of robust design optimization at NUMECA."

[94] Wuillemin, Z., Antonetti, Y., Beetschen, C., Millioud, O., Ceschini, S., Madi, H., and Van herle, J., 2013, "Local Activation and Degradation of Electrochemical Processes in a SOFC," ECS Trans., **57**(1), pp. 561–570.

[95] Wuillemin, Z., Nakajo, A., Müller, A., Schuler, A. J., Diethelm, S., Van Herle, J., and Favrat, D., 2009, "Locally-Resolved Study of Degradation in a SOFC Repeat-Element," S.C. Singhal, and H. Yokokawa, eds., ECS, Vienna, Austria, pp. 457–466.

[96] Gass, S. I., and Fu, M. C., eds., 2013, Encyclopedia of Operations Research and Management Science, Springer US, Boston, MA.

[97] JCGM/WG 2, 2012, International vocabulary of metrology – Basic and general concepts and associated terms, JCGM.

[98] Christian F. Durach, Andreas Wieland, and Jose A.D. Machuca, 2015, "Antecedents and dimensions of supply chain robustness: a systematic literature review," Int. J. Phys. Distrib. Logist. Manag., **45**(1/2), pp. 118–137.

[99] Dodge, Y., ed., 2006, The Oxford dictionary of statistical terms, Oxford Univ. Press, Oxford.

Thierry CORNU
La Rottatte 22
CH-2345 Les Breuleux JU
+41 79 586 65 77
thierry.cornu@alumni.epfl.ch

1st February 1986
Swiss
Single

SOFT SKILLS

Conscientious, dedicated and attentive,
I willingly share my experience to grow with my colleagues.

PROFESSIONAL EXPERIENCE

Laboratory for Industrial Energy Systems (EPFL)

Doctoral Assistant **2010 – 2015**

- Objective of the PhD thesis: Develop a methodology and a framework for the **optimisation under uncertainty** of the **design** of **fuel cells**, i.e. taking into account the variability and uncertainties related to modelling and manufacturing while optimizing the design.
- Finality: maximize lifetime, performance, and economic competitiveness.
- Choice and development of methods to find a tread-off between computing resources and modelling accuracy, while also respecting manufacturing constraints.
- PhD thesis in collaboration with industry:
    1) **SOLIDpower S.p.a.** (SOFCpower−HTceramix), Italy−Switzerland.
    2) **SwissHydrogen S.A.** (formerly Belenos CPH, Swatch Group), Switzerland.
- Homogenization of flow distributions: +100% for 1) and +200% for 2).

Scientific Assistant **2009 – 2010**

- Mandate given by SOFCpower−HTceramix, following their satisfaction during my Master's and Minor's projects. Modelling of direct internal reforming of methane.

EDUCATION

PhD in Energy, EPFL, Switzerland **2010 – 2016**

Master of Sciences in Mechanical Engineering, EPFL, Switzerland **2004 – 2009**

Specialisations: Aero-Hydrodynamics & Minor in Energy

Federal Matura in Physics and Applied Mathematics **2001 – 2004**
Lycée Blaise-Cendrars, La Chaux-de-Fonds, Switzerland

Highest distinction awarded for the Federal Matura and the diploma's project

Specific courses followed during the PhD

- *Uncertainty Quantification in CFD,* VKI Lecture series, Von Kármán Institute, Belgium, 2014.
- *Fundamentals of Microscale Heat Transfer*, summer school, EPFL, 2011.
- *Design of Experiment*, EPFL, 2014.
- *Environmental Economics for Engineers*, EPFL, 2011.
- *Optimization & Simulation*, EPFL, 2010.
- *Computational Science on Graphics Cards using CUDA*, EPFL, 2010.

TECHNICAL SKILLS

- Computational Fluid Dynamics (CFD) and associated multi-physics phenomena
- Solid Oxide Fuel Cells (SOFC) and Polymer Electrolyte Membrane Fuel Cells (PEMFC)
- Energetics & Heat Transfers
- Uncertainty quantification & statistical analyses
- Optimization under uncertainty (robustness, reliability)
- Improvement of the quality of a product

Computer literacy

CFD tools: ANSYS CFD: Fluent, Meshing, Icemcfd ; Gambit, Trelis
Programming: MatLab, C++, bash/batch
Analysis: DAKOTA (Sandia Lab.), ANSYS DesignXplorer
CAD tools: DASSAULT SYSTÈMES SolidWorks & Catia, ANSYS DesignModeler
Office: Microsoft Office, LATEX
Multimedia: Adobe Creative Suite
Windows, Linux, usage of High-Performance Computing (HPC) servers

LANGUAGES

French	Mother tongue	
English	Professional proficiency	C1
German	Basic knowledge	B1

SCIENTIFIC PUBLICATIONS

"Impact of random geometric distortions on the performance and reliability of an SOFC"
T. Cornu, Z. Wuillemin
In *Fuel Cells -Weinheim-*, 11(4), p. 553-564, 2011.

"Robust design optimization of fuel cells: about the uncertainty of decision variables"
T. Cornu, A. Nakajo, J. Van herle
In *Proceedings of the 11th Symposium "ModVal"*, Winterthur, CH, 2014.

"Design and analysis of a computer experiment of the anode-gas-flow distribution in fuel cells"
T. Cornu, P. Caliandro, A. Nakajo, J. Van herle
In *Proceedings of the 11th European SOFC and SOE Forum*, Lucerne, CH, A1509, 2014.

"High-performance SOFC stacks tested under different reformate compositions"
Z. Wuillemin, S. Ceschini, Y. Antonetti, C. Beetschen, S. Modena, D. Montaniro, T. Cornu, et al.
In *Proceedings of the 11th European SOFC and SOE Forum*, Lucerne, CH, A0901, 2014.

PARTICIPATION TO CONFERENCES & WORKSHOPS

- Oral presentation at the 7th Symposium for Fuel Cell and Battery Modeling and Experimental Validation (ModVal), March 2010, Morges, Switzerland.
- Attendance at the 9th & 10th European SOFC Forum, July 2010 & 2012, Lucerne, Switzerland.
- Attendance at the SOF-CH Workshop, 2014, Morat, Switzerland.
- Oral presentation at the 11th Symposium for Fuel Cell and Battery Modeling and Experimental Validation (ModVal), March 2014, Winterthur, Switzerland.
- Oral presentations for the CTI-project with Belenos CPH, Oct. 2013 & May 2014, EPFL.
- Poster presentation at the 11th European SOFC and SOE Forum, July 2014, Lucerne, Switzerland.
- Oral presentations at SOFCpower S.p.a., Mezzolombardo, Italy (3×).
- Oral presentations at HTceramix S.A., Yverdon, Switzerland (3×).

TEACHING / ASSISTANTSHIP

Practical applications and mini-projects for 4 courses

- *Numerical flow simulations* fall 2011 – 2013
- *Engines & fuel cells* fall 2012 – 2013
- *Advanced fossil and renewable energy-systems* fall 2012
- *Renewable energy* spring 2012

Elaboration and coaching for the projects of 17 students

- *Analysis of the effect of dimensional variability in the design of fuel cells*,
  Roberto PASSINI, Master semester 3 fall 2013
- *A comparative study of mass-distribution at cathode-side of PEMFC stack-configurations*
  Vinit K. MITTAL, summer internship summer 2013
- *Réduction de modèle d'une pile à combustible pour analyser la sensibilité de la distribution des gaz aux tolérances géométriques*
  Xavier BEDNAREK, Master sem. 2 spring 2013
- *CFD electrochemical model of PEMFC*
  Roberto PASSINI, Master sem. 2 spring 2013
- *Uniformisation of the gas-distribution in a fuel cell with CFD*
  Pieter DERMONT, Master sem. 3 fall 2012
- *Sensitivity analysis to reduce the complexity of a SOFC CFD model*
  Roberto PASSINI, Master sem. 1 fall 2012
- *Amélioration d'un logiciel d'analyse des effets stochastiques dans une pile à combustible*
  Kevin ARRANDEL, Master sem. 2 spring 2012
- *Simulations de la distribution des gaz dans une pile à combustible de qualité hétérogène*
  Kévin ROSSET, Master sem. 1 fall 2011
- 2 group projects (simultaneous engineering), Bachelor sem. 6 2011, 2012

EXTRACURRICULAR ACTIVITIES & INTERESTS

Aeronautics, photography (club EPFL), typography
Monitoring about information & communication technologies